Exploring kidney organoid vascularization

Koning, M.

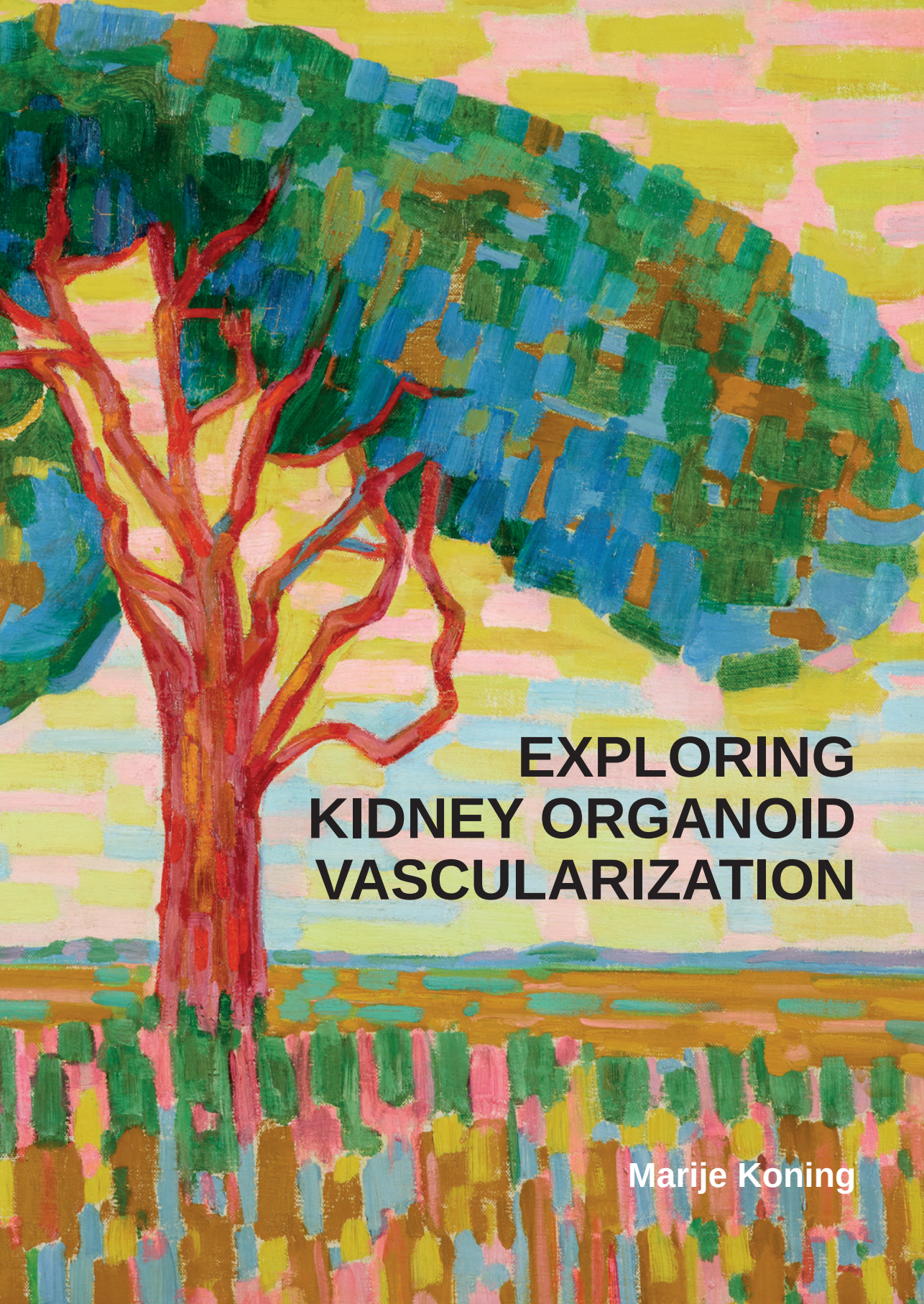

EXPLORING KIDNEY ORGANOID VASCULARIZATION

Marije Koning

Exploring kidney organoid vascularization

Marije Koning

The work described in this thesis was performed at the department of internal medicine and Einthoven laboratory, Leiden University Medical Center, the Netherlands. It was supported by the Nephrosearch Foundation and the partners of Regenerative Medicine Crossing Borders (RegMedXB).

Layout: Parntawan Kidtam | www.ridderprint.nl
Print: Ridderprint | www.ridderprint.nl
Cover Art: Twee Bomen, olieverf op canvas 70,5 x 88,2cm, Jacoba van Heemskerck 1910. Kunstmuseum Den Haag - schenking particuliere collectie.

ISBN: 978 94 6522 978 2

Exploring kidney organoid vascularization

Proefschrift

ter verkrijging van
de graad van doctor aan de Universiteit Leiden,
op gezag van rector magnificus prof.dr. S. de Rijcke,
volgens besluit van het college voor promoties
te verdedigen op woensdag 4 februari 2026
klokke 13:00 uur

door

Marije Koning

Promotor

Prof. Dr. A.J. Rabelink

Co-promotor

Dr. C.W. van den Berg

Leden promotiecommissie

Prof. dr. N. Geijsen

Prof. dr. D.J.M. Peters

Dr. V. Orlova

Dr. T. Jaffredo (Sorbonne Université)

Prof. dr. P. Carmeliet (Katholieke Universiteit Leuven)

Table of contents

CHAPTER 1

Introduction and outline of this thesis

Chronic kidney disease (CKD) is highly prevalent worldwide, affecting more than 10% of the general population[1]. It significantly increases the risk of cardiovascular and all-cause mortality[1-4] and carries a substantial economic burden that rises with disease severity[5]. Treatment options to prevent or slow progression of CKD are limited and a proportion of patients develops kidney failure. Once kidney failure occurs, patients can be treated with conservative management, dialysis, or kidney transplantation. Conservative management consists of the management of symptoms of kidney failure and preservation of residual kidney function for as long as possible, without dialysis or transplantation. Dialysis, in the form of hemodialysis or peritoneal dialysis, can replace around 10-15% of kidney function. These are strenuous treatments, with great impact on daily life and high morbidity and mortality. Kidney transplantation is currently the treatment option with the best outcomes. However, the shortage of donor organs leads to waiting lists that in the Netherlands are lengthening every year[6]. Also, some patients are too frail to undergo transplant surgery and the lifelong immunosuppressive treatment that is required after transplantation. There is therefore an urgent need for new methods to treat patients with CKD.

Kidney organoids

Kidney organoids generated from human stem cells hold great promise in this respect. In 2007, it was discovered that adult cells can be reprogrammed to stem cells[7]. These human induced pluripotent stem cells (hiPSCs) can be generated from healthy or diseased individuals, and possess the same properties as embryonic stem cells. They can proliferate indefinitely as stem cells and have the potential to differentiate to any specialized cell type in the human body. The significance of this discovery was immediately recognized by researchers, and since then protocols have been developed for the differentiation of hiPSCs to all kinds of cell types, including kidney organoids[8-12].

Protocols for the generation of kidney organoids from hiPSCs are based on embryonic kidney development. In embryology, kidneys develop from 2 progenitor populations: the metanephric mesenchyme, which forms the nephron, and the ureteric bud, which gives rise to the collecting duct and ureter. Both progenitor populations are derived from the intermediate mesoderm, which develops from primitive streak cells that migrate anteriorly. Kidney organoid differentiation protocols attempt to mimic this process in vitro: hiPSCs are treated with CHIR to mimic Wnt signaling inducing differentiation to primitive streak, followed by FGF9 to induce intermediate mesoderm. An additional CHIR pulse as well as interaction between the different developing cells in the organoids leads to further differentiation. Interestingly, the relatively straightforward protocols for the generation of kidney organoids yield highly complex nephron structures, consisting of glomerular,

proximal tubular, and distal tubular cells that are surrounded by stromal and endothelial cells (ECs). Organoids in their current form have already been used to screen for drug toxicity and model certain early onset kidney diseases[13-18], which will hopefully in the future reduce the need for laboratory animals. However, their impact would be much greater if they could be used for transplantation as auxiliary kidney tissue or even to fully replace kidney function.

Several important limitations currently hinder kidney organoids from achieving their full potential: Kidney organoids contain off-target cell populations causing safety concerns[19,20], they are far too small to generate sufficient kidney function to keep patients off dialysis, and 3D organization with a urine drainage system is lacking. Another major concern is that kidney organoids lack a functional vasculature and are (ultra)structurally, functionally and metabolically immature.

Vascularization of human kidneys versus kidney organoids

Kidneys are highly vascularized organs, receiving 20-25% of cardiac output. Blood flow is indispensable for kidney function, allowing for oxygenation of renal cells, glomerular filtration, blood pressure regulation, tubular reabsorption and secretion. In addition to blood flow, the ECs lining the renal vasculature play a crucial role in kidney development and maintenance. Renal ECs are phenotypically heterogeneous to support the specific functions of each region of the kidney[21,22]. Glomerular ECs are the most well-known example in this respect. These highly fenestrated cells, together with podocyte foot processes and the glomerular basement membrane (GBM), form the glomerular filtration barrier that allows for the continuous filtration of large volumes of blood. The development of this intricate structure requires interaction between glomerular podocytes, mesangial cells and ECs. In embryology, podocyte precursors attract ECs by producing vascular endothelial growth factor A (VEGF-A), which start to invade nephron structures in the S-shaped body stage of development. It has been shown in mouse models that a reduction of podocyte-derived VEGF-A leads to severe damage to ECs, with a complete absence of VEGF-A resulting in unvascularized glomeruli and perinatal death[23]. In turn, podocytes lacking interaction with ECs fail to mature, displaying effacement of foot processes and absence of slit diaphragms[23].

Kidney organoids cultured in vitro do contain ECs, but these are mainly located at the periphery of the organoid and fail to invade the clusters of podocytes that form the glomerular structure (Fig. 1). The interaction required for proper development of both

cell types as well as the glomerular filtration barrier consequently does not occur and the organoid glomeruli and nephrons remain immature. This poses important restrictions to the use of kidney organoids for modeling glomerular diseases as well as for regenerative medicine.

Strategies to enhance vascularization and maturation of kidney organoids

Transplantation of kidney organoids under the kidney capsule or subcutaneously in mice has been shown to induce vascularization and enhance maturation[24,25]. These transplanted organoids become functionally perfused by blood vessels that are lined mainly by host derived ECs and have even been shown to be capable of glomerular sieving[26]. The disadvantage of this model is that it is labour intensive, not allowing for high throughput experiments. Also, the factors responsible for inducing vascularization upon transplantation remain unknown. It has been hypothesized that exposure of ECs to flow, hypoxia, growth factors and the presence of mature ECs from the host might play a role.

Attempts to vascularize kidney organoids in vitro by mimicking these condition through culture under laminar flow, in a hypoxic environment, or after addition of VEGF-A to the culture medium have been only partially successful[27-29]. These strategies mainly induced an increase in the number of ECs but no or at most sporadic invasion of glomerular structures by ECs. Functional vascularization of in vitro kidney organoids by perfusable endogenous ECs therefore remains elusive.

Analyzing kidney organoids at a single cell level

For the development of new strategies to enhance kidney organoid vascularization and maturation, detailed analysis of the organoids at a molecular level can be of great value. Unfortunately, the interpretation of kidney organoid gene expression data from quantitative PCR or bulk RNA sequencing analysis is challenging. These techniques provide average gene expression levels for organoids as a whole, but do not inform about cell type specific transcriptomes. This does not do justice to the complexity of kidney organoids, as differences in gene expression between the many different cell types remain undetected. The development of single cell RNA sequencing (scRNAseq) analysis has overcome this problem. It enables the measurement of transcriptome profiles for individual cells at great scale and high resolution. This provides the possibility to distinguish cell populations, identify possible target genes for differentiation, maturation or disease modeling, and analyse potential interactions between cell populations. In this manner, it could provide important clues to enhance kidney organoid vascularization and maturation.

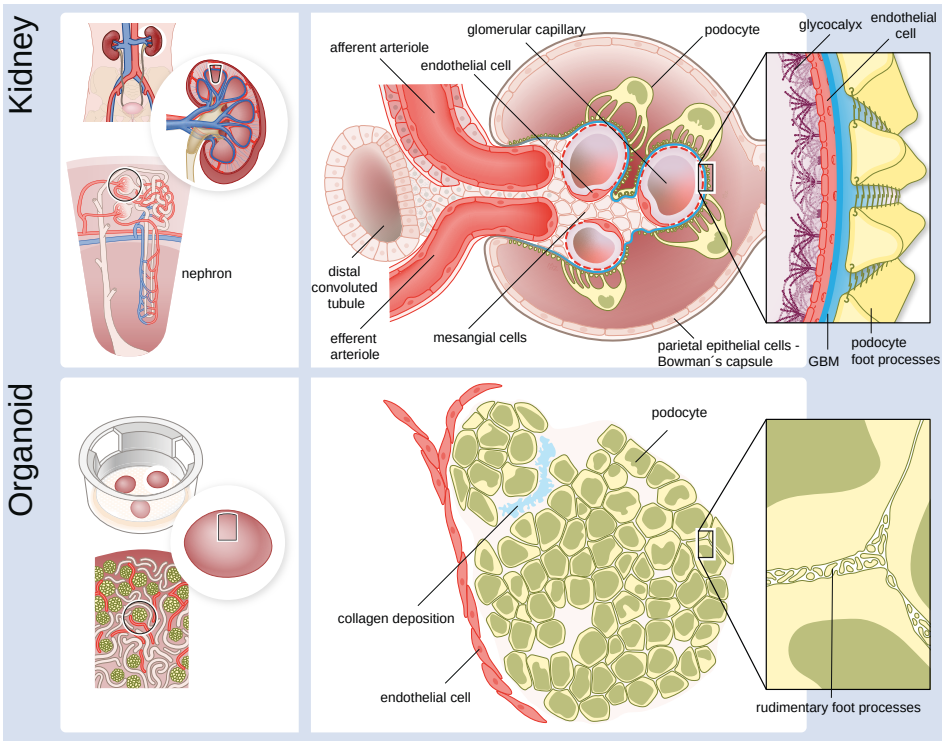

Figure 1: glomerular structures in the adult kidney (top) and kidney organoid (bottom).
The glomerulus in the adult kidney consists of a network of capillaries, lined with fenestrated endothelial cells, that are supported by mesangial cells and surrounded by podocytes. Blood enters the glomerulus through the afferent arteriole. Filtration occurs through the glomerular filtration barrier, the filtrate enters Bowman's space and flows into the proximal tubule. Blood exits the glomerulus through the efferent arteriole. The glomerular filtration barrier (zoom of boxed area) consists of fenestrated endothelial cells, the glomerular basement membrane and podocyte foot processes.
Kidney organoids contain glomerular structures, tubular structures and endothelial cells. Glomerular structures in kidney organoids consist of clusters of podocytes that in some areas deposit unorganized collagen and are surrounded with but not invaded by endothelial cells. The podocytes display rudimentary foot processes, but a glomerular filtration barrier does not form.

General outline of this thesis

The aim of this thesis is to explore the process of kidney organoid vascularization and its effect on organoid development and maturation.

In **Chapter 2**, methods for the generation of kidney organoids from human iPSCs and their limitations are discussed, with a focus on vascularization. Although currently available protocols yield organoids containing nephron-like structures, the lack of a functional vasculature and consequent immaturity of the organoids limits their applicability. Existing strategies to enhance vascularization include transplantation in mice. However, this is labour intensive and unsuitable for studying large numbers of organoids.

To improve organoid vascularization, we initially attempted in vitro co-culture with ECs. In **Chapter 3,** we discuss the different strategies we applied, including exposure to flow and modifications of the extracellular matrix. Despite adaptations to the differentiation protocol and culture conditions it seems challenging to induce functional vascularization.

We therefore decided to take a step back, and study the process of organoid vascularization in more detail. For this purpose, we developed a method for intracoelomic transplantation of kidney organoids in chicken embryos. In **Chapter 4**, we show that transplanted organoids are functionally vascularized within 8 days, leading to perfusion of organoid glomeruli. Compared to untransplanted controls, transplanted organoids display enhanced maturation at a transcriptional as well as ultrastructural level. The interaction between ECs and podocytes in transplanted organoids enables the development of a rudimentary GBM. The detailed protocol for intracoelomic transplantation of kidney organoids in chicken embryos, followed by injection of fluorescently labelled lectin to visualize perfused blood vessels, can be found in **Chapter 5**.

Considering the phenotypic heterogeneity of ECs in the adult kidney, in **Chapter 6** we next evaluate the characteristics of organoid ECs in untransplanted and transplanted organoids. Human ECs were isolated from transplanted organoids and untransplanted controls and analysed using single cell RNA sequencing (scRNAseq). We show that organoid ECs are heterogeneous and that transplantation sustains EC proliferation and induces a major shift from venous to arterial ECs that resemble fetal kidney ECs. In addition, we identify possible targets to enhance vascularization.

Chapter 7 provides a discussion of the findings presented in this thesis and the future possibilities of kidney organoids for research and regenerative medicine purposes.

References

1 Kovesdy, C. P. Epidemiology of chronic kidney disease: an update 2022. Kidney Int Suppl (2011) ***12***, 7-11 (2022). https://doi.org:10.1016/j.kisu.2021.11.003

2 Matsushita, K. et al. Association of estimated glomerular filtration rate and albuminuria with all-cause and cardiovascular mortality in general population cohorts: a collaborative meta-analysis. Lancet ***375***, 2073-2081 (2010). https://doi.org:10.1016/S0140-6736(10)60674-5

3 Go, A. S., Chertow, G. M., Fan, D., McCulloch, C. E. & Hsu, C. Y. Chronic kidney disease and the risks of death, cardiovascular events, and hospitalization. N Engl J Med ***351***, 1296-1305 (2004). https://doi.org:10.1056/NEJMoa041031

4 van der Velde, M. et al. Lower estimated glomerular filtration rate and higher albuminuria are associated with all-cause and cardiovascular mortality. A collaborative meta-analysis of high-risk population cohorts. Kidney Int ***79***, 1341-1352 (2011). https://doi.org:10.1038/ki.2010.536

5 Jha, V. et al. Global Economic Burden Associated with Chronic Kidney Disease: A Pragmatic Review of Medical Costs for the Inside CKD Research Programme. Adv Ther ***40***, 4405-4420 (2023). https://doi.org:10.1007/s12325-023-02608-9

6 Nederlandse Transplantatie Stichting, Cijferoverzicht 2021. (2021).

7 Takahashi, K. et al. Induction of pluripotent stem cells from adult human fibroblasts by defined factors. Cell ***131***, 861-872 (2007). https://doi.org:10.1016/j.cell.2007.11.019

8 Taguchi, A. et al. Redefining the in vivo origin of metanephric nephron progenitors enables generation of complex kidney structures from pluripotent stem cells. Cell Stem Cell ***14***, 53-67 (2014). https://doi.org:10.1016/j.stem.2013.11.010

9 Morizane, R. et al. Nephron organoids derived from human pluripotent stem cells model kidney development and injury. Nat Biotechnol ***33***, 1193-1200 (2015). https://doi.org:10.1038/nbt.3392

10 Takasato, M. et al. Kidney organoids from human iPS cells contain multiple lineages and model human nephrogenesis. Nature ***526***, 564-568 (2015). https://doi.org:10.1038/nature15695

11 Freedman, B. S. et al. Modelling kidney disease with CRISPR-mutant kidney organoids derived from human pluripotent epiblast spheroids. Nat Commun ***6***, 8715 (2015). https://doi.org:10.1038/ncomms9715

12 Taguchi, A. & Nishinakamura, R. Higher-Order Kidney Organogenesis from Pluripotent Stem Cells. Cell Stem Cell (2017). https://doi.org:10.1016/j.stem.2017.10.011

13 Tanigawa, S. et al. Organoids from Nephrotic Disease-Derived iPSCs Identify Impaired NEPHRIN Localization and Slit Diaphragm Formation in Kidney Podocytes. Stem Cell Reports (2018). https://doi.org:10.1016/j.stemcr.2018.08.003

14 Forbes, T. A. et al. Patient-iPSC-Derived Kidney Organoids Show Functional Validation of a Ciliopathic Renal Phenotype and Reveal Underlying Pathogenetic Mechanisms. Am J Hum Genet ***102***, 816-831 (2018). https://doi.org:10.1016/j.ajhg.2018.03.014

15 Hale, L. J. et al. 3D organoid-derived human glomeruli for personalised podocyte disease modelling and drug screening. Nat Commun ***9***, 5167 (2018). https://doi.org:10.1038/s41467-018-07594-z

16 Cruz, N. M. et al. Organoid cystogenesis reveals a critical role of microenvironment in human polycystic kidney disease. Nat Mater (2017). https://doi.org:10.1038/nmat4994

17 Dorison, A. et al. Kidney Organoids Generated Using an Allelic Series of NPHS2 Point Variants Reveal Distinct Intracellular Podocin Mistrafficking. J Am Soc Nephrol (2022). https://doi.org:10.1681/ASN.2022060707

18 Vanslambrouck, J. M. et al. Enhanced metanephric specification to functional proximal tubule enables toxicity screening and infectious disease modelling in kidney organoids. Nat Commun ***13***, 5943 (2022). https://doi.org:10.1038/s41467-022-33623-z

19 Wu, H. et al. Comparative Analysis and Refinement of Human PSC-Derived Kidney Organoid Differentiation with Single-Cell Transcriptomics. Cell Stem Cell (2018). https://doi.org:10.1016/j.stem.2018.10.010

20 Phipson, B. et al. Evaluation of variability in human kidney organoids. Nat Methods ***16***, 79-87 (2019). https://doi.org:10.1038/s41592-018-0253-2

21 Dumas, S. J. Single-Cell RNA Sequencing Reveals Renal Endothelium Heterogeneity and Metabolic Adaptation to Water Deprivation. JASN (2019).

22 Dumas, S. J. et al. Phenotypic diversity and metabolic specialization of renal endothelial cells. Nat Rev Nephrol ***17***, 441-464 (2021). https://doi.org:10.1038/s41581-021-00411-9

23 Eremina, V. et al. Glomerular-specific alterations of VEGF-A expression lead to distinct congenital and acquired renal diseases. J Clin Invest ***111***, 707-716 (2003). https://doi.org:10.1172/JCI17423

24 van den Berg, C. W. et al. Renal Subcapsular Transplantation of PSC-Derived Kidney Organoids Induces Neo-vasculogenesis and Significant Glomerular and Tubular Maturation In Vivo. Stem Cell Reports ***10***, 751-765 (2018). https://doi.org:10.1016/j.stemcr.2018.01.041

25 Bantounas, I. et al. Generation of Functioning Nephrons by Implanting Human Pluripotent Stem Cell-Derived Kidney Progenitors. Stem Cell Reports ***10***, 766-779 (2018). https://doi.org:10.1016/j.stemcr.2018.01.008

26 van den Berg, C. W., Koudijs, A., Ritsma, L. & Rabelink, T. J. In Vivo Assessment of Size-Selective Glomerular Sieving in Transplanted Human Induced Pluripotent Stem Cell-Derived Kidney Organoids. J Am Soc Nephrol ***31***, 921-929 (2020). https://doi.org:10.1681/ASN.2019060573

27 Homan, K. A. et al. Flow-enhanced vascularization and maturation of kidney organoids in vitro. Nat Methods ***16***, 255-262 (2019). https://doi.org:10.1038/s41592-019-0325-y

28 Menéndez, A. B. C. et al. Creating a kidney organoid-vasculature interaction model using a novel organ-on-chip system. Sci Rep-Uk ***12*** (2022). https://doi.org:ARTN 20699 10.1038/s41598-022-24945-5

29 Schumacher, A. et al. Enhanced Microvasculature Formation and Patterning in iPSC-Derived Kidney Organoids Cultured in Physiological Hypoxia. Front Bioeng Biotechnol ***10***, 860138 (2022). https://doi.org:10.3389/fbioe.2022.860138

CHAPTER 2

Stem cell-derived kidney organoids: engineering the vasculature

M. Koning, C.W. van den Berg, A.J. Rabelink

Cellular and Molecular Life Sciences, 2019

Abstract

Kidney organoids can be generated from human pluripotent stem cells (PSCs) by using protocols that resemble the embryonic development of the kidney. The renal structures thus generated offer great potential for disease modeling, drug screening and possibly future therapeutic application. At the same time, use of these PSC derived organoids is hampered by lack of maturation and off-target differentiation. Here, we review the main protocols for the generation of kidney organoids from human induced PSCs, discussing their advantages and limitations. In particular, we will focus on the vascularization of the kidney organoids, which appears to be one of the critical factors to achieve maturation and functionality of the organoids.

Introduction

Chronic kidney disease (CKD) is highly prevalent worldwide and increases the risk of cardiovascular and all-cause mortality[1-3]. Treatment options are limited and once patients progress to end stage renal disease (ESRD) they become dependent on renal replacement therapy, requiring either dialysis or kidney transplantation. Dialysis is a strenuous treatment associated with high morbidity and mortality. Kidney transplantation is currently the best available treatment for ESRD, but suffers from a shortage of donor kidneys and necessitates the lifelong use of immunosuppressive drugs.

The publication of protocols to generate 3D kidney organoids from human induced pluripotent stem cells (hiPSCs) was therefore met with great enthusiasm. Human iPSCs can be obtained by reprogramming adult cells from any individual, either healthy or diseased, offering unprecedented possibilities for treatment and disease modeling[4]. Over the past 5 years, several protocols have been developed to differentiate human PSCs to kidney organoids[5-8]. All are based on the development of the kidney in an embryo. Here, the nephron including the glomerulus, proximal and distal tubules, loop of Henle and connecting tubule is derived from the metanephric mesenchyme (MM)[9-11], whereas the collecting duct and ureter are derived from the ureteric bud (UB). Inductive interaction between these two progenitor populations is essential for correct development and 3D organization of the kidney[12,13].

Protocols for iPSC derived kidney organoids generally yield nephron structures containing glomerular, proximal tubular and distal tubular structures that, in many cases, are surrounded by stromal and endothelial cells (ECs)[5-8,14]. In addition, some authors claim the generation of collecting duct like structures[7,14].

Kidney organoids have already been used to study kidney development[5,6,15], model certain (early onset) kidney diseases[8,16-19] and screen for tubular nephrotoxicity[6-8]. However, before they can be applied for regenerative medicine purposes there are still many limitations to overcome. Kidney organoids frequently contain off-target cell populations[20-23], suffer from interexperimental variability[21], display limited 3D organization, contain far too few nephrons to replace renal function and, unless they are generated from a patient's own cells, are likely to elicit an immune response upon transplantation[24,25]. Another great concern is that, although kidney organoids frequently contain some ECs, they lack a functional vasculature.

Kidneys are highly vascularized organs whose correct development, functionality and maintenance require the presence of blood flow and the interaction with vascular ECs. In

embryology, glomerular podocytes and mesangial cells develop in close conjunction with ECs and their maturation as well as the development of the glomerular filtration barrier are disturbed when ECs are lacking [26-28]. In adult kidneys, specialized ECs in the glomerulus, peritubular capillaries and ascending and descending vasa recta contribute to glomerular filtration, tubular urine concentrating ability and interstitial fluid drainage[29]. Consequently, the applicability of kidney organoids lacking a perfused vascular network is limited.

It has been shown that transplantation of kidney organoids in mice results in vascularization by perfused blood vessels as well as significant maturation, confirming the benefit of a functional vasculature for progressive organoid development[30-32]. Very recently, researchers aimed to achieve similar results in vitro by culturing kidney organoids with flow over their top surface. They observed an increase in the number of ECs, which formed networks that, in some cases, invaded organoid glomerular structures. However, they were unable to convincingly show that the vascular networks were fully perfusable[33]. In addition, for both the transplantation studies and the in vitro culture under flow, it is unclear to what degree the blood vessels that are formed possess the properties of the specialized renal vasculature in vivo.

Here, we review the main protocols to generate 3D kidney organoids from human PSCs and discuss the importance of a functional vasculature in kidney organoids. We compare the process of kidney vascularization in embryology to that occurring after transplantation of PSC-derived organoids to murine hosts and upon culturing them under flow in vitro. Finally, we consider the potential and limitations of in vivo and in vitro vascularized kidney organoids.

Human pluripotent stem cell-derived kidney organoids

In order to differentiate iPSCs to a specific tissue type, detailed knowledge about its embryonic development is indispensable. The protocols for the generation of iPSC-derived kidney organoids are, therefore, based on extensive research in mammalian nephrogenesis and their establishment was accompanied by important developmental discoveries.

In embryology, the metanephric kidneys are derived from the intermediate mesoderm (IM), which gives rise to both the MM and the UB[34,35]. In response to glial derived neurotrophic factor (GDNF) produced by the MM, the UB protrudes from the nephric duct into the MM and branches to form the collecting duct system[36-38]. The MM cells surrounding the UB tips condense to form the cap mesenchyme (CM), which contains the progenitor cells for the entire nephron[9-11].

Dependent on canonical Wnt signalling activated by UB-derived Wnt9b, the CM forms a pretubular aggregate (PTA)[39,40]. The PTA expresses Wnt4, which induces mesenchyme-to-epithelial transition (MET) through non-canonical signalling and gives rise to the renal vesicle (RV)[41,42]. Recently, it was discovered that the formation of the RV occurs gradually over time with the recruitment of nephron progenitor cells (NPCs) from the CM into the RV. The timing of recruitment plays an important role in the proximal-distal patterning of the nephron. NPCs that are recruited first form the distal tubular precursors and are located closest to the ureteric bud tip, the second recruits form the proximal tubular precursors, and the last cells to enter the RV give rise to podocyte precursors[43]. The RV subsequently develops into the comma-shaped body, S-shaped body, capillary loop stage and, finally, the mature nephron, which is connected to the UB-derived collecting duct system.

Protocols for human iPSC-derived kidney organoids

Since renal organogenesis depends on the interaction between the MM and UB, induction of both progenitor populations will be essential to eventually generate complete kidneys from iPSCs. Researchers, therefore, set out to determine their precise developmental origin. Although it was known that both progenitor populations derive from the IM, the processes responsible for the differentiation towards either the UB or the MM lineage had not been elucidated.

To investigate this, Taguchi et al. extensively studied the development of NPCs in mice, starting at the MM stage and moving backwards to the PS stage step by step. Possible precursor populations were identified, isolated, and tested for their capacity to differentiate to the next stage in vitro. This enabled them to test their hypotheses as well as differentiation conditions for mouse embryonic nephron precursors.

It was discovered that the presence of metanephric nephron progenitors was restricted to the posterior IM (PIM), with cells in the anterior IM (AIM) contributing to mesonephric nephrons and the ureteric bud. Additional experiments demonstrated that the PIM is derived from caudal Brachyury positive (T+) primitive streak (PS) cells that remain posteriorized until E8.5, while the AIM cells migrate anteriorly in an earlier stage[5].

The obtained knowledge was used by Taguchi et al. and several other research groups to develop protocols for the differentiation of human PSCs to 3D kidney organoids[5-8].

The protocol by Taguchi et al. entails the generation of embryoid bodies, followed by mesoderm induction with BMP4 and CHIR (Wnt agonist), stimulation of the obtained mesoderm with Activin A, BMP4, CHIR and retinoic acid to achieve differentiation to PIM and, finally, addition of CHIR and FGF9 to generate MM cells. Co-culture of the hiPSC-

derived MM with mouse embryonic spinal cord results in the formation of 3D kidney organoids containing nephron-like structures[5] (Fig. 1).

Morizane et al. developed a chemically defined protocol for the generation of NPCs and kidney organoids[6]. They tested varying doses and duration of CHIR treatment and growth factors to determine the optimal conditions for the induction of late PS and PIM. By treating hiPSCs with CHIR and Noggin for 4 days to obtain PS, followed by stimulation with Activin A for 3 days, they generate PIM cells with 80-90% efficiency. Subsequent addition of FGF9 to the PIM cells is sufficient to achieve differentiation to MM within 2 days. The obtained MM cells are replated in 96-well round bottom low attachment plates and the formation of renal vesicles is induced by treatment with CHIR and FGF9 during 2 days, followed by 3 days with FGF9 only. From day 14 of differentiation onwards, no growth factors are added to the media and kidney organoids with nephron-like structures form through self-organization (Fig. 1).

Freedman et al. cultured hiPSCs between 2 layers of Matrigel to induce the formation of cavitated spheroids that maintain pluripotency. By treating these spheroids with CHIR for 1,5 days, differentiation to mesenchyme is induced, which subsequently undergoes MET upon culture in B27-supplemented media, resulting in the formation of organoids with nephron like-structures[8] (Fig. 1).

Takasato et al. hypothesized that, since the AIM is formed by cells that migrate anteriorly from the PS early on, these are exposed to the strong Wnt signalling in the PS for a shorter period of time than those that migrate in a later stage to form the PIM. Therefore, it might be possible to induce both the AIM and the PIM from PSCs by optimizing the duration of CHIR treatment prior to replacement by FGF9[7]. They tested this theory by treating PSCs with CHIR for 3, 4 or 5 days and checking for the expression of AIM / UB (LHX1, GATA3) and PIM / MM (HOXD11, EYA1) markers at day 7 and 18 of differentiation using qPCR (day 7) and immunofluorescent stainings (day 7 and 18). Based on these experiments, they claimed that exposing hPSCs to CHIR for 4 days followed by FGF9 for 3 days induces both PIM and AIM simultaneously. To subsequently generate organoids, the cells were dissociated, reaggregated to form cell pellets, and cultured on transwell filters where they were treated with a CHIR pulse followed by FGF9 for 5 more days. Afterwards, growth factors were removed and it was reported that over the next 6-13 days, 3D kidney organoids containing nephron-like structures as well as collecting duct networks formed[7] (Fig. 1).

Collecting ducts were defined by the authors as tubular structures that co-expressed GATA3 and ECAD. However, these markers are not specific for the collecting duct only, and have been shown to be expressed in the MM derived distal tubules and connecting tubules as well[44]. In addition, the collecting duct tree in vivo is a highly organized branching structure that connects the tubular system to the calyces and ureter, ensuring a single

urinary exit path. The structures termed collecting ducts in the in vitro kidney organoids did not display this morphology. Also, single cell RNA sequencing analysis of the organoids failed to identify a clear ureteric bud and / or collecting duct cell population[20,23]. These limitations have led to discussion in the field about the nature of the GATA3+, ECAD+ structures in the kidney organoids. Future research aimed specifically at unravelling the identity of these cells will hopefully clarify this.

Despite the differences in culture conditions between the protocols discussed above, the resulting organoids as reported by the authors show many similarities. In all cases, nephron-like structures containing podocytes (WT1/NPHS1+/PODXL+), proximal tubules (LTL+/CUBN+/LRP2+) and distal tubules (ECAD+) were demonstrated through immunofluorescent stainings and confocal microscopy[5-8]. Some, but not all, authors also described the presence of ECs (CD31+, vWF+)[7,8], stromal cells, 'early mesangial cells'[7] and / or epithelial cells expressing a marker specific for the ascending loop of Henle (UMOD+)[6,7]. Bowman's capsule like structures were demonstrated in several of the previously discussed papers[6-8] and it was shown later on that these consist of parietal epithelial cells (CLDN1+, PAX8+)[22] that display aberrant morphology in organoids generated from PAX2 knockout iPSCs[45]. However, it is unclear whether this variation in reported cell types represents true differences between the obtained organoids. The methods used to characterize the organoids were not identical and reports of direct comparisons between protocols are scarce. One study compared organoids generated through the Takasato and Morizane protocol using single cell RNA sequencing (scRNAseq), and demonstrated that these were very similar with regard to the cell populations present, although differences in the fractions of these populations were detected[20]. Of note, this and other scRNAseq studies have demonstrated that kidney organoids do not consist solely of renal cell types, but also contain off-target stromal, neural and/or muscle cell populations[20-22,46].

Three dimensional organization of kidney organoids

An important question regarding the organoids generated through all the above protocols is to what degree their 3D organization resembles that in the in vivo kidney. The in vivo kidney is a complex structure consisting of many different cell types which are meticulously organized. In organoids, glomerular, proximal tubular and distal tubular structures have been reported to connect in the right order[5-8], but this is not always the case and the lack of a branching collecting duct system precludes the development of a morphologically correct structure with full corticomedullary organization. This is also illustrated by the 'Loop of Henle' cells in the organoids. Although these cells express Uromodulin, a marker specific for epithelial cells in the ascending Loop of Henle, they have not been shown to form the elongated U-shaped structure that in vivo extends deep into the medulla before looping back to the renal cortex. In this area, there is ample room for improvement.

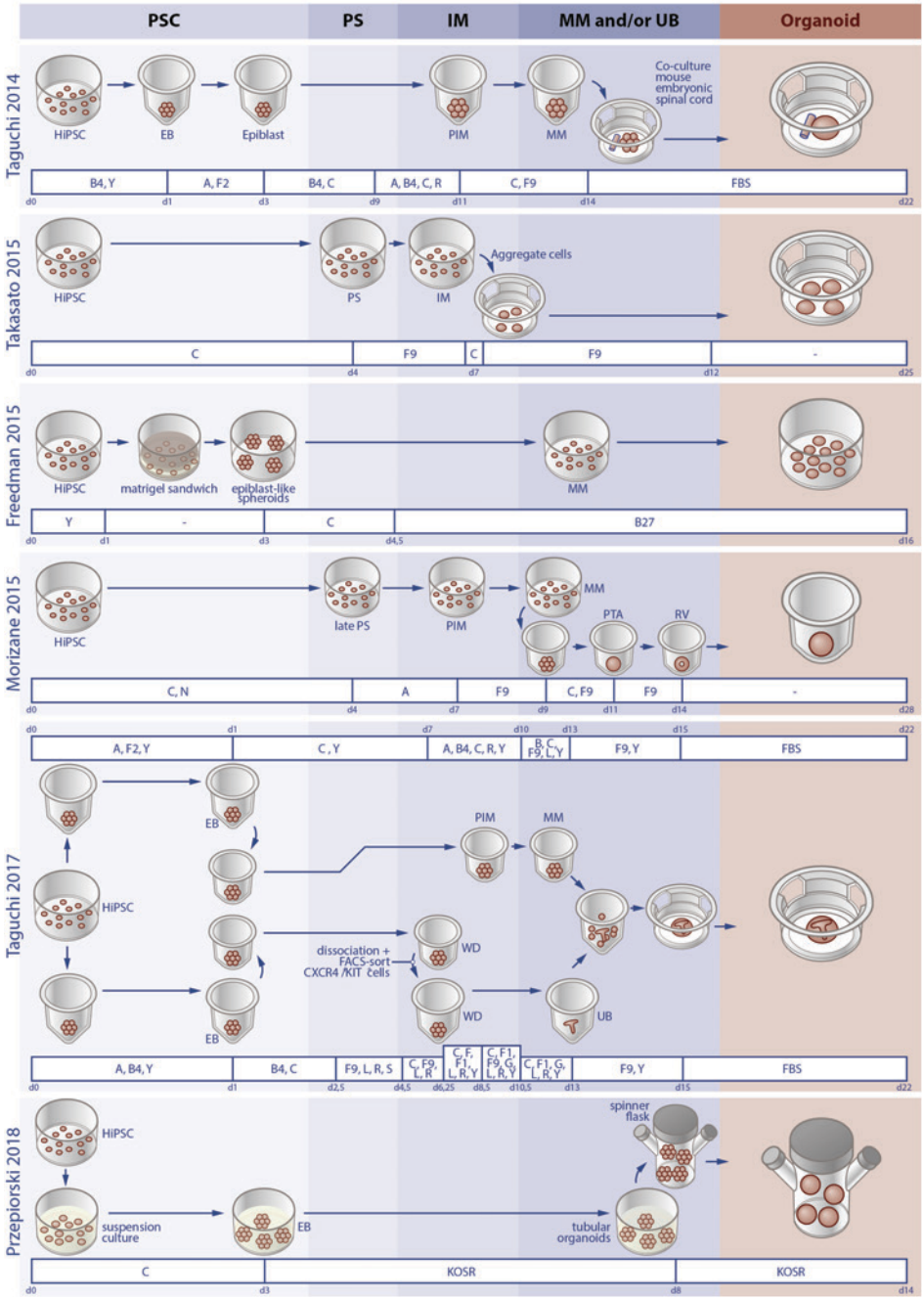

Figure 1: Overview of protocols for the generation of kidney organoids from human iPSCs. The schematically shown protocols are described in the main text and include the co-culture of MM with mouse embryonic spinal cord or separately induced UB, culturing on an air-liquid interface, using a Matrigel sandwich, induction of nephron progenitor cells followed by renal vesicle formation, and suspension culture.

Abbreviations: A = activin A; B = BMS493; B4 = bone morphogenetic protein 4; B27 = B27 medium; C = CHIR 99021; EB = embryoid Body; F = fibroblast growth factor; FBS = fetal bovine serum; G = glial cell derived neurotrophic factor; hiPSC = human induced pluripotent stem cells; IM = intermediate mesoderm; KOSR = knockout serum replacement; L = LDN193189; MM = metanephric mesenchyme; N = noggin; PIM = posterior intermediate mesoderm; PS = primitive streak; PSC = pluripotent stem cells; PTA = pretubular aggregate; R = retinoic acid; RV = renal vesicle; S = SB431542; UB = ureteric bud; WD = wolffian duct; Y = Y27632.

Last year, Taguchi et al. developed a new protocol with the aim of improving the 3D organization of kidney organoids by generating a branching collecting duct system[14] (Fig. 1). The authors utilized a method reminiscent of the dissociation-reaggregation strategies applied for primary fetal tissue derived kidney organoids[47,48]. Instead of aggregating MM and UB tissue that was isolated from murine embryos, they used separately induced mouse ESC derived MM and UB. For the generation of MM, they employed an adapted version of their earlier protocol[5]. The protocol for the induction of UB was newly developed based on the developmental processes involved in the differentiation to the UB lineage in mice, which the authors studied using a backward approach. As discussed previously, UB progenitors migrate anteriorly from the T+ PS stage earlier on than MM progenitors and are therefore exposed to Wnt signalling for a shorter period of time. However, the authors found that solely reducing the duration of CHIR treatment was insufficient to induce UB progenitors and developed a complex protocol that includes a step in which cells are dissociated and FACS-sorted for the Wolffian duct (WD) progenitor markers CXCR4+/KIT+, to obtain PSC derived UB[14]. Upon combination of separately induced mouse ESC derived MM and UB with primary mouse embryonic stromal progenitors, kidney organoids containing nephrons connected to an arborized collecting duct were formed[14]. Unfortunately, when the protocol was adapted for human iPSCs, it was much less successful. The obtained UB displayed only minimal branching capacity when cultured in matrigel, and upon combination with hiPSC derived MM, branching morphogenesis did not occur, nor did the formation of nephrons from the MM.

This might be due to the lack of stromal progenitors, a suboptimal differentiation of either the MM or the UB or a problem with the reaggregation assay[14].

Scaling up organoid production

All of the previously discussed protocols for kidney organoid differentiation are labor intensive, often requiring manual pipetting and/or aggregation steps. This limits the efficiency and reproducibility of organoid generation, both of which are essential to apply them for drug and nephrotoxicity screening or renal replacement therapy. Recently, several strategies aimed at improving these aspects were published.

Przepiorski et al. showed that the laboriousness and cost of kidney organoid generation can be reduced by using suspension culture in BPEL supplemented with CHIR followed by DMEM with KnockOut Serum Replacement (KOSR). To further scale up production, the organoids can be transferred to spinner flasks on day 8 of differentiation[49] (Fig. 1). The organoids generated seem similar to those obtained with earlier protocols based on immunofluorescent stainings, but a direct comparison was not performed. This straightforward protocol is inexpensive due to the use of BPEL and the replacement of FGF9 or B27 by KOSR. However, the use of BPEL, which contains bovine serum albumin, makes the protocol susceptible to batch variation and might reduce the reproducibility of the organoids.

Czerniecki et al. took a different approach to increasing the efficiency of kidney organoid generation and focused on their suitability for high throughput screening (HTS). To this end, the previously discussed Matrigel-sandwich protocol[8] was adapted to adherent culture in 96- or 384-well plates[22] In each well, many very small organoids containing about 5 nephron-like structures per organoid appeared, surrounded by areas with non renal cells, indicating that the protocol is not fully efficient in inducing differentiation to the kidney lineage. However, as the authors demonstrated, culturing in 384 well plates facilitates efficient testing of differentiation conditions and toxicity screening.

In summary, various protocols have been developed to generate kidney organoids containing nephron like structures. Important limitations of these organoids are their limited 3D organization, the presence of off target cell populations, the lack of a functional vasculature and of a single urinary exit tract.

However, in their current form, the organoids have already been shown to be suitable to model certain kidney diseases.

Using PSC-derived kidney organoids for disease modeling

Over the past few years, the first studies reporting the use of 3D hPSC-derived kidney organoids for disease modeling were published. Generally, two main approaches are employed to obtain diseased organoids: Inducing mutations/knockouts in healthy hPSC lines using CRISPR/Cas9 or generating hiPSCs from patients. In both cases, it is of great importance to distinguish differences between affected and healthy organoids caused by the disease from those due to line to line variability. HPSC lines from different donors can exhibit marked variation in differentiation potential[50,51] and kidney organoids generated from different cell lines or even in a different batch from the same cell line vary in composition and maturation[21]. To reduce the influence of line to line variability,

organoids derived from diseased cell lines should be compared to those from isogenic controls and ideally, multiple cell lines should be investigated.

Freedman et al. focussed on polycystic kidney disease (PKD) and generated PKD1 and PKD2 knockout PSCs from a human ESC line using CRISPR/Cas9[8,19]. Upon differentiation to kidney organoids using their adherent protocol, about 7% of the organoids formed fluid filled cysts[8,19]. This percentage rose to 75% when they removed the organoids from the surrounding stroma on day 21 of differentiation and subsequently cultured them in suspension, indicating a role for adherent forces in preventing tubular cyst formation. The high number of cysts in the PKD organoids was not due solely to the adapted culture conditions, as only 5% of organoids from isogenic control hPSCs developed cysts under the same circumstances[19].

In addition to the PKD1 and 2 knockout PSCs, the authors differentiated cell lines from 2 patients with autosomal dominant PKD (ADPKD) and 1 with autosomal recessive PKD (ARPKD) to kidney organoids. Due to great variability in the capacity to differentiate as well as the propensity to form cysts in these patient cell lines, they were not used for additional experiments[19].

The PKD knockout model can be useful to study the process of early (prenatal) cyst formation and to perform drug screening. However, the immaturity of tubules in kidney organoids, the lack of a collecting duct and the scarcity of stromal tissue in this model might limit its applicability for modeling postnatal PKD, in which the majority of cysts arise from distal nephron segments and collecting ducts and extensive fibrosis is a characteristic feature. Also, it cannot be used for personalized medicine purposes, as it does not reflect the variable phenotype of PKD in patients. This would require the optimization of kidney organoid culture from patient iPSC lines.

Forbes et al. generated an uncorrected and a gene-corrected hiPSC line from a patient with nephronophthisis related ciliopathy (NPHP-RC) due to compound-heterozygous mutations in IFT140. After differentiation of both cell lines to kidney organoids, they analyzed the morphology of the cilia through manual, blinded scoring of individual cilia. In organoids derived from the uncorrected iPSCs, they found that 59% of the cilia displayed the clubbed morphology that was previously described in IFT140 null mice, compared to 12% in the gene-corrected organoids[17]. In addition, they performed differential gene expression analysis, which indicated downregulation of genes involved in apicobasal polarity in epithelial cells derived from patient organoids. Spheroid culture of these epithelial cells after isolation from the organoids was impaired accordingly[17].

However, studying disease related defects in apicobasal polarity in intact kidney organoids will be very challenging as their immature tubular epithelium is characterized by incomplete polarization[30]. More advanced modeling of NPHP-RC in kidney organoids will therefore require tubular maturation.

Kim et al. and Freedman et al. investigated the effect of the knockout of podocalyxin, which leads to early postnatal death in mice, on the podocytes in iPSC derived kidney organoids[8,15]. They demonstrated that the formation of microvilli by these podocytes was greatly reduced compared to isogenic controls, with the podocytes clustering closer together and forming lateral cell-cell junctions. Subsequent analysis of podocytes in prenatal PODXL-/- mice revealed a similar phenotype[15]. Although podocalyxin mutations in patients with kidney disease are uncommon, these results demonstrate the suitability of kidney organoids to study developmental processes.

Recently, two different research groups used kidney organoids to study congenital nephrotic syndrome (CNS)[16,18]. Tanigawa et al. investigated early podocyte abnormalities in CNS due to an NPHS1 missense mutation[16,18]. They differentiated patient-derived iPSCs to kidney organoids using a modified version of the Taguchi 2017 protocol and detected a difference in NEPHRIN localization when comparing these to organoids derived from a gene corrected control cell line[16]. Similarly, Hale et al. used iPSCs derived from a CNS patient with compound heterozygous NPHS1 mutations to generate kidney organoids and observed reduced levels of NEPHRIN and PODOCIN protein compared to healthy controls[18]. Of note, the control cell line used in this study was not isogenic.

Unfortunately, slit diaphragm formation, which is impaired in patients with NPHS1 mutations, could not be studied in organoids in vitro, since the slit diaphragm does not develop under these conditions.

These studies demonstrate that in vitro kidney organoids are suitable to study certain genetic tubular and (early onset) podocyte diseases. However, there are some general limitation to consider. First, CRISPR/Cas9 was used by most authors to either induce or correct disease causing mutations. Although this is a very potent technology, it is important to realize that it can also have off target effects, which might influence results[52-54]. Second, in all studies using patient derived diseased cell lines, these were generated from a single patient and thus a single genetic background. Considering the previously discussed line to line variability of hPSCS, replicating the findings with a cell line from a different background would enhance the strength of the results. Third, beside the PKD organoids, the phenotypes demonstrated are mainly those of the early stages of disease. This is likely due to the immature character and the lack of a functional vasculature of the organoids.

Unfortunately, this limits their applicability. For instance, diseases affecting the GBM or slit diaphragms cannot be modelled since these do not develop in organoids in vitro. Diabetic nephropathy, in which injury of the glomerular ECs plays an important role, cannot be fully recapitulated in their absence, and the modeling of tubular channelopathies would require the maturation of the involved electrolyte channels and transporters, which has not yet been shown. Also, more advanced disease modeling and drug screening with functional read-outs would require glomerular filtration and urine production by the organoids, which is not possible without a functional vasculature.

We, therefore, believe that the vascularization of kidney organoids will be an important step to increase their potential and will focus on this aspect in the remainder of this review.

Vascularization is essential for kidney functionality and development

Mature mammalian kidneys receive approximately 20-25% of cardiac output. Renal blood flow is essential for virtually all kidney functions, including but not limited to glomerular filtration, blood pressure regulation and acid-base and electrolyte balance.

Each human kidney is supplied with blood through the renal artery that, at the site of the renal hilum, branches into segmental arteries which give rise to the interlobar arteries travelling towards the cortex. Around the border between the cortex and medulla, the interlobar arteries form the arcuate arteries, from which the interlobular arteries branch towards the periphery of the kidney[55]. There, they give rise to the afferent arterioles which are lined with continuous endothelium and, at the glomerular hilum, contain juxtaglomerular cells that produce and secrete renin in response to blood pressure changes. The afferent arteriole branches to form the glomerular capillary network. The highly fenestrated ECs in this network are part of the glomerular filtration barrier and contribute to its development and maintenance through paracrine cross-talk with podocytes and mesangial cells[26,27,56]. The glomerular capillaries drain into the efferent arteriole which, in the case of cortical glomeruli, supplies the cortical peritubular capillary network that enables reabsorption of fluid and electrolytes through ECs with diaphragmed fenestrae[57]. In juxtamedullary glomeruli, the efferent arterioles form the medullary microcirculation by giving rise to the descending vasa recta (DVR), which are lined with continuous endothelium and descend into the medulla in vascular bundles. In the inner medulla, they drain into the diaphragmed fenestrated ascending vasa recta (AVR)[55,58] which possess lymphatic like qualities that are essential for fluid drainage from the medullary interstitium[29]. Together, the DVR and AVR play an important role in urinary concentrating ability through the countercurrent exchange mechanism.

In kidney development, the importance of vascularization becomes apparent early on and has been demonstrated most extensively for the glomerulus. Glomerular vascularization begins once the renal vesicle has developed through the comma- into the S-shaped body stage, with the development of a vascular cleft between the podocyte precursors and proximal tubular segment. Endothelial progenitor cells expressing VEGFR-2 (Flk1) enter the vascular cleft dependent on VEGF-A produced by immature podocytes[59,60]. They join to form capillary loops which subsequently develop a lumen through TGF-β1 mediated apoptosis of superfluous ECs[61]. The capillary loops branch to form the capillary tuft and the ECs develop fenestrae. These are initially, like in the peritubular capillaries, bridged by diaphragms, but lose these as the cells mature into specialized glomerular ECs with undiaphragmed fenestrae[62,63].

Disturbance of the glomerular vascularization process can have severe consequences. In mice, heterozygosity for podocyte-specific VEGF-A leads to glomerular endotheliosis and severe proteinuria, whereas a complete absence of podocyte-derived VEGF-A results in glomeruli lacking ECs, disabling the development of a functional filtration barrier, and perinatal death[26]. Antibody mediated blockade of VEGF activity in newborn mice, in which nephrogenesis is still ongoing, leads to the development of many glomerular structures lacking capillaries[64]. Postnatally, deletion of VEGFR-2 leads to significant damage to glomerular ECs[65]. These severe phenotypes demonstrate the importance of podocyte-to-endothelial cell signaling for glomerular endothelial cell recruitment as well as survival. Conversely, ECs are essential for podocyte maturation. In the absence of ECs podocytes do develop but retain an immature phenotype, with effacement of foot processes and lack of slit diaphragms[26].

Signaling between mesangial cells, the third major cell type in the glomerulus, and ECs also plays a pivotal role in glomerular development. PDGFRβ-positive mesangial cells enter the glomerulus in response to PDGFβ produced by ECs[27]. Mesangial cells, in turn, contribute to the looping of glomerular capillaries, which fails to occur in the absence of mesangial cells[66,67]

Therefore, cross-talk between ECs, podocytes and mesangial cells is indispensable for the development, maturation and maintenance of functional glomeruli.

Unfortunately, none of the previously discussed protocols for kidney organoid generation produce organoids containing a functional vasculature. Some iPSC-derived organoids do contain ECs, but these are not organized into blood vessels and do not enter the glomerulus[7,8,30]. Addition of vascular endothelial growth factor (VEGF) during organoid differentiation increases the number of ECs, but fails to induce invasion of the glomerulus[22].

The process of embryonic kidney vascularization can provide important clues for the generation kidney organoids with a perfusable vascular network.

Kidney vascularization in embryonic development: vasculogenesis or angiogenesis?

The development of the human embryonic vasculature starts with the formation of a primitive vascular plexus by differentiation of mesoderm-derived angioblasts, a process called vasculogenesis. Subsequently, this network is expanded and remodeled through angiogenesis; the formation of blood vessels from the existing vasculature by sprouting and intussusception[68,69].

The process responsible for kidney vascularization and the origin of renal ECs are still debated. Possibilities are vasculogenesis by in situ differentiation of angioblasts that either arise from progenitors in the metanephros or migrate into it from the systemic circulation, angiogenesis from pre-existent systemically connected blood vessels or a combination of both.

Most studies exploring the mechanisms of embryonic kidney vascularization are based on murine models. Support for vasculogenesis came from studies demonstrating the presence of endogenous endothelial progenitor cells within mouse embryonic kidneys. In E10 mouse metanephric kidneys, Flk1+ angioblasts[70] and Tie1 expressing cells[71] unconnected to the systemic vasculature were found and a lineage tracing study in mice showed that a portion of the peritubular capillary endothelium is derived from Foxd1-positive renal stromal cells[72]. More elaborate support for vasculogenesis comes from transplantation studies in which embryonic kidneys were transplanted into murine hosts, followed by the analysis of the origin of the blood vessels inside the graft. Although the results of these experiments were variable, in most cases, at least a part of the glomerular vasculature was graft-derived, indicating a role for vasculogenesis[71,73,74] (Table 1). A limitation of these studies is the difficulty in establishing the origin of the donor-derived ECs. Although their presence supports the vasculogenesis theory, it does not provide solid proof, since either endothelial progenitor cells or mature ECs may have entered the metanephric kidney through angiogenesis prior to transplantation. Researchers tried to preclude this possibility by transplanting avascular grafts, but since blood vessels are present within the metanephric kidney from E11, this is nearly impossible.

Evidence for angiogenesis in embryonic kidney vascularization is convincing. In the transplantation studies discussed above, the larger vasculature was host-derived in almost all cases[73,75-77] (Table 1). Furthermore, a recent elaborate spatiotemporal analysis

of kidney vascularization in mice indicated such a large role for angiogenesis that the authors proposed an angiogenesis-only mechanism[78]. In this study, high resolution confocal imaging of normally developed whole metanephric mouse kidneys was performed from the start of metanephric kidney development at E10.5 until birth. At E10.5, CD31+ capillaries were detected neighbouring the UB and the avascular MM was surrounded by scattered CD31+ ECs. Next, the capillaries formed a vascular ring around the UB stalk and a dense network between the Wolffian duct and the MM. By E11.5, vessels from this dense capillary network had entered the MM and by E12.5, the entire MM was vascularized. Further analysis showed that from E11 onwards, all blood vessels in the metanephric kidney were connected to the embryonic circulation and contained erythroid cells[78].

Although this meticulously performed study provides strong support for angiogenesis, it does not rule out a contribution of vasculogenesis. The scattered CD31+ ECs surrounding the MM at E10.5 may have formed through vasculogenesis and the erythroid cells present in the metanephric vasculature through hemovasculogenesis.

The elaborate research discussed above has provided strong evidence for angiogenesis and largely ruled out a vasculogenesis-only mechanism, although a contribution of vasculogenesis cannot be rejected.

Therefore, we believe the embryonic development of the intricate vascular network of the kidney depends on either a combination of angio- and vasculogenesis or on angiogenesis only (Fig. 2).

Vascularization and maturation of kidney organoids in in vivo and in vitro models

Considering the role of angiogenesis in the vascularization of embryonic metanephroi, it seemed likely that vascularizing kidney organoids would require co-culture with blood vessels possessing angiogenic potential. This is challenging to establish in vitro, but in vivo models are available. As discussed previously, transplantation of human, murine or pig metanephroi to the omentum, anterior eye chamber or under the kidney capsule of murine hosts leads to vascularization of the graft[71,73-77,79,80]. Subsequently, the transplanted metanephroi grow and differentiate[75,77,79-83], developing mature looking nephrons that function to a certain degree[77,79,81-83].

Table 1: Studies reporting the origin of endothelial cells in blood vessels supplying the graft after transplantation of embryonic metanephroi, embryonic organoids or PSC-derived kidney organoids to a murine host

Author	Journal	Year	Graft	Host	Graft location	Duration Tx	Origin ECs in vascularized graft
Hyink	Am J Physiol	1996	Metanephroi mice E11-12	Mice	Anterior eye chamber	6 days	Small vessels predominantly donor Large vessels predominantly host
Robert	Am J Physiol	1996	Metanephroi mice E12	Mice - Neonatal - Adult	Neonatal mice - kidney capsule Adult mice - kidney capsule - anterior eye chamber	6-7 days	Neonatal host: combination of host and donor Adult host: - Kidney capsule: mostly donor - Anterior eye chamber: small vessels donor, large vessels host
Loughna	Angiogenesis	1997	Metanephroi mice E11/ E12	Mice - neonatal	Nephrogenic renal cortex	7-10 days	Predominantly donor
Rogers	Am J Physiol Regul Integr Comp Physio	2001	Metanephroi rats E15	Mice - immunosuppressed, uninephrectomized	Omentum	2 weeks	At least partly host (did not stain for donor EC)
Takeda	Transplant Immunology	2006	Metanephroi pigs week 4	Rats - immunosuppressed	Omentum	5, 7 or 8 weeks	Host
Dekel	Nature Medicine	2003	Metanephroi - human: week 7-8 - pig: week 4	Mice - immunodeficient	Kidney capsule	4 weeks	At least partly host (did not stain for donor ECs)
Xinaris	JASN	2012	Embryonic kidney organoids (mice E11.5)	Rats - athymic nude, uninephrectomized	Kidney capsule	3 weeks	Donor
Sharmin	JASN	2016	hiPSC-derived kidney organoids	Mice - immunodeficient	Kidney capsule	20 days	Host
Bantounas	Stem Cell Reports	2018	hESC-derived kidney organoids	Mice - SCID/beige	Subcutaneous	12 weeks	At least partly donor (did not stain for host ECs)
Van den Berg	Stem Cell Reports	2018	hESC and hiPSC-derived kidney organoids	Mice - NOD / SCID	Kidney capsule	7-28 days	Combination of host and donor
Tran	Developmental Cell	2019	hESC-derived kidney organoids	Mice - NOD / SCID	Kidney capsule	10 days	Host

In vivo vascularization of kidney organoids derived from embryonic mouse tissue

Researchers hypothesized that the transplantation of embryonic organoids generated through dissociation and reaggregation of E11.5 mouse kidneys would yield similar results. However, upon transplantation under the kidney capsule of rats for 3 weeks, vascularization was minimal and maturation of tubular but not of glomerular structures occurred[84]. This seemed to be due to insufficient VEGF production by the graft, as pre- and post- treatment with this growth factor markedly improved both vascularization and maturation. Inside the transplanted organoids, identified by a staining for mouse specific anti-CENP-A, the authors demonstrated the presence of peritubular and glomerular capillaries lined by donor-derived endothelium (MECA32+, RECA-1-) and containing red blood cells. Transmission electron microscopy (TEM) imaging of glomerular structures demonstrated that glomerular ECs were not fully mature and frequently lacked fenestrations. Podocytes were in varying stages of maturation and in some areas, a glomerular basement membrane (GBM) appeared between ECs and podocytes[84]. The presence of mesangial cells was not convincingly shown. Although it is difficult to distinguish between host and donor derived cells in TEM images, it is unlikely that these glomerular structures were derived from the adult rat host, considering their immature features.

The authors further showed that the transplanted organoids achieved a certain level of functionality by injecting FITC-conjugated BSA and FITC-labeled dextran into the host vasculature prior to fixation. Both were found to colocalize with megalin in proximal tubular structures, suggesting that glomerular filtration and tubular endocytosis had occurred[84].

Although these results are promising, the requirement of external VEGF-administration to obtain them implies that the intrinsic capability to produce VEGF is reduced in these embryonic organoids compared to metanephric kidneys. This might be due to the relatively small proportion of VEGF producing podocyte precursors in the in vitro organoids; although these were not quantified by the authors, the number of cells stained for the early podocyte marker WT-1 seems limited in the published image and nephrin positive cells were not detected.

In a different study, similar outcomes were observed upon transplantation of ‘organ buds’, consisting of dissociated E13.5 mouse embryonic kidney cells, human umbilical vein endothelial cells (HUVECs) and mesenchymal stem cells (MSCs) inside the cranium. The organ buds were quickly vascularized and the injection of Lucifer Yellow combined with intravital microscopy revealed glomerular perfusion and filtration[85].

In vivo vascularization of hPSC derived kidney organoids

In 2016, Sharmin et al. transplanted hiPSC-derived kidney organoids generated using the Taguchi 2014 protocol under the renal capsule of immunodeficient mice[31]. Two rods soaked in VEGF and aggregates of HUVECs and MSCs were transplanted along with the organoids. 20 days after transplantation, the glomeruli in the organoids were vascularized by host-derived mouse ECs and showed signs of maturation, with the formation of foot processes, slit diaphragm-like structures, a double layered glomerular basement membrane (GBM) and fenestrated ECs[31]. The effect of transplantation on the tubular structures was not described. Although VEGF or aggregates of HUVECs and MSCs were co-transplanted in most experiments, they were omitted in a few cases. This did not hamper vascularization, raising doubts concerning the necessity of adding these factors when transplanting hiPSC-derived kidney organoids[31].

Indeed, in 2018, it was shown that hPSC-derived kidney organoids are capable of producing VEGF themselves[30] and 2 papers were published simultaneously describing their successful vascularization and improved maturation upon transplantation in immunodeficient mice without external VEGF administration[30,32].

Van den Berg et al. differentiated hiPSCs and hESCs to kidney organoids using an adapted version of the Takasato 2015 protocol and transplanted these under the renal capsule of mice[30]. After 7 to 28 days, vascularization and functional perfusion of the organoids by a combination of host and graft derived blood vessels was demonstrated using live in vivo imaging through an abdominal imaging window (Fig. 2). In addition, transmission electron microscopy (TEM) analysis showed progressive maturation of glomerular and tubular structures over time. The level of maturity varied between structures, but overall improved markedly compared to the in vitro situation. In the glomeruli, which were surrounded by a Bowman's capsule, a trilaminar GBM, podocyte foot processes and fenestrated endothelium had appeared. Slit diaphragms between foot processes were starting to form, but were not mature yet. Tubular structures had developed widened lumina with areas displaying an apical brush border[30].

Bantounas et al. generated NPCs from hESCs in 2D culture using a method that was developed by Takasato et al. and entails treatment with CHIR for 3 days followed by FGF9 and heparin for 10 days[32,86]. On day 12 of differentiation, they dissociated the NPCs and injected them subcutaneously. 12 weeks later, blood vessels lined with human ECs and containing erythrocytes were observed inside and around kidney structures in the grafts and mesangial cells were shown to be present inside the glomerular structures. As a staining for mouse ECs was not performed, it is unclear whether these contributed to organoid

vascularization. Similar to the study by van den Berg et al., maturation of transplanted kidney structures was demonstrated using TEM. Upon injection of FITC-labeled dextran into the host, this was found back in some of the organoid tubules, strongly suggesting that glomerular filtration had occurred[32]. However, because glomerular filtration was not directly visualized, it cannot be ruled out that the injected dextran ended up in the tubular structures through a different route. For instance, it could have diffused from neighboring capillaries into the peritubular space and the tubules.

The vascularization and increased maturation of kidney organoids that occurs upon transplantation improves their resemblance to the in vivo human kidney. However, there are several important limitations to this model.

The vasculature in transplanted organoids is still far from perfect. As discussed previously, the adult human kidney relies on an intricate vascular network lined with ECs that differ in structure and function between kidney compartments for its blood supply and functionality. In the transplanted organoids, fenestrated glomerular ECs resembling those in the adult human kidney have been demonstrated, but the blood vessels outside the glomerular structures have not been extensively characterized. It is therefore unclear to what degree their 3D organization and ECs resemble those in vivo. Upon transplantation, the vasculature that is formed does not seem to derive from a main artery, nor does it drain into a main vein. Also, it remains to be elucidated whether the organoid glomerular structures are supplied by 1 afferent arteriole with their capillary network draining into 1 efferent arteriole, or by several capillaries that enter the glomeruli at different locations. The second option may result in insufficient glomerular perfusion and on the longer term loss of functionality of the kidney organoids. With regard to the medullary microcirculation, it is unlikely that this is present in the transplanted organoids, considering their corticomedullary organization is limited and Loops of Henle have not convincingly been demonstrated.

Besides vascularization, a main outcome of these transplantation studies was maturation of structures in transplanted organoids evaluated using TEM imaging. A limitation of TEM analysis is the inability to distinguish between graft and host cells. Theoretically, kidney structures from the mouse host could therefore be confused with organoid structures when these are transplanted under the kidney capsule. This risk can be reduced by selecting areas for TEM analysis based on histological sections analyzed with light microscopy, in which organoid and host kidney are easily distinguishable. Inside the transplanted organoids, our experience is that all glomerular structures are of human origin based on stainings for human nuclei. Also, the glomeruli in the mouse kidney are usually not located in the area directly adjacent to the transplanted organoid, further lowering the risk of misidentification.

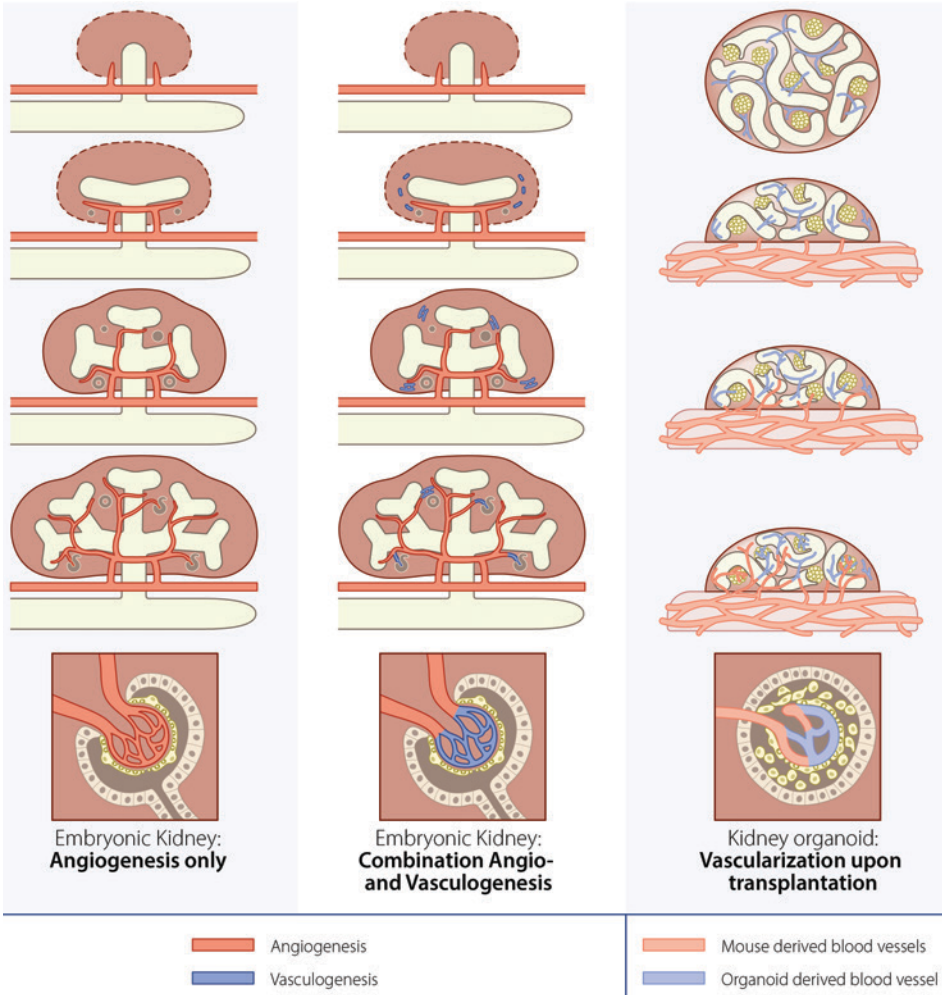

Figure 2: Schematic representation of possible mechanisms of kidney vascularization in embryonic development versus hPSC-derived kidney organoid vascularization upon transplantation. Left and middle: The ureteric bud (white) protrudes from the nephric duct into the metanephric mesenchyme (dark red) and branches over time to form the collecting duct system. Left: Angiogenesis only hypothesis. The metanephric kidney is vascularized exclusively through angiogenesis by blood vessels connected to the systemic vasculature (red). Middle: Combination angio- and vasculogenesis hypothesis. The metanephric kidney is vascularized through a combination of angiogenic vessels (red) and vessels formed through vasculogenesis (blue) from endothelial progenitor cells (blue) present in the metanephric mesenchyme. Right: vascularization of hPSC-derived kidney organoids upon transplantation under the kidney capsule of a murine host. Prior to transplantation the organoid (dark red circle) contains glomerular structures (clusters of yellow podocytes), tubular structures (white tubes) and endothelial cells (light blue). Upon transplantation, host derived blood vessels (light red) invade the organoid, and connect to some of the organoid-derived endothelial cells. The organoid is vascularized by a combination of host and donor derived endothelial cells.
Note: This schematic representation is not based on quantification studies.

Another restriction of TEM is its relative subjectiveness. As discussed previously, areas imaged by TEM are selected based on histological sections. This is very useful, but also enables selective analysis. Researchers, therefore, must be careful to image representative regions of the sample and are encouraged to provide a low magnification histological overview of the sample in addition to the detailed TEM images. An elegant way to reduce cherry picking in TEM imaging is the generation of tile scans, as was done in the study by van den Berg et al., which allows detailed visualization of larger areas.

Of note, in both studies not all glomerular and tubular structures in the transplanted organoids displayed the same level of maturation and it never reached that of the adult human kidney. In organoids, the glomerular vascular network remains less extensive, the podocyte foot processes and slit diaphragms are not fully mature, glomerular mesangial cells have not been completely characterized and the apical brush border in tubular structures is not always well developed.

Additional problems that were observed upon in vivo transplantation of kidney organoids are the formation of excessive stromal tissue surrounding the renal structures[30-32] and the lack of a single urinary exit tract.

Despite the limitations discussed above, vascularization and maturation of kidney organoids through transplantation can be useful to improve the modeling of diseases, especially those affecting the podocytes, glomerular ECs or GBM. In a recent study, it was shown using scRNAseq of week 17 human fetal kidneys and kidney organoids generated through the Morizane protocol, that podocytes in organoids follow a similar developmental process as those in human fetal kidneys. However, on day 28 of differentiation, in vitro organoid podocytes are a mix of early and late podocyte like cells, displaying incomplete downregulation of early podocyte genes[28]. Interestingly, they lack expression of several disease related genes, including COL4A3, which encodes the alpha 3 chain of collagen IV, a major component of the GBM, and is linked to Alport disease. Upon transplantation of day 13-14 organoids under the kidney capsule of NOD SCID mice for 10 days, the organoids were vascularized and did express COL4A3 (IF stainings, not scRNAseq), demonstrating the necessity of vascularization for the normal development of the GBM and consequently for the modeling of Alport disease[28].

The modeling of diseases caused by mutations in genes that are expressed in untransplanted organoids can also be enhanced by vascularization, as was demonstrated in the previously discussed study investigating CNS due to an NPHS1 mutation[16]. In vitro, the authors could detect a difference in NEPHRIN localization between patient and control organoids, but only upon transplantation under the renal capsule of mice and the resulting

formation of podocyte foot processes did the impaired development of slit diaphragms in the patient-derived organoids become clear[16]. To enable evaluation of the proteinuric phenotype caused by CNS, functional assessment of kidney organoids, organoid urine production and analysis of this urine will be necessary which, to our knowledge, has not been achieved yet.

Although vascularization of kidney organoids can improve disease modeling, it also complicates experiments. It will, therefore, depend on the research question and on the disease being studied if vascularized organoids are the most suitable model.

In vitro vascularization of hPSC derived kidney organoids

Recently, Homan et al. aimed to generate kidney organoids containing a perfusable vascular network in vitro by culturing them under flow[33]. They differentiated PSCs to kidney organoids using the protocol developed by Morizane et al.[6] and on day 11 of differentiation placed them on perfusable millifluidic chips, on which the medium flows over the top of the organoids. This induced the expansion of the organoid-derived endothelial cell network that, in some cases, entered the glomerular structures and aligned the tubuli. The authors claimed that some of the blood vessels were perfusable based on the apparent overlap of fluorescent beads which were added to the media with ECs stained with ulex europaeus lectin or CD31[33]. Due to the diffuse presence of the fluorescent beads in the image and video published by the authors and the small number of vessels for which the overlap was shown, this claim is not irrefutable. TEM imaging of the organoids cultured under flow demonstrated the appearance of a Bowman's capsule like structure and improved maturation of podocyte foot processes. A GBM was not demonstrated in the published TEM images of organoid glomeruli, indicating that the interaction between the ECs and podocytes was not optimal.

Neither the vascular network nor the maturation in this model were therefore as extensive as those observed after transplantation. There was, however, an expansion of the endothelial cell network which invaded some of the organoid glomerular structures. The addition of flow to the system seems to have been an important factor causing this, although the large changes that were made to the extracellular matrix and the addition of fetal bovine serum to the medium likely contributed as well.

In summary, in vivo transplantation of kidney organoids leads to a certain degree of vascularization and maturation, which can improve the modeling of glomerular kidney disease and glomerulotoxicity and is an important step towards using kidney organoids for regenerative medicine. However, the 3D organization of the vasculature as well as

the nephrons in transplanted kidney organoids are not as advanced as that in the adult human kidney. In vitro, functional perfusion of vascularized kidney organoids has yet to be achieved.

Conclusions and future perspectives

Since the discovery of iPSCs, great progress has been made in the field of kidney organoid generation. Robust protocols have been developed for the differentiation of PSCs to segmented nephrons and adapting culture conditions enables large-scale production. In their current form, organoids are useful to study early developmental processes, model certain early onset kidney diseases and screen for tubular nephrotoxicity. Transplantation of kidney organoids in murine hosts or in vitro culture under flow can be performed to accomplish a certain degree of vascularization and maturation, increasing the applicability of the organoids. Nonetheless, we still have a long way to go towards generating fully functional kidney tissue with a specialized vasculature and organized urine drainage system. Also, before kidney organoids can be introduced for regenerative medicine applications, pressing safety issues must be addressed. Organoids are subject to interexperimental variability, frequently contain off-target cell populations and upon transplantation avoiding immunological rejection is a great challenge.

For the future, we expect that achieving functional vascularization of kidney organoids in vitro combined with advancements increasing their safety will markedly enhance their potential.

References

1 Matsushita, K. et al. Association of estimated glomerular filtration rate and albuminuria with all-cause and cardiovascular mortality in general population cohorts: a collaborative meta-analysis. Lancet ***375***, 2073–2081 (2010). https://doi.org/10.1016/S0140-6736(10)60674-5

2 Go, A. S., Chertow, G. M., Fan, D., McCulloch, C. E. & Hsu, C. Y. Chronic kidney disease and the risks of death, cardiovascular events, and hospitalization. N Engl J Med ***351***, 1296–1305 (2004). https://doi.org/10.1056/NEJMoa041031

3 van der Velde, M. et al. Lower estimated glomerular filtration rate and higher albuminuria are associated with all-cause and cardiovascular mortality. A collaborative meta-analysis of high-risk population cohorts. Kidney Int ***79***, 1341–1352 (2011). https://doi.org/10.1038/ki.2010.536

4 Takahashi, K. et al. Induction of pluripotent stem cells from adult human fibroblasts by defined factors. Cell ***131***, 861–872 (2007). https://doi.org/10.1016/j.cell.2007.11.019

5 Taguchi, A. et al. Redefining the in vivo origin of metanephric nephron progenitors enables generation of complex kidney structures from pluripotent stem cells. Cell Stem Cell ***14***, 53–67 (2014). https://doi.org/10.1016/j.stem.2013.11.010

6 Morizane, R. et al. Nephron organoids derived from human pluripotent stem cells model kidney development and injury. Nat Biotechnol ***33***, 1193–1200 (2015). https://doi.org/10.1038/nbt.3392

7 Takasato, M. et al. Kidney organoids from human iPS cells contain multiple lineages and model human nephrogenesis. Nature ***526***, 564–568 (2015). https://doi.org/10.1038/nature15695

8 Freedman, B. S. et al. Modelling kidney disease with CRISPR-mutant kidney organoids derived from human pluripotent epiblast spheroids. Nat Commun ***6***, 8715 (2015). https://doi.org/10.1038/ncomms9715

9 Boyle, S. et al. Fate mapping using Cited1-CreERT2 mice demonstrates that the cap mesenchyme contains self-renewing progenitor cells and gives rise exclusively to nephronic epithelia. Dev Biol ***313***, 234–245 (2008). https://doi.org/10.1016/j.ydbio.2007.10.014

10 Herzlinger, D., Koseki, C., Mikawa, T. & al-Awqati, Q. Metanephric mesenchyme contains multipotent stem cells whose fate is restricted after induction. Development ***114***, 565–572 (1992).

11 Kobayashi, A. et al. Six2 defines and regulates a multipotent self-renewing nephron progenitor population throughout mammalian kidney development. Cell Stem Cell ***3***, 169–181 (2008). https://doi.org/10.1016/j.stem.2008.05.020

12 Grobstein, C. Inductive interaction in the development of the mouse metanephros. Journal of Experimental Zoology, 319–339 (1955).

13 Auerbach, R. & Grobstein, C. Inductive interaction of embryonic tissues after dissociation and reaggregation. Exp Cell Res ***15***, 384–397 (1958).

14 Taguchi, A. & Nishinakamura, R. Higher-Order Kidney Organogenesis from Pluripotent Stem Cells. Cell Stem Cell (2017). https://doi.org/10.1016/j.stem.2017.10.011

15 Kim, Y. K. et al. Gene-Edited Human Kidney Organoids Reveal Mechanisms of Disease in Podocyte Development. Stem Cells ***35***, 2366–2378 (2017). https://doi.org/10.1002/stem.2707

16 Tanigawa, S. et al. Organoids from Nephrotic Disease-Derived iPSCs Identify Impaired NEPHRIN Localization and Slit Diaphragm Formation in Kidney Podocytes. Stem Cell Reports (2018). https://doi.org/10.1016/j.stemcr.2018.08.003

17 Forbes, T. A. et al. Patient-iPSC-Derived Kidney Organoids Show Functional Validation of a Ciliopathic Renal Phenotype and Reveal Underlying Pathogenetic Mechanisms. Am J Hum Genet ***102***, 816–831 (2018). https://doi.org/10.1016/j.ajhg.2018.03.014

18 Hale, L. J. et al. 3D organoid-derived human glomeruli for personalised podocyte disease modelling and drug screening. Nat Commun ***9***, 5167 (2018). https://doi.org/10.1038/s41467-018-07594-z

19 Cruz, N. M. et al. Organoid cystogenesis reveals a critical role of microenvironment in human polycystic kidney disease. Nat Mater (2017). https://doi.org/10.1038/nmat4994

20 Wu, H. et al. Comparative Analysis and Refinement of Human PSC-Derived Kidney Organoid Differentiation with Single-Cell Transcriptomics. Cell Stem Cell (2018). https://doi.org/10.1016/j.stem.2018.10.010

21 Phipson, B. et al. Evaluation of variability in human kidney organoids. Nat Methods ***16***, 79–87 (2019). https://doi.org/10.1038/s41592-018-0253-2

22 Czerniecki, S. M. et al. High-Throughput Screening Enhances Kidney Organoid Differentiation from Human Pluripotent Stem Cells and Enables Automated Multidimensional Phenotyping. Cell Stem Cell ***22***, 929–940 e924 (2018). https://doi.org/10.1016/j.stem.2018.04.022

23 Combes, A. N., Zappia, L., Er, P. X., Oshlack, A. & Little, M. H. Single-cell analysis reveals congruence between kidney organoids and human fetal kidney. Genome Med ***11***, 3 (2019). https://doi.org/10.1186/s13073-019-0615-0

24 Gornalusse, G. G. et al. HLA-E-expressing pluripotent stem cells escape allogeneic responses and lysis by NK cells. Nat Biotechnol ***35***, 765–772 (2017). https://doi.org/10.1038/nbt.3860

25 Sasaki, H. et al. New Immunosuppressive Cell Therapy to Prolong Survival of Induced Pluripotent Stem Cell-Derived Allografts. Transplantation ***99***, 2301–2310 (2015). https://doi.org/10.1097/TP.0000000000000875

26 Eremina, V. et al. Glomerular-specific alterations of VEGF-A expression lead to distinct congenital and acquired renal diseases. J Clin Invest ***111***, 707–716 (2003). https://doi.org/10.1172/JCI17423

27 Lindahl, P. et al. Paracrine PDGF-B/PDGF-Rbeta signaling controls mesangial cell development in kidney glomeruli. Development ***125***, 3313–3322 (1998).

28 Tran, T. et al. In Vivo Developmental Trajectories of Human Podocyte Inform In Vitro Differentiation of Pluripotent Stem Cell-Derived Podocytes. Developmental Cell ***50***, 102–+ (2019). https://doi.org/10.1016/j.devcel.2019.06.001

29 Kenig-Kozlovsky, Y. et al. Ascending Vasa Recta Are Angiopoietin/Tie2-Dependent Lymphatic-Like Vessels. J Am Soc Nephrol ***29***, 1097–1107 (2018). https://doi.org/10.1681/ASN.2017090962

30 van den Berg, C. W. et al. Renal Subcapsular Transplantation of PSC-Derived Kidney Organoids Induces Neo-vasculogenesis and Significant Glomerular and Tubular Maturation In Vivo. Stem Cell Reports ***10***, 751–765 (2018). https://doi.org/10.1016/j.stemcr.2018.01.041

31 Sharmin, S. et al. Human Induced Pluripotent Stem Cell-Derived Podocytes Mature into Vascularized Glomeruli upon Experimental Transplantation. J Am Soc Nephrol ***27***, 1778–1791 (2016). https://doi.org/10.1681/ASN.2015010096

32 Bantounas, I. et al. Generation of Functioning Nephrons by Implanting Human Pluripotent Stem Cell-Derived Kidney Progenitors. Stem Cell Reports ***10***, 766–779 (2018). https://doi.org/10.1016/j.stemcr.2018.01.008

33 Homan, K. A. et al. Flow-enhanced vascularization and maturation of kidney organoids in vitro. Nat Methods ***16***, 255–262 (2019). https://doi.org/10.1038/s41592-019-0325-y

34 Mugford, J. W., Sipila, P., McMahon, J. A. & McMahon, A. P. Osr1 expression demarcates a multi-potent population of intermediate mesoderm that undergoes progressive restriction to an Osr1-dependent nephron progenitor compartment within the mammalian kidney. Dev Biol ***324***, 88–98 (2008). https://doi.org/10.1016/j.ydbio.2008.09.010

35 Saxen, L. & Sariola, H. Early organogenesis of the kidney. Pediatr Nephrol ***1***, 385–392 (1987).

36 Moore, M. W. et al. Renal and neuronal abnormalities in mice lacking GDNF. Nature ***382***, 76–79 (1996). https://doi.org/10.1038/382076a0

37 Pichel, J. G. et al. Defects in enteric innervation and kidney development in mice lacking GDNF. Nature ***382***, 73–76 (1996). https://doi.org/10.1038/382073a0

38 Sanchez, M. P. et al. Renal agenesis and the absence of enteric neurons in mice lacking GDNF. Nature ***382***, 70–73 (1996). https://doi.org/10.1038/382070a0

39 Carroll, T. J., Park, J. S., Hayashi, S., Majumdar, A. & McMahon, A. P. Wnt9b plays a central role in the regulation of mesenchymal to epithelial transitions underlying organogenesis of the mammalian urogenital system. Dev Cell ***9***, 283–292 (2005). https://doi.org/10.1016/j.devcel.2005.05.016

40 Karner, C. M. et al. Canonical Wnt9b signaling balances progenitor cell expansion and differentiation during kidney development. Development ***138***, 1247–1257 (2011). https://doi.org/10.1242/dev.057646

41 Tanigawa, S. et al. Wnt4 induces nephronic tubules in metanephric mesenchyme by a non-canonical mechanism. Dev Biol ***352***, 58–69 (2011). https://doi.org/10.1016/j.ydbio.2011.01.012

42 Burn, S. F. et al. Calcium/NFAT signalling promotes early nephrogenesis. Dev Biol ***352***, 288–298 (2011). https://doi.org/10.1016/j.ydbio.2011.01.033

43 Lindstrom, N. O. Progressive Recruitment of Mesenchymal Progenitors Reveals a Time-Dependent Process of Cell Fate Acquisition in Mouse and Human Nephrogenesis. Developmental Cell (2018).

44 Combes, A. N. et al. Single cell analysis of the developing mouse kidney provides deeper insight into marker gene expression and ligand-receptor crosstalk. Development (2019). https://doi.org/10.1242/dev.178673

45 Kaku, Y. et al. PAX2 is dispensable for in vitro nephron formation from human induced pluripotent stem cells. Sci Rep ***7***, 4554 (2017). https://doi.org/10.1038/s41598-017-04813-3

46 Combes, A. N. et al. High throughput single cell RNA-seq of developing mouse kidney and human kidney organoids reveals a roadmap for recreating the kidney. bioRxiv Preprint (2017).

47 Unbekandt, M. & Davies, J. A. Dissociation of embryonic kidneys followed by reaggregation allows the formation of renal tissues. Kidney Int ***77***, 407–416 (2010). https://doi.org/10.1038/ki.2009.482

48 Ganeva, V., Unbekandt, M. & Davies, J. A. An improved kidney dissociation and reaggregation culture system results in nephrons arranged organotypically around a single collecting duct system. Organogenesis ***7***, 83–87 (2011). https://doi.org/10.4161/org.7.2.14881

49 Przepiorski, A. et al. A Simple Bioreactor-Based Method to Generate Kidney Organoids from Pluripotent Stem Cells. Stem Cell Reports (2018). https://doi.org/10.1016/j.stemcr.2018.06.018

50 Boulting, G. L. et al. A functionally characterized test set of human induced pluripotent stem cells. Nat Biotechnol ***29***, 279–286 (2011). https://doi.org/10.1038/nbt.1783

51 Bock, C. et al. Reference Maps of human ES and iPS cell variation enable high-throughput characterization of pluripotent cell lines. Cell ***144***, 439–452 (2011). https://doi.org/10.1016/j.cell.2010.12.032

52 Fu, Y. et al. High-frequency off-target mutagenesis induced by CRISPR-Cas nucleases in human cells. Nat Biotechnol ***31***, 822–826 (2013). https://doi.org/10.1038/nbt.2623

53 Hsu, P. D. et al. DNA targeting specificity of RNA-guided Cas9 nucleases. Nat Biotechnol ***31***, 827–832 (2013). https://doi.org/10.1038/nbt.2647

54 Lin, Y. et al. CRISPR/Cas9 systems have off-target activity with insertions or deletions between target DNA and guide RNA sequences. Nucleic Acids Res ***42***, 7473–7485 (2014). https://doi.org/10.1093/nar/gku402

55 Moffat, D. B. & Fourman, J. A vascular pattern of the rat kidney. 1963. J Am Soc Nephrol ***12***, 624–632 (2001).

56 Eremina, V. et al. Vascular endothelial growth factor a signaling in the podocyte-endothelial compartment is required for mesangial cell migration and survival. J Am Soc Nephrol ***17***, 724–735 (2006). https://doi.org/10.1681/ASN.2005080810

57 Bearer, E. L. & Orci, L. Endothelial fenestral diaphragms: a quick-freeze, deep-etch study. J Cell Biol ***100***, 418–428 (1985). https://doi.org/10.1083/jcb.100.2.418

58 Beeuwkes, R., 3rd. Efferent vascular patterns and early vascular-tubular relations in the dog kidney. Am J Physiol ***221***, 1361–1374 (1971). https://doi.org/10.1152/ajplegacy.1971.221.5.1361

59 Breier, G., Albrecht, U., Sterrer, S. & Risau, W. Expression of vascular endothelial growth factor during embryonic angiogenesis and endothelial cell differentiation. Development ***114***, 521–532 (1992).

60 Bartlett, C. S., Jeansson, M. & Quaggin, S. E. Vascular Growth Factors and Glomerular Disease. Annu Rev Physiol ***78***, 437–461 (2016). https://doi.org/10.1146/annurev-physiol-021115-105412

61 Fierlbeck, W., Liu, A., Coyle, R. & Ballermann, B. J. Endothelial cell apoptosis during glomerular capillary lumen formation in vivo. J Am Soc Nephrol ***14***, 1349–1354 (2003).

62 Ichimura, K., Stan, R. V., Kurihara, H. & Sakai, T. Glomerular endothelial cells form diaphragms during development and pathologic conditions. J Am Soc Nephrol ***19***, 1463–1471 (2008). https://doi.org/10.1681/ASN.2007101138

63 Reeves, W. H., Kanwar, Y. S. & Farquhar, M. G. Assembly of the glomerular filtration surface. Differentiation of anionic sites in glomerular capillaries of newborn rat kidney. J Cell Biol ***85***, 735–753 (1980). https://doi.org/10.1083/jcb.85.3.735

64 Kitamoto, Y., Tokunaga, H. & Tomita, K. Vascular endothelial growth factor is an essential molecule for mouse kidney development: glomerulogenesis and nephrogenesis. J Clin Invest ***99***, 2351–2357 (1997). https://doi.org/10.1172/JCI119416

65 Sison, K. et al. Glomerular structure and function require paracrine, not autocrine, VEGF-VEGFR-2 signaling. J Am Soc Nephrol ***21***, 1691–1701 (2010). https://doi.org/10.1681/ASN.2010030295

66 Leveen, P. et al. Mice deficient for PDGF B show renal, cardiovascular, and hematological abnormalities. Genes Dev ***8***, 1875–1887 (1994).

67 Soriano, P. Abnormal kidney development and hematological disorders in PDGF beta-receptor mutant mice. Genes Dev ***8***, 1888–1896 (1994).

68 Risau, W. Mechanisms of angiogenesis. Nature ***386***, 671–674 (1997). https://doi.org/10.1038/386671a0

69 Carmeliet, P. Mechanisms of angiogenesis and arteriogenesis. Nat Med ***6***, 389–395 (2000). https://doi.org/10.1038/74651

70 Robert, B., St John, P. L. & Abrahamson, D. R. Direct visualization of renal vascular morphogenesis in Flk1 heterozygous mutant mice. Am J Physiol ***275***, F164–172 (1998).

71 Loughna, S. et al. A molecular and genetic analysis of renalglomerular capillary development. Angiogenesis ***1***, 84–101 (1997). https://doi.org/10.1023/A:1018357116559

72 Sims-Lucas, S. et al. Endothelial Progenitors Exist within the Kidney and Lung Mesenchyme. PLoS One ***8***, e65993 (2013). https://doi.org/10.1371/journal.pone.0065993

73 Hyink, D. P. et al. Endogenous origin of glomerular endothelial and mesangial cells in grafts of embryonic kidneys. Am J Physiol ***270***, F886–899 (1996). https://doi.org/10.1152/ajprenal.1996.270.5.F886

74 Robert, B., St John, P. L., Hyink, D. P. & Abrahamson, D. R. Evidence that embryonic kidney cells expressing flk-1 are intrinsic, vasculogenic angioblasts. Am J Physiol ***271***, F744–753 (1996). https://doi.org/10.1152/ajprenal.1996.271.3.F744

75 Rogers, S. A. & Hammerman, M. R. Transplantation of rat metanephroi into mice. Am J Physiol Regul Integr Comp Physiol ***280***, R1865–1869 (2001). https://doi.org/10.1152/ajpregu.2001.280.6.R1865

76 Takeda, S., Rogers, S. A. & Hammerman, M. R. Differential origin for endothelial and mesangial cells after transplantation of pig fetal renal primordia into rats. Transpl Immunol ***15***, 211–215 (2006). https://doi.org/10.1016/j.trim.2005.10.003

77 Dekel, B. et al. Human and porcine early kidney precursors as a new source for transplantation. Nat Med ***9***, 53–60 (2003). https://doi.org/10.1038/nm812

78 Munro, D. A. D., Hohenstein, P. & Davies, J. A. Cycles of vascular plexus formation within the nephrogenic zone of the developing mouse kidney. Sci Rep ***7***, 3273 (2017). https://doi.org/10.1038/s41598-017-03808-4

79 Rogers, S. A., Lowell, J. A., Hammerman, N. A. & Hammerman, M. R. Transplantation of developing metanephroi into adult rats. Kidney Int ***54***, 27–37 (1998). https://doi.org/10.1046/j.1523-1755.1998.00971.x

80 Rogers, S. A., Talcott, M. & Hammerman, M. R. Transplantation of pig metanephroi. ASAIO J ***49***, 48–52 (2003).

81 Dekel, B. et al. Engraftment and differentiation of human metanephroi into functional mature nephrons after transplantation into mice is accompanied by a profile of gene expression similar to normal human kidney development. J Am Soc Nephrol ***13***, 977–990 (2002).

82 Dilworth, M. R. et al. Development and functional capacity of transplanted rat metanephroi. Nephrol Dial Transplant ***23***, 871–879 (2008). https://doi.org/10.1093/ndt/gfm671

83 Rogers, S. A., Liapis, H. & Hammerman, M. R. Transplantation of metanephroi across the major histocompatibility complex in rats. Am J Physiol Regul Integr Comp Physiol ***280***, R132–136 (2001). https://doi.org/10.1152/ajpregu.2001.280.1.R132

84 Xinaris, C. et al. In vivo maturation of functional renal organoids formed from embryonic cell suspensions. J Am Soc Nephrol ***23***, 1857–1868 (2012). https://doi.org/10.1681/ASN.2012050505

85 Takebe, T. et al. Vascularized and Complex Organ Buds from Diverse Tissues via Mesenchymal Cell-Driven Condensation. Cell Stem Cell ***16***, 556–565 (2015). https://doi.org/10.1016/j.stem.2015.03.004

86 Takasato, M. et al. Directing human embryonic stem cell differentiation towards a renal lineage generates a self-organizing kidney. Nat Cell Biol ***16***, 118–126 (2014). https://doi.org/10.1038/ncb2894

CHAPTER 3

Co-culture of kidney organoids with a perfusable endothelial cell network in a scalable organ-on-chip system

M. Koning, S. Previdi, D. Kurek, P. Vulto, C.W. van den Berg, A.J. Rabelink

Abstract

Kidney organoids cultured in vitro contain some endothelial cells (ECs), but lack a functional vasculature. This is an important limitation for disease modeling and regenerative medicine. Transplantation under the kidney capsule in mice has been shown to induce vascularization by mainly host-derived ECs, which are attracted by VEGF-A produced by the organoid podocytes. This is consistent with the process of vascularization in embryology, which is thought to be at least partly based on sprouting angiogenesis from previously formed blood vessels. We therefore hypothesized that in vitro vascularization of kidney organoids might require an external source of ECs. Here, we used the commercially available OrganoPlate Graft to co-culture kidney organoids with an EC network. This plate contains culture chips that each consist of 1 graft chamber flanked by 2 perfusable lanes and can be placed on a rocker to mimic shear stress. Human umbilical vein endothelial cells (HUVECs) or human induced pluripotent stem cell (hiPSC)-derived ECs seeded into the perfusion lanes formed a continuous endothelium from which vessels sprouted towards the kidney organoid after placing it in the graft chamber. This vascular network was perfusable, as shown by injection of fluorescently labeled dextran. As expected, podocyte-derived VEGF-A was a major inducer of angiogenic sprouting, and blocking of VEGF-A activity by VEGF neutralizing antibody strongly inhibited vessel growth. Unfortunately, although the vessels moved towards the organoid, a connection between the vascular network and the kidney organoid did not form. Adaptation of the extracellular matrix, the differentiation stage of the organoids, the location of the ECs and addition of pericytes to the culture system did not improve the results. In conclusion, co-culture of kidney organoids and ECs in the Organoplate Graft results in the formation of a perfusable vascular network that sprouts towards the kidney organoid, but fails to invade it. This implies that an essential unknown cue for vascularization is still missing in the organoid and culture environment.

Introduction

Kidney organoids derived from human induced pluripotent stem cells (hiPSCs) offer great possibilities for disease modeling and regenerative medicine. They contain glomerular, tubular, stromal and endothelial cells (ECs) and have been shown at a transcriptional level to resemble third trimester fetal kidneys[1]. However, to harness their full potential, limitations with regard to maturity and functionality will have to be overcome. Vascularization is essential for kidney maturation and functionality. It provides the developing kidney with oxygen and nutrients and enables the interaction between ECs and podocyte precursors that leads to the formation of the glomerular basement membrane and the maturation of podocytes and ECs[2-4]. Unfortunately, the ECs present in kidney organoids fail to form the blood vessels and glomerular capillary tufts that are required for this interaction. Transplantation of kidney organoids in mice has been shown to induce functional vascularization and even enables glomerular filtration[5-8]. Interestingly, the blood vessels in these transplanted organoids are mainly host-derived, formed through sprouting angiogenesis in response to vascular endothelial growth factor (VEGF-A) produced by the organoid. This matches the process of kidney vascularization in embryology, which is believed to be at least partly based on angiogenesis from existing vasculature induced by podocyte-derived VEGF-A[9-11]. Although transplantation in mice is an effective method for functional vascularization, variability is difficult to control and it lacks scalability. We therefore aimed to develop a model for in vitro vascularization of kidney organoids. Based on the in vivo findings, we hypothesized that this might require a pre-formed vascular network that could function as a source for sprouting angiogenesis.

The development of microfluidic chips has enabled high-throughput 3D culture of ECs as perfusable microvessels that display more resemblance to in vivo vasculature than 2D monolayer cultures[12]. In this study, we used the Organoplate Graft, a microfluidic chip system specifically designed for co-culture of a graft with perfused microvessels. We demonstrate that kidney organoids, through production of VEGF-A, induce the formation of angiogenic sprouts from the microvessels towards the organoids. Unfortunately, we did not observe the formation of a vascular network within the kidney organoids.

Results

Kidney organoids induce angiogenesis upon co-culture with endothelial cells

The Organoplate Graft contains 64 chips that each consist of a graft chamber supported by an extracellular matrix (ECM) channel, flanked by 2 perfusion lanes (Fig. 1a). The ECM

channel, perfusion lanes, and graft chamber can be accessed separately to add ECM, seed ECs, and insert a graft. By placing the Organoplate on a rocker, bidirectional flow can be generated in the perfusion channels. We aimed to use this system to enhance kidney organoid vascularization by co-culturing kidney organoids with ECs. Kidney organoids were generated from hiPSCs using a previously published protocol[1,6]. This entails differentiation of hiPSCs in monolayer culture in APEL2 medium for 7 days, followed by the formation of aggregates that are further maintained at an air-liquid interface on transwell filters (Fig. 1b). The characteristics of the Organoplate Graft required adaptation of several aspects of the protocol: The size of the graft chamber necessitates sectioning of the organoids, the chip only allows for submerged culture, and the culture medium has to support co-culture. To analyze the effects of these modifications on kidney organoid morphology, we evaluated the impact of each adaptation separately in a regular 24 well plate with transwell inserts (supplementary Fig. 1). Sectioning organoids did not have a major impact on organoid morphology. Organoids in submerged culture in the organoid medium APEL2 maintained their structure, although they appeared slightly more dense. The EC medium MV2, however, had a detrimental effect on the organoids in submerged as well as air-liquid interface culture, with organoids losing recognizable structures (supplementary Fig. 1). In the Organoplate Graft, we therefore decided to use APEL2 medium in the graft chamber and MV2 medium in the perfusion lanes, to provide optimal support to both organoids and ECs.

For co-culture experiments, the ECM channel was loaded with Collagen I followed by incubation for 15 min (Fig. 1b, bottom, day -2). Subsequently, red fluorescent protein expressing human umbilical vein endothelial cells (RFP-HUVECs) were seeded in the perfusion lanes, positioning them against the collagen I, and allowed to attach before placing the Organoplate on the rocker (Fig. 1b, bottom, day -2). Once the ECs had formed a confluent lining of the perfusion channels, usually 2-3 days after seeding, a kidney organoid fragment was added to the graft chamber (Fig. 1b, bottom, day 0). Kidney organoids were prepared for co-culture by generating and maintaining them under standard conditions until day 7+12 or day 7+18 of differentiation (Fig. 1b, top), when they were sectioned using a surgical knife and added to the Organoplate. These timepoints were based on the previously demonstrated increasing production of VEGF by kidney organoids between d7+10 and d7+17 of differentiation[6]. In contrast to standard culturing conditions, in which the organoids are maintained directly on a polyester transwell membrane, the Organoplate contains Collagen I in the ECM channel, a suitable matrix to support ECs in microfluidic culture systems[12]. To evaluate the optimal ECM for kidney organoids, we compared the effect of using no additional ECM to placing a layer of Matrigel (Growth factor reduced, phenol red free) or Collagen I in the graft chamber before adding the organoid.

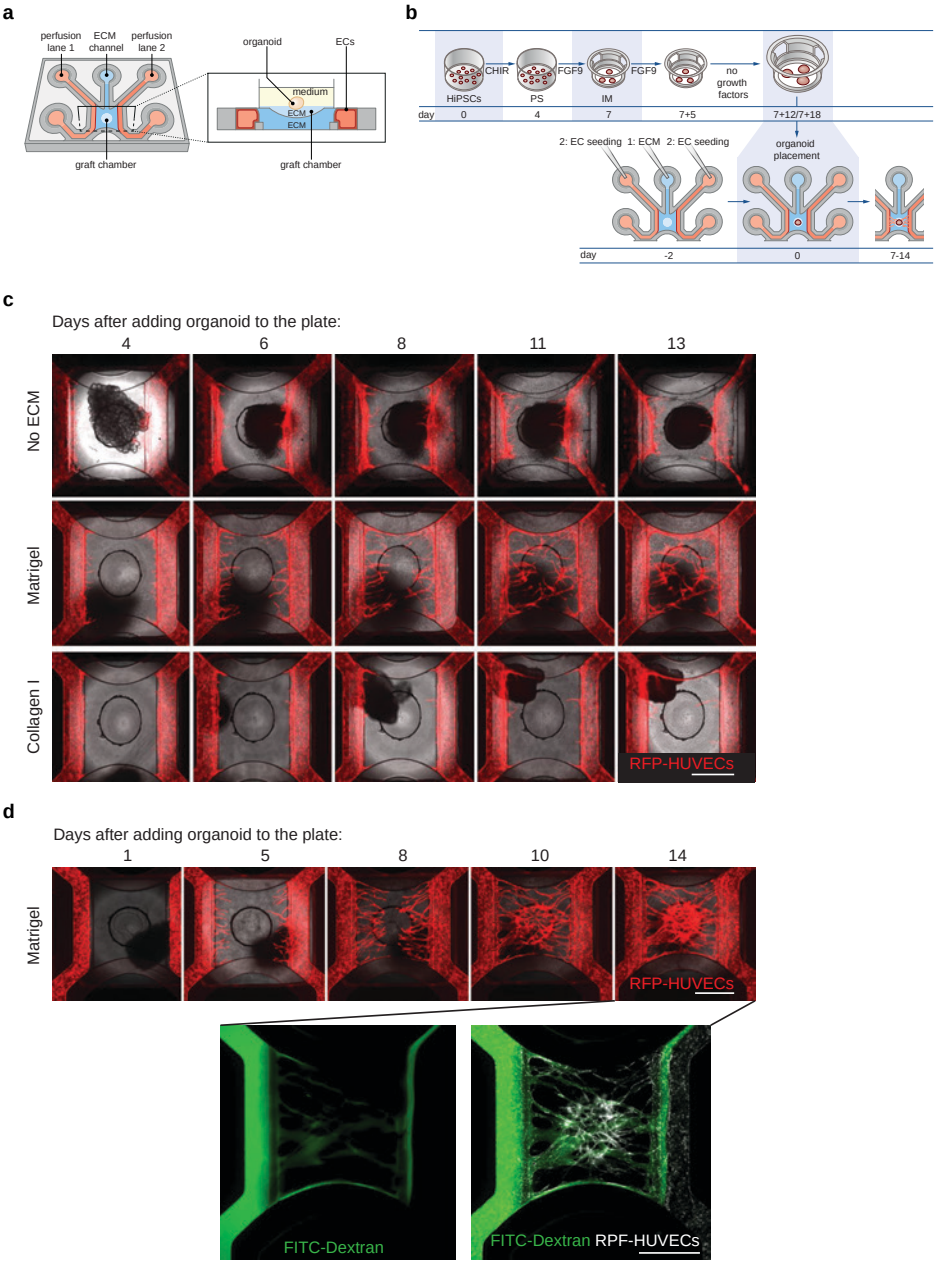

Figure 1: Kidney organoids induce angiogenesis upon co-culture with endothelial cells. a Schematic of culture chips in the Organoplate Graft. Each chip consists of a graft chamber supported by an extracellular matrix (ECM) channel and flanked by 2 perfusion lanes. ECM channel, both perfusion lanes and the graft chamber can be accessed separately for gel loading, cell seeding, graft placement and medium change. **b** Timeline of differentiation of hiPSCs to kidney organoids (top), and preparation of the Organoplate followed by co-culture of organoids and ECs on the Organoplate Graft (bottom). Differentiating iPSCs are cultured as a monolayer for 7 days, followed by aggregation

to organoids that are maintained at an air liquid interface. On day 7+12 or day 7+18 of differentiation, organoids are sectioned and an organoid fragment is added to the graft chamber of the Organoplate Graft, that has been prepared 2-3 days earlier by loading the ECM channel with Collagen I and seeding ECs in the perfusion lanes. Kidney organoids and ECs are co-cultured for 7-14 days. HiPSC human induced pluripotent stem cells PS primitive streak IM intermediate mesoderm**. c** Co-culture of kidney organoids with ECs in the Organoplate. Top: Without additional ECM in the graft chamber. Middle: With Matrigel coating of the graft chamber. Bottom: With Collagen I coating of the graft chamber. Matrigel coating of the graft chamber yields optimal results, with abundant sprouting of ECs from the perfusion lanes into the graft chamber. RFP-HUVECs are shown in red. **d** Upon injection of FITC-labelled dextran into the left perfusion lane, dextran flows through the EC network to the opposite perfusion lane, demonstrating that the angiogenic sprouts connect to each other and are perfusable. RFP-HUVECs are shown in white, FITC-labelled dextran in green.

In co-culture experiments without ECM in the graft chamber, the ECs displayed sprouting angiogenesis from day 6 to 8 after adding the organoid, before the sprouts deteriorated (Fig. 1c, top panel). The addition of Collagen I to the graft chamber yielded similar results (Fig. 1c, bottom panel). Adding Matrigel to the graft chamber resulted in extensive sprouting of ECs from the perfusion channels (Fig. 1c, middle panel). These newly formed vessels appeared to connect to each other in the middle of the chip (Fig. 1d, top panel). Further experiments were therefore performed with Matrigel in the graft chamber. To evaluate connectivity and perfusability of the vessels, FITC-labeled Dextran (150 kDa, Sigma-Aldrich 46946) was added to one side of the perfusion channel. The Dextran remained inside the lumen of the blood vessels and travelled through them to reach the perfusion channel on the opposite side (Fig. 1d, bottom panel). Not all of the vascular network was perfusable, as RFP-positive, FITC-negative HUVECs were also visible. These might be the youngest sprouts that have yet to become functional.

VEGF-A is an important driver of organoid-induced angiogenesis

We hypothesized that the angiogenic sprouting that occurred upon co-culture of kidney organoids with ECs was induced by factors secreted by the organoids. To test this, conditioned APEL2 medium was collected from kidney organoids cultured under standard conditions in transwells, and added to the graft chamber of a chip with RFP-HUVECs seeded in the perfusion lane. As a negative control, unconditioned APEL2 medium was used. Indeed, in the chips with conditioned medium, sprouts appeared after 4 days and expanded over time, whereas in the control chips, no sprouting was observed (Fig. 2a). A Luminex Assay was then performed to assess the levels of several known modulators of angiogenesis in conditioned medium from the Organoplate Graft: Vascular Endothelial Growth Factor A (VEGF-A), Angiopoietin-1 (Ang1), Angiopoietin-2 (Ang2), and platelet derived growth factor BB (PDGF-BB) (Fig. 2b). Medium was collected from the perfusion lanes and graft chambers of chips with organoid monoculture or organoid-EC co-culture on day 5 and 12 after adding the organoid.

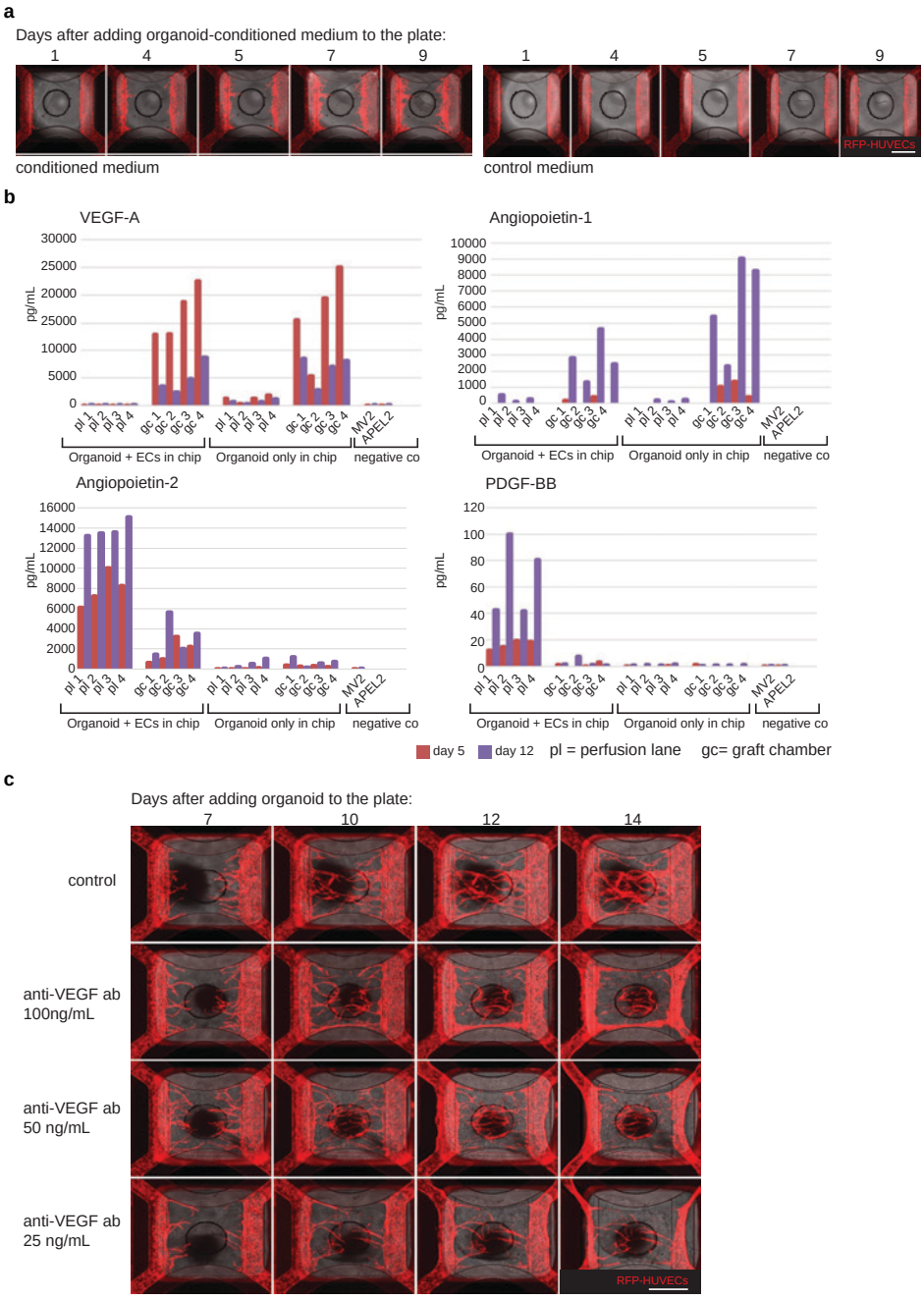

Figure 2: VEGF-A secretion is an important driver of organoid-induced angiogenesis. a Organoid-conditioned medium induces sprouting of ECs in the Organoplate (left), while control APEL2 medium does not (right), indicating that organoids secrete an angiogenic factor. **b** Levels of Angiopoietin-1, Angiopoietin-2, VEGF-A, and PDGF-BB measured by Luminex screening in conditioned medium from the perfusion lanes and the graft chamber of Organoplate chips after 5 and 12 days and in unconditioned MV2 and APEL2 medium. Kidney organoids produce VEGF-A at day 5 and at a lower

level at day 12 and ANGPT1 at day 12. ECs produce ANGPT2 and PDGF-BB with the highest levels detected at day 12. pl perfusion lane gc graft chamber. **c** VEGF-blockade with anti-VEGF antibody starting on day 7 after adding the organoid to the Organoplate leads to demise of the vascular network.

On day 5, the graft chambers contained high levels of VEGF-A in organoid monoculture as well as organoid-EC co-culture. In the perfusion lanes of chips containing ECs, Ang-2 was detected at this timepoint. On day 12, VEGF-A levels in the graft chambers were still detectable although clearly lower than at day 5, and a striking increase in Ang-1 concentration occurred in the graft chambers. In the perfusion lanes, Ang-2 expression was even higher than at day 5. In addition, PDGF-BB was detected (Fig. 2b). VEGF-A and Ang-1 were clearly produced by the organoids, as these factors were detected in the graft chamber irrespective of the presence of ECs. This fits with their role in embryonic kidney development, in which both factors are known to be secreted by podocyte precursors. VEGF-A is essential for the attraction of ECs into the vascular cleft of the S-shaped body stage nephron[2,13]. Ang-1 is produced by podocytes and mural cells and promotes EC survival and quiescence[14]. Ang-2 and PDGF-BB appear to be secreted by ECs, since they are mainly detected in medium from the perfusion lanes of chips with organoid-EC co-culture. The effect of EC-derived Ang-2 on ECs is context-dependent, stimulating angiogenesis and vascular remodeling in the presence of VEGF-A while inducing vessel regression in its absence[15,16]. In this co-culture model with high VEGF-A levels, it is expected to support the formation of the vascular network. PDGF-B is released by angiogenic ECs to attract pericytes for vessel stabilization[17,18]. To confirm the role of VEGF-A in the formation of a vascular network in the Organoplate Graft, we blocked its activity through the addition of an anti-VEGF antibody in 3 different concentrations (25, 50 and 100ng/mL) 7 days after placing the organoid in the graft chamber (Fig. 2c). This led to the regression of formed sprouts and affected the confluency of the ECs in the perfusion lanes over the following week (Fig. 2c).

Endothelial cells do not invade kidney organoids

Although the VEGF-A and ANGPT-1 produced by the organoids induced EC sprouting, 3D reconstruction of whole mount stained and imaged organoids revealed that the ECs did not invade the organoids (Fig. 3a). A connection between the newly formed microvessels and the endogenous organoid ECs did not occur. The explanation for the limited success of this co-culture method could lie in any one or multiple components of the system: ECs, organoids, proximity between organoids and ECs, the lack of mural cells supporting the microvessels, the characteristics of the flow in the chip, or suboptimal interplay between any of these elements. In an attempt to enhance our experimental set-up, we made stepwise adaptations to several of these components, namely the ECs, the proximity and the mural cells. ECs in vivo are heterogeneous and display organ specificity. Even within the kidney, ECs are phenotypically

diverse to support organ functionality[19-21]. HUVECs, although frequently used as an easily accessible EC source, display their own tissue-specific phenotype[22-24].

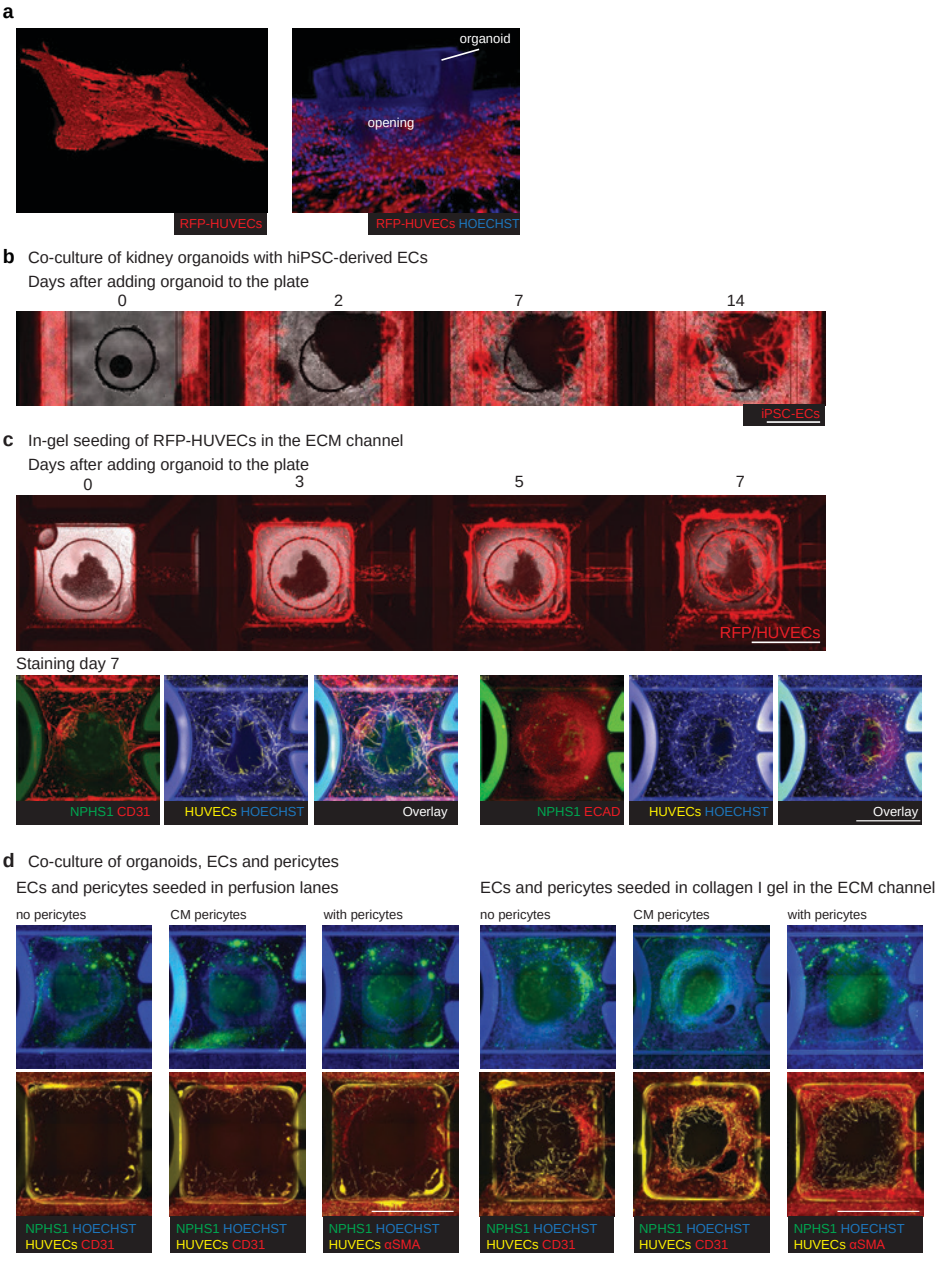

Figure 3: strategies to improve co-culture. a 3D reconstruction of kidney organoid and EC co-culture demonstrates that, although ECs move towards the organoid, they fail to invade them. **b** Co-culturing kidney organoids with hiPSC-ECs instead of HUVECs leads to similar results, with the induction of sprouting angiogenesis without invasion of kidney organoids by the hiPSC-ECs.

c Seeding HUVECs in hydrogel in the ECM channel to minimize the distance between ECs and organoid does not enhance vascularization after 7 days of co-culture. Left: Organoids were stained for NPHS1 (green), CD31 (red), HOECHST (blue). Right: Organoids were stained for ECAD (green), CD31 (red), HOECHST (blue). RFP-HUVECs are depicted in yellow. Overlay of RFP-HUVECs and CD31 is shown in white. **d** Co-culture of organoids and ECs in pericyte conditioned medium (CM pericytes) or with pericytes does not induce invasion of ECs into the organoid. Left: ECs and pericytes seeded in the perfusion lanes. Right: ECs and pericytes seeded in collagen I in the graft chamber. Organoids were stained for NPHS1 (green), CD31 (red), HOECHST (blue). RFP-HUVECs are depicted in yellow.

They might therefore lack the characteristics required for optimal interaction with renal cells as well as the plasticity to acquire these. As an alternative EC source we used hiPSC-derived ECs, generated through an established protocol[25]. Similar to the experiments with HUVECS, co-culture of organoids with hiPSC-ECs led to sprouting of ECs towards the organoid, but did not result in vascularization (Fig. 3b). Next, we enhanced the proximity between organoid and ECs by seeding HUVECs in hydrogel in the ECM channel directly below the organoid instead of in the perfusion lanes. Although the ECs formed microvessels, invasion of the organoids did not occur (Fig. 3c). Finally, we addressed the lack of mural cells in our system. In vivo, pericytes play an important role promoting vessel stabilization and integrity[26]. For practical reasons, we used commercially available brain pericytes. However, addition of pericytes or pericyte-conditioned medium to the co-culture system, either in the perfusion lanes or the ECM channel, did not induce the development of a more extensive vascular network or the establishment of a connection to the organoid (Fig. 3d). Also, the αSMA positive pericytes did not appear to support the newly forming blood vessels, but remained instead within the perfusion lanes or ECM channel depending on where they were seeded.

Discussion

In this study, we developed a method to co-culture kidney organoids and ECs in a microfluidic chip. The design of the Organoplate Graft enabled the maintenance of 64 organoids per plate, each flanked by 2 perfusion lanes. ECs seeded in the perfusion lanes formed a continuous lining within days, and upon addition of an organoid fragment to the graft chamber gave rise to perfusable angiogenic sprouts. Unfortunately, a connection between the microvessels and the organoids was not established.

Angiogenesis in vivo is regulated by the balance between angiogenic and quiescent stimuli. Quiescent ECs are maintained under the influence of autocrine and pericyte-derived signals such as Ang-1, VEGF-A, FGF and NOTCH. Upon sensing an angiogenic signal like VEGF-A, VEGF-C or Ang-2 released from hypoxic cells, vessel permeability is increased and ECs migrate toward the angiogenic signal, one EC forming the tip cell

and the others following as stalk cells[27]. The VEGF family plays an essential role in angiogenesis, and deficiency of either VEGF-A or its receptor VEGFR2 results in defects in vascular development and embryonic lethality[28-30]. It is therefore not surprising that in our model VEGF-A secretion by kidney organoids was indispensable for inducing angiogenesis, with VEGF blockade leading to the demise of the vascular network. Also, the increase over time of Ang-2 in the perfusion lanes matches the in vivo situation, in which Ang2 is released by sprouting ECs to enhance pericyte detachment, vessel permeability and further sprouting[27]. Despite the presence of angiogenesis promoting factors in the co-culture system, vascularization of the organoids did not occur, illustrating the complexity of angiogenesis regulation. Sprouting angiogenesis is induced by a gradient of proangiogenic factors that is established due to secretion by hypoxic and nutrient deprived cells. Once these cells are vascularized, the gradient diminishes and ECs obtain a quiescent phenotype [31]. It is perceivable that our culture method did not provide the optimal conditions to support the development of a gradient. As demonstrated in the Luminex assay, the organoids released VEGF-A into the medium in the graft chamber. Organoid medium was refreshed 3 times a week, allowing accumulation of proangiogenic factors in the medium. This may have led to the formation of a gradient with the highest concentration of VEGF-A in the medium instead of the organoid itself, explaining the development of microvessels into the graft chamber but not the organoid.

Once sprouting angiogenesis has occurred, functionality of newly formed blood vessels requires their stabilization and maturation. For this purpose, ECs attract pericytes through the production of PDGF-B[27]. The ECs in the co-culture system secreted low levels of PDGF-B which increased over time, implying the acquisition of a quiescent cell state by a proportion of the ECs. However, the absence of mural cells in the Organoplate Graft precluded coverage of the vessels by pericytes in response to PDGF-B. Upon addition of brain pericytes to the chip, these did not encase the ECs, possibly due to a mismatch in origin of ECs and pericytes. The inability to stabilize the microvascular network in the co-culture system could have contributed to the failure to establish a connection to the organoid.

ECs display extensive phenotypic diversity between and within different tissues[32-34]. This allows them to optimally support the diverse physiological functions of the organs and tissues. In this study, we utilized HUVECs and human iPSC-ECs as accessible EC sources, with the added advantage that fluorescently labeled cell lines are available. As discussed, neither cell type invaded the kidney organoids. Since HUVECs are terminally differentiated umbilical cord specific ECs, their lack of plasticity might play a role in the failure to integrate into the kidney organoids. On the contrary, the limitation of hiPSC-ECs is their immaturity, lacking a functional glycocalyx and displaying reduced

mitochondrial function[35]. Beside the characteristics of the ECs that were used, the type of flow in the Organoplate Graft likely influenced the outcome. One of the advantages of the Organoplate Graft is the possibility to subject cells and tissues to flow without an extensive pump and tubing system, by placing the plate on a rocker. In contrast to the in vivo situation, in which ECs are exposed to unidirectional flow, this induces alternating flow in opposite directions. In vivo, shear stress plays an important role in arterialization of ECs[36]. In addition, it enables the synthesis of the glycocalyx by inhibiting PFKFB3 through increasing the inhibitory effects of Krüppel-like factor 2 (KLF2) and nitric oxide[37,38]. It is unclear to what extent alternating flow such as in our system can mimic these effects. Laminar shear stress has been applied to kidney organoids in vitro in different forms[39-41]. Application of flow over the top of organoids increased organoid ECs compared to static conditions, but with only limited development of perfusable vessels[39]. Co-culture of kidney organoids with HUVECs subjected to laminar flow in different designs of microfluidic chips resulted in angiogenesis from the microvessel to the organoid[40] or, when adding VEGF to the medium in the microvessel, from the organoid to the microvessel[41]. In both cases, a connection between organoid and microvessels was established. Unfortunately, glomerular vascularization did not occur. Recently, a new Organoplate Graft became available that allows for unidirectional flow without the need for a tubing system. Utilization of this or a similar microfluidic system combined with more frequent medium changes to maintain an angiogenic gradient, and optimization of EC type and timing of co-culture might contribute to optimization of kidney organoid vascularization in vitro.

In conclusion, the Organoplate Graft enables the co-culture of kidney organoids with a perfusable EC network that is formed in response to VEGF-A secreted by the organoids. Unfortunately, although the microvessels and organoids come in close proximity, they do not form a connection. This study identifies possible culprits, such as an insufficient gradient of proangiogenic factors, suboptimal EC characteristics, lack of laminar flow and of mural cells, that can be addressed to enhance methods for in vitro vascularization of kidney organoids.

Methods

iPSC maintenance and differentiation to kidney organoids

HiPSC lines hiPSC-CRL1502 clone C32, and LUMC0072iCTRL01 were maintained in Essential 8 medium (E8, Thermo Fisher Scientific) with 0.5% Penicillin-Streptomycin (Thermo Fisher Scientific) on recombinant human Vitronectin (Thermo Fisher Scientific). Cell lines were mycoplasma free. hiPSCs were passaged twice a week using 0.5 mM UltraPure EDTA (Thermo Fisher Scientific). They were differentiated to kidney organoids using a previously published protocol.[6] Briefly this entails monolayer culture for 7 days

in STEMdiff APEL2 medium (Stem Cell Technologies) containing 1% PFHMII (Life Technologies) and Antibiotic-Antimycotic solution supplemented with 8 µM CHIR99021 (Tocris) for 4 days, followed by 200 ng mL^{-1} rhFGF9 (R&D Systems) and 1 µg mL^{-1} heparin (Sigma-Aldrich) for 3 days. On day 7, the cells were treated with a CHIR pulse, dissociated to single cells and centrifuged to form aggregates of 500,000 cells, which were placed on Transwell 0.4 µM pore polyester membranes and further cultured at an air-liquid interface. Until day 7+5, the developing organoids were cultured in APEL2-medium supplemented with 200 ng mL^{-1} rhFGF9 and 1 µg mL^{-1} heparin (only bottom compartment), and from day 7+5 onwards in APEL2 without supplements.

Endothelial cell maintenance

RFP-HUVECs (VeraVec, Angiocrine Bioscience or Alphabioregen, #RFP4) were cultured in Endothelial Cell Growth Medium MV2 (Promocell). ECs derived from NCRM1 hiPSCs with constitutive mCherry and Venus reporter, kindly provided by Valeria Orlova (LUMC), were cultured in Endothelial cell serum-free medium (EC-SFM, Gibco, Thermo Fisher Scientific). All ECs were maintained until 80% confluency in T75 tissue culture flask. The cells were dissociated with TrypLE™ Express Enzyme (Thermo, #12604021), before introducing them to the OrganoPlate Graft.

Co-culture in the Organoplate Graft

Co-culture of kidney organoids and ECs was performed using the OrganoPlate Graft with 400 µm x 220 µm (w x h) channels (Mimetas BV, the Netherlands). The ECM channel was loaded with 2.5 µL of gel composed of 4 mg/mL Collagen I (AMSbio Cultrex 3D Collagen I Rat Tail, 5 mg/mL, #3447-020-01), 100 mM HEPES (Life Technologies, #15630-122) and 3.7 mg/mL NaHCO3 (Sigma, #S5761) followed by incubation for 15 min at 37 °C. HUVECs or hiPSC-ECs were dissociated to single cells using TrypLE™ Express Enzyme (Thermo, #12604021), and 20000 cells suspended in 2 µL were seeded in each perfusion channel through the inlet. Subsequently, 50 µL of MV2 (HUVECs) or EC-SFM (hiPSC-ECs) medium was added to each inlet and the OrganoPlate Graft was incubated at 37 °C for at least 1 hour until the ECs attached to the bottom of the perfusion channels. 50 µL of MV2 (HUVECs) of EC-SFM (hiPSC-ECs) medium was then added to the perfusion channel outlets. The OrganoPlate Graft was placed in the incubator (37°C and 5% CO2) on a rocker switching between a +14° and -14° inclination every 8 min (OrganoFlow S, Mimetas) allowing bi-directional flow. Medium (50 µL in each inlet and outlet) was refreshed 3 times per week. ECs were maintained in monoculture for ~2-3 days until confluent vessels were formed in the perfusion channels. The graft chambers were

then prepared for the organoids by aspirating the medium, and adding 10µL of Matrigel (growth factor reduced, phenol red free, Corning) followed by incubation at 37°C for 20 min. Kidney organoids at day d7+12 or 7+18 of differentiation were sectioned using a surgical knife and one organoid fragment was added to each graft chamber, suspended in 30µL STEMdiff APEL2 medium (Stem Cell Technologies). Alternatively, an organoid fragment suspended in 10ul Matrigel was introduced to the graft chamber and incubated for 20 min before 30µL STEMdiff APEL2 medium was added. Sectioning of the organoids was required due to the size mismatch between organoids and graft chamber. Medium in the graft chamber was refreshed 3 times per week. For the experiments with EC in-gel seeding in hydrogrel, 3D Life ToGro Hydrogel from Cellendes (cat G94-1) was used. ECs were suspended in the hydrogel before loading the gel in the ECM channel.

Immunofluorescence analysis

Organoids and ECs were imaged periodically during the experiments using the ImageXpress Confocal Imaging system (Molecular Devices, ImageXpress Micro Confocal). HUVECs and hiPSC-ECs were fluorescently labeled, allowing for their identification during culture without prior fixation and staining. For more detailed analysis of organoid structures and the interaction between organoids and ECs, they were fixed and stained for immunofluorescence analysis within the Organoplate Graft after completing the experiment. Organoids and ECs were fixed in 2% paraformaldehyde (PFA) at 4°C for 20 min. They were permeabilized and blocked in 0.3% TritonX in PBS containing 10% donkey serum for 2 h. Primary antibodies were diluted in blocking solution and incubated for 24 h. Upon washing, secondary antibodies were incubated for 2–4 h at room temperature. Kidney organoids were characterized for NPHS1 (AF4269), ECAD (610181), CD31 (555444), α-SMA (ab5694). Primary antibodies were detected with donkey-α-sheep Alexa, donkey-α-mouse Alexa, donkey-α-rabbit Alexa conjugated with Fluorofores 488, 568 and 647. Nuclei were stained with Hoechst33258 (Thermo Fisher Scientific). All antibodies and isotype controls were validated in human kidney samples. Image Xpress Confocal Imaging system and Leica White Light Laser Confocal Microscope TCS SP8 using LAS-X Image software with 3D module (Leica) was used for analysis of the tissues.

Growth factor analysis

Cell culture supernatant of organoids cultured in transwells was collected during each media change between day 7+7 and day 7+18. It was pooled together and added to the graft chamber of the Organoplate Graft to evaluate its potential to induce angiogenesis.

For the measurement of growth factor concentrations in medium from the Organoplate Graft, cell culture supernatant was collected from the perfusion lanes and graft chamber of 4 chips containing organoids and ECs and 4 chips containing organoids only. Unconditioned MV2 and APEL2 medium was used as a negative control. Medium was collected 5 and 12 days after adding the organoid to the chips. The levels of VEGF-A, Ang1, Ang2 and PDGF-BB were assessed using the Human Luminex Discovery Assay. The Bio-Plex Luminex system (Bio-Rad) was used for readout and growth factor concentration was expressed as pg/mL

Blockade of VEGF-A activity was performed through the addition of human VEGF165 antibody (R&D Systems AF-293-NA) in 3 different concentrations (25, 50 and 100ng/mL), 7 days after placing the organoid in the graft chamber.

Pericyte culture

Primary human brain pericytes (Sciencell, 1200) were cultured on Poly-L-lysine (Cultrex, 3438-100-01) coated flask in pericyte medium (Pericyte Medium Kit (PM, cat#1201) including FBS (2%) (#0010), PGS (#1252) and P/S (#0503)). Cells were detached by use of TrypLE™ Express Enzyme (Thermo, #12604021), counted and pelleted (5 min, 300 x g), before addition to the OrganoPlate Graft.

Acknowledgements

We acknowledge the support of Manon Zuurmond (LUMC, Leiden, the Netherlands) in the generation of the schematic figures, and thank Valeria Orlova (LUMC, Leiden, the Netherlands) for providing the NCRM1 hiPSCs with constitutive mCherry and Venus reporter.

References

1 Takasato, M. et al. Kidney organoids from human iPS cells contain multiple lineages and model human nephrogenesis. Nature ***526***, 564–568 (2015). https://doi.org/10.1038/nature15695

2 Eremina, V. et al. Glomerular-specific alterations of VEGF-A expression lead to distinct congenital and acquired renal diseases. J Clin Invest ***111***, 707–716 (2003). https://doi.org/10.1172/JCI17423

3 Kitamoto, Y., Tokunaga, H. & Tomita, K. Vascular endothelial growth factor is an essential molecule for mouse kidney development: glomerulogenesis and nephrogenesis. J Clin Invest ***99***, 2351–2357 (1997). https://doi.org/10.1172/JCI119416

4 Sison, K. et al. Glomerular structure and function require paracrine, not autocrine, VEGF-VEGFR-2 signaling. J Am Soc Nephrol ***21***, 1691–1701 (2010). https://doi.org/10.1681/ASN.2010030295

5 van den Berg, C. W., Koudijs, A., Ritsma, L. & Rabelink, T. J. In Vivo Assessment of Size-Selective Glomerular Sieving in Transplanted Human Induced Pluripotent Stem Cell-Derived Kidney Organoids. J Am Soc Nephrol ***31***, 921–929 (2020). https://doi.org/10.1681/ASN.2019060573

6 van den Berg, C. W. et al. Renal Subcapsular Transplantation of PSC-Derived Kidney Organoids Induces Neo-vasculogenesis and Significant Glomerular and Tubular Maturation In Vivo. Stem Cell Reports ***10***, 751–765 (2018). https://doi.org/10.1016/j.stemcr.2018.01.041

7 Bantounas, I. et al. Generation of Functioning Nephrons by Implanting Human Pluripotent Stem Cell-Derived Kidney Progenitors. Stem Cell Reports ***10***, 766–779 (2018). https://doi.org/10.1016/j.stemcr.2018.01.008

8 Sharmin, S. et al. Human Induced Pluripotent Stem Cell-Derived Podocytes Mature into Vascularized Glomeruli upon Experimental Transplantation. J Am Soc Nephrol ***27***, 1778–1791 (2016). https://doi.org/10.1681/ASN.2015010096

9 Munro, D. A. D., Hohenstein, P. & Davies, J. A. Cycles of vascular plexus formation within the nephrogenic zone of the developing mouse kidney. Sci Rep ***7***, 3273 (2017). https://doi.org/10.1038/s41598-017-03808-4

10 Rogers, S. A. & Hammerman, M. R. Transplantation of rat metanephroi into mice. Am J Physiol Regul Integr Comp Physiol ***280***, R1865–1869 (2001). https://doi.org/10.1152/ajpregu.2001.280.6.R1865

11 Takeda, S., Rogers, S. A. & Hammerman, M. R. Differential origin for endothelial and mesangial cells after transplantation of pig fetal renal primordia into rats. Transpl Immunol ***15***, 211–215 (2006). https://doi.org/10.1016/j.trim.2005.10.003

12 van Duinen, V. et al. 96 perfusable blood vessels to study vascular permeability in vitro. Sci Rep ***7***, 18071 (2017). https://doi.org/10.1038/s41598-017-14716-y

13 Eremina, V. & Quaggin, S. E. The role of VEGF-A in glomerular development and function. Curr Opin Nephrol Hypertens ***13***, 9–15 (2004).

14 Bartlett, C. S., Jeansson, M. & Quaggin, S. E. Vascular Growth Factors and Glomerular Disease. Annu Rev Physiol ***78***, 437–461 (2016). https://doi.org/10.1146/annurev-physiol-021115-105412

15 Lobov, I. B., Brooks, P. C. & Lang, R. A. Angiopoietin-2 displays VEGF-dependent modulation of capillary structure and endothelial cell survival in vivo. Proc Natl Acad Sci U S A ***99***, 11205–11210 (2002). https://doi.org/10.1073/pnas.172161899

16 Gale, N. W. et al. Angiopoietin-2 is required for postnatal angiogenesis and lymphatic patterning, and only the latter role is rescued by angiopoietin-1. Developmental Cell ***3***, 411–423 (2002). https://doi.org/Doi 10.1016/S1534-5807(02)00217-4

17 Hellstrom, M., Kalen, M., Lindahl, P., Abramsson, A. & Betsholtz, C. Role of PDGF-B and PDGFR-beta in recruitment of vascular smooth muscle cells and pericytes during embryonic blood vessel formation in the mouse. Development ***126***, 3047–3055 (1999). https://doi.org/10.1242/dev.126.14.3047

18 Lindahl, P., Johansson, B. R., Leveen, P. & Betsholtz, C. Pericyte loss and microaneurysm formation in PDGF-B-deficient mice. Science ***277***, 242–245 (1997). https://doi.org/10.1126/science.277.5323.242

19 Dumas, S. J. Single-Cell RNA Sequencing Reveals Renal Endothelium Heterogeneity and Metabolic Adaptation to Water Deprivation. JASN (2019).

20 Molema, G. & Aird, W. C. Vascular heterogeneity in the kidney. Semin Nephrol ***32***, 145–155 (2012). https://doi.org/10.1016/j.semnephrol.2012.02.001

21 Jourde-Chiche, N. et al. Endothelium structure and function in kidney health and disease. Nat Rev Nephrol (2019). https://doi.org/10.1038/s41581-018-0098-z

22 Dienemann, S., Schmidt, V., Fleischhammer, T., Mueller, J. H. & Lavrentieva, A. Comparative analysis of hypoxic response of human microvascular and umbilical vein endothelial cells in 2D and 3D cell culture systems. J Cell Physiol ***238***, 1111–1120 (2023). https://doi.org/10.1002/jcp.31002

23 Dib, H. et al. Proteomes of umbilical vein and microvascular endothelial cells reflect distinct biological properties and influence immune recognition. Proteomics ***12***, 2547–2555 (2012). https://doi.org/10.1002/pmic.201200060

24 Browning, A. C. et al. Comparative gene expression profiling of human umbilical vein endothelial cells and ocular vascular endothelial cells. Br J Ophthalmol ***96***, 128–132 (2012). https://doi.org/10.1136/bjophthalmol-2011-300572

25 Orlova, V. V. et al. Generation, expansion and functional analysis of endothelial cells and pericytes derived from human pluripotent stem cells. Nat Protoc ***9***, 1514–1531 (2014). https://doi.org/10.1038/nprot.2014.102

26 Bergers, G. & Song, S. The role of pericytes in blood-vessel formation and maintenance. Neuro Oncol ***7***, 452–464 (2005). https://doi.org/10.1215/S1152851705000232

27 Carmeliet, P. & Jain, R. K. Molecular mechanisms and clinical applications of angiogenesis. Nature ***473***, 298–307 (2011). https://doi.org/10.1038/nature10144

28 Shalaby, F. et al. Failure of blood-island formation and vasculogenesis in Flk-1-deficient mice. Nature ***376***, 62–66 (1995). https://doi.org/10.1038/376062a0

29 Ferrara, N. et al. Heterozygous embryonic lethality induced by targeted inactivation of the VEGF gene. Nature ***380***, 439–442 (1996). https://doi.org/10.1038/380439a0

30 Carmeliet, P. et al. Abnormal blood vessel development and lethality in embryos lacking a single VEGF allele. Nature ***380***, 435–439 (1996). https://doi.org/10.1038/380435a0

31 Eelen, G., Treps, L., Li, X. & Carmeliet, P. Basic and Therapeutic Aspects of Angiogenesis Updated. Circ Res ***127***, 310–329 (2020). https://doi.org/10.1161/CIRCRESAHA.120.316851

32 Nolan, D. J. et al. Molecular signatures of tissue-specific microvascular endothelial cell heterogeneity in organ maintenance and regeneration. Dev Cell ***26***, 204–219 (2013). https://doi.org/10.1016/j.devcel.2013.06.017

33 Kalucka, J. et al. Single-Cell Transcriptome Atlas of Murine Endothelial Cells. Cell ***180***, 764–779.e720 (2020). https://doi.org/10.1016/j.cell.2020.01.015

34 Dumas, S. J. et al. Phenotypic diversity and metabolic specialization of renal endothelial cells. Nat Rev Nephrol ***17***, 441–464 (2021). https://doi.org/10.1038/s41581-021-00411-9

35 Tiemeier, G. L. et al. Closing the Mitochondrial Permeability Transition Pore in hiPSC-Derived Endothelial Cells Induces Glycocalyx Formation and Functional Maturation. Stem Cell Reports ***13***, 803–816 (2019). https://doi.org/10.1016/j.stemcr.2019.10.005

36 Fang, J. S. et al. Shear-induced Notch-Cx37-p27 axis arrests endothelial cell cycle to enable arterial specification. Nat Commun ***8***, 2149 (2017). https://doi.org/10.1038/s41467-017-01742-7

37 Cantelmo, A. R. et al. Inhibition of the Glycolytic Activator PFKFB3 in Endothelium Induces Tumor Vessel Normalization, Impairs Metastasis, and Improves Chemotherapy. Cancer Cell ***30***, 968–985 (2016). https://doi.org/10.1016/j.ccell.2016.10.006

38 van den Berg, C. W., Dumas, S. J., Little, M. H. & Rabelink, T. J. Challenges in maturation and integration of kidney organoids for stem cell-based renal replacement therapy. Kidney Int ***107***, 262–270 (2025). https://doi.org/10.1016/j.kint.2024.10.028

39 Homan, K. A. et al. Flow-enhanced vascularization and maturation of kidney organoids in vitro. Nat Methods ***16***, 255–262 (2019). https://doi.org/10.1038/s41592-019-0325-y

40 Menéndez, A. B. C. et al. Creating a kidney organoid-vasculature interaction model using a novel organ-on-chip system. Sci Rep-Uk ***12*** (2022). https://doi.org/ARTN 20699 10.1038/s41598-022-24945-5

41 Kroll, K. T. et al. A perfusable, vascularized kidney organoid-on-chip model. Biofabrication ***16*** (2024). https://doi.org/10.1088/1758-5090/ad5ac0

Supplementary Figures

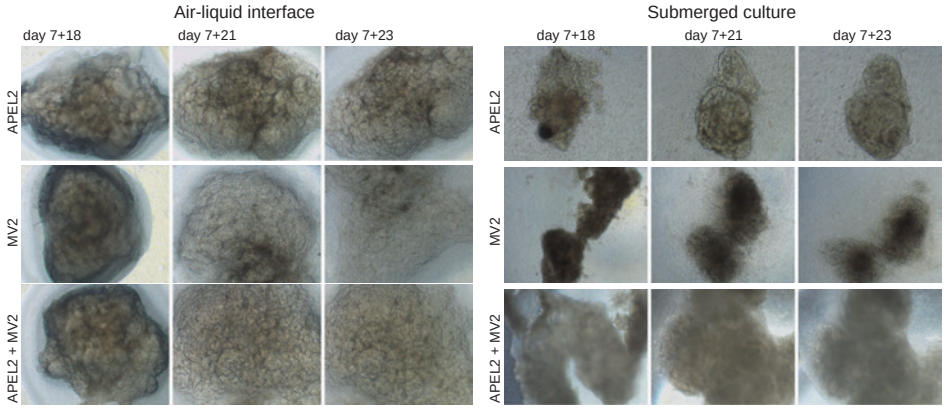

Supplementary Fig. 1: Culturing kidney organoid fragments at air-liquid interface (left) versus submerged culture (right) in APEL2, MV2 or mixed medium

CHAPTER 4

Vasculogenesis in kidney organoids upon transplantation

M. Koning*, S.J. Dumas*, M.C. Avramut, R.I. Koning, E. Meta, E. Lievers, L.E. Wiersma, M. Borri, X. Liang, L. Xie, P. Liu, F. Chen, L. Lin, Y. Luo, J. Mulder, H.S. Spijker, T. Jaffredo, B.M. van den Berg, P. Carmeliet, C.W. van den Berg, A.J. Rabelink
* authors contributed equally to the work

NPJ Regenerative Medicine, 2022

Abstract

Human induced pluripotent stem cell-derived kidney organoids have potential for disease modeling and to be developed into clinically transplantable auxiliary tissue. However, they lack a functional vasculature and the sparse endogenous endothelial cells (ECs) are lost upon prolonged culture in vitro, limiting maturation and applicability. Here, we use intracoelomic transplantation in chicken embryos followed by single-cell RNA sequencing and advanced imaging platforms to induce and study vasculogenesis in kidney organoids. We show expansion of human organoid-derived ECs that reorganize into perfused capillaries and form a chimeric vascular network with host-derived blood vessels. Ligand-receptor analysis infers extensive potential interactions of human ECs with perivascular cells upon transplantation, enabling vessel wall stabilization. Perfused glomeruli display maturation and morphogenesis to capillary loop stage. Our findings demonstrate the beneficial effect of vascularization on not only epithelial cell types, but also the mesenchymal compartment, inducing the expansion of ´on target´ perivascular stromal cells which in turn are required for further maturation and stabilization of the neo-vasculature. The here described vasculogenic capacity of kidney organoids will have to be deployed to achieve meaningful glomerular maturation and kidney morphogenesis in vitro.

Introduction

Since the publication of protocols for the generation of three-dimensional (3D) kidney organoids from human induced pluripotent stem cells (hiPSCs) [1-4], expectations regarding their potential for the modeling of kidney development and disease have been very high. Over the past few years, it has become increasingly clear that the level of maturation in vitro is an important limiting factor in this respect. Although many aspects including culture environment, restricted time in culture, off-target differentiation, and limited corticomedullary organization play a role in restricting maturation, the absence of a functional vasculature is of particular importance. In embryology, the development of the kidney depends on the presence of perfused blood vessels. These supply the tissue with oxygen and nutrients and enable the interaction between podocytes and vascular endothelial cells (ECs) that is necessary for their maturation and development of the glomerular basement membrane (GBM) [5-7]. In kidney organoids maintained in vitro, this interaction does not occur, limiting their maturation as well as their resemblance to in vivo kidney tissue.

We and others have shown previously that transplantation in mice leads to vascularization and progressive maturation of hiPSC-derived kidney organoids [8-10], which even enables functional glomerular filtration [11]. However, this model is labor intensive and unsuitable to study large numbers of organoids. Transplantation on the chicken chorioallantoic membrane (CAM) is much more straightforward and was demonstrated to induce vascularization [12]. Because the CAM takes time to develop, this method allowed for only 5 days of transplantation, limiting the extent of the vasculature and maturation. Therefore, we aimed to develop an easy, efficient, reproducible and accessible model to induce and study vascularization and maturation of kidney organoids through transplantation in the coelomic cavity of chicken embryos. Chicken embryos can develop normally after opening the egg shell, lack a fully functional immune system, and their coelomic cavity is a favorable environment for vascularization and differentiation of transplanted embryonic tissues [13-17]. Unlike grafting on the CAM, the coelom permits transplantation as early as day 3–4 of embryonic development, allowing for a longer duration of transplantation, and quite unlimited expansion of the transplanted tissue in all directions [16].

Here, we transplanted hiPSC-derived kidney organoids inside the coelom of chicken embryos and extensively investigated the effect of transplantation on the vasculature, cellular composition and maturation of the organoids using immunofluorescence (IF), single cell RNA sequencing (scRNAseq), and ultra-large scale transmission electron microscopy (TEM) [18]. To enable analysis of the 3D organization of organoid glomeruli, we

performed serial block face scanning electron microscopy (SBF-SEM) followed by artificial intelligence-based segmentation, annotation and 3D reconstruction. We demonstrate the development of a chimeric perfused vascular network inside transplanted organoids, which invades the glomerular structures and induces enhanced nephron maturation as well as improved stromal composition.

Results

Kidney organoids are vascularized upon intracoelomic transplantation in chicken embryos

Chicken embryos are easily accessible, require very little maintenance, and their coelomic cavity is a favorable environment for the differentiation of embryonic tissues[15-17,19]. Therefore, we aimed to investigate the suitability of intracoelomic transplantation to induce and study vascularization and maturation of hiPSC-derived kidney organoids. Kidney organoids were generated from hiPSCs using previously published protocols (Fig. 1a)[10,20]. Although organoids generated in this manner contain some ECs, these fail to invade glomerular structures and diminish upon prolonged in vitro culture (supplementary Fig. 1a)[21]. To ensure the presence of endogenous ECs at the time of transplantation, we decided to transplant organoids at a relatively early stage, on d7+11 or d7+12 of differentiation. Organoids were bisected and inserted into the coelomic cavity of day 4 (Hamburger Hamilton stage 23) chicken embryos (Fig. 1a,b)[19,22]. At this stage of development, the coelom is large enough to accommodate half an organoid and the body wall is not yet fully closed, allowing straightforward transplantation that takes around 5 min per embryo. Transplanted organoids and untransplanted controls were harvested 1 day after transplantation for scRNAseq analysis and 8 days after transplantation for scRNAseq, IF, TEM and SBF-SEM analysis (Fig. 1a). Embryos selected for IF analysis were injected with Rhodamine labeled *lens culinaris agglutinin* (LCA)[23] to stain the endothelium of perfused blood vessels before sacrificing them. Organoids had most frequently become attached to the liver, but could also be found connected to the intestines or ribs. Upon visual inspection through a stereo microscope, they appeared to be vascularized with apparent blood perfusion (Fig. 1c).

For scRNAseq analysis, we performed enzymatic dissociation of 94 untransplanted and 75 bisected transplanted organoids (150 chicken embryos) at d7+13 and 93 untransplanted and 46,5 bisected transplanted organoids (93 chicken embryos) at d7+20 from the same differentiation to single cells. Pooling such a high number of organoids for each condition allows for mitigating potential inter- organoid variability.

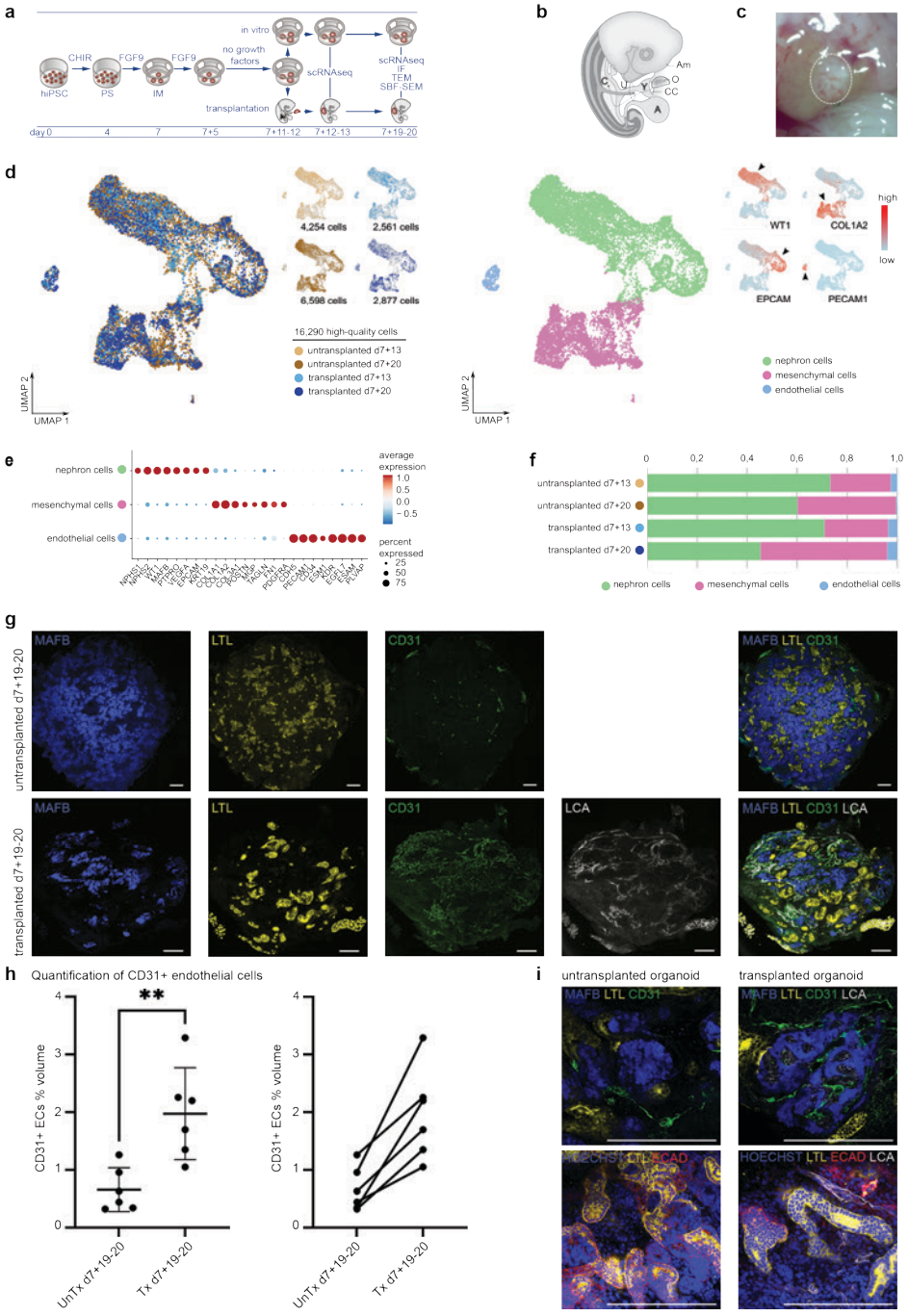

Figure 1: hiPSC-derived kidney organoids become vascularized upon transplantation in the coelomic cavity of chicken embryos. a Schematic of the in vitro generation of kidney organoids and transplantation inside chicken embryos. HiPSCs were differentiated for 7 days as monolayer,

followed by culture as organoids on an air liquid interface. On d7+11 or d7+12 of differentiation, they were either transplanted inside the coelomic cavity of HH23 chicken embryos or maintained in vitro. Transplanted organoids and untransplanted controls were harvested for analysis with scRNAseq 1 day after transplantation and for scRNAseq, IF, TEM, and SBF-SEM 8 days after transplantation. **b** Schematic of the method of transplantation inside the coelomic cavity of chicken embryos (modified from Dossel et al. Science 1954, with permission)[19]: a small hole is made in the chorion and amnion membrane using forceps, the bisected organoid is inserted into the coelom with a blunt instrument through this hole and the opening in the body wall that is still present at this stage of development. A allantois, Am amnion, C coelom, CC cut chorion membrane, O organoid, U umbilical ring, Y yolk stalk. **c** Macroscopic image of a vascularized kidney organoid (circled area) attached to the liver inside a day 12 chicken embryo **d** UMAP visualization of a total of 16,290 high-quality human organoid cells obtained from untransplanted (4254 cells from d7+13, 6598 from d7+20) and transplanted (2561 cells from d7+13, 2877 from d7+20) kidney organoids, color-coded by condition (left) or main cell populations: nephron cells, mesenchymal cells and endothelial cells (right). Top right inset: UMAP plot color-coded by the expression level of WT1, COL1A2, EPCAM and PECAM1 genes (red: high expression level, blue: low expression level). **e** Dot plot representing marker gene expression in organoid cell clusters. Dot size indicates proportion of cells in cluster expressing a gene, colour intensity indicates the level of expression. **f** Relative cluster quantification for each condition, showing endothelial cell loss upon prolonged culture in vitro and maintenance upon transplantation. The proportion of nephron cells decreased in favor of mesenchymal cells in d7+20 compared to d7+13 organoids, with the highest proportion of mesenchymal cells in transplanted d7+20 organoids. **g** Immunofluorescent images of untransplanted (top) and transplanted (bottom) kidney organoids, showing glomerular (MAFB-BFP2 (blue)) and tubular (LTL (yellow)) structures and endothelial cells (CD31 (green)). In transplanted organoids the endothelial cells have formed a vascular network and have become perfused as demonstrated by the presence of injected LCA (white). Scale bars 200µm. **h** Quantification of CD31 positive ECs as percent volume of organoid volume in whole mount untransplanted (untx) and transplanted (tx) organoids at d7+19-20. n=6 untransplanted and 6 matched transplanted organoids from 6 different experiments. Left: Transplanted organoids contain significantly more EC volume than untransplanted controls ($p<0,01$). Data are presented as individual data points, mean (SD). Unpaired two-tailed t-test was performed to compare means between group. Right: Alternative visualization demonstrating the increase in EC percent volume upon transplantation for each differentiation. ***i*** Top: Glomerular structures (MAFB-BFP2 (blue)) in untransplanted kidney organoids did not contain human endothelial cells (CD31 (green)), while these structures were invaded by endothelial cells (CD31 (green), LCA (white)) upon transplantation. Bottom: After incubation inside the chicken embryo, tubular structures (LTL (yellow) and ECAD (red)) were aligned by perfused capillaries (LCA (white)). Scale bars 200µm. Images in **g, i** are based on >5 separate experiments and 3 cell lines (iPSC-MAFB (shown here), LUMC0072 (supplementary Fig. 3), LUMC0020 (supplementary Fig. 3).

An aliquot was taken from the single cell suspension of each condition and processed for sequencing. After species demultiplexing (for transplanted organoids), quality controls and filtering, a total of 16,290 high quality human organoid cells and 6866 high quality chicken host cells were retained for downstream analyses (Fig. 1d, supplementary Fig. 2a, 3a, supplementary data 1). Unsupervised clustering of the organoid-derived human cells revealed three main cell populations, which were identified as nephron, mesenchymal and endothelial cells based on expression of established marker genes (Fig. 1d, e, supplementary data 2). The proportion of nephron cell types was the highest at d7+13 (73% of the total cell number in untransplanted and 71% in transplanted organoids) and had decreased in favor of mesenchymal cell types at d7+20 (60% in untransplanted, 45% in transplanted). As expected, in organoids cultured in vitro the proportion of ECs decreased over time from 2.6% at d7+13 to 0.4% at d7+20. Upon transplantation, however, we observed an increase to 4% of ECs at d7+20 (Fig. 1f, supplementary data 3). Whole

mount IF staining of untransplanted and transplanted organoids at d7+19-20 followed by quantification of organoid-derived ECs (human CD31+) confirmed the higher percentage of ECs in transplanted organoids (Fig. 1g,h). The presence of injected rhodamine-labeled LCA demonstrated perfusion of the vasculature (Fig. 1g and supplementary Fig. 1b). All investigated transplanted organoids had become vascularized. In addition, the perfused blood vessels (CD31+, LCA+) were shown to invade the organoid glomerular structures marked by an mTagBFP2 podocyte reporter (MAFB+) or stained for nephrin (NPHS1+) and align with tubular structures (LTL+ / ECAD+) (Fig. 1l and supplementary Fig. 1b). Host-derived ECs also appear to contribute to the vasculature, as evidenced by the presence of CD31-, LCA+ (perfused chicken derived) vessels beside CD31+, LCA+ (perfused organoid derived) and CD31+, LCA- (unperfused organoid derived) vessels (supplementary Fig. 4a). Unperfused chicken-derived endothelial cells could not be identified, because a specific antibody for these cells is not available. Within the chicken cells collected with transplanted organoids for scRNAseq, an angiogenic EC population was identified (supplementary Fig. 3b-d, supplementary data 4). Some of these might reflect host-derived ECs that invaded the kidney organoids upon transplantation in addition to the endogenous human ECs. However, liver-specific sinusoidal ECs, as well as hepatocytes and other non-renal cell types were also identified, likely emerging from chicken tissue that remained attached to the kidney organoids during collection despite careful dissection, resulting in challenging interpretation of the chicken cell dataset (supplementary Fig. 3b-d).

Since vascularization was already quite extensive after only 8 days of transplantation, we investigated the development of the vasculature in the organoids over time. On day 1 after transplantation, perfused blood vessels (LCA+) could already be detected at the edge of the transplanted organoids (supplementary Fig. 4b). Three days after transplantation, the first glomerular-like structures (MAFB+) started to be invaded by human ECs (CD31+/LCA+). On day 5, vascularized glomerular structures could be seen throughout the organoid and on day 7, the majority of glomerular structures were perfused (supplementary Fig. 4b).

Heterogeneity of nephron cell types in kidney organoids is preserved upon transplantation

Next, we evaluated the effect of transplantation and vascularization on the cellular composition of kidney organoids, starting with the nephron compartment. Unsupervised subclustering of a total of 10,198 high quality nephron cells obtained from untransplanted (3116 cells from d7+13; 3963 cells from d7+20) and transplanted (1816 cells from d7+13;

1303 cells from d7+20) organoids resulted in 16 subclusters, which we identified based on the top marker genes for each cluster (Fig. 2a,b, supplemenary Fig. 2b-d, supplementary data 5, 6). Organoids from all conditions contained proliferative cell clusters, nephron precursors (pretubular aggregate / renal vesicle and nephron progenitor cells), tubular cells and podocytes (Fig. 2a). Supporting our cluster identification, further unsupervised hierarchical clustering of the delineated nephron cell phenotypes revealed higher similarity of the different identified podocyte clusters as compared with nephron precursors and proliferating nephron cells, as well as a greater distance with tubular cell clusters (Fig. 2c). More specifically, 4 subclusters of tubular cells were distinguished: 2 types of proximal tubule cells (#1 and 2), loop of Henle-like cells, and distal tubule / collecting duct-like cells (Fig 2b, c, supplementary Fig. 2c, and supplementary data 5, 7). We did not identify a clear distal convoluted tubule (*SLC12A3*) or pure collecting duct (*AQP2/4*) population.

The podocytes displayed more heterogeneity, resulting in 7 subclusters, mainly reflecting different levels of maturation. The podocyte-committed progenitor cluster highly expressed *OLFM3*, a podocyte-specific lineage marker, but no other markers for podocyte identity. The immature podocyte, early podocyte #1 and 2 and late podocyte clusters expressed increasing levels of markers for podocyte identity (*MAFB, WT1*), and differentiation (*NPHS1* and *2*, *PODXL*, *CLIC5*) (Fig. 2b, supplementary Fig. 2b and supplementary data 5). In addition, we found a subcluster of late podocytes expressing genes associated with stress and a subcluster of hypoxic podocytes (Fig. 2b and supplementary Fig. 2b,e). Since all organoids from the same condition were pooled, it is not possible to definitively distinguish whether these podocyte subclusters are the result of different maturation stages within the same or between different organoids. However, based on variation observed through TEM imaging, we believe it reflects intra- rather than inter-organoid variability.

All nephron subclusters were represented in all organoid conditions, and major shifts in populations were not observed (Fig. 2d). However, there were some interesting differences between conditions. In transplanted organoids (d7+13 and d7+20), the proportion of hypoxic podocytes appeared increased, which can be explained by the hypoxia in the intracoelomic cavity prior to vascularization. This did not lead to a larger proportion of stress-induced podocytes, which were most abundant in untransplanted d7+20 organoids.

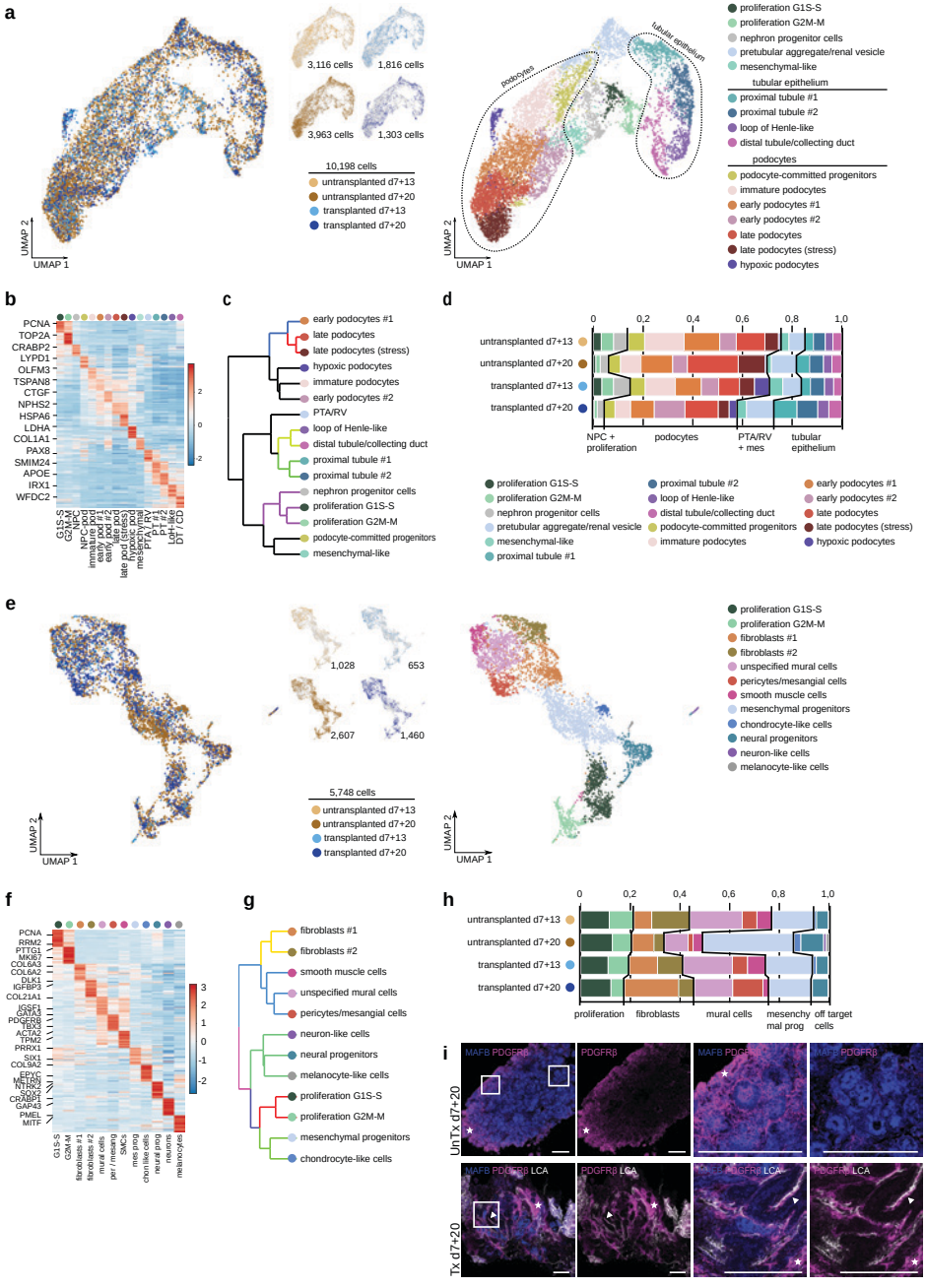

Figure 2: Heterogeneity of nephron and mesenchymal cell types in untransplanted and transplanted kidney organoids. a UMAP visualization of a total of 10,198 high-quality nephron cells obtained from untransplanted (3116 cells from d7+13, 3963 from d7+20) and transplanted (1816 cells from d7+13, 1303 from d7+20) kidney organoids, color-coded by condition (left) and by cluster (n=16; right). **b** Expression-level scaled heatmap of the top 20 marker genes in nephron subclusters. Scale: z-score of the gene expression level. Abbreviations: G1S-S: proliferative nephron

cells G1S-S, G2M-M: proliferative nephron cells G2M-M, NPC: nephron progenitor cells, NPC-pod: podocyte-committed progenitors, immature pod; immature podocytes, early pod #1: early podocytes #1, early pod #2: early podocytes #2, late pod: late podocytes, late pod (stress): late podocytes (stress-induced), hypoxic pod: hypoxic podocytes, mesenchymal: mesenchymal-like nephron cells, PTA/RV: pretubular aggregate/renal vesicle, PT #1: proximal tubules #1, PT #2: proximal tubules #2, LoH-like: loop of Henle-like, DT/CD: distal tubules/collecting duct. **c** Hierarchical clustering of nephron cell types, color-coded according to P-value from multiscale bootstrap resampling analysis on all highly variable genes. **d** Relative cluster quantification of the nephron cell types in transplanted versus untransplanted kidney organoids (d7+13 and d7+20). **e** UMAP visualization of a total of 5748 high-quality mesenchymal cells obtained from untransplanted (1028 cells from d7+13, 2607 from d7+20) and transplanted (653 cells from d7+13, 1460 from d7+20) kidney organoids, color-coded by condition (left) and by cluster (n=12; right). **f** Expression-level scaled heatmap of the top 20 marker genes in mesenchymal subclusters. Scale: z-score of the gene expression level. Abbreviations: G1S-S: proliferative mesenchymal cells G1S-S, G2M-M: proliferative mesenchymal cells G2M-M, mural cells: unspecified mural cells, per / mesang: pericytes/mesangial cells, SMCs: smooth muscle cells, mes prog: mesenchymal progenitors, chon like cells: chondrocyte-like cells, neural prog: neural progenitors. **g** Hierarchical clustering of mesenchymal cell types, color-coded according to P-value from multiscale bootstrap resampling analysis on all highly variable genes. **h** Relative cluster quantification of the mesenchymal cell types in transplanted versus untransplanted kidney organoids (d7+13 and d7+20). **i** Staining of PDGFRβ+ stromal cells in untransplanted and transplanted kidney organoids reveals abundant PDGFRβ+ stromal cells in the periphery of untransplanted organoids (asterix and first magnification) and scarce PDGFRβ+ cells in the center (second magnification). Transplantation induces the appearance of perivascular stromal cells (PDGFRβ+, arrowhead and magnifications) supporting perfused blood vessel (LCA+). Magnifications of boxed areas are shown. Scale bars 200μm.

Transplantation induces an increase in perivascular cell types

Mesenchymal cells are essential for kidney development and function. However, they can also contribute to kidney fibrosis and subpopulations of stromal cells have been reported in organoids to give rise to off-target cell populations such as cartilage[24]. To investigate the identity of the mesenchymal cells in our kidney organoids, we performed unsupervised subclustering of the 5748 high quality mesenchymal cells obtained from untransplanted (1028 cells from d7+13; 2607 cells from d7+20) and transplanted (653 cells from d7+13; 1460 cells from d7+20) organoids (Fig. 2e). This revealed 12 clusters, which we identified as proliferating cells, fibroblasts, mural cells, mesenchymal progenitor cells and off-target cell populations based on their top marker gene expression (Fig. 2e, f and supplementary data 8). Further unsupervised hierarchical clustering supported our cluster identification with grouping clusters by cell types: fibroblasts, mural cells, off-target cells derived from neural lineage, and proliferating cells together with mesenchymal progenitors and derivative off-target chondrocyte-like cells (Fig. 2g). More specifically, off-target cells consisted of chondrocyte-like cells, neural progenitors, neuron-like cells and melanocyte-like cells. Three types of mural cells, namely pericytes/mesangial cells, smooth muscle cells, and unspecified mural cells could be distinguished (Fig. 2e,f, supplementary Fig. 2f). In untransplanted organoids at d7+20, the proportion of off-target cell types and mesenchymal progenitor cells was increased compared to d7+13, at the expense of mural cells. In transplanted organoids at d7+20, the increase in off-target cell types and mesenchymal progenitors was much less pronounced, but we did observe an increase in pericytes/mesangial cells and fibroblasts

(Fig. 2h, supplementary data 3). We confirmed the presence of perivascular stromal cells in transplanted organoids through IF staining with a PDGFRβ antibody, combined with injected rhodamine labeled LCA. In untransplanted organoids, PDGFRβ positive stromal cells were present mainly in the periphery of the organoid and only sporadically in the center scattered between the epithelial structures. In transplanted organoids, perivascular PDGFRβ+ stromal cells supporting the LCA+ perfused blood vessels had appeared, although some areas with PDGFRβ+ stromal cells were still visible between epithelial structures (Fig. 2i).

These data imply that, although transplantation in chicken embryos may increase the proportion of mesenchymal cells, it favors their differentiation to 'on-target' pericytes and mesangial cells, while reducing the amount of off-target cell types compared to in vitro controls.

Vessel wall stabilization in transplanted organoids

Stabilization and maturation of newly formed blood vessels requires the establishment of inter-EC contacts and pericyte-EC interactions[25,26]. We evaluated the occurrence of these events in our model through gene set enrichment analysis (GSEA) of ECs in d7+20 transplanted compared with respective untransplanted organoids and ligand-receptor (LR) network analysis. Differential gene expression analysis (DGEA) followed by GSEA in ECs demonstrated upregulation of, amongst others, gene sets associated with vascularization, regulation of vasomotor tone, immunity (likely due to the connection to the chicken embryo circulation), and extracellular matrix organization (occurs in but is not specific for angiogenesis and vessel stabilization). Interestingly, a gene set associated with cell-cell junction organization, an important event in vessel wall stabilization, as well as a gene set involved in the regulation of vasoconstriction, reflecting maturation of the vasculature were significantly enriched (Fig. 3a, supplementary data 9). Indeed, expression of many individual genes involved in these processes were upregulated in transplanted kidney organoids at d7+20 compared to all other conditions (Fig. 3b).

To investigate the interaction of ECs with pericytes, we performed LR network analysis. Because of the low number of both pericytes / mesangial cells and ECs, especially in untransplanted d7+20 organoids, we decided to pool the cells from this condition with those from untransplanted and transplanted d7+13 organoids, and compare them to transplanted d7+20 organoids for further LR analysis. Since the observed increase in proportion and change in localization of pericytes was clearly present in transplanted d7+20 organoids compared to the other conditions, changes in interactions between ECs and pericytes upon transplantation were expected to remain detectable after pooling of cells from these 3 conditions.

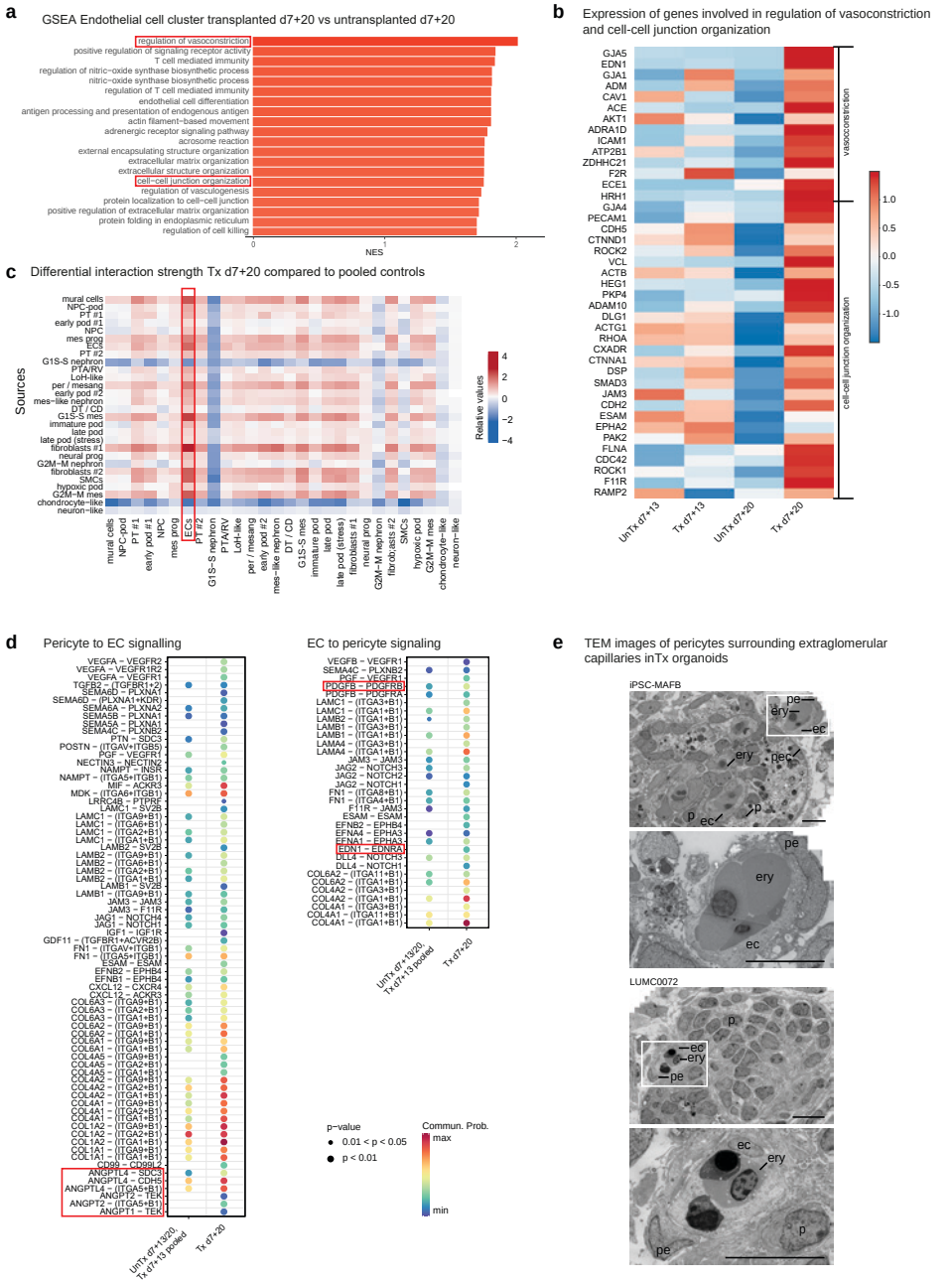

Figure 3: Vessel wall stabilization in transplanted kidney organoids a Gene set enrichment analysis (GSEA) for EC cluster in transplanted d7+20 versus untransplanted d7+20 organoids demonstrating enrichment of gene sets associated with vasoconstriction and cell-cell junction organization. NES: normalized enrichment score. **b** Expression-level scaled heatmap of genes involved in vasoconstriction and cell-cell junction organization, demonstrating upregulation of the majority of these genes in d7+20 transplanted endothelial cells compared to all other conditions. Scale: z-score of the gene expression level. **c** Heatmap demonstrating differential interaction strength (probability

of interactions) per cluster for d7+20 transplanted organoids compared to pooled controls (d7+13 transplanted and untransplanted and d7+20 untransplanted organoids). Abbreviations: mural cells: unspecified mural cells, NPC-pod: podocyte-committed progenitors, PT #1: proximal tubules #1, early pod #1: early podocytes #1, NPC: nephron progenitor cells, mes prog: mesenchymal progenitors, ECs: endothelial cells, PT #2: proximal tubules #2, G1S-S nephron: proliferative nephron cells G1S-S, PTA/RV: pretubular aggregate/renal vesicle, LoH-like: loop of Henle-like, per/mesang: pericytes/mesangial cells, early pod #2: early podocytes #2, mes-like nephron: mesenchymal-like nephron cells, DT/CD: distal tubules/collecting duct, G1S-S mes: proliferative mesenchymal cells G1S-S, imm pod; immature podocytes, late pod: late podocytes, late pod (stress): late podocytes (stress-induced), fibroblasts #1: fibroblasts #1, neural prog: neural progenitors, G2M-M nephron: proliferative nephron cells G2M-M, fibroblasts #2; fibroblasts #2, SMC: smooth muscle cells, hypoxic pod: hypoxic podocytes, G2M-M mes: proliferative mesenchymal cells G2M-M, chondrocyte-like: chondrocyte-like cells, neuron-like: neuron-like cells. **d** Dot plot of the ligand-receptor pairs for which interaction strength between pericytes and endothelial cells is increased in d7+20 transplanted organoids compared to pooled controls with (left) pericytes as source and (right) endothelial cells as source. **e** In transplanted kidney organoids, extraglomerular capillaries are supported by pericytes. ec endothelial cell, p podocyte, pe pericyte, pec parietal epithelial cell, ery erythrocyte. Scale bars 10μm.

Investigation of the differential interaction strength (reflecting the probability of interactions) for all clusters revealed an increase of inferred interactions between ECs and mesenchymal cell types in transplanted d7+20 organoids compared to pooled controls, especially with the ECs as receiver (Fig. 3c). We subsequently analyzed which ligand-receptor interactions were newly detected or increased from pericytes to ECs and vice versa (Fig. 3d). We observed an increase in a large number of LR-pairs, the majority of which have been reported to play a role in angiogenesis (SEMA-PLXN[27], PTN-SDC3[28], EFN-EPH[29-32], IGF1-IGF1R, GDF11-TGFBR1+ACVR2B[33]), vascular development (CXCL12-CXCR[34], FN1-ITGA[35]), pericyte recruitment to neovasculature (PDGFB-PDGFRB, EDN1-EDNRA), vessel wall stabilization (ANGPT-TEK, JAG/DLL4-NOTCH[36,37]), or generally in pericyte-endothelial cell interaction (TGFB2-TGFBR[38], VEGF-VEGFR[39], ESAM-ESAM[40]). For the two most relevant identified upregulated pathways, ANGPT-TEK and PDGF-PDGFR, we generated heatmaps to visualize the expression of the genes encoding the ligands and receptors in all organoid cell clusters (supplementary Fig. 5a, b). *ANGPT1* was expressed by pericytes and unspecified mural cells, but also by podocytes, which is in accordance with the reported expression in kidney development[41]. *ANGPT2* was expressed by endothelial cells and mural cells. As expected, all receptors for angiopoietins were most highly expressed in endothelial cells. *PDGFB* was strongly expressed by endothelial cells and its receptor *PDGFRB* in mural cells and to a lesser degree in other mesenchymal cell types and several subsets of podocytes.

Inferred interactions with collagens and laminins were broadly upregulated in transplanted organoids, which can play a role in but is not specific for vessel maturation. Also, several upregulated LR-pairs have not been described previously in physiological vascularization, namely *POSTN-ITGAV + ITGB5* (*POSTN* implicated in kidney fibrosis), *PGF-VEGFR1* (mainly described in pathological angiogenesis), *CD99-CD99L2* and *MIF-ACKR3* (involved in neutrophil extravasation and attraction), *JAM3-JAM3* and *NECTIN3-NECTIN2* (part of

endothelial cell tight and adherens junctions) and *LRRC4B-PTPRF* (mainly described in neurons). These could be examples of unwanted effects of transplantation or previously unrecognized physiological interactions. Distinguishing between these would require further investigation.

Finally, to add spatial information to these sequencing data, we performed TEM to evaluate the presence of perivascular stromal cells in transplanted organoids, and identified pericyte-like cells supporting extraglomerular capillaries (Fig. 3e).

Vascularization improves maturation of the kidney organoids

Cell-cell communication is essential for kidney development and maintenance. Interestingly, a comparison of the total number of interactions and interaction strength of all cell clusters between conditions showed a marked decrease in interactions in untransplanted d7+20 organoids compared to all other conditions, suggesting overall loss of cell-cell communication in in vitro culture (supplementary Fig. 2g). To further evaluate the effect of transplantation and vascularization on nephron cell types, we compared late stage transplanted organoids with respective untransplanted controls through DGEA followed by GSEA. This analysis was performed for the late podocyte cluster and tubular epithelial cells (proximal, loop of Henle and distal clusters combined). In transplanted late podocytes, we observed enrichment of gene sets associated with VEGF production, vasculogenesis, organization of cell-cell junctions, and establishment and maintenance of cell polarity (supplementary Fig. 6a, supplementary data 10). This is consistent with the observed vascularization and indicates differentiation of podocytes from immature simple columnar epithelium to a more mature phenotype displaying apicobasal polarity and forming intercellular junctions at their basal side. Interestingly, a gene set associated with positive regulation of collagen biosynthetic processes was also enriched in transplanted podocytes. We hypothesized that this was related to the establishment of a GBM, which in embryonic development is formed by the fusion of two basement membranes produced by both podocytes and ECs. Therefore, we investigated the expression of genes encoding specific collagens, laminins and heparan sulfate proteoglycans (HSPGs) involved in the formation and maturation of the GBM by podocytes in untransplanted and transplanted organoids (Fig. 4a). We observed upregulation of *COL4A3-5* and *LAMB2* in d7+20 transplanted podocytes compared to all other conditions, fitting with the switch from collagen IV α1α2α1 to collagen IV α3α4α5 and from laminin β1 to laminin β2 during GBM maturation. Also, *SULF1*, a regulator of heparan sulfates, is highly expressed in d7+20 transplanted podocytes. *LAMC1* and *AGRN*, encoding laminin γ1 and agrin, a dominant laminin and HSPG in the mature GBM, and *SULF2* are not upregulated in d7+20 transplanted podocytes, implying the GBM in the organoids is not fully matured.

To assess whether glomerular maturation and GBM formation were also detectable at an ultrastructural level, we performed TEM imaging followed by stitching (Fig. 4b, supplementary Fig. 1c). In contrast to traditional TEM, in which only small areas selected based on low-resolution overviews are imaged at higher magnification, this yields large 2D high-resolution virtual slides [18]. After 8 days of transplantation, the invasion of organoid glomerular structures by capillaries containing chicken-derived nucleated erythrocytes and leukocytes had resulted in the rearrangement of podocytes around the capillaries and the deposition of a GBM between the podocytes and ECs. Podocyte cell bodies stretched out along the GBM, cell junctions between adjacent podocytes moved to the basal side of the cells, and primitive foot processes were formed. Rudimentary slit diaphragms were observed between these primitive foot processes. ECs were variable in appearance but generally contained large nuclei surrounded by relatively thick cell bodies, lacking the fenestrations typical for mature human glomeruli (Fig. 4b). Mesangial cells were visible in the stalk of some of the glomeruli, adjacent to the ECs (Fig. 4b). The vascularized glomerular structures were surrounded by a single layer of parietal epithelial-like cells and a clearly distinguishable Bowman's space had appeared between the podocytes and parietal epithelial-like cells (Fig. 4b).

The GSEA for d7+20 transplanted tubular epithelial cells versus untransplanted controls demonstrated enrichment of gene sets associated with establishment and maintenance of cell polarity and of potassium ion transport (supplementary Fig. 6b, supplementary data 11). Since the development of transporters is indispensable for tubular functionality, we evaluated the expression of genes encoding several major tubular transporters in untransplanted and transplanted organoids. We observed upregulation of genes encoding the sodium-potassium pump Na^+/K^+-ATP-ase (*ATP1A1*, *ATP1B1*, *ATP1B3*), the sodium potassium chloride cotransporter NKCC2 (*SLC12A1*) and the renal outer medullary potassium channel ROMK (*KCNJ1*) in d7+20 transplanted organoids compared to the other conditions (Fig. 4c). The expression of *SCNN1A*, which encodes the α-subunit of the epithelial sodium channel (ENaC) in the distal convoluted tubule, connecting tubule and collecting duct, was surprisingly highest in transplanted d7+13 organoids (Fig. 4c). Expression of *SLC12A3* and *AQP2*, encoding the sodium chloride cotransporter (NCC) in the distal convoluted tubule and the water channel aquaporin 2 in the collecting duct, was not detected in any condition, consistent with the lack of clearly distinct distal convoluted tubule and collecting duct cell clusters (Fig. 2a-c). TEM analysis of tubular structures demonstrated that the lumen widened upon transplantation, the epithelial cells formed a monolayer and, in accordance with the GSEA, showed signs of apicobasal polarity with their nuclei moving towards the basolateral membrane. Abundant mitochondria were observed in their cytoplasm, and some of the tubular cells displayed cilia and microvilli, further reflecting ongoing maturation (Fig. 4d and supplementary Fig. 1d).

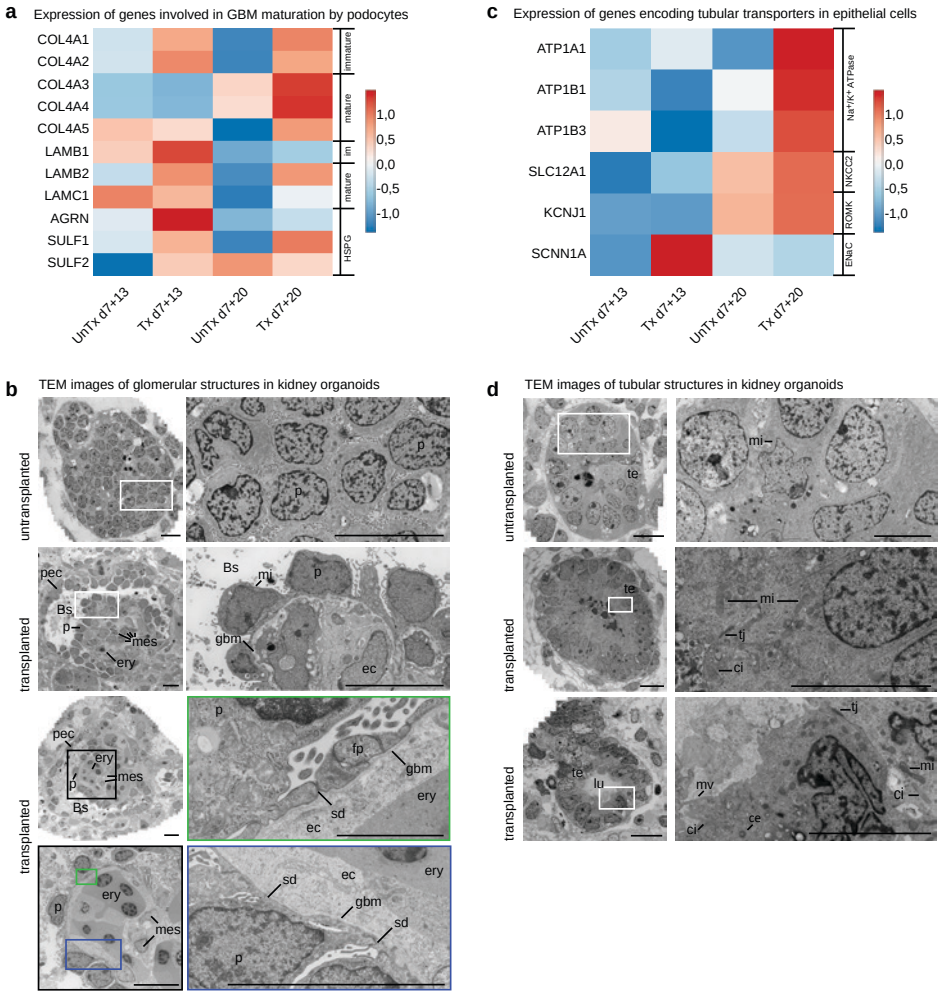

Figure 4: hiPSC-derived kidney organoids mature upon transplantation. a Expression-level scaled heatmap of genes involved in GBM development in podocytes in untransplanted versus transplanted kidney organoids at different timepoints. COL4A3-5 and LAMB2 are upregulated in d7+20 transplanted podocytes compared to all other conditions, fitting with the switch from collagen IV α1α2α1 to collagen IV α3α4α5 and from laminin β1 to laminin β2 during GBM maturation. LAMC1 and AGRN, encoding laminin γ1 and agrin (a heparan sulfate proteoglycan HSPG) in the mature GBM are not upregulated in d7+20 transplanted podocytes, implying the GBM in the organoids is not fully matured. Scale: z-score of the gene expression level. **b** Transmission Electron Microscopy (TEM) imaging displays maturation of glomerular structures upon transplantation for 8 days. Podocyte clusters are invaded with capillaries containing erythrocytes and supported by mesangial cells. Parietal epithelial cells form a Bowman's capsule, a glomerular basement membrane is deposited between the podocytes and endothelial cells, and rudimentary slit diaphragms are formed between primitive foot processes . Magnifications of the boxed areas are displayed, Bs Bowman's space, ec endothelial cell, ery erythrocyte, fp foot process, gbm glomerular basement membrane, leu leukocyte, mes mesangial cell, mi mitochondrion, p podocyte, pec parietal epithelial cell, sd slit diaphragm. Scale bars 10µm. Scale bar magnification marked in green 2µm. **c** Expression-level scaled heatmap of genes encoding tubular transporters in untransplanted versus transplanted kidney organoids at different timepoints. Expression of genes encoding the transporters Na^+/K^+ ATPase, NKCC2 and ROMK are upregulated in transplanted organoids at d7+20. SCNN1A, which encodes the α-subunit

of the ENaC channel, is not upregulated. Scale: z-score of the gene expression level. **d** Upon transplantation for 8 days, tubular structures also show signs of maturation. Tubular epithelial cells have formed a monolayer and their nuclei have moved toward the basolateral side of the cell. Tight junctions, cilia, a centriole, microvilli and abundant mitochondria are visible. ce centriole, ci cilium, lu lumen, mi mitochondrion, mv microvilli, te tubular epithelium, tj tight junction. Scale bars images left row 10μm, scale bars magnifications right row 5μm. TEM Images based on 5 transplanted organoids from 2 experiments using 2 cell lines (MAFB (here)) and LUMC0072 (Fig S3)).

Glomerular morphogenesis to capillary loop stage

To evaluate the 3D organization of glomerular cells and structures in untransplanted and transplanted organoids, we performed SBF-SEM. This technique utilizes an ultramicrotome mounted inside the vacuum chamber of a scanning electron microscope to serially image the block face of a tissue sample, of which ultrathin sections are cut after the generation of each image. The result is a Z-stack of images that allows for the evaluation of the 3D tissue structure as well as ultrastructural analysis at a subcellular level[42]. After generating datasets of 4 untransplanted and 3 transplanted glomerular structures (supplementary movies 1-4), artificial intelligence-based segmentation and annotation was performed on 2 datasets (1 untransplanted and 1 transplanted) (supplementary movies 1,2), followed by manual annotation of cell types, segmentation and 3D visualization (Fig. 5a, supplementary movies 5-6).

The untransplanted glomerular structure consisted of a cluster of podocytes, surrounded by a layer of parietal epithelial-like cells (Fig. 5b, c, supplementary movies 1,5). After 8 days of transplantation, the glomerular structure had become vascularized. A perfused capillary containing erythrocytes as well as leukocytes was clearly visible running along the side of the glomerular structure, before invading it and forming a single loop reaching deep into the center of the glomerulus before exiting it (Fig. 5b, c, supplementary movies 2, 6). The podocytes reorganized into a layer surrounding the capillary and their cell bodies stretched out along the ECs (Fig. 5c). The parietal epithelial-like cells assumed a more flattened morphology and formed a nearly complete capsule around the podocytes (Fig. 5c and supplementary movie 6).

Discussion

In this study, we demonstrate a new model to induce and study vasculogenesis and maturation in hiPSC-derived kidney organoids through transplantation inside the coelomic cavity of chicken embryos. The procedure is easy and efficient, requiring around 5 min per embryo, and provides a scalable alternative to the labor-intensive transplantation in mice. We limited transplantation duration to 8 days in order to sacrifice the embryos on day 12 of incubation, a day before it is believed they start experiencing pain[43,44]. An

extension to a maximum of 15 days is theoretically possible, sacrificing the embryos on day 19 of incubation to avoid hatching. Endogenous organoid-derived ECs which diminish in in vitro culture, thrive upon transplantation, invade glomerular structures and form a chimeric vasculature with invading host-derived endothelium. This implies that organoid vascularization occurs through a combination of vasculogenesis (human, organoid-derived vessels) and angiogenesis (chicken-derived vessels), and is consistent with the main accepted theory that kidney vascularization in embryology depends on angiogenic[45-49] as well as vasculogenic mechanisms[46,50-52]. The ability of organoid-derived endothelium to contribute to the glomerular vasculature after intracoelomic transplantation signifies the absence of unidentified cues for vascularization in in vitro culture conditions. It is well known that the production of VEGF-A by podocytes during embryonic development is essential for recruitment, differentiation and maintenance of glomerular ECs[5,53]. Although it has been demonstrated that organoids in vitro produce VEGF[10], either the levels produced or the concentration gradient within the organoid could be insufficient. The addition of VEGF to organoid culture media, which increases VEGF level but does not establish a gradient, supports EC proliferation, but fails to induce glomerular vascularization[54]. In our transplanted podocytes, we found upregulation of a gene set associated with VEGF production (supplementary Fig. 6a), and gene expression of VEGFA was clearly enhanced in podocytes compared to all other organoid cell clusters (supplementary Fig. 5c) implying that the establishment of a larger VEGF gradient by the podocytes could be a major facilitator of vascularization upon transplantation. Other factors that could play a role are shear stress and hypoxia. Shear stress is an important regulator of EC maturation and establishment of the endothelial glycocalyx[55-57]. The static culture of kidney organoids is therefore likely to be suboptimal for vascular development. Indeed, it has been shown that culturing organoids under flow leads to proliferation of ECs, although invasion of glomerular structures was still rare[58]. However, shear stress in this study was much lower than reported as physiological in embryology[57,59,60] and modifications were made to the culture conditions, such as addition of fetal bovine serum and ECM, which could also have contributed to the observed changes. In embryology, nephron progenitor cells are thought to reside in a hypoxic environment until they are properly vascularized[61-63]. The cells in our organoids, cultured at an air-liquid interface in an incubator with 20% oxygen, are exposed to much higher oxygen levels. The temporary hypoxic conditions they are exposed to in the coelomic cavity of chicken embryos might therefore mimic physiologic conditions more closely. Unfortunately, the number of ECs in our scRNAseq dataset was too small to evaluate the influence of the conditions discussed above on transplanted ECs.

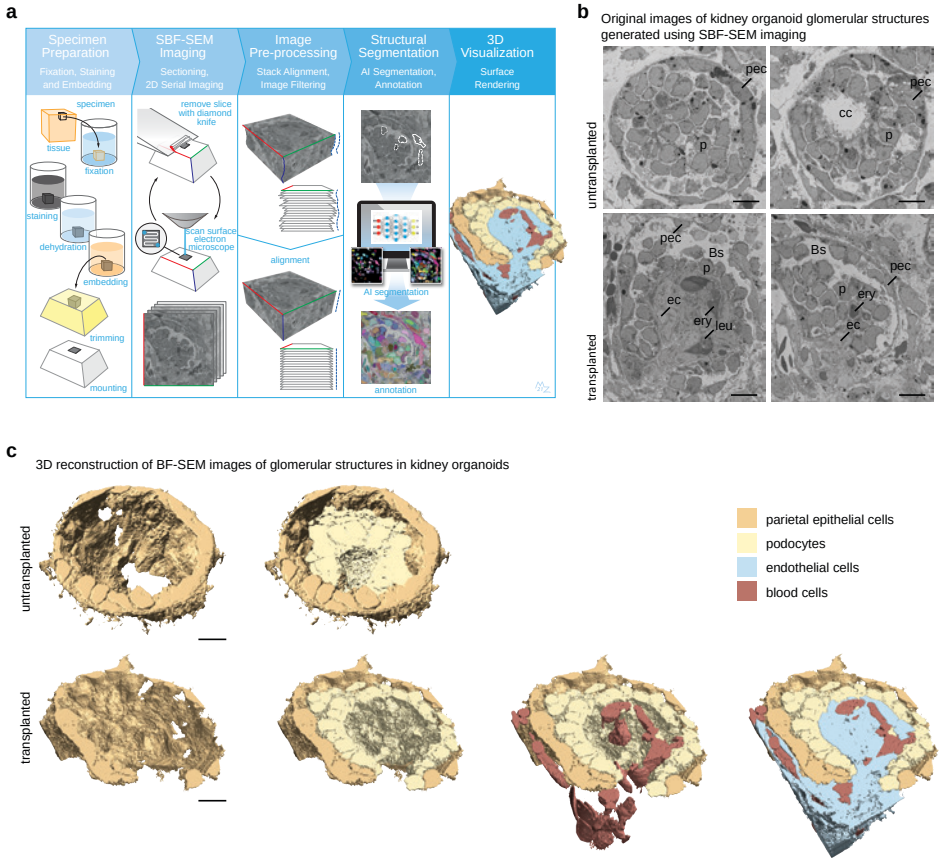

Figure 5: SBF-SEM followed by 3D reconstruction enables analysis of the 3D organization of organoid glomerular structures and reveals maturation to capillary loop stage. a The SBF-SEM imaging workflow comprises five steps. First the specimen is prepared for imaging by chemical fixation, staining with heavy metals, dehydration and embedding in resin, after which it is prepared for imaging by trimming the block and mounting for SEM. SBF-SEM imaging is performed inside the microscope and consists of alternating sectioning and imaging steps, by which a stack of images through the specimen block is generated. Image pre-processing is performed by image alignment and filtering. Segmentation of cell structures, such as nucleus, mitochondria and endoplasmic reticulum was performed by Artificial Intelligence methods followed by manual annotation of cell types. Visualization of images and movies is performed by surface rendering of segmented structures. **b** Images generated by SBF-SEM of glomerular structures in untransplanted (top) and transplanted (bottom) kidney organoids (iPSC-MAFB). For full Z-stacks, see supplementary movies 1, 2. Bs Bowman's space, cc central cavity, ec endothelial cell, ery erythrocyte, leu leukocyte, p podocyte, pec parietal epithelial cell. Scale bar 10µm. **c** 3D reconstruction of the SBF-SEM datasets in A and supplementary movies 1, 2. In the untransplanted glomerular structure (left) a layer of parietal epithelial-like cells (beige) is visible surrounding a cluster of podocytes (yellow) containing a central cavity. In the transplanted glomerular structure (right) a perfused capillary (endothelial cells in blue, blood cells in red) invades the glomerulus and forms a single loop inside the glomerulus. The podocytes (yellow) have reorganized around the capillary and the PECs (beige) have adopted a more flattened phenotype. For 360° view of the 3D reconstructions, see supplementary movies 5, 6. Scale bar 10µm. For SBF-SEM analysis, 2 transplanted organoids and 1 untransplanted organoid, all differentiated from iPSC-MAFB, were used to generate 4 datasets of untransplanted and 3 datasets of transplanted glomerular structures. 2 datasets (1 transplanted and 1 untransplanted) were used for the 3D visualization shown in (c).

Analysis of the effect of transplantation on the cellular composition of kidney organoids revealed an increase in proportion of mesenchymal cells in d7+20 compared to d7+13 organoids, with the highest proportion in transplanted d7+20 organoids. As concerns have been raised about the proliferation of off-target cell types upon transplantation[64], we analyzed the identity of the mesenchymal cells in our organoids. Interestingly, we found a lower percentage of off-target cells and a higher proportion of pericytes / mesangial cells and fibroblasts in transplanted organoids at d7+20 compared to untransplanted controls. This is consistent with the reduction of off-target cell types previously reported upon transplantation in mice[24]. The relatively short duration of transplantation in this paper (14 days) and our model (8 days) may partly explain the lack of proliferation of off-target cell types, but not the observed difference with timepoint-matched in vitro controls. The increase in the pericyte/mesangial cell population upon transplantation is an interesting finding. In the human kidney, pericytes play a role in angiogenesis, blood vessel stabilization and blood pressure regulation and have been implied as a source of mesenchymal stem cells[65]. Mesangial cells are specialized pericytes that interact with glomerular ECs and podocytes to enable glomerular functionality[66]. Through LR network analysis and TEM, we were able to demonstrate that the chimeric neovasculature in transplanted organoids is supported by perivascular stromal cells that interact with the ECs to stabilize and mature the vascular network.

Although the duration of transplantation in our study is relatively short compared to that reported in mouse studies, we observed significant maturation of transplanted organoids. Comparison of our scRNAseq data to different transplantation methods would be very valuable. However, only one dataset of kidney organoids transplanted in mice is currently publicly available[24]. Differences in cell line, differentiation protocol, duration of transplantation and dissociation method between this and our study prevent a fair comparison. Hence, further studies, including direct comparison of kidney organoids submitted to different transplantation methods, would be required to investigate this.

GSEA of the late podocyte cluster and tubular epithelial cells revealed upregulation of genes involved in maturation of the GBM and in the development of tubular transporters upon transplantation. Evaluation of the organoids at an ultrastructural level using TEM image mosaics confirmed the deposition of a GBM between the podocytes and the ECs that invaded the glomerular structures. In addition, it demonstrated maturation of the podocytes with the formation of primitive foot processes and rudimentary slit diaphragms. Mesangial cells had followed the ECs into the glomerular structures, providing support to the glomerular vasculature and enabling the interaction with podocytes and ECs that in in vivo kidneys is required for functionality[66]. Tubular epithelial cells in transplanted organoids

formed a monolayer, displayed signs of apicobasal polarization, and the tubular lumen widened. Through SBF-SEM followed by 3D reconstruction, we evaluated the spatial organization of organoid glomeruli and visualized the trajectory of the vasculature in a transplanted glomerular structure. A single capillary was visible penetrating deep into the glomerular structure and forming a single loop. It had not yet undergone intussusceptive angiogenesis to form a capillary tuft. The podocytes had reorganized around the capillary.

In conclusion, we have developed a new model to efficiently induce and study the development of a stabilized vascular network in kidney organoids through transplantation in the coelomic cavity of chicken embryos, and demonstrate the essential role of vascularization for organoid maturation and glomerular morphogenesis. This scalable model can be used to identify essential early cues for vasculogenesis and maturation of kidney organoids.

Methods

iPSC maintenance and differentiation

hiPSC lines were maintained in Essential 8 medium (E8, Thermo Fisher Scientific) supplemented with 0.5% Penicillin-Streptomycin (Thermo Fisher Scientific) on recombinant human Vitronectin (Thermo Fisher Scientific). All cell lines were mycoplasma free. hiPSCs were passaged twice a week as small clumps using 0.5 mM UltraPure EDTA (Thermo Fisher Scientific). hiPSC reporter MAFB:mTagBFP2 (hiPSC-MAFB)[67], LUMC0072iCTRL01, and LUMC0020iCTRL6.4 lines (Detailed information can be found at https://hpscreg.eu/) were plated as single cells at 15,000 – 25,000 cells / cm^2 one day prior to differentiation using TrypLE Select (Thermo Fisher Scientific) and the addition of RevitaCell Supplement (ThermoFisher Scientific). hiPSCs were incubated from day 0–4 in 8 µM CHIR99021 (R&D Systems) in STEMdiff APEL2 medium (Stem Cell Technologies) supplemented with 1% Protein Free Hybridoma Medium II (PFHMII, Thermo Fisher Scientific) and Antibiotic-Antimycotic solution (Thermo Fisher Scientific). From day 4 – day 7 cells were treated with 200 ng mL^{-1} rhFGF9 (R&D Systems) and 1 µg mL^{-1} heparin (Sigma Aldrich) in APEL2-medium. After an 1 h 5 µM CHIR pulse on day 7, cells were dissociated using Trypsin-EDTA (0.25%, Thermo Fisher Scientific), counted and plated on Transwell 0.4 µM pore polyester membranes as pellets of 500,000 cells. These were cultured on an air-liquid interface for another 5 days in APEL2-medium containing 200 ng mL^{-1} rhFGF9 and 1 µg mL^{-1} heparin (only bottom compartment). For the remaining days, the organoids were cultured in medium without FGF9 and heparin and medium was changed every 2 days. Organoids were maintained on the transwell membranes until transplantation or day 7+20.

Transplantation in chicken embryos

In accordance with Dutch law, approval by the animal welfare committee was not required for these experiments. Fertilized White Leghorn eggs (*Gallus gallus domesticus*, Drost Loosdrecht B.V.) were placed horizontally in a humidified incubator at 37 °C. After 3 days of incubation, a small hole was made in the tip of each egg by tapping it with the sharp end of a pair of dissecting scissors (Hammacher Karl, HAMMHSB391-10), and 2–3 mL of albumen was removed using a syringe with a 19 gauge needle to lower the embryo inside the egg. A window was then cut into the egg shell using dissecting scissors. 2–3 drops of DPBS with calcium and magnesium (Thermo Fisher Scientific) were added to the egg to avoid dehydration before sealing the window and the hole in the tip of the egg with transparent tape (Tesa 4120). The window was made a day prior to transplantation, because we found that the chorioallantoic membrane as well as the embryo have frequently become attached to the egg shell by day 4 of incubation, leading to bleeding and embryo death when attempting to create a window at this timepoint. On day 4 of incubation (Hamburger Hamilton stage 23), kidney organoids on day 7+11 or day 7+12 of differentiation were bisected with a surgical knife and half an organoid was transplanted inside the coelomic cavity of each chicken embryo (Fig, 1a)[22]. Bisection of the organoids was necessary because the coelomic cavity is not large enough to accommodate a whole organoid at this stage of development. Transplantation was performed by creating a small hole in the chorion and amnion membrane with forceps (Hammacher Karl, HAMMHTC090-11), and inserting the bisected organoid through this hole and the opening in the body wall that is still present at this stage of development into the coelom using a blunt instrument (Fig. 1b). The eggs were resealed with transparent tape and further incubated for a maximum of 8 days until the end of the experiment. The whole process of transplantation takes about 5 min per egg, allowing for transplantation in up to 100 chicken embryos per person per day. Since maintenance of the embryos before and after transplantation only requires a humidified incubator, this does not limit the number of embryos used for transplantation. On day 5 and day 12 (respectively 1 and 8 days after transplantation) of incubation, the chicken embryos were sacrificed and the organoids harvested. To enable analysis of the vasculature, some of the embryos were carefully injected with 20 µL of 2,5 mg mL^{-1} rhodamine labelled *lens culinaris agglutinin* (LCA) (RL-1042, Vector Laboratories) [23] in the vitelline vein using a glass microcapillary needle before being sacrificed. The injected lectin was allowed to circulate for 10 min before these embryos were sacrificed. For the timeline experiment (supplementary Fig. 4b), the volume of injected LCA was adjusted based on the age of the embryos: 10µL was injected in day 5-7 embryos, 12µL in day 8-9 embryos, 15µL in day 10 embryos and 20µL in day 11 embryos. To retrieve the organoids, the abdominal wall of the embryos was opened along the longitudinal axis using forceps

under a stereo microscope. Organoids were localized based on tissue morphology and removed using micro scissors and a surgical knife.

Immunofluorescence analysis

Organoids in vitro were fixed in 2% paraformaldehyde (PFA) at 4°C for 20 min. Transplanted organoids were fixed using 4% PFA at 4°C overnight and thoroughly washed with PBS. They were used for whole mount staining. Non-transplanted organoids or transplanted tissues were permeabilized and blocked in 0.3% TritonX in PBS containing 10% donkey serum for 2 h. Primary antibodies were diluted in blocking solution and incubated 24–72 h. Upon washing, secondary antibodies were incubated for 2–4 h at room temperature. Kidney organoids were characterized for NPHS1 (AF4269, dilution 1:100), CD31 (555444, dilution 1:100), ECAD (610181, dilution 1:300), LTL-biotin (B-1325, dilution 1:300), and PDGFRβ (MAB1263, dilution 1:50). Primary antibodies were detected with donkey-α-sheep Alexa Fluor 568 (A-21099, dilution 1:500) and 647 (A-21448, dilution 1:500), donkey-α-mouse Alexa Fluor 405 (ab175658, dilution 1:500) and 488 (A-212-02, dilution 1:500), streptavidin Alexa Fluor 532 (S11224, dilution 1:200) and 647 (S21374, dilution 1:200) (supplementary data 12). All antibodies and isotype controls were validated in human kidney samples. Nuclei were stained with Hoechst33258 (Thermo Fisher Scientific) and tissues embedded in ProLong Gold Antifade Mountant (Thermo Fisher Scientific) in 35 mm glass bottom dishes (MatTek corporation) or adhesive microscope slides (StarFrost, Knittel glass). Leica White Light Laser Confocal Microscope TCS SP8 using LAS-X Image software with 3D module (Leica) was used for analysis of the tissues.

Quantification of CD31 positive endothelial cells

Quantification of CD31 positive endothelial cells was performed in whole mount half or whole untransplanted and transplanted organoids at d7+19-20. Imaris Software was used to calculate the volume of CD31 positive cells as a percentage of whole organoid volume. To select the organoid tissue, a surface was generated manually by drawing a contour around the organoids every 5 slides of the Z-stack. This surface was used to calculate the volume of the organoid with the statistics function in Imaris. Next, a surface was created for the CD31 channel and the volume of this surface was obtained in the same manner. In case of transplanted organoids with high background signal in the surrounding chicken tissue, a mask was created for the CD31 channel based on the previously generated organoid surface. This masked CD31 channel was then used to create a surface and calculate the CD31 volume. Threshold and minimum number of voxels for CD31 surface generation were set separately for each sample, to be able to

correct for differences in background and if necessary, background falsely identified as endothelial cells by the software was removed manually. This analysis was performed for 6 untransplanted organoids, all from different differentiation batches (3 from iPSC-MAFB, 3 from LUMC0072) and 6 matched transplanted organoids. Graphpad Prism 9.0.1 was used for statistical analysis. Means were compared between groups using an unpaired two-tailed t-test. Normality of the distribution was tested and confirmed using the Shapiro-Wilk and Kolmogorov-Smirnov test. Individual data points and mean (SD) are presented.

Single cell RNA sequencing sample preparation

Untransplanted and transplanted (on day 7+12) organoids from the same differentiation of the hiPSC-MAFB line were dissociated to single cells at day 7+13 and d7+20 using a collagenase I buffer consisting of 600U ml^{-1} collagenase Type I (Worthington) and 0,75U ml^{-1} DNAse (Sigma Aldrich) in HBSS with calcium and magnesium (Thermo Fisher Scientific) followed by a TrypLE buffer consisting of 5U ml^{-1} DNAse I (Sigma Aldrich) and 4µg ml^{-1} heparin (Sigma Aldrich) in 80% TrypLE select 10x (Thermo Fisher Scientific) in DPBS (Thermo Fisher Scientific). 5 organoids were placed in Collagenase I buffer and incubated in a water bath at 37°C for 40 min with repeated pipetting. The cell suspensions were centrifuged at 300G and the cell pellet was incubated at 37°C for another 5 min in TrypLE buffer. The dissociation was stopped by adding cold HBSS+/+ with 10% FCS, and the suspension further diluted with HBSS+/+. The single cell suspension was centrifuged at 400G and the cell pellet was resuspended in PBS+0,1% BSA. All cells from organoids from the same condition were pooled (d7+13 untransplanted: 94 organoids, transplanted: 75 bisected organoids (transplanted in 150 chicken embryos) d7+20 untransplanted: 95 organoids, transplanted: 46,5 bisected organoids (transplanted in 93 chicken embryos)) and 30mL of PBS + 0,1%BSA was added to enable cell counting. The single cell suspensions were converted to barcoded scRNA-seq libraries with a targeted cell recovery of 9000 cells/condition using the Chromium Single Cell 3' v3 Library, Gel Bead & Multiplex Kit and Chip Kit (10x Genomics).

Deep sequencing and data pre-processing

The scRNA-seq libraries were converted into DNA nanoballs (DNB) using a standard circularization protocol optimized for the DNBSEQ-T7 sequencer, and all subsequent steps were carried out following the standard operation procedure, as previously described[68,69]. The scRNA-seq libraries were sequenced aiming for at least 50,000 reads/cells, and using 28+100+8 bp paired-end sequencing to determine (1) the cell barcode and UMI, (2) the transcript and (3) the sample index, respectively. Demultiplexing according to the

sample barcodes, and subsequent read alignment were performed using Cell Ranger (10x Genomics, v3.1.0). For untransplanted kidney organoid samples, reads were aligned to human genome (GRCh38) only. For transplanted kidney organoid samples, a combined genome including human (GRCh38) and chicken (GRCg6a) genomes, was prepared using the *mkgtf* and *mkref* commands from Cell Ranger (10X genomics), following 10X genomics instructions. Reads associated to these samples were then aligned to this reference. Key sequencing metrics are summarized in supplementary data 1.

Raw unfiltered data matrices from the Cell Ranger output were then further processed with R (v4.1.1) and Seurat package (v4.0.4). For multi-species samples, the percentage of genes belonging to each species was determined using the *PercentageFeatureSet* function from Seurat package, and cells were labelled either “human” or “chicken” when >85% of total genes were mapped to the respective species, whereas ambiguous cells (unlabeled) were discarded. Cells from multi-species samples were then segregated per species for downstream processing, resulting in both a human and a chicken dataset, for each transplanted kidney organoid sample. The following quality control steps were performed for each dataset: (i) genes expressed by less than 10 cells were removed; (ii) cells that expressed fewer than 600 genes (for human datasets) and 200 genes (for chicken datasets) were discarded as low-quality cells (supplementary data 1); (iii) cells with a detected number of genes exceeding a “doublet” threshold as listed in supplementary data 1 were excluded (determined by inspecting the cell frequency per total number of genes expressed, for each sample); (iv) cells with a fraction of mitochondrial genes >15% (for human datasets) and >5% (for chicken datasets) were also removed (cells with compromised cell membrane/dying or dead cells). After pre-processing, human cells-containing samples were merged as well as chicken cells-containing samples, resulting in 24,988 human cells (27,349 human cells before removal of dying/dead cells), and in 8018 chicken cells (8279 chicken cells before removal of dying/dead cells).

ScRNAseq data analysis

Data were normalized using the *NormalizeData* function from Seurat Package, and the top 2,000 highly variable genes were identified using *FindvariableFeatures*. Data were scaled with the *Scaledata* function and reduced with principal component (PC) analysis using *RunPCA* function. The top 30 PCs (40 PCs for chicken cells) were used for visualization using uniform manifold approximation and projection (UMAP) with the *RunUMAP* function as implemented in Seurat. Next, a shared nearest-neighbor graph (SNN) was determined using *FindNeighbors* function, and used to calculate clusters with the *FindClusters* function. Top marker genes were calculated with the *Findallmarkers* function using default settings.

Remaining low-quality cell and doublet clusters were characterized by a low number of genes expressed per cell, and an overlap of different cell type markers with high number of genes expressed per cell, respectively, and removed from the dataset. High-quality cells were split according to condition (transplantation & timepoint) and aligned using *Seurat* integration tool: *FindintegrationAnchors* and *IntegrateData* functions, with 2000 anchors and 40 PCs as settings. Clustering was performed as described above using 40 PCs and main cell types for human and chicken datasets were identified. For the human dataset, nephron cell (*NPHS1, NPHS2, MFAB, WT1, EPCAM, KRT19, …*) and mesenchymal cell clusters (*COL1A1, COL1A2, COL3A1, TAGLN, PDGFRA,* …) were subsetted using the *subset* function for more in-depth analysis. Briefly, for both the mesenchymal and nephron cell clusters, 2000 highly variable genes were identified and data were integrated per condition (transplantation & timepoint) using 2,000 anchors and 40 PCs as settings, as described above. Integrated data were further scaled, reduced within 40 PCs that were further used for UMAP visualization, and clustering, as described above. Upregulated markers were identified using the *FindAllMarkers* function including genes for which Log2FC>0 only, and using other parameters as default. Cluster identity was determined according to cell-(sub)type specific top marker genes: podocyte markers as *MAFB, NPHS1, NPHS2, WT1*, epithelial cell markers as *EPCAM* and *KRT19* for tubular epithelial cells, and fibroblast markers as *COL1A1, COL1A2, COL3A1*, smooth muscle cell markers as *ACTA2*, *TAGLN*, *MYL9*, pericyte/mesangial cell markers as *REN, GATA3, PDGFRB*, mesenchymal progenitor markers as *PRRX1 and PRRX2*, neural-like cell markers as *NTREK2, METRN, GAP43, STMN2,* chondrocyte-like cell markers as *COL9A1, COL9A2, COL9A3, MATN4*, and melanocyte-like cell markers as *PMEL, MITF, MLANA*. As for the chicken cells, the following markers were used to identify clusters: erythroid cells (*HBA1, HBAD, HBE1*), megakaryocytes (*GP9, ITGB3, GP1BB*), endothelial cells (*PECAM1, CDH5, PROX1*), macrophages (*CD74, C1QB*), granulocytes (*DEFB4A, AvBD1*), lymphoid cells (*CD3D, IGLL1*), fibroblasts (*COL3A1, COL14A1*), pericytes (*KCNJ8, RGS5, ABCC9*), smooth muscle cells (*ACTA2, TAGLN, ACTG2*), hepatic stellate cells (*COLEC11, HGF*), epithelioid cells (*KRT24, KRT1*), hepatocytes (*ALB, FGB, FGG*), Leydig cells (*CYP11A1, STAR, HSD3B1*), Sertoli cells (*AMH, SOX9*), Schwann cells (*NRN1, SOX10, CRYAB*) and neurons (*GAP43, NEFM, NSG1*). Proliferative cell clusters were identified as either within G1/S phases or G2/M phases according to canonical marker genes, as listed in Seurat.

Dot plot and heatmap visualization

All dotplots were prepared using *DotPlot* function as implemented in Seurat. All heatmaps were prepared with BIOMEX software (v1.5 - https://carmelietlab.sites.vib.be/en/biomex)[70], except heatmaps displaying gene expression of ligand and receptors,

which were prepared with the ComplexHeatmap package (v2.11.1) in R. For heatmaps prepared in BIOMEX, briefly, count data matrix was exported from the Seurat object using the *GetAssayData* function (selected assay "RNA") and uploaded in BIOMEX altogether with the corresponding metadata information. Data were normalized ("Standard" parameter) and (auto)scaled for heatmap visualization within BIOMEX. Cluster-averaged gene expression was used to account for cell-to-cell transcriptomic stochastics. Top marker gene heatmaps were prepared including uniquely upregulated genes resulting from the marker gene identification tool from BIOMEX. For heatmaps prepared with the ComplexHeatmap package, briefly, the averaged expression profiles per each cluster and for all genes were calculated using the *AverageExpression()* function from Seurat package. Next, scaled data were obtained from the RNA assay using *GetAssayFunction()* function and selected gene data were extracted from the resulting matrix. These values were used as input for the *Heatmap()* function from the ComplexHeatmap package.

Cluster similarity analysis

Hierarchical clustering was performed with BIOMEX using highly variable genes as identified in BIOMEX, with Euclidean distance and complete linkage. The confidence of each branch of the tree was estimated by the bootstrap resampling approach from the R-package *pvclust* [71], using a confidence score of > 0.05. Number of bootstrapping was set at 1,000.

Metadata quantification

Metadata from the Seurat object were exported, as described above and uploaded in BIOMEX. Metadata were quantified and visualized using the metadata quantification tool, as implemented in BIOMEX. "barplots" was used as plot setting.

Differential gene expression analysis (DGEA)

For DGEA according to the transplantation condition, the *FindMarkers* function from Seurat was used on the "RNA" assay. Differential expression was run with the MAST package. The number of UMIs per cell was used as latent variable to correct for unequal sequencing depth between cells.

Geneset enrichment analysis (GSEA)

DGEA outputs were used for GSEA using the *ClusterProfiler* package (v4.0.5). GSEA was performed on gene ontology genesets (biological processes only) with *gseGO*

function, as implemented in *ClusterProfiler*. Genesets including less than 10 genes were not included. All other parameters were used as default. In order to remove as much as possible redundant terms, results were simplified using the online Revigo tool (http://revigo.irb.hr) for both significantly up- and down-regulated genesets with Normalized Enrichment Scores used as ranking method. The resulting list was aimed to be small (selected 0.5 parameter). Output from Revigo was exported and plotted using *ggplot* function, as implemented within the *ggplot2* package (v3.3.5).

Ligand/Receptor interaction analysis (L/R analysis)

For L/R analysis, *CellChat* package (v1.1.3) was used. First, the melanocyte-like cluster was removed from the analysis since it was absent from the transplanted d7+20 kidney organoid condition. The normalized data matrix "data" slot, from the "RNA" assay within the Seurat object was extracted for each condition (d7+20 condition, and the other conditions as pooled, or taken separately for the comparison of the total number of interactions and interaction probabilities between the four conditions) using *GetAssayData()* function from the Seurat package. The metadata containing final cluster identities were extracted as a data frame. Data and metadata were used to create CellChat objects using *createCellChat()* function. The complete human cellchat database was used. Expression data was subsetted to genes present in the database using *subsetData()* function and overexpressed genes and interactions were identified for each condition with *identifyOverExpressedGenes()* and *identifyOverExpressedInteractions()* functions, respectively. Communication probabilities and inference of the cellular communication network were calculated using *computeCommunProb()*, *computeCommunProbPathway()*, *aggregateNet()* and *netAnalysis_computeCentrality()* functions. Cellchat objects were merged with the dedicated *mergeCellChat()* function. Comparison of the total number of interaction and interaction strength was performed using *compareInteraction()* function setting the "measure" argument as "weight" when appropriate. The *netVisual_heatmap()* function, setting the "measure" argument as "weight", was used to generate a heatmap of differential interaction strength between cell populations. To identify the up-regulated signaling ligand-receptor pairs between ECs and pericytes/mesangial cells, we compared the communication probabilities between conditions and visualized the results as a dot plot using the *netVisual_bubble()* function, with "max.dataset" argument set as "2".

Transmission Electron Microscopy (TEM)

For morphological analysis, small sections of in vitro kidney organoids and transplanted organoids were fixed for 2 h at room temperature in 1.5% glutaraldehyde (Electron

Microscopy Sciences) in 0.1M sodium cacodylate buffered solution (pH 7.4). The tissues were further rinsed with sodium cacodylate buffer and fixed in a solution of 1% osmium tetroxide (Electron Microscopy Sciences) in 0.1M sodium cacodylate buffer for 1 h on ice. Afterwards, samples were washed with sodium cacodylate buffer and dehydrated in a series of 70%, 80%, 90% and 100% ethanol. The probes were infiltrated with a mixture of 1:1 Epon LX-112 (Ladd Research) and propylene oxide (Electron Microscopy Sciences) for 1 h, followed by infiltration with pure Epon for 2h. Subsequently, the samples were embedded in pure Epon, mounted in BEEM capsules (Agar Scientific) and polymerized for 48 h at 60 °C. Ultrathin sections (100 nm) were collected onto copper slot grids (Storck Veco B.V.), covered with formvar film and a 7 nm carbon layer. The sections were contrasted with an aqueous solution of 7% uranyl acetate for 20 min, followed by Reynolds lead citrate for 10 min. The imaging was performed at an acceleration voltage of 120 kV with a FEI Tecnai G^2 Spirit BioTWIN transmission electron microscope (FEI), equipped with an Eagle 4K slow-scan charge-coupled device (CCD) camera (FEI). Data were collected at 18,500x magnification, corresponding to a 1.2 nm pixel size at the specimen level. Large virtual slides showing glomerular structures were acquired using automated large-scale data collection combined with stitching software.[18] These extensive digital images provide an overview of entire glomeruli and the possibility to zoom in to high detail, allowing for qualitative analysis.

Serial Block Face Scanning Electron Microscopy (SBF-SEM)

For SBF-SEM analysis, 2 transplanted organoids and 1 untransplanted organoid, all generated using iPSC-MAFB were used. Kidney organoid fixation, staining and embedding was done according to an adapted protocol from Deerink et al.[72] Samples were fixed for 2 h on ice with 2.5% glutaraldehyde and 2% paraformaldehyde (Electron Microscopy Sciences) in 0.15M sodium cacodylate buffer containing 2mM calcium chloride. A first post-fixation step was performed for 1 h on ice, using a solution of 2% osmium tetroxide and 1.5% potassium ferrocyanide in 0.15M sodium cacodylate buffer containing 2mM calcium chloride. Subsequently samples were treated for 20 min at room temperature with 1% aqueous solution of thiocarbohydrazide, followed by 2% aqueous osmium tetroxide for 30 min at room temperature and incubated overnight at 4 °C in a 1% aqueous solution of uranyl acetate. The probes were then stained for 30 min at 60 °C, using Walton's lead aspartate, and dehydrated in series of 20% up to 100% ethanol, followed by dehydration in anhydrous acetone. Tissue samples were infiltrated in mixtures of 1:3, 1:1, 3:1 Durcupan ACM resin (Ladd Research) and acetone, in 2 h steps, then overnight at room temperature in 100% Durcupan. A final infiltration step with fresh

Durcupan was performed for 2 h at room temperature. The samples were then placed in BEEM capsules, embedded in Durcupan and polymerized for 48 h at 60 °C. Sample blocks were trimmed and 300 nm thick sections were cut and stained with toluidine blue for light microscopy to find regions of interest containing glomerular structures. For SBF-SEM, small blocks of approximately 800 x 800 x 400 µm were trimmed and glued on aluminum pins (Gatan) using Conductive Silver Epoxy Kit (Agar Scientific), then coated with a thin layer of gold right before imaging. A data set from transplanted and non-transplanted organoid was collected on a GeminiSEM 300 microscope (ZEISS) equipped with a 3View 2XP system (Gatan). The SEM was operated at a chamber pressure of 5 Pa, in variable pressure mode, using an acceleration voltage of 1.6 kV and the 60 µm aperture. Back-scattered electron images were acquired using the OnPoint BSE detector (Gatan). 4 datasets were generated of untransplanted glomerular structures and 3 of transplanted glomerular structures, of which 2 (1 untransplanted and 1 transplanted) were used for 3D visualization. The data set from the non-transplanted organoid was acquired at 10,000x magnification, with a pixel size of 9 nm, a dwell time of 2.8 µs and a 50 nm slice thickness. The sample size was 61 x 61 x 28 µm, and the image size 6,800 x 6,800 pixels x 557 slices. The data set from the transplanted kidney organoid was acquired at 9,000x magnification, a pixel size of 10 nm, a dwell time of 1.5 µs and a 60 nm slice thickness. The sample size was 65 x 75 x 27 µm, and the image size 6,500 x 7,500 pixels x 451 slices. SBF-SEM image stacks were acquired as dm4 files and aligned using Digital Micrograph software (Gatan).

Annotation and Visualization of SBF-SEM data

2 SBF-SEM datasets (1 untransplanted and 1 transplanted) were annotated using artificial intelligence-based image segmentation by Ariadne (Ariadne-Service GmbH). In short, nuclei, extracellular space (ECS), and plasma membrane labels were predicted using a convolutional neural network (CNN) architecture based on the U-Net. [73] Stochastic weight averaging was used in the ER prediction. [74] Somata were segmented by running the watershed algorithm on the plasma membrane probability map, using the predicted nucleus locations as seeds and excluding the ECS regions. CNNs were implemented in the ELEKTRONN deep learning library (www.elektronn.org). Image stacks of segmented structures (~12 Gb or ~25 Gb in size) were binned (in X and Y) using Fiji [75] or IMOD [76] to decrease the file size, and converted to mrc stacks and the headers were corrected using IMOD. Cell types were annotated by hand according to morphology and location and surfaces were smoothed, simplified and visualized using AMIRA 3D software for life sciences (Thermo-Fisher Scientific). Surfaces were imported into Cinema4D (Maxon) for final rendering using Redshift (Maxon).

Data availability

Both raw and processed sequencing data are available in ArrayExpress under accession number E-MTAB-11429. Other data are available from the authors upon request.

Code availability statement

Custom code is available upon reasonable request.

Acknowledgements

We are grateful to Christian Freund (hiPSC core facility, LUMC, Leiden, the Netherlands) for providing hiPSC lines (LUMC0072 and LUMC0020), and Melissa Little (Murdoch Children's Research Institute, Melbourne, Australia) for iPSC-MAFB. We acknowledge the support of Saskia van der Wal-Maas (Department of Anatomy & Embryology, LUMC, Leiden, the Netherlands), Conny van Munsteren (Department of Anatomy & Embryology, LUMC, Leiden, the Netherlands), Manon Zuurmond (LUMC, Leiden, the Netherlands), George Galaris (LUMC, Leiden, the Netherlands), and Annemarie de Graaf (LUMC, Leiden, the Netherlands).

References

1 Taguchi, A. et al. Redefining the in vivo origin of metanephric nephron progenitors enables generation of complex kidney structures from pluripotent stem cells. Cell Stem Cell ***14***, 53–67 (2014). https://doi.org/10.1016/j.stem.2013.11.010

2 Morizane, R. et al. Nephron organoids derived from human pluripotent stem cells model kidney development and injury. Nat Biotechnol ***33***, 1193–1200 (2015). https://doi.org/10.1038/nbt.3392

3 Takasato, M. et al. Kidney organoids from human iPS cells contain multiple lineages and model human nephrogenesis. Nature ***526***, 564–568 (2015). https://doi.org/10.1038/nature15695

4 Freedman, B. S. et al. Modelling kidney disease with CRISPR-mutant kidney organoids derived from human pluripotent epiblast spheroids. Nat Commun ***6***, 8715 (2015). https://doi.org/10.1038/ncomms9715

5 Eremina, V. et al. Glomerular-specific alterations of VEGF-A expression lead to distinct congenital and acquired renal diseases. J Clin Invest ***111***, 707–716 (2003). https://doi.org/10.1172/JCI17423

6 Kitamoto, Y., Tokunaga, H. & Tomita, K. Vascular endothelial growth factor is an essential molecule for mouse kidney development: glomerulogenesis and nephrogenesis. J Clin Invest ***99***, 2351–2357 (1997). https://doi.org/10.1172/JCI119416

7 Sison, K. et al. Glomerular structure and function require paracrine, not autocrine, VEGF-VEGFR-2 signaling. J Am Soc Nephrol ***21***, 1691–1701 (2010). https://doi.org/10.1681/ASN.2010030295

8 Sharmin, S. et al. Human Induced Pluripotent Stem Cell-Derived Podocytes Mature into Vascularized Glomeruli upon Experimental Transplantation. J Am Soc Nephrol ***27***, 1778–1791 (2016). https://doi.org/10.1681/ASN.2015010096

9 Bantounas, I. et al. Generation of Functioning Nephrons by Implanting Human Pluripotent Stem Cell-Derived Kidney Progenitors. Stem Cell Reports ***10***, 766–779 (2018). https://doi.org/10.1016/j.stemcr.2018.01.008

10 van den Berg, C. W. et al. Renal Subcapsular Transplantation of PSC-Derived Kidney Organoids Induces Neo-vasculogenesis and Significant Glomerular and Tubular Maturation In Vivo. Stem Cell Reports ***10***, 751–765 (2018). https://doi.org/10.1016/j.stemcr.2018.01.041

11 van den Berg, C. W., Koudijs, A., Ritsma, L. & Rabelink, T. J. In Vivo Assessment of Size-Selective Glomerular Sieving in Transplanted Human Induced Pluripotent Stem Cell-Derived Kidney Organoids. J Am Soc Nephrol ***31***, 921–929 (2020). https://doi.org/10.1681/ASN.2019060573

12 Garreta, E. et al. Fine tuning the extracellular environment accelerates the derivation of kidney organoids from human pluripotent stem cells. Nat Mater ***18***, 397–405 (2019). https://doi.org/10.1038/s41563-019-0287-6

13 Jankovic, B. D. et al. Immunological capacity of the chicken embryo. I. Relationship between the maturation of lymphoid tissues and the occurrence of cell-mediated immunity in the developing chicken embryo. Immunology ***29***, 497–508 (1975).

14 Alkie, T. N. et al. Development of innate immunity in chicken embryos and newly hatched chicks: a disease control perspective. Avian Pathol ***48***, 288–310 (2019). https://doi.org/10.1080/03079457.2019.1607966

15 Hamburger, V. Morphogenetic and axial self-differentiation of transplanted limb primordia of 2-day chick embryos. Journal of Experimental Zoology ***77***, 379–399 (1938).

16 Rawles, M. E. Transplantation of normal embryonic tissues. Ann N Y Acad Sci ***55***, 302–312 (1952).

17 Rawles, M. E. The Development of Melanophores from Embryonic Mouse Tissues Grown in the Coelom of Chick Embryos. Proc Natl Acad Sci U S A ***26***, 673–680 (1940).

18 Faas, F. G. et al. Virtual nanoscopy: generation of ultra-large high resolution electron microscopy maps. J Cell Biol ***198***, 457–469 (2012). https://doi.org/10.1083/jcb.201201140

19 Dossel, W. E. New method of intracoelomic grafting. Science ***120***, 262–263 (1954).

20 Takasato, M., Er, P. X., Chiu, H. S. & Little, M. H. Generation of kidney organoids from human pluripotent stem cells. Nat Protoc ***11***, 1681–1692 (2016). https://doi.org/10.1038/nprot.2016.098

21 Ryan, A. R. et al. Vascular deficiencies in renal organoids and ex vivo kidney organogenesis. Dev Biol ***477***, 98–116 (2021). https://doi.org/10.1016/j.ydbio.2021.04.009

22 Hamburger, V. & Hamilton, H. L. A series of normal stages in the development of the chick embryo. 1951. Dev Dyn ***195***, 231–272 (1992). https://doi.org/10.1002/aja.1001950404

23 Jilani, S. M. et al. Selective binding of lectins to embryonic chicken vasculature. J Histochem Cytochem ***51***, 597–604 (2003).

24 Subramanian, A. et al. Single cell census of human kidney organoids shows reproducibility and diminished off-target cells after transplantation. Nat Commun ***10***, 5462 (2019). https://doi.org/10.1038/s41467-019-13382-0

25 Carmeliet, P. Angiogenesis in health and disease. Nat Med ***9***, 653–660 (2003). https://doi.org/10.1038/nm0603-653

26 Dejana, E. Endothelial cell-cell junctions: happy together. Nat Rev Mol Cell Biol ***5***, 261–270 (2004). https://doi.org/10.1038/nrm1357

27 Gu, C. & Giraudo, E. The role of semaphorins and their receptors in vascular development and cancer. Exp Cell Res ***319***, 1306–1316 (2013). https://doi.org/10.1016/j.yexcr.2013.02.003

28 Brunskill, E. W. & Potter, S. S. Changes in the gene expression programs of renal mesangial cells during diabetic nephropathy. BMC Nephrol ***13***, 70 (2012). https://doi.org/10.1186/1471-2369-13-70

29 Kida, Y., Ieronimakis, N., Schrimpf, C., Reyes, M. & Duffield, J. S. EphrinB2 reverse signaling protects against capillary rarefaction and fibrosis after kidney injury. J Am Soc Nephrol ***24***, 559–572 (2013). https://doi.org/10.1681/ASN.2012080871

30 Gerety, S. S. & Anderson, D. J. Cardiovascular ephrinB2 function is essential for embryonic angiogenesis. Development ***129***, 1397–1410 (2002). https://doi.org/10.1242/dev.129.6.1397

31 Foo, S. S. et al. Ephrin-B2 controls cell motility and adhesion during blood-vessel-wall assembly. Cell ***124***, 161–173 (2006). https://doi.org/10.1016/j.cell.2005.10.034

32 Salvucci, O. & Tosato, G. Essential roles of EphB receptors and EphrinB ligands in endothelial cell function and angiogenesis. Adv Cancer Res ***114***, 21–57 (2012). https://doi.org/10.1016/B978-0-12-386503-8.00002-8

33 Lu, L. et al. Growth Differentiation Factor 11 Promotes Neurovascular Recovery After Stroke in Mice. Front Cell Neurosci ***12***, 205 (2018). https://doi.org/10.3389/fncel.2018.00205

34 Takabatake, Y. et al. The CXCL12 (SDF-1)/CXCR4 axis is essential for the development of renal vasculature. J Am Soc Nephrol ***20***, 1714–1723 (2009). https://doi.org/10.1681/ASN.2008060640

35 Astrof, S. & Hynes, R. O. Fibronectins in vascular morphogenesis. Angiogenesis ***12***, 165–175 (2009). https://doi.org/10.1007/s10456-009-9136-6

36 Kofler, N. M., Cuervo, H., Uh, M. K., Murtomaki, A. & Kitajewski, J. Combined deficiency of Notch1 and Notch3 causes pericyte dysfunction, models CADASIL, and results in arteriovenous malformations. Sci Rep ***5***, 16449 (2015). https://doi.org/10.1038/srep16449

37 Kofler, N. M. et al. Notch signaling in developmental and tumor angiogenesis. Genes Cancer ***2***, 1106–1116 (2011). https://doi.org/10.1177/1947601911423030

38 Armulik, A., Genove, G. & Betsholtz, C. Pericytes: developmental, physiological, and pathological perspectives, problems, and promises. Dev Cell ***21***, 193–215 (2011). https://doi.org/10.1016/j.devcel.2011.07.001

39 Darland, D. C. et al. Pericyte production of cell-associated VEGF is differentiation-dependent and is associated with endothelial survival. Dev Biol ***264***, 275–288 (2003). https://doi.org/10.1016/j.ydbio.2003.08.015

40 Kosyakova, N. et al. Differential functional roles of fibroblasts and pericytes in the formation of tissue-engineered microvascular networks in vitro. NPJ Regen Med ***5***, 1 (2020). https://doi.org/10.1038/s41536-019-0086-3

41 Woolf, A. S., Gnudi, L. & Long, D. A. Roles of angiopoietins in kidney development and disease. J Am Soc Nephrol ***20***, 239–244 (2009). https://doi.org/10.1681/ASN.2008020243

42 Denk, W. & Horstmann, H. Serial block-face scanning electron microscopy to reconstruct three-dimensional tissue nanostructure. PLoS Biol ***2***, e329 (2004). https://doi.org/10.1371/journal.pbio.0020329

43 ACUC. ACUC Guideline: The Use and Euthanasia Procedures of Chicken/Avian Embryos., <https://www.cpp.edu/research/research-compliance/iacuc/docs/iacuc-guidelines-on-euthanasia-of-chicken-and-embryos.pdf> (2012).

44 Aleksandrowicz, E. & Herr, I. Ethical euthanasia and short-term anesthesia of the chick embryo. ALTEX ***32***, 143–147 (2015). https://doi.org/http://dx.doi.org/10.14573/altex.1410031

45 Munro, D. A. D., Hohenstein, P. & Davies, J. A. Cycles of vascular plexus formation within the nephrogenic zone of the developing mouse kidney. Sci Rep ***7***, 3273 (2017). https://doi.org/10.1038/s41598-017-03808-4

46 Hyink, D. P. et al. Endogenous origin of glomerular endothelial and mesangial cells in grafts of embryonic kidneys. Am J Physiol ***270***, F886–899 (1996). https://doi.org/10.1152/ajprenal.1996.270.5.F886

47 Rogers, S. A. & Hammerman, M. R. Transplantation of rat metanephroi into mice. Am J Physiol Regul Integr Comp Physiol ***280***, R1865–1869 (2001). https://doi.org/10.1152/ajpregu.2001.280.6.R1865

48 Takeda, S., Rogers, S. A. & Hammerman, M. R. Differential origin for endothelial and mesangial cells after transplantation of pig fetal renal primordia into rats. Transpl Immunol ***15***, 211–215 (2006). https://doi.org/10.1016/j.trim.2005.10.003

49 Dekel, B. et al. Human and porcine early kidney precursors as a new source for transplantation. Nat Med ***9***, 53–60 (2003). https://doi.org/10.1038/nm812

50 Robert, B., St John, P. L., Hyink, D. P. & Abrahamson, D. R. Evidence that embryonic kidney cells expressing flk-1 are intrinsic, vasculogenic angioblasts. Am J Physiol ***271***, F744–753 (1996). https://doi.org/10.1152/ajprenal.1996.271.3.F744

51 Sims-Lucas, S. et al. Endothelial Progenitors Exist within the Kidney and Lung Mesenchyme. PLoS One ***8***, e65993 (2013). https://doi.org/10.1371/journal.pone.0065993

52 Loughna, S. et al. A molecular and genetic analysis of renalglomerular capillary development. Angiogenesis ***1***, 84–101 (1997). https://doi.org/10.1023/A:1018357116559

53 Bartlett, C. S., Jeansson, M. & Quaggin, S. E. Vascular Growth Factors and Glomerular Disease. Annu Rev Physiol ***78***, 437–461 (2016). https://doi.org/10.1146/annurev-physiol-021115-105412

54 Czerniecki, S. M. et al. High-Throughput Screening Enhances Kidney Organoid Differentiation from Human Pluripotent Stem Cells and Enables Automated Multidimensional Phenotyping. Cell Stem Cell ***22***, 929–940 e924 (2018). https://doi.org/10.1016/j.stem.2018.04.022

55 Arora, S., Lam, A. J. Y., Cheung, C., Yim, E. K. F. & Toh, Y. C. Determination of critical shear stress for maturation of human pluripotent stem cell-derived endothelial cells towards an arterial subtype. Biotechnol Bioeng ***116***, 1164–1175 (2019). https://doi.org/10.1002/bit.26910

56 Arisaka, T. et al. Effects of shear stress on glycosaminoglycan synthesis in vascular endothelial cells. Ann N Y Acad Sci ***748***, 543–554 (1995). https://doi.org/10.1111/j.1749-6632.1994.tb17359.x

57 Adamo, L. et al. Biomechanical forces promote embryonic haematopoiesis. Nature ***459***, 1131–1135 (2009). https://doi.org/10.1038/nature08073

58 Homan, K. A. et al. Flow-enhanced vascularization and maturation of kidney organoids in vitro. Nat Methods ***16***, 255–262 (2019). https://doi.org/10.1038/s41592-019-0325-y

59 Gautam, M., Shen, Y., Thirkill, T. L., Douglas, G. C. & Barakat, A. I. Flow-activated chloride channels in vascular endothelium. Shear stress sensitivity, desensitization dynamics, and physiological implications. J Biol Chem ***281***, 36492–36500 (2006). https://doi.org/10.1074/jbc.M605866200

60 Buchanan, C. F., Verbridge, S. S., Vlachos, P. P. & Rylander, M. N. Flow shear stress regulates endothelial barrier function and expression of angiogenic factors in a 3D microfluidic tumor vascular model. Cell Adh Migr ***8***, 517–524 (2014). https://doi.org/10.4161/19336918.2014.970001

61 Hemker, S. L., Sims-Lucas, S. & Ho, J. Role of hypoxia during nephrogenesis. Pediatr Nephrol ***31***, 1571–1577 (2016). https://doi.org/10.1007/s00467-016-3333-5

62 Gerosa, C. et al. Low vascularization of the nephrogenic zone of the fetal kidney suggests a major role for hypoxia in human nephrogenesis. Int Urol Nephrol ***49***, 1621–1625 (2017). https://doi.org/10.1007/s11255-017-1630-y

63 Rymer, C. et al. Renal blood flow and oxygenation drive nephron progenitor differentiation. Am J Physiol Renal Physiol ***307***, F337–345 (2014). https://doi.org/10.1152/ajprenal.00208.2014

64 Nam, S. A. et al. Graft immaturity and safety concerns in transplanted human kidney organoids. Exp Mol Med ***51***, 145 (2019). https://doi.org/10.1038/s12276-019-0336-x

65 Shaw, I., Rider, S., Mullins, J., Hughes, J. & Péault, B. Pericytes in the renal vasculature: roles in health and disease. Nat Rev Nephrol ***14***, 521–534 (2018). https://doi.org/10.1038/s41581-018-0032-4

66 Vaughan, M. R. & Quaggin, S. E. How do mesangial and endothelial cells form the glomerular tuft? J Am Soc Nephrol ***19***, 24–33 (2008). https://doi.org/10.1681/ASN.2007040471

67 Vanslambrouck, J. M. et al. A Toolbox to Characterize Human Induced Pluripotent Stem Cell-Derived Kidney Cell Types and Organoids. J Am Soc Nephrol (2019). https://doi.org/10.1681/ASN.2019030303

68 Huang, J. et al. A reference human genome dataset of the BGISEQ-500 sequencer. Gigascience ***6***, 1–9 (2017). https://doi.org/10.1093/gigascience/gix024

69 Korostin, D. et al. Comparative analysis of novel MGISEQ-2000 sequencing platform vs Illumina HiSeq 2500 for whole-genome sequencing. PLoS One ***15***, e0230301 (2020). https://doi.org/10.1371/journal.pone.0230301

70 Taverna, F. et al. BIOMEX: an interactive workflow for (single cell) omics data interpretation and visualization. Nucleic Acids Res ***48***, W385–W394 (2020). https://doi.org/10.1093/nar/gkaa332

71 Suzuki, R. & Shimodaira, H. Pvclust: an R package for assessing the uncertainty in hierarchical clustering. Bioinformatics ***22***, 1540–1542 (2006). https://doi.org/10.1093/bioinformatics/btl117

72 Deerinck, T. J., Bushong, E. A., Thor, A. & Ellisman, M. H. NCMIR Methods for 3D EM: a new protocol for preparation of biological specimens for serial block face scanning electron microscopy. . (National Center for Microscopy and Imaging Research (NCMIR), La Jolla, CA,, NCMIR, 2010).

73 Ronneberger, O., Fischer, P. & Brox, T. in Medical Image Computing and Computer-Assisted Intervention (MICCAI) Vol. 9351 234 –241 (Springer, 2015).

74 Izmailov, P., Podoprikhin, D., Garipov, T., Vetrov, D. & Wilson, A. G. Averaging weights leads to wider optima and better generalization. 876–885 (Association For Uncertainty in Artificial Intelligence (AUAI), 2018).

75 Schindelin, J. et al. Fiji: an open-source platform for biological-image analysis. Nat Methods ***9***, 676–682 (2012). https://doi.org/10.1038/nmeth.2019

76 Kremer, J. R., Mastronarde, D. N. & McIntosh, J. R. Computer visualization of three-dimensional image data using IMOD. J Struct Biol ***116***, 71–76 (1996). https://doi.org/10.1006/jsbi.1996.0013

Supplementary Figures

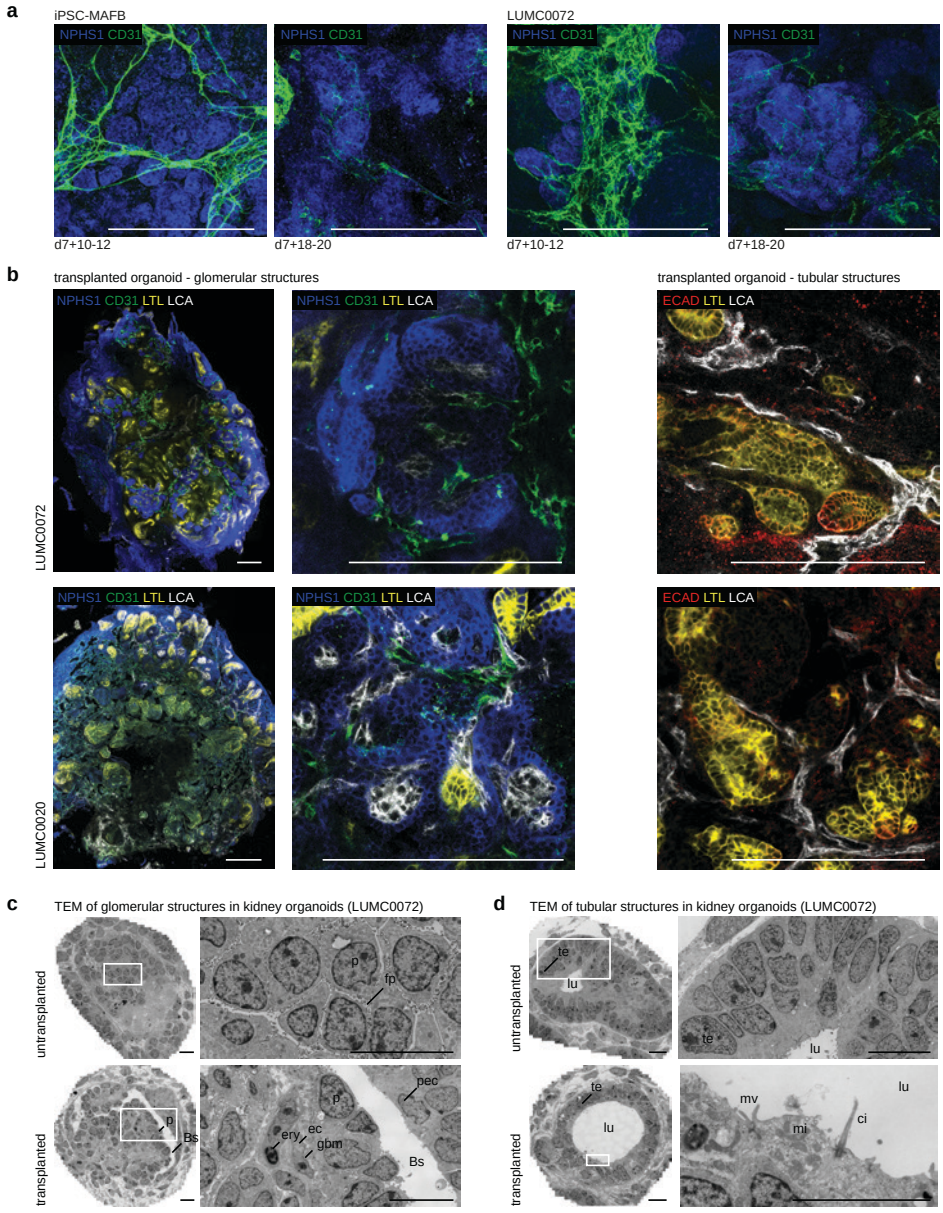

Supplementary figure 1: Vascularization of untransplanted and transplanted kidney organoids in multiple cell lines. a Maximum projection images of Z-stacks of untransplanted kidney organoids derived from hiPSC-MAFB and LUMC0072 at d7+10-12 and d7+18-20 of differentiation. Endothelial cells are more abundant at the earlier time point. Scalebar 200µm. **b** Kidney organoids derived from LUMC0072 and LUMC0020 are vascularized upon transplantation for 8 days. Glomerular structures (NPHS1+, blue) are invaded by perfused capillaries (LCA+, white and CD31+, green) and proximal (LTL+, yellow) and distal (ECAD+, red) tubular structures are aligned by them. Scalebar 200µm. **c** TEM imaging of kidney organoids derived from LUMC0072 demonstrates increased maturation

of glomerular structures upon transplantation for 8 days. Podocyte clusters are invaded with capillaries containing erythrocytes, parietal epithelial cells form a Bowman's capsule, a glomerular basement membrane is deposited between the podocytes and endothelial cells. Bs Bowman's space, ec endothelial cell, ery erythrocyte, fp foot process, gbm glomerular basement membrane, p podocyte, pec parietal epithelial cell. Scalebar 10μm. **d** TEM imaging of kidney organoids derived from LUMC0072 demonstrates increased maturation of tubular structures. Tubular epithelial cells have formed a monolayer and their nucleus has moved toward the basolateral side of the cell. A wide tubular lumen is visible. Cilia, microvilli and abundant mitochondria are visible. ci cilium, lu lumen, mi mitochondrion, mv microvilli, te tubular epithelium. Scalebar untransplanted overview and magnification and transplanted overview 10μm. Scalebar transplanted magnification 5μm.

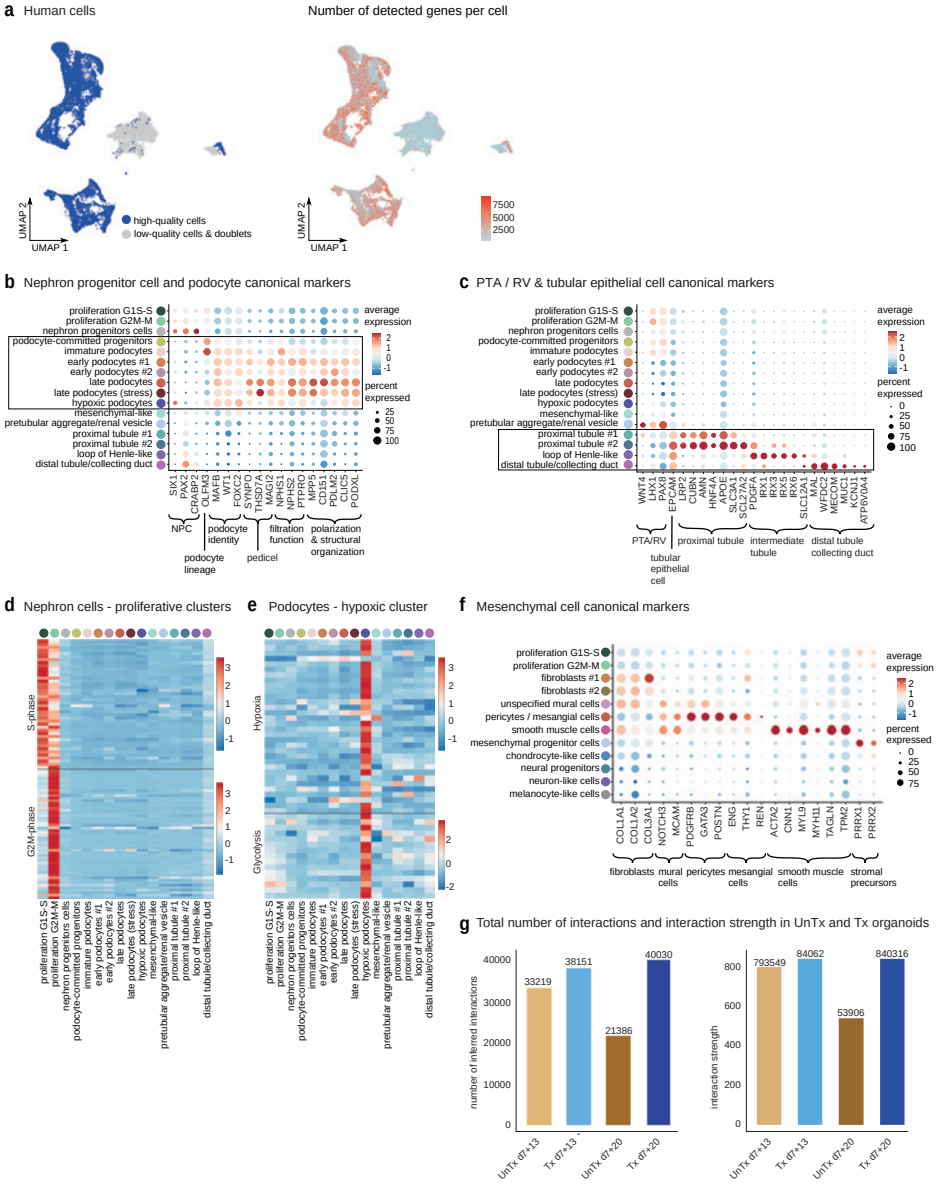

Supplementary figure 2: Selection of high quality organoid cells and subclustering of nephron and mesenchymal cell types. a UMAP visualization of (left) all human cells and selection of high-quality cells (high-quality cells: blue, low-quality cells and doublets: grey), and (right) number of detected genes per cell. **b** Dot plot of canonical nephron progenitor cell (NPC) and podocyte markers used to characterize podocyte cluster identity. Dot size indicates proportion of cells in cluster expressing a gene, colour intensity indicates the level of expression. **c** Dot plot of canonical renal vesicle / pretubular aggregate (RV/PTA) and tubular epithelial cell markers used to characterize tubular epithelium cluster identity. Dot size indicates proportion of cells in cluster expressing a gene, colour intensity indicates the level of expression. **d** Expression-level scaled heatmap of S-phase and G2M-phase genes, upregulated in nephron proliferation clusters. Scale: z-score of the gene expression level. **e** Expression-level scaled heatmap of hypoxia and glycolysis-related genes, upregulated in the hypoxic podocytes clusters. Scale: z-score of the gene expression level. **f** Dot plot of canonical mesenchymal cell markers used

to characterize cluster identity. Dot size indicates proportion of cells in cluster expressing a gene, colour intensity indicates the level of expression. **g** Bar plot of the total number of inferred interactions (left) and total interaction strength (right) in transplanted and untransplanted organoids at different timepoints (d7+13 and d7+20).

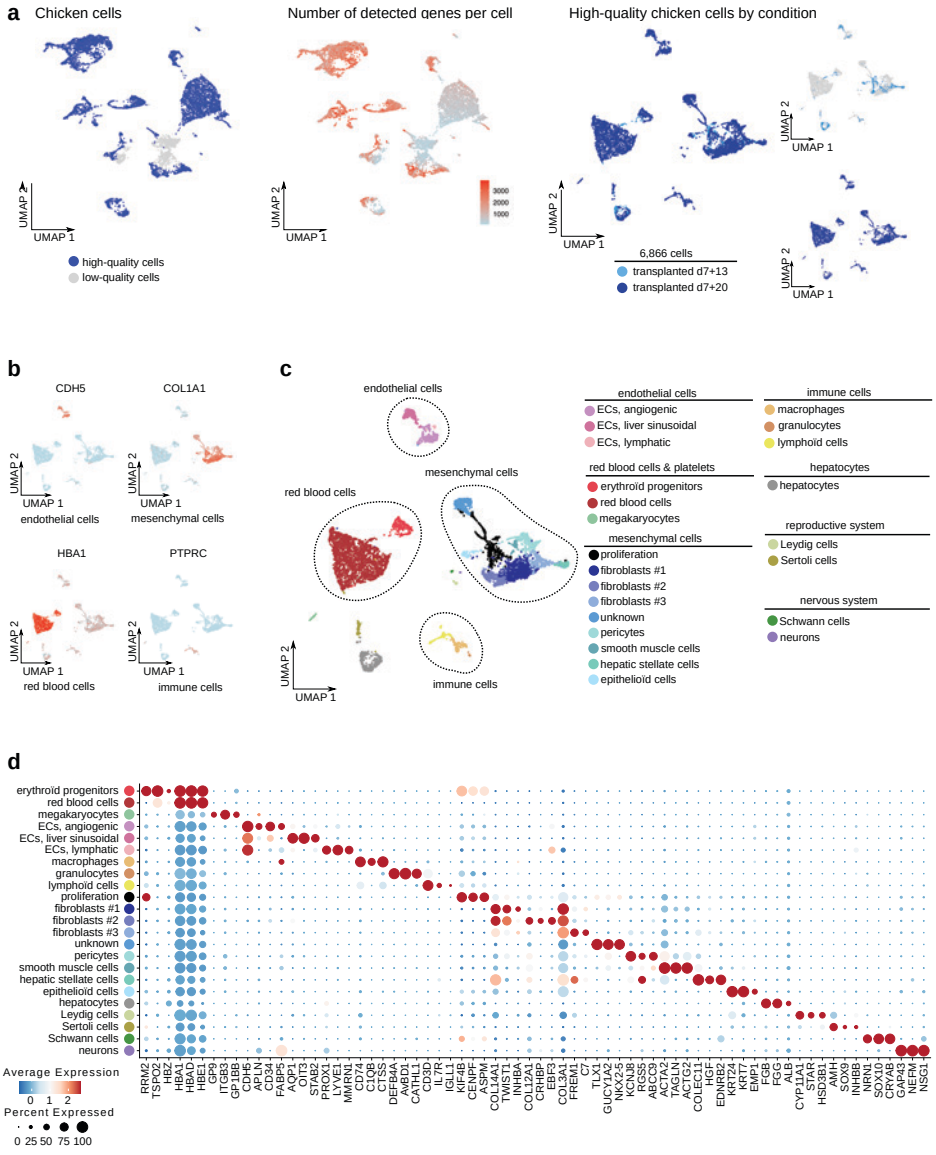

Supplementary figure 3: Selection and subclustering of high-quality chicken cells. a UMAP visualization of all chicken cells color-coded by (left) cell quality (high= blue, low= grey), (middle) number of detected genes per cell. (Right) UMAP visualization of a total of 6,866 high-quality chicken cells from transplanted kidney organoids color-coded by timepoint condition (857 cells from d7+13, 6,009 cells from d7+20). Note that these cells are partly derived from the organoid itself and partly from chicken tissue attached to the organoid. **b** UMAP visualization of all high-quality chicken cells, color-coded by the expression level of CDH5, COL1A1, HBA1, and PTPRC genes, canonical markers

for endothelial cells, mesenchymal cells, red blood cells and immune cells (red: high expression level, blue: low expression level). **c** UMAP visualization of all high-quality chicken cells, color-coded by identified chicken cell clusters: endothelial cells (n=3 clusters), red blood cells & platelets (n=3 clusters), mesenchymal cells (n=9 clusters), immune cells (n=3 clusters), hepatocyte (n=1 cluster), cells from the reproductive system (n=2 clusters) and cells from the nervous system (n=2 clusters). **d** Dot plot representing canonical marker gene expression in chicken cell clusters. Dot size indicates proportion of cells in cluster expressing a gene, colour intensity indicates the level of expression.

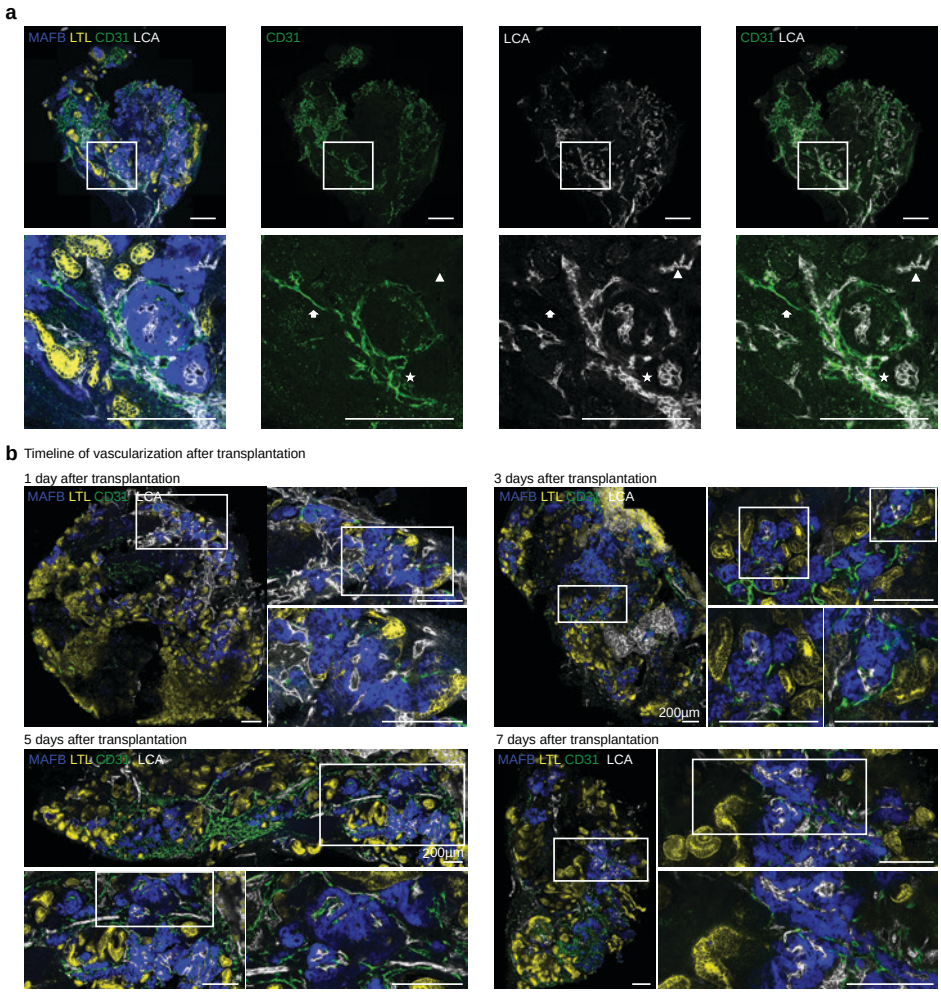

Supplementary figure 4: Origin of endothelial cells and timeline of vascularization. a Combined staining for human CD31 (green) and injected LCA (white) demonstrates the presence of an extensive perfused vascular network in transplanted organoids d7+19-20. Three types of blood vessels can be distinguished: perfused human organoid derived endothelial cells, (CD31+, LCA+) unperfused human organoid derived endothelial cells (CD31+, LCA-), and perfused chicken derived endothelial cells (CD31-, LCA+). Examples are marked in the magnifications of the boxed areas by a star (perfused human), arrow (unperfused human), and arrowhead (perfused chicken). Scalebar 200µm. **b** Timeline demonstrating the rapid vascularization of kidney organoids upon transplantation. On day 1 after transplantation, blood vessels have entered the organoid, but not the glomerular structures. On day 3, some glomerular structures have become vascularized, which increases markedly on day 5 and 7 after transplantation. Magnifications of the boxed areas are displayed. Scalebar 200µm.

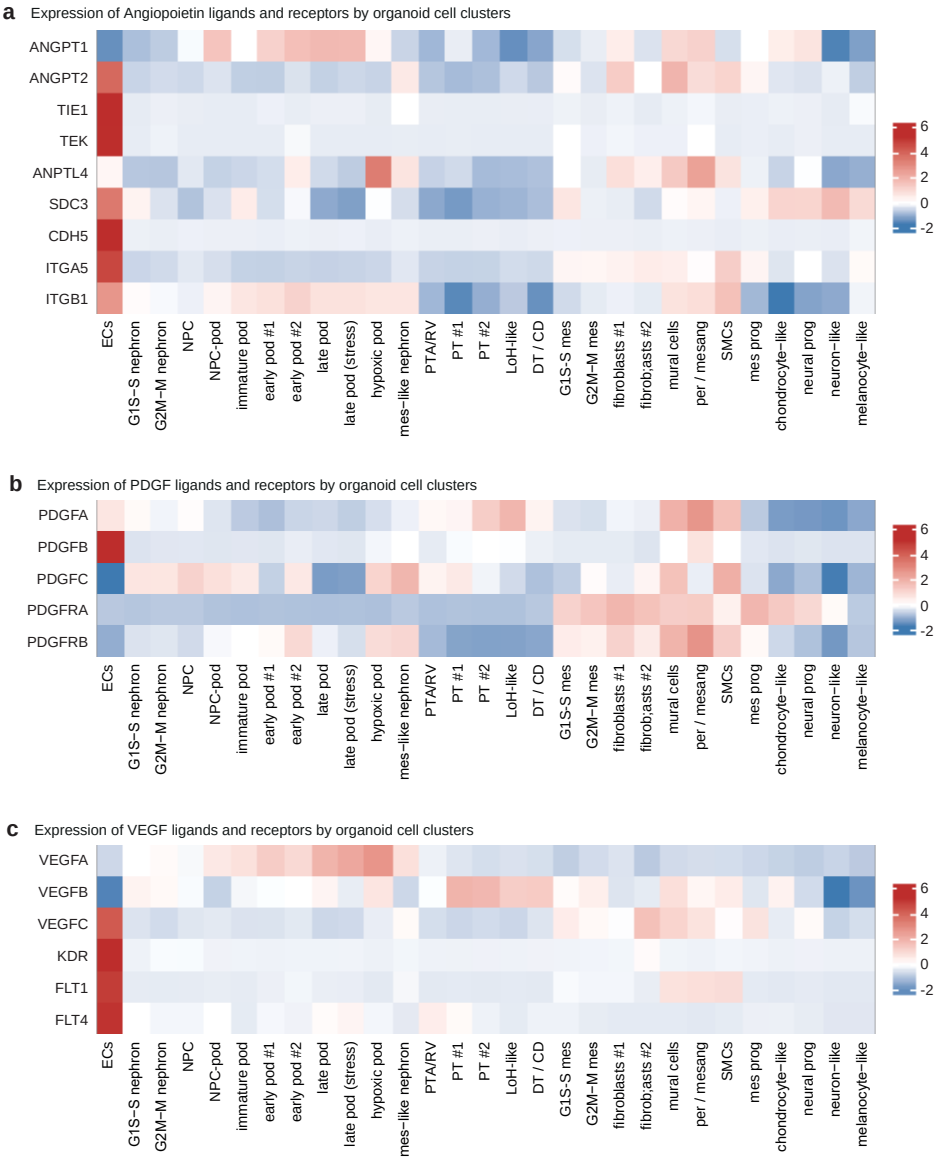

Supplementary figure 5: Gene expression of ANGPT, PDGF and VEGF ligands and receptors. **a** Expression-level scaled heatmap of genes encoding angiopoietin ligands and receptors in organoid cell clusters (cells from all conditions pooled). Scale: z-score of the gene expression level. **b** Expression-level scaled heatmap of genes encoding PDGF ligands and receptors in organoid cell clusters (cells from all conditions pooled). Scale: z-score of the gene expression level. **c** Expression-level scaled heatmap of genes encoding VEGF ligands and receptors in organoid cell clusters (cells from all conditions pooled). Scale: z-score of the gene expression level.

a
GSEA Late podocyte cluster transplanted d7+20 vs untransplanted d7+20
feeding behavior
positive regulation of cytosolic calcium ion concentration involved in phospholipase C−activating G protein−coupled signaling pathway
regulation of synapse assembly
heterophilic cell−cell adhesion via plasma membrane cell adhesion molecules
vasculogenesis
somite development
phospholipase C−activating G protein−coupled receptor signaling pathway
inositol lipid−mediated signaling
phosphatidylinositol−mediated signaling
receptor signaling pathway via JAK−STAT
positive regulation of vascular endothelial growth factor production
receptor signaling pathway via STAT
regulation of fibroblast growth factor receptor signaling pathway
secondary palate development
positive regulation of collagen biosynthetic process
positive chemotaxis
cell−cell junction organization
endothelial cell apoptotic process
platelet−derived growth factor receptor signaling pathway
negative regulation of translation
regulation of protein maturation
striated muscle cell proliferation
heat generation
peptidyl−tyrosine phosphorylation
response to prostaglandin E
positive regulation of tyrosine phosphorylation of STAT protein
protein localization to cell−cell junction
ovulation cycle process
negative regulation of lymphocyte proliferation
establishment or maintenance of cell polarity
intermediate filament cytoskeleton organization
roof of mouth development
cellular response to glucose starvation
regulation of protein processing
interleukin−6−mediated signaling pathway
detection of biotic stimulus
intermediate filament−based process
regulation of heat generation
negative regulation of leukocyte apoptotic process
chromatin assembly
organ growth
negative regulation of stem cell differentiation
trans−synaptic signaling modulating synaptic transmission
regulation of DNA recombination
establishment of cell polarity
mRNA transport
cellular response to inorganic substance
protein processing
protein localization to nucleus
rhythmic process
protein autophosphorylation
regulation of DNA metabolic process
positive regulation of cell migration
regulation of cell−cell adhesion
wound healing
regulation of GTPase activity
0.0
0.5
1.0
1.5
NES

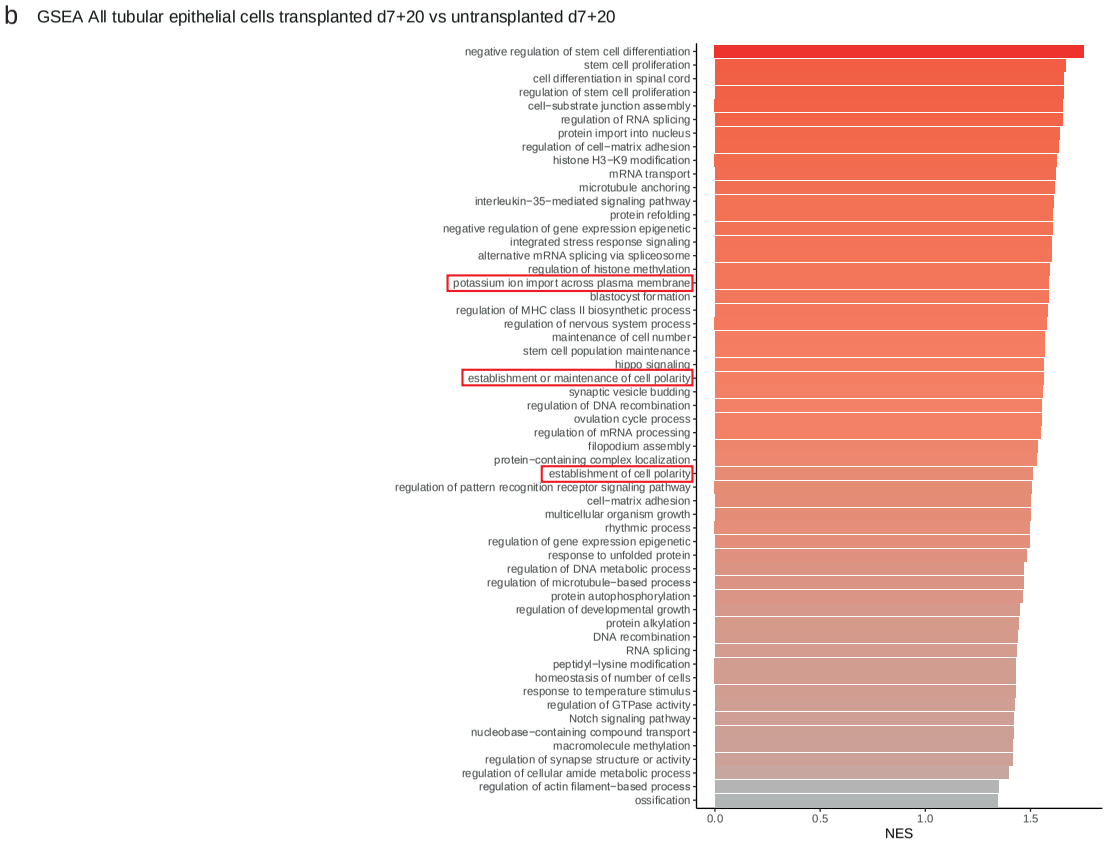

Supplementary figure 6: Gene set enrichment analysis podocytes and tubular epithelial cells. a Gene set enrichment analysis (GSEA) for late podocyte cluster in transplanted d7+20 versus untransplanted d7+20 organoids. NES: normalized enrichment score. **b** Gene set enrichment analysis (GSEA) for all tubular epithelial cells in transplanted d7+20 versus untransplanted d7+20 organoids. NES: normalized enrichment score.

Supplementary tables and movies can be accessed through the following QR code:

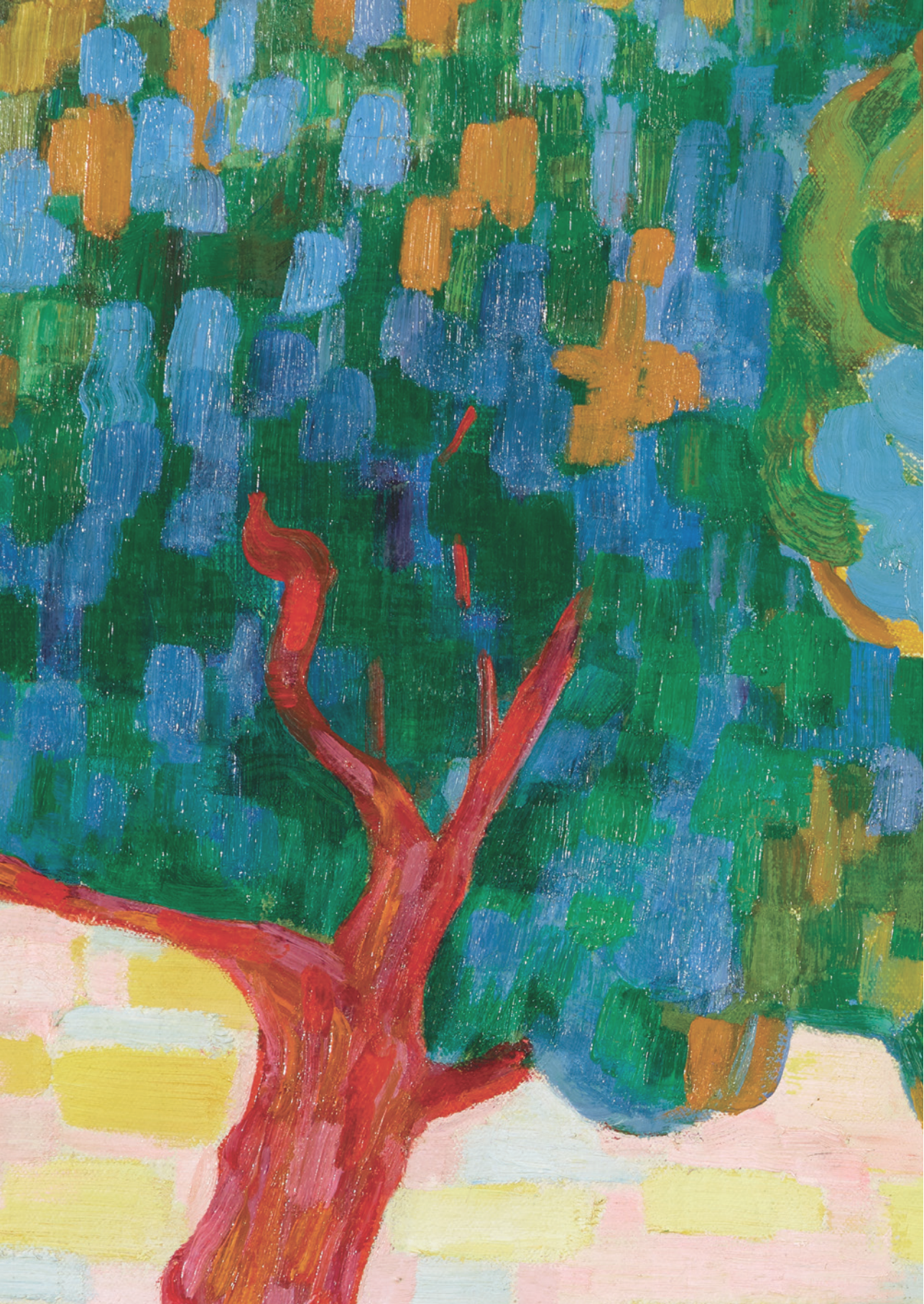

CHAPTER 5

Efficient vascularization of kidney organoids through intracoelomic transplantation in chicken embryos

M. Koning, E. Lievers, T. Jaffredo, C.W. van den Berg, A.J. Rabelink

Journal of Visualized Experiments, 2023

Abstract

Kidney organoids derived from human induced pluripotent stem cells contain nephron-like structures that resemble those in the adult kidney to a certain degree. Unfortunately, their clinical applicability is hampered by the lack of a functional vasculature and consequently limited maturation in vitro. The transplantation of kidney organoids in the coelomic cavity of chicken embryos induces vascularization by perfused blood vessels, including the formation of glomerular capillaries, and enhances their maturation. This technique is very efficient, allowing for the transplantation and analysis of large numbers of organoids. This paper describes a detailed protocol for the intracoelomic transplantation of kidney organoids in chicken embryos, followed by the injection of fluorescently labeled lectin to stain the perfused vasculature, and the collection of transplanted organoids for imaging analysis. This method can be used to induce and study organoid vascularization and maturation to find clues for enhancing these processes in vitro and improve disease modeling.

Introduction

Human induced pluripotent stem cell (hiPSC)-derived kidney organoids have been shown to have potential for developmental studies[1-4], toxicity screening[5,6], and disease modeling[5,7-13]. However, their applicability for these and eventual clinical transplantation purposes is limited by the lack of a vascular network. During embryonic kidney development, podocytes, mesangial cells, and vascular endothelial cells (ECs) interact to form the intricate structure of the glomerulus. Without this interaction, the glomerular filtration barrier, consisting of podocytes, the glomerular basement membrane (GBM), and ECs cannot develop properly[14-16]. Although kidney organoids in vitro do contain some ECs, these fail to form a proper vascular network and diminish over time[17]. It is therefore not surprising that the organoids remain immature. Transplantation in mice induces vascularization and maturation of kidney organoids[18-21]. Unfortunately, this is a labor-intensive process that is unsuitable for the analysis of large numbers of organoids.

Chicken embryos have been used to study vascularization and development for over a century[22]. They are easily accessible, require low maintenance, lack a fully functional immune system, and can develop normally after opening the eggshell[23-26]. The transplantation of organoids on their chorioallantoic membrane (CAM) has been shown to lead to vascularization[27]. However, the duration of transplantation on the CAM, as well as the level of maturation of the graft, are limited by CAM formation, which takes until embryonic day 7 to complete. Therefore, a method was recently developed to efficiently vascularize and mature kidney organoids through intracoelomic transplantation in chicken embryos[28]. The coelomic cavity of chicken embryos has been known since the 1930s to be a favorable environment for the differentiation of embryonic tissues[29,30]. It can be accessed early in embryonic development and allows for relatively unlimited expansion of the graft in all directions.

This paper outlines a protocol for the transplantation of hiPSC-derived kidney organoids in the coelomic cavity of day 4 chicken embryos. This method induces vascularization and enhanced maturation of the organoids within 8 days. Injection of fluorescently labeled lens culinaris agglutinin (LCA) prior to sacrificing the embryos enables visualization of perfused blood vessels within the organoids through confocal microscopy.

Protocol

In accordance with Dutch law, approval by the animal welfare committee was not required for this research.

1. Preparing hiPSC-derived kidney organoids for transplantation

1. Differentiate hiPSCs to kidney organoids using the protocol developed by Takasato et al.[4,18,31]. Culture the organoids following this protocol on polyester cell culture inserts with 0.4 μm pores (cell culture inserts) until day 7+12 of differentiation. Each cell culture insert will contain three organoids.

2. Remove the organoids from the cell culture insert.

1. Make a hole in the middle of the membrane of the cell culture insert with a pair of dissecting forceps. Using dissecting scissors, make three cuts in the membrane from the hole in the middle to the edge of the cell culture insert, cutting between the organoids. This will result in three pieces of membrane, each with one organoid attached, which are still connected to the cell culture insert at their outer edge.
2. Take hold of one of the pieces of membrane close to its outer edge with a pair of forceps and tear it loose from the cell culture insert. Place the piece of membrane with the attached organoid in a Petri dish. Add a few drops of DPBS without calcium and magnesium (DPBS $^{-/-}$) to the organoid to avoid dehydration. Repeat for the other two organoids.
3. Bisect the organoids by holding their membrane in place with forceps and cutting them in half with a double-edge stainless steel razor blade (a whole organoid is too large for the coelom to accommodate at this stage of development). Gently push the two organoid halves off the membrane with a dura dissector. Discard the membrane and leave the organoids in DPBS$^{-/-}$ until transplantation.

NOTE: Prepare a maximum of three organoids at a time for transplantation to avoid stress to the organoids prior to transplantation. Ideally one person prepares the organoids while another performs the transplantation.

2. Preparing chicken embryos for transplantation

1. Incubate fertilized white leghorn eggs. Start incubation of the eggs on kidney organoid differentiation day 7+8 to ensure correct timing of transplantation.

1. Place fertilized white leghorn eggs (*Gallus domesticus)* horizontally on a holder (Fig. 1a, day 0), marking the middle of the upward-facing side with a pencil. NOTE: Either custom-made plastic holders or egg cartons can be used as holders to incubate the eggs.
2. Place the holder with the eggs in a humidified incubator at 38 ± 1 ^{o}C (Fig. 1a, day 0).
3. Incubate the eggs for 3 days, keeping the water basin in the incubator filled.

2. Create a window in the eggshell on day 3 of incubation.

1. On day 3 of incubation, place a small piece (~1 cm x 0.5 cm) of transparent tape on the pointed tip of the egg (small end). Make a small hole in the eggshell in the middle of the transparent tape by tapping it with the sharp end of a pair of dissecting scissors.
2. Insert a 19 G needle on a 5 mL syringe into the hole at a 45^{o} angle, avoiding damage to the yolk sac, and aspirate 2–3 mL of albumen from the egg to lower the embryo inside the egg. Seal the hole with a second piece (~1 cm x 0.5 cm) of transparent tape.
3. Place a large piece (~5 cm x 5 cm) of transparent tape on the pencil-marked, upward-facing side of the egg. Make a hole in the eggshell in the middle of the transparent tape by tapping it with the sharp end of a pair of dissecting scissors (Fig. 1a, day 3).
4. Starting from this hole, cut a small circular window in the eggshell using curved dissecting scissors. Look through this window to locate the embryo, then enlarge the window to optimize access to the embryo (Fig. 1a, day 3).
5. Remove any large pieces of eggshell that may have fallen on top of the embryo using forceps. Remove smaller pieces by placing a few drops of DPBS with calcium and magnesium (DPBS$^{+/+}$) on the embryo with a plastic transfer pipette, then aspirating the DPBS$^{+/+}$ with the eggshell into the pipette.
6. Add three drops of DPBS$^{+/+}$ supplemented with 0.5% penicillin/streptomycin to the egg using a plastic transfer pipette.
7. Carefully seal the window with a large piece (±5 x 5 cm) of transparent tape before placing the egg back in the incubator until day 4 of incubation, when the embryo will be in HH Hamilton stage 23–24 (HH 23–24)[32]. NOTE: Sealing the window is very important to avoid dehydration and death of the embryo.
8. Check the embryos daily for viability by looking at them through the tape (do not remove the tape to avoid dehydration). During these first days of incubation, the egg yolk color will change from bright to matte yellow upon embryo death. Discard deceased embryos.
9. Keep the water basin in the incubator filled.

3. Intracoelomic transplantation on day 4 of incubation

1. Gaining access to the coelomic cavity

1. Cut the tape from the window with curved dissecting scissors.
2. Place the egg under a dissecting microscope on a rubber holder or egg carton.

3. The chicken embryo is now in HH 23–24 and lying on its left side with its right side facing the viewer (Fig. 1a, day 4). Locate the right wing and leg bud of the embryo, as the coelom will be accessed between these two limb buds. In the area between the right wing and leg bud, create an opening consecutively in the vitelline membrane, the chorion, and the amnion by holding them with two pairs of dissecting forceps and gently pulling these in opposite directions. NOTE: The vitelline membrane is the first membrane that is encountered after opening the egg, and in some cases, has already been damaged when making the window on day 3. If the embryo is rotated, lying on its right side with its left side facing the viewer (Fig. 1a, day 4), it is necessary to turn it around to enable transplantation. To do this, make a large opening in the vitelline and chorion membrane, then carefully turn the embryo around using forceps.
4. Check whether there is unobstructed access to the coelomic cavity: gently take hold of the edge of the body wall between the wing and limb bud with a pair of dissecting forceps and pull it slightly towards the viewer. The coelomic cavity must be clearly visible. Carefully insert a blunt but slim instrument (e.g., a blunt tungsten wire in a microscalpel holder) into the coelomic cavity. NOTE: If insertion of the blunt instrument into the coelomic cavity is not possible, one or more of the membranes have not been properly opened.

2. Transplantation

1. Place half an organoid inside the egg on top of the allantois using a dura dissector.
2. Using dissecting forceps, carefully take hold of the edge of the body wall and pull it slightly towards the viewer to make the opening to the coelom visible. NOTE: Avoid damaging the blood vessels in the body wall.
3. Gently move the organoid towards and through the opening in the body wall into the coelom with blunt Tungsten wire in a microscalpel holder. Push the organoid slightly cranially to lodge it inside the coelom. It is now visible just behind the wing bud (Fig. 1a, day 4).
4. Add three drops of $DPBS^{+/+}$ to the egg using a plastic transfer pipette.
5. Carefully seal the window with a large piece (±5 x 5 cm) of transparent tape before placing the egg back in the incubator until day 12 of incubation (8 days after transplantation).
6. Keep checking the embryos daily for viability by looking at them through the tape (do not remove the tape to avoid dehydration). Discard deceased embryos. NOTE: As the embryos and their chorioallantoic membranes grow, these become more clearly visible through the tape. A lack of movement by the embryo and collapsed or sparse blood vessels are a sign of embryo death.
7. Check the water basin in the incubator daily and keep it filled.

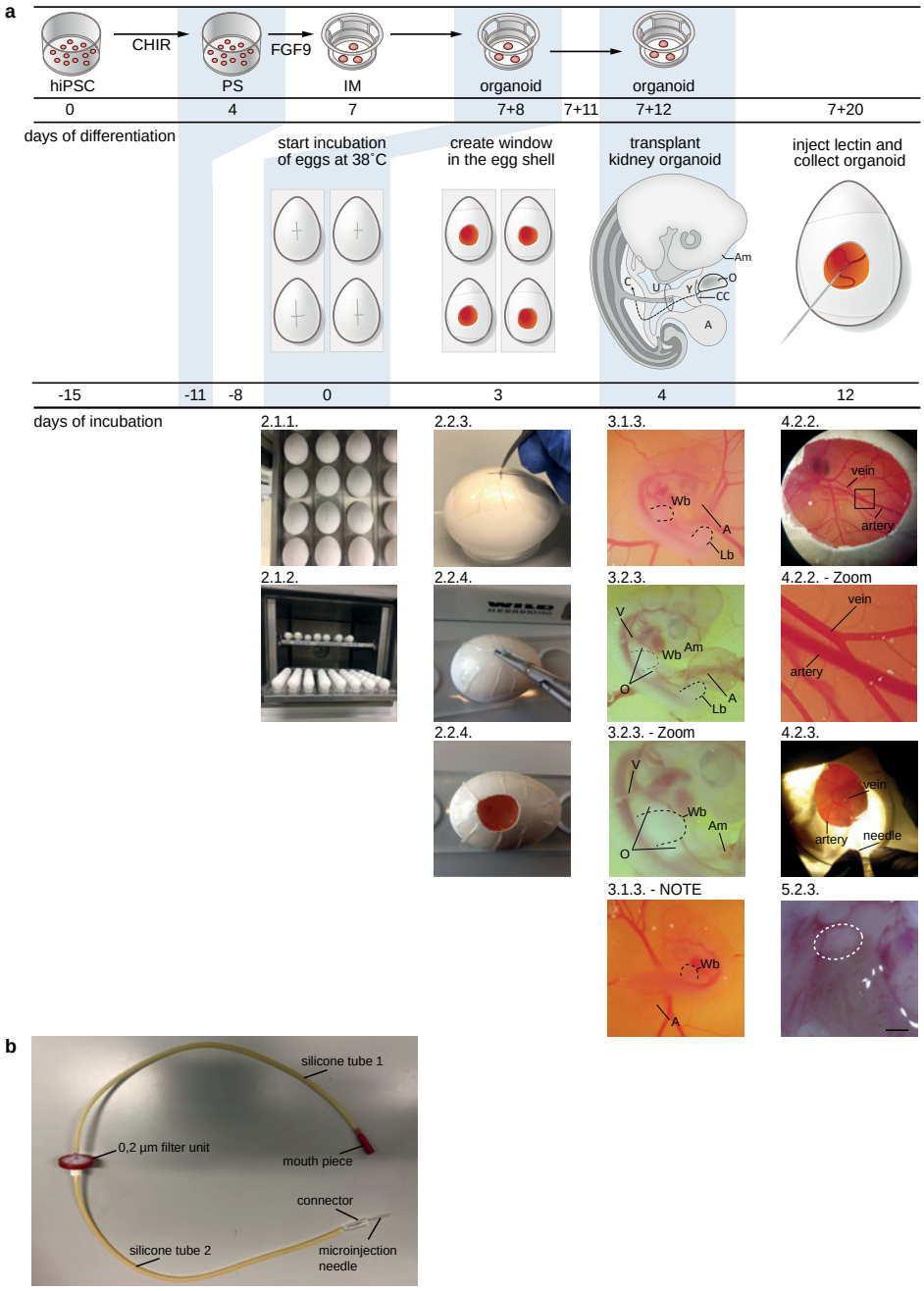

Figure 1: Intracoelomic transplantation method. a Timeline of differentiation of hiPSCs to kidney organoids, incubation of fertilized chicken eggs, and intracoelomic transplantation of kidney organoids. Differentiation of hiPSCs to kidney organoids is initiated 15 days before incubation of the chicken eggs is started (differentiation day 0 = incubation day -15), to enable transplantation of kidney organoids on day 7+12 of differentiation in chicken embryos on day 4 of inbubation. Days

of incubation: Day 0: Fertilized chicken eggs are positioned horizontally on holders (step 2.1.1.), which are placed in an incubator at 38 ^{o}C ± 1 ^{o}C (protocol step 2.1.2.). Day 3: A window is created in each egg by making a small hole in the upward-facing side of the egg with the sharp end of a pair of curved dissecting scissors (step 2.2.3.) and cutting a circular window starting from this hole (step 2.2.4.). The window is sealed with transparent tape before placing the egg back in the incubator. Day 4: Intracoelomic transplantation of kidney organoids on day 7+12 of differentiation is performed. The embryo is in HH 23–24 and lying on its left side, with its right side facing the viewer (step 3.1.3.). Between the wing and leg bud, an opening is made in the vitelline membrane, chorion, and amnion to obtain access to the coelomic cavity, and the organoid is inserted through these openings into the coelom. After transplantation, the organoid is visible as a white structure located just behind the wing bud. The edges of the opened vitelline and amnion membranes are visible (steps 3.2.3 and 3.2.3–Zoom). In some cases, embryos are rotated, lying on their right instead of left side (3.1.3–NOTE) and must be turned around prior to transplantation. Day 12: Fluorescently labeled lectin is injected intravenously. Veins are distinguished from arteries by their color; the blood in the veins is oxygen-rich, coming from the CAM, so they are slightly brighter red than the arteries that are coming from the embryo (steps 4.2.2., 4.2.2–Zoom, and 4.2.3.). The embryo is sacrificed and the organoid retrieved. The organoid (circled) has become attached to the chicken liver and appears to be vascularized (step 5.2.3). Scalebar = 1 mm. The schematic image depicting intracoelomic transplantation image in the top panel was reprinted with permission from Koning et al.[28]. **b** Image of the assembled injection system, consisting of a mouthpiece, two pieces of 38 cm silicone tubing, a 0.2 μm filter, a connector, and a glass microinjection needle that was generated by pulling glass microcapillaries in a micropipette puller. Abbreviations: A = allantois; Am = amnion; C = coelom; CC = cut chorion membrane; CHIR = CHIR99021; FGF9 = Fibroblast Growth Factor 9; hiPSCs = human induced pluripotent stem cells; IM = Intermediate Mesoderm; Lb = leg bud; O = organoid; PS = Primitive Streak; U = umbilical ring; V vitelline membrane; Wb = wing bud; Y = yolk stalk.

4. Injection of fluorescently labeled lectin

1. Preparing for injection

1. Make glass microinjection needles by pulling glass microcapillaries in a micropipette puller with the following settings: Heat 533, Pull 60, Velocity 150, Time 200. While looking through the dissecting microscope, carefully break the tips off the microinjection needles using dissecting forceps to create an opening. NOTE: The required settings for the micropipette puller may differ depending on the machine.
2. Assemble the injection system. Take two pieces of 38 cm silicone tubing and connect them to each other by placing a 0.2 μm filter between them. Insert a mouthpiece into the end of the tube that is connected with the filter outlet (silicone tube 1), and a connector to the end of the tube that is connected with the filter inlet (silicone tube 2). Finally, insert the microinjection needle into the connector (Fig. 1b).
3. Dilute fluorescently labeled lens culinaris agglutinin (LCA) with $DPBS^{-/-}$ to a concentration of 2.5 mg mL^{-1} in a 0.5 mL tube and spin down for ±30 s in a microcentrifuge to move aggregates to the bottom of the tube.
4. Pipette 20 μL of LCA onto a piece of parafilm.
5. Aspirate the 20 μL of LCA from the parafilm into the microcapillary needle of the assembled injection system.

2. Injection

1. Cut the tape from the window with curved dissecting scissors. Place the egg under a dissecting microscope in a rubber holder.
2. Evaluate the vasculature and locate the veins, which can be distinguished from the arteries by their slightly brighter red color (Fig. 1a, day 12). To improve access to the vasculature, carefully enlarge the window by cutting with curved dissecting scissors. Select a vein for injection based on accessibility and size.
3. Insert the tip of the microcapillary needle into the selected vein at a 0–20^{o} angle. Ensure the needle is in the vein by gently moving the tip from side to side. Gently and steadily blow into the injection system to inject the LCA (Fig. 1a, day 12). NOTE: If the needle in the vein is in the correct position, it should stay within the boundaries of the vein.
4. Place the egg back in the incubator for 10 min to let the LCA circulate. NOTE: It is not necessary to seal the egg with tape during this time.

5. Collecting transplanted organoids on day 12 of incubation

1. Sacrificing the chicken embryo

1. Place the egg in a rubber holder on the bench. Cut the tape from the window with curved dissecting scissors. Then, cut through the membranes surrounding the embryo with curved dissecting scissors. NOTE: A dissecting microscope is not required for this step.
2. Scoop the embryo up from the egg with a perforated spoon and immediately decapitate the embryo using scissors. Place the body of the embryo in a Petri dish under the dissection microscope.

2. Locating and collecting organoids.

1. Place the embryo on its back in the Petri dish and spread its limbs.
2. Carefully open the abdominal wall of the embryo along the longitudinal axis using forceps.
3. Locate the organoid inside the embryo. The organoid most frequently has become attached to the right liver lobe, either at the caudal tip or cranially just below the rib cage (Fig. 1a, day 12). It is therefore recommended to start by looking in these locations.
4. Once the organoid is located, remove it from the embryo by cutting around it with micro scissors. Place the organoid and the chicken tissue that is inevitably attached to it in a Petri dish under the dissecting microscope. Remove as much chicken tissue as possible with a double-edge stainless steel razor blade.
5. Process the organoid depending on the desired analysis.

6. Whole-mount immunofluorescence staining

1. Place a transplanted organoid in a 24-well plate and fix in 500 µL of paraformaldehyde (PFA) 4% at 4 °C for 24 h. Wash 3x with $DPBS^{-/-}$.

2. Permeabilize and block the organoid in 300 µL of blocking solution (0.3% TritonX in $DPBS^{-/-}$ containing 10% donkey serum) for 2 h at room temperature.

3. Prepare primary antibody mix: for one organoid, dilute primary antibodies NPHS1 (sheep-α-human, dilution 1:100), CD31 (mouse-α-human, dilution 1:100), and LTL (biotin-conjugated, dilution 1:300) in 300 µL of blocking solution. Add the antibody mix to the organoid and incubate for 72 h at 4 ºC.

4. Wash 3x with 0.3% TritonX in $DPBS^{-/-}$.

5. Prepare secondary antibody mix: for one organoid, dilute secondary antibodies donkey-α-sheep Alexa Fluor 647 (dilution 1:500), donkey-α-mouse Alexa Fluor 488, and streptavidin Alexa Fluor 405 (dilution 1:200) in 300 µL of blocking solution. Add the secondary antibody mix to the organoid and incubate for 2–4 h at room temperature. Cover with aluminum foil to avoid exposure of the secondary antibodies to light.

6. Wash 3x with $DPBS^{-/-}$.

7. Embed the organoid in ±30 µL of mounting medium in a 35 mm glass bottom dish and let it dry overnight at room temperature covered with aluminum foil. Store at 4 ºC.

8. Image using a confocal microscope.

Representative Results:

The method and timeline for differentiation of hiPSCs to kidney organoids, incubation of fertilized chicken eggs, transplantation of kidney organoids, injection of LCA, and collection of the organoids are summarized in Fig. 1a. It is important to coordinate the timing of organoid differentiation and chicken egg incubation, starting differentiation 15 days before incubation. The actions on day 0, 3, 4, and 12 of incubation are illustrated by photographs below the timeline. Organoids are transplanted at day 7+12 of differentiation into day 4 (HH 23–24) chicken embryos. LCA is injected into the venous system of the embryo 8 days after transplantation to stain the perfused vasculature, before sacrificing the embryo and retrieving the organoid. The assembled injection system is shown in Fig. 1b.

Chicken embryos are sacrificed on day 12 of incubation (Fig. 1a). Upon careful dissection of the embryo, the transplanted organoid can usually be found attached to the liver.

Looking through a dissection microscope, it appears vascularized (Fig. 1a, day 12, 5.2.3.). Confocal imaging of transplanted organoids injected with LCA and stained for nephron structures and human ECs confirms vascularization by perfused blood vessels (Fig. 2a), which also invade glomerular structures (Fig. 2b). The vasculature is chimeric: perfused human ECs (CD31+, LCA+), unperfused human ECs (CD31+, LCA-), and perfused chicken-derived ECs (CD31-, LCA+) can be distinguished (Fig. 2a, panel III, IV, V).

Discussion

In this manuscript, a protocol for intracoelomic transplantation of hiPSC-derived kidney organoids in chicken embryos is demonstrated. Upon transplantation, organoids are vascularized by perfused blood vessels that consist of a combination of human organoid-derived and chicken-derived ECs. These are spread throughout the organoid and invade the glomerular structures, enabling interaction between the ECs and podocytes. It was previously shown that this leads to enhanced maturation of the organoid glomerular and tubular structures [28]. The transplantation is very efficient, taking ~5 min per embryo, and the only maintenance that the embryos require is a regular refill of the water basin in the incubator. This method is therefore very suitable for the analysis of large numbers of organoids.

Vascularization and maturation of kidney organoids have been previously demonstrated through transplantation in mice [18,20]. In these labor-intensive mouse models, organoids were transplanted for 2 to up to 12 weeks. In the intracoelomic transplantation experiments shown here, the duration of transplantation was limited to 8 days. This allows for the sacrifice of the embryos before day 13 of incubation, when they are thought to start experiencing pain [33,34]. Since chicken embryos hatch on day 21, the duration of transplantation could be extended to 15 days, sacrificing the embryos on day 19 to avoid hatching. This would, however, require the use of anesthetics. Despite the relatively short transplantation duration in this model, it induces extensive vascularization and significant maturation of organoid nephrons compared to in vitro organoids, including the formation of a GBM between organoid podocytes and the invading ECs [28].

When performing intracoelomic transplantation experiments, it is important to consider that not all chicken embryos will develop normally and survive. Usually, ~65% of the embryos placed in the incubator at day 0 reach the end point of the experiment. This is due to a combination of acute bleeding caused by vessel damage during transplantation (5–10% in our hands), and the stress that is induced by the windowing and transplantation procedures. When embryos are in an earlier or later stage than HH 23–24, this will complicate transplantation due to limited space and more extensive vasculature, respectively. If embryos are not in the correct stage at the expected time, this can be due to the temperature of incubation, as a higher temperature generally leads to faster development.

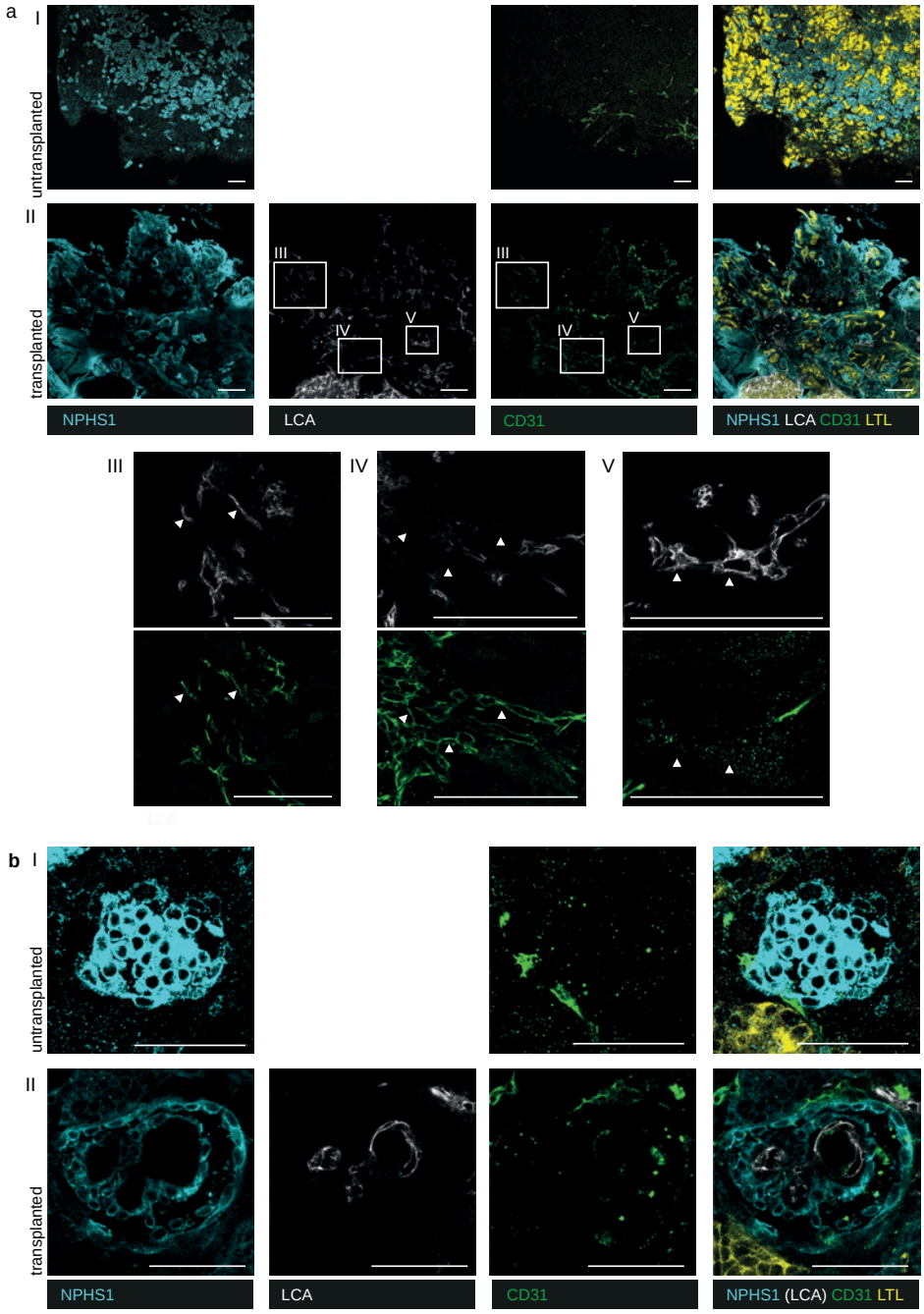

Figure 2: Vascularized transplanted kidney organoids. a Immunofluorescent images of (I) an untransplanted kidney organoid and (II) a transplanted kidney organoid. In both conditions, glomerular (NPHS1+, cyan) and tubular (LTL+, yellow) structures are visible. In the untransplanted organoids, some human ECs (CD31+, green) are present. In the transplanted organoid, a perfused

vascular network (CD31+, green and injected rhodamine-labeled LCA+, white) is visible throughout the organoid. In panel III, IV and V, magnifications of the boxed areas in panel II are shown, to demonstrate the three types of ECs that can be distinguished in transplanted organoids: Panel III contains perfused human ECs (CD31+, LCA+), marked with arrowheads. Panel IV contains unperfused human ECs (CD31+, LCA-), marked with arrowheads. Panel V contains perfused chicken-derived ECs (CD31-, LCA+), marked with arrowheads. Scale bar = 200 μm. **b** In untransplanted organoids (I), ECs (CD31+, green) surround glomerular structures (NPHS1+, cyan) but do not invade them. In transplanted organoids (II, glomerular structures (NPHS1+, blue) are vascularized by perfused capillaries (LCA+, white, CD31+, green). Scale bar = 50 μm.

Moreover, keeping fertilized eggs at room temperature for a prolonged period before incubation induces more variability in development. To avoid this, the temperature of the incubator must be kept stable throughout and between experiments, and incubation started within 3 days after delivery of the fertilized eggs. Unexpectedly high percentages of embryo death between procedures can be caused by dehydration. To avoid this, it is essential to add 2–3 drops of $DPBS^{+/+}$ to each egg after opening it and after transplantation and sealing the egg very carefully with tape, smoothing out creases in the tape as much as possible. Combining the windowing and transplantation steps to reduce the number of times the eggs are opened is not recommended, as windowing on day 4 considerably increases embryo death. This is the result of damage to blood vessels that have frequently become attached to the eggshell at this stage.

In conclusion, this method provides an efficient and powerful tool to induce vascularization and enhance maturation in kidney organoids. It can be used to study these processes in large numbers of organoids and has potential for the modeling of renal diseases that require a higher level of maturation than can currently be acquired in vitro.

Acknowledgements

We thank George Galaris (LUMC, Leiden, the Netherlands) for his help with chicken embryo infection. We acknowledge the support of Saskia van der Wal-Maas (Department of Anatomy & Embryology, LUMC, Leiden, the Netherlands), Conny van Munsteren (Department of Anatomy & Embryology, LUMC, Leiden, the Netherlands), Manon Zuurmond (LUMC, Leiden, the Netherlands), and Annemarie de Graaf (LUMC, Leiden, the Netherlands).

References

1 Taguchi, A. et al. Redefining the in vivo origin of metanephric nephron progenitors enables generation of complex kidney structures from pluripotent stem cells. Cell Stem Cell ***14***, 53–67 (2014). https://doi.org/10.1016/j.stem.2013.11.010

2 Morizane, R. et al. Nephron organoids derived from human pluripotent stem cells model kidney development and injury. Nat Biotechnol ***33***, 1193–1200 (2015). https://doi.org/10.1038/nbt.3392

3 Kim, Y. K. et al. Gene-Edited Human Kidney Organoids Reveal Mechanisms of Disease in Podocyte Development. Stem Cells ***35***, 2366–2378 (2017). https://doi.org/10.1002/stem.2707

4 Takasato, M. et al. Kidney organoids from human iPS cells contain multiple lineages and model human nephrogenesis. Nature ***526***, 564–568 (2015). https://doi.org/10.1038/nature15695

5 Hale, L. J. et al. 3D organoid-derived human glomeruli for personalised podocyte disease modelling and drug screening. Nat Commun ***9***, 5167 (2018). https://doi.org/10.1038/s41467-018-07594-z

6 Vanslambrouck, J. M. et al. Enhanced metanephric specification to functional proximal tubule enables toxicity screening and infectious disease modelling in kidney organoids. Nat Commun ***13***, 5943 (2022). https://doi.org/10.1038/s41467-022-33623-z

7 Tanigawa, S. et al. Organoids from Nephrotic Disease-Derived iPSCs Identify Impaired NEPHRIN Localization and Slit Diaphragm Formation in Kidney Podocytes. Stem Cell Reports (2018). https://doi.org/10.1016/j.stemcr.2018.08.003

8 Forbes, T. A. et al. Patient-iPSC-Derived Kidney Organoids Show Functional Validation of a Ciliopathic Renal Phenotype and Reveal Underlying Pathogenetic Mechanisms. Am J Hum Genet ***102***, 816–831 (2018). https://doi.org/10.1016/j.ajhg.2018.03.014

9 Freedman, B. S. et al. Modelling kidney disease with CRISPR-mutant kidney organoids derived from human pluripotent epiblast spheroids. Nat Commun ***6***, 8715 (2015). https://doi.org/10.1038/ncomms9715

10 Cruz, N. M. et al. Organoid cystogenesis reveals a critical role of microenvironment in human polycystic kidney disease. Nat Mater (2017). https://doi.org/10.1038/nmat4994

11 Gupta, N. et al. Modeling injury and repair in kidney organoids reveals that homologous recombination governs tubular intrinsic repair. Sci Transl Med ***14***, eabj4772 (2022). https://doi.org/10.1126/scitranslmed.abj4772

12 Hiratsuka, K. et al. Organoid-on-a-chip model of human ARPKD reveals mechanosensing pathomechanisms for drug discovery. Sci Adv ***8***, eabq0866 (2022). https://doi.org/10.1126/sciadv.abq0866

13 Dorison, A. et al. Kidney Organoids Generated Using an Allelic Series of NPHS2 Point Variants Reveal Distinct Intracellular Podocin Mistrafficking. J Am Soc Nephrol (2022). https://doi.org/10.1681/ASN.2022060707

14 Eremina, V. et al. Glomerular-specific alterations of VEGF-A expression lead to distinct congenital and acquired renal diseases. J Clin Invest ***111***, 707–716 (2003). https://doi.org/10.1172/JCI17423

15 Kitamoto, Y., Tokunaga, H. & Tomita, K. Vascular endothelial growth factor is an essential molecule for mouse kidney development: glomerulogenesis and nephrogenesis. J Clin Invest ***99***, 2351–2357 (1997). https://doi.org/10.1172/JCI119416

16 Sison, K. et al. Glomerular structure and function require paracrine, not autocrine, VEGF-VEGFR-2 signaling. J Am Soc Nephrol ***21***, 1691–1701 (2010). https://doi.org/10.1681/ASN.2010030295

17 Ryan, A. R. et al. Vascular deficiencies in renal organoids and ex vivo kidney organogenesis. Dev Biol ***477***, 98–116 (2021). https://doi.org/10.1016/j.ydbio.2021.04.009

18 van den Berg, C. W. et al. Renal Subcapsular Transplantation of PSC-Derived Kidney Organoids Induces Neo-vasculogenesis and Significant Glomerular and Tubular Maturation In Vivo. Stem Cell Reports ***10***, 751–765 (2018). https://doi.org/10.1016/j.stemcr.2018.01.041

19 Sharmin, S. et al. Human Induced Pluripotent Stem Cell-Derived Podocytes Mature into Vascularized Glomeruli upon Experimental Transplantation. J Am Soc Nephrol ***27***, 1778–1791 (2016). https://doi.org/10.1681/ASN.2015010096

20 Bantounas, I. et al. Generation of Functioning Nephrons by Implanting Human Pluripotent Stem Cell-Derived Kidney Progenitors. Stem Cell Reports ***10***, 766–779 (2018). https://doi.org/10.1016/j.stemcr.2018.01.008

21 van den Berg, C. W., Koudijs, A., Ritsma, L. & Rabelink, T. J. In Vivo Assessment of Size-Selective Glomerular Sieving in Transplanted Human Induced Pluripotent Stem Cell-Derived Kidney Organoids. J Am Soc Nephrol ***31***, 921–929 (2020). https://doi.org/10.1681/ASN.2019060573

22 Asai, R., Bressan, M. & Mikawa, T. Avians as a Model System of Vascular Development. Methods Mol Biol ***2206***, 103–127 (2021). https://doi.org/10.1007/978-1-0716-0916-3_9

23 Jankovic, B. D. et al. Immunological capacity of the chicken embryo. I. Relationship between the maturation of lymphoid tissues and the occurrence of cell-mediated immunity in the developing chicken embryo. Immunology ***29***, 497–508 (1975).

24 Alkie, T. N. et al. Development of innate immunity in chicken embryos and newly hatched chicks: a disease control perspective. Avian Pathol ***48***, 288–310 (2019). https://doi.org/10.1080/03079457.2019.1607966

25 Rawles, M. E. Transplantation of normal embryonic tissues. Ann N Y Acad Sci ***55***, 302–312 (1952).

26 Rawles, M. E. The Development of Melanophores from Embryonic Mouse Tissues Grown in the Coelom of Chick Embryos. Proc Natl Acad Sci U S A ***26***, 673–680 (1940).

27 Garreta, E. et al. Fine tuning the extracellular environment accelerates the derivation of kidney organoids from human pluripotent stem cells. Nat Mater ***18***, 397–405 (2019). https://doi.org/10.1038/s41563-019-0287-6

28 Koning, M. et al. Vasculogenesis in kidney organoids upon transplantation. NPJ Regen Med ***7***, 40 (2022). https://doi.org/10.1038/s41536-022-00237-4

29 Hamburger, V. Morphogenetic and axial self-differentiation of transplanted limb primordia of 2-day chick embryos. Journal of Experimental Zoology ***77***, 379–399 (1938).

30 Dossel, W. E. New method of intracoelomic grafting. Science ***120***, 262–263 (1954).

31 Takasato, M., Er, P. X., Chiu, H. S. & Little, M. H. Generation of kidney organoids from human pluripotent stem cells. Nat Protoc ***11***, 1681–1692 (2016). https://doi.org/10.1038/nprot.2016.098

32 Hamburger, V. & Hamilton, H. L. A series of normal stages in the development of the chick embryo. 1951. Dev Dyn ***195***, 231–272 (1992). https://doi.org/10.1002/aja.1001950404

33 Aleksandrowicz, E. & Herr, I. Ethical euthanasia and short-term anesthesia of the chick embryo. ALTEX ***32***, 143–147 (2015). https://doi.org/http://dx.doi.org/10.14573/altex.1410031

34 ACUC. ACUC Guideline: The Use and Euthanasia Procedures of Chicken/Avian Embryos., <https://www.cpp.edu/research/research-compliance/iacuc/docs/iacuc-guidelines-on-euthanasia-of-chicken-and-embryos.pdf> (2012).

CHAPTER 6

Single cell transcriptomics of human kidney organoid endothelium reveals vessel growth processes and arterial maturation upon transplantation

M. Koning*, S.J. Dumas*, E. Meta, E. Lievers, A.M.A. de Graaf, M. Borri, L.J. Nai Chung Tong, X. Liang, P. Liu, F. Chen, L. Lin, Y. Luo, P. Carmeliet, C.W. van den Berg, A.J. Rabelink
* authors contributed equally to the work

NPJ Regenerative Medicine, 2025

Abstract

Kidney organoids derived from human induced pluripotent stem cells lack a proper vasculature, hampering their applicability. Transplantation prevents the loss of organoid endothelial cells (ECs) observed in vitro, and promotes vascularization. In this study, we transplanted kidney organoids in chicken embryos and deployed single-cell RNA sequencing of ~12,000 organoid ECs to delineate their molecular landscape and identify key changes associated with transplantation. Transplantation significantly altered EC phenotypic composition. Consistent with angiogenesis, proliferating EC populations expanded 8 days after transplantation. Importantly, ECs underwent a major vein-to-arterial phenotypic shift. One of the transplantation-specific arterial EC populations, characterized by laminar shear stress response and Notch signalling, showed a similar transcriptome as human fetal kidney arterial/afferent arteriolar ECs. Consistently, transplantation-induced transcriptional changes involved proangiogenic and arteriogenic SOX7 transcription factor upregulation and regulon enrichment. These findings point to blood flow and candidate transcription factors such as SOX7 as possible targets to enhance kidney organoid vascularization.

Introduction

The absence of a functional vasculature in cultured human induced pluripotent stem cell (hiPSC)-derived kidney organoids is a major limitation. It precludes full maturation and functionality of organoid nephron structures, thus restricting their applicability. In organoids maintained in vitro, the sparse endothelial cells (ECs) that are initially formed during differentiation perish over time, suggesting the absence of essential cues for EC maintenance in the culture conditions. We have previously shown that transplantation in the coelomic cavity of chicken embryos induces functional vascularization and enhanced maturation of kidney organoids. Interestingly, the vasculature in these transplanted organoids is chimeric, consisting of both chicken and human ECs which, contrary to the in vitro situation, are maintained in vivo. To date, it is unclear what leads to the demise of human ECs in vitro as well as what sustains them upon transplantation.

Renal ECs are known to display extensive molecular and phenotypic heterogeneity to support the specific functions of each nephron segment[1-4]. Glomerular ECs display fenestrae without diaphragms and play a role in glomerular filtration. ECs in peritubular capillaries have bridged fenestrae and contribute to the tubular reabsorption of solutes. In the larger renal vessels, the EC lining is continuous. A recent study demonstrated that renal EC heterogeneity is even more extensive than was previously thought by identifying at least 24 distinct renal EC phenotypes in the adult mouse kidney based on single cell RNA sequencing (scRNAseq) analysis[1]. However, it is unknown whether and to what extent kidney organoid-derived ECs resemble renal ECs. Although previous studies provided scRNA-seq data of kidney organoid cells, the absence or paucity of ECs recovered from the organoids precluded the extensive analysis of this critical cell population. In this study, we isolated a total of 11,966 high-quality human ECs from untransplanted and transplanted kidney organoids and analyzed them using scRNAseq. We demonstrate that organoid ECs in vitro display phenotypic heterogeneity, but lack similarity to fetal kidney ECs. Transplantation in chicken embryos stimulates EC proliferation and induces a new, more mature, arterial EC phenotype, resembling fetal kidney arterial-afferent arteriolar ECs.

Results

Transplantation greatly affects the kidney organoid endothelial cell transcriptome

To evaluate the molecular effects of transplantation on kidney organoid ECs, we compared human ECs from organoids cultured in vitro with those from organoids transplanted in chicken embryos. HiPSCs were differentiated to kidney organoids using a

previously published protocol (Fig 1a, step 1)[5]. On day 7+12 of differentiation they were either transplanted in the coelomic cavity of Hamburger Hamilton stage 22-23 (HH22-23) chicken embryos or maintained in vitro (Fig 1a, step 2). This timepoint was selected to ensure the presence of endogenous ECs in the organoids at the time of transplantation[6]. On day 7+13 and d7+20 of differentiation, transplanted organoids and untransplanted controls were collected for analysis. The 24 h post-transplantation timepoint was included to isolate the effects of the microenvironmental changes resulting from transplantation, from the effects of blood perfusion, which we observe throughout the organoids from day 3 after transplantation[6]. Since kidney organoids contain a limited number of ECs, in-depth scRNAseq analysis of these cells requires their enrichment. We therefore isolated ECs from dissociated organoids through fluorescence activated cell sorting (FACS) using human CD31 as EC marker for purification (Fig 1a, step 3). Sorted ECs were processed for sequencing. After quality control and EC filtering, a total of 11,966 high quality human ECs were subjected to downstream analyses: 2777 and 1505 ECs from untransplanted d7+13 and d7+20 organoids, and 307 and 7377 ECs from transplanted D7+13 and d7+20 organoids, respectively (Fig 1b, supplementary Fig. 1, supplementary data 1). Correlation analysis demonstrated that both time and transplantation altered organoid EC transcriptomes, with the latter having a greater impact (Fig 1c). We identified significantly differentially expressed genes in each condition (supplementary data 2, Fig 1d). Subsequent geneset enrichment analysis (GSEA) revealed that in organoids cultured in vitro, ECs at d7+13 upregulated genes associated with aerobic respiration (e.g. *NDUFC2*, *ATP5PO*, *NDUFB8*), and active replication, whereas at d7+20, upregulation of genes associated with DNA damage/growth arrest (e.g. *CDKN1A, CCND1, MDM2*, *SNAI2*) was observed. Upon transplantation, ECs at d7+13 upregulated genes associated with glycolysis (e.g. *SLC2A1*, *LDHA*, *ENO1*, *ENO2*, *ALDOA*, *PGK1*) rather than oxidative phosphorylation, along with hypoxia-induced genes (e.g. *BNIP3*, *FAM162A*) (Fig. 1e, supplementary data 3). This metabolic transcriptome shift from aerobic respiration to glycolysis is consistent with the change in environment from in vitro culture at 21% oxygen to the hypoxic coelomic cavity. Eight days after transplantation, genes associated with angiogenesis (e.g. *EPAS1*, *AQP1*, *GJA5*, *ESM1*), blood coagulation (e.g. *MYL9*), circulation (e.g. *EPAS1*, *GJA5*), matrix deposition (e.g. *COL12A1*), and antigen presentation (e.g. *HLA-B*, *B2M*, *HLA-C*), were upregulated, indicating vessel growth, response to blood perfusion and interaction with the host immune system (Fig. 1d, e, supplementary data 3).

To identify the potential drivers of the transcriptional phenotypes adopted by kidney organoid ECs in these 4 conditions, transcription factor inference analysis was conducted using the SCENIC workflow[7]. Our analysis revealed dynamic changes in the expression of specific transcription factors and their regulons (Fig. 1f).

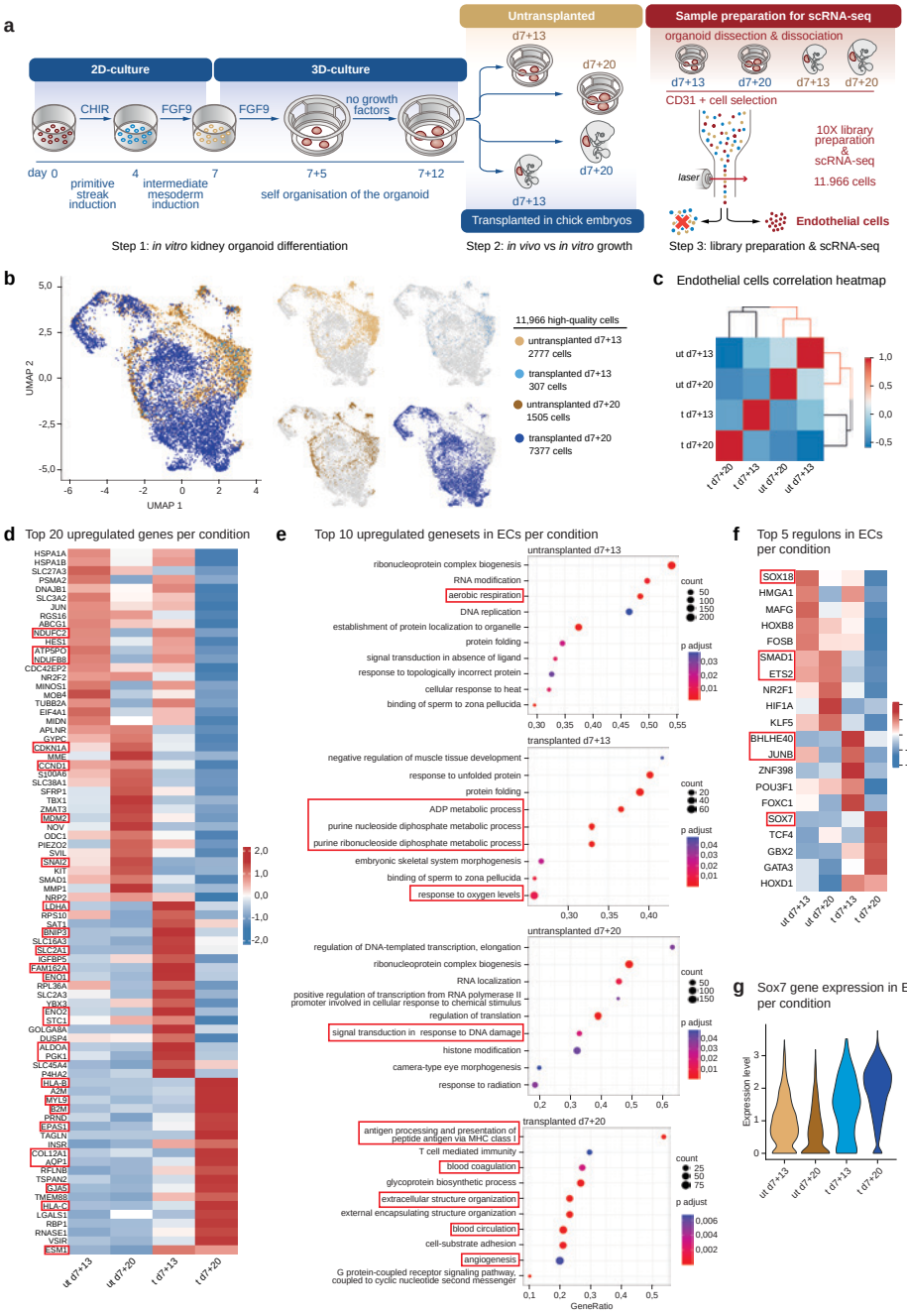

Figure 1: scRNAseq of enriched ECs from untransplanted and transplanted kidney organoids. **a** Workflow of step 1: kidney organoid differentiation from hiPSCs, step 2: in vitro culture versus intracoelomic transplantation in chicken embryos, and step 3: organoid collection, dissociation to single cells, endothelial cell enrichment and scRNAseq. **b** UMAP visualization of a total of 11,966 high-quality human endothelial cells obtained from untransplanted (2777 cells from d7+13,

1505 from d7+20) and transplanted (307 cells from d7+13, 7377 from d7+20) kidney organoids, color-coded by condition. **c** Heatmap visualization of similarity analysis of ECs from the different conditions. ECs from each condition had unique transcriptome profiles but showed a higher similarity based on transplantation conditions than timepoints. Scale: z-score of the gene expression level. Abbreviations: ut = untransplanted. t = transplanted. **d** Expression-level scaled heatmap of the top 20 upregulated genes per condition. Highlighted genes are discussed in the text. Scale: z-score of the gene expression level. **e** Top 10 upregulated gene sets in ECs for each condition. Dot size indicates proportion of cells expressing a gene. Color intensity indicates the level of expression. Highlighted gene sets are discussed in the text. **f** Top 5 upregulated regulons in ECs for each condition, generated by transcription factor inference analysis conducted using the SCENIC method. Highlighted regulons are discussed in the text. Scale: z-score of the regulon enrichment score. **g** Violin plot visualization of the expression level of the SOX7 gene in ECs from the different conditions.

At day 7+13, ECs from untransplanted organoids exhibited a significant enrichment of the SOX18 regulon, a transcription factor known for its transient expression during embryonic development, particularly in nascent ECs[8]. This finding suggests activation of SOX18 in the early stages of EC differentiation in kidney organoids in vitro. By day 7+20, we observed an upregulation of the SMAD1 and ETS2 regulons in the remaining ECs, transcription factors promoting EC survival and angiogenesis[9,10]. Upon transplantation, we detected an upregulation of the hypoxia-inducible BHLHE40 transcription factor, along with the stress-induced JUNB regulon, consistent with an adaptive response of ECs to the altered microenvironment post-transplantation. At day 7+20 in transplanted organoids, ECs displayed a significant enrichment of the SOX7 regulon as well as *SOX7* upregulation (Fig. 1f, g). SOX7 is recognized for its roles in vasculogenesis, angiogenesis during embryonic development, and arterial EC specification[11,12]. This enrichment suggests that SOX7 plays a pivotal role in the maturation and specification of ECs under transplantation conditions, consistent with the observed response to blood perfusion.

Kidney organoid transplantation sustains endothelial cell proliferation

It is known that ECs in kidney organoids regress over time in vitro[13], whereas they persist upon transplantation[6]. To further investigate possible changes in proliferation, we performed unsupervised clustering of the 11,966 high quality human ECs, which resulted in 13 subclusters (Fig. 2a), each with a distinct transcriptome profile (top marker genes in Fig. 2b and supplementary data 4, marker genes in supplementary data 5). Clusters 1 and 2 both displayed a clear proliferative transcriptome. The distinction between the two clusters was based on cell cycle phases: ECs in cluster 1 showed the highest S phase module score, mainly upregulating genes associated with the G1S-S phase. ECs in cluster 2 showed the highest G2M phase module score, upregulating genes associated with the G2M-M phase (Fig. 2c, d). Clusters 3 to 13 did not exhibit an upregulation of any proliferation genes, indicating rather a quiescent or a migrating cell state.

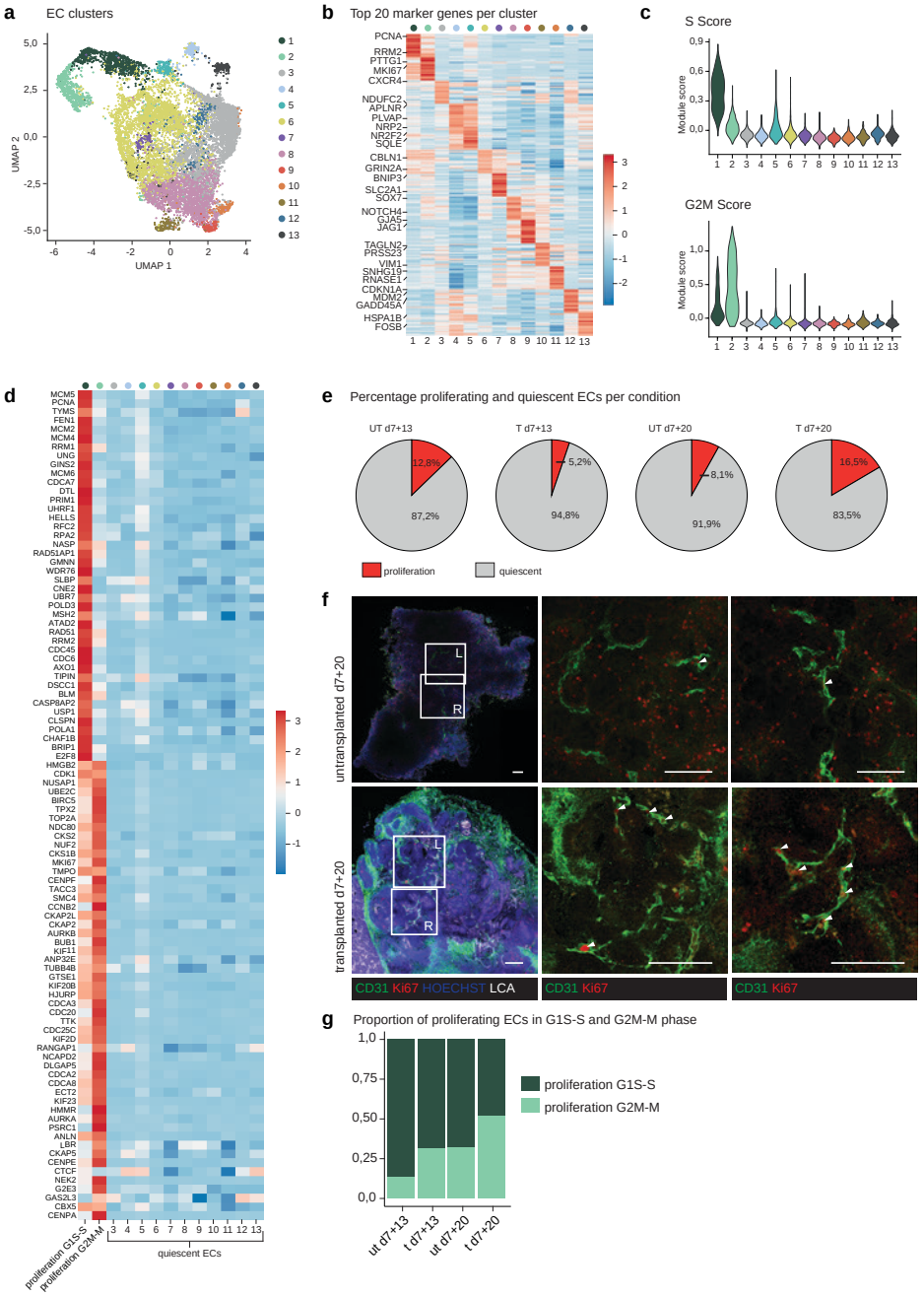

Figure 2: Endothelial cell proliferation is sustained after transplantation. a UMAP visualization of a total of 11,966 high-quality human endothelial cells obtained from untransplanted (2777 cells from d7+13, 1,505 from d7+20) and transplanted (307 cells from d7+13, 7377 from d7+20) kidney organoids, color-coded by cluster (n=13). **b** Expression-level scaled heatmap of the top 20 marker genes per EC cluster. Scale = z-score of the gene expression level. **c** Violin plots depicting Module scores for S phase (top) and G2M phase (bottom) of the cell cycle for each EC cluster. Cluster 1 displayed the highest S module score, whereas cluster 2 had the highest G2M module score. Cluster 3 – 13 had

low S and G2M scores. **d** Expression- level scaled heatmap of genes associated with proliferation per EC cluster. Cluster 1 and 2 express proliferation genes, with cluster 1 expressing genes associated with G1S-S phase and cluster 2 expressing genes associated with G2M-M phase. Cluster 3-13 did not express proliferation genes and were classified as quiescent EC clusters. Scale = z-score of the gene expression level. **e** Pie charts of the percentage of proliferating (red) and quiescent (grey) ECs per condition. The percentage of proliferating ECs is highest in transplanted day 7+20 organoids. **f** Immunofluorescent images of untransplanted day 7+20 (top) and transplanted d7+20 (bottom) kidney organoids, stained for human CD31 (green) ki67 (red) and HOECHST. Injected LCA (white) is visible in the transplanted organoid. In untransplanted organoids, few proliferating endothelial cells (CD31+, ki67+, arrowheads) can be identified, whereas in transplanted organoids, they appear more abundant. Scale bar: 100μm. Images are based on 3 separate experiments. **g** Bar graph depicting the proportion of proliferating ECs in G1S-S (dark green) and G2M-M (light green) phase per condition.

Comparison of the proportion of proliferating and quiescent or migrating ECs between the different conditions revealed a decrease in proliferating ECs in untransplanted organoids over time, from 12.8% at d7+13 to 8.1% at d7+20, consistent with a decreased proliferative potential of these ECs.

The percentage of proliferating ECs was lowest in transplanted d7+13 organoids (5.2%). This is possibly due to the extensive changes in microenvironment upon transplantation, requiring metabolic rewiring of transplanted ECs and likely affecting their proliferative capacity temporarily. However, in transplanted d7+20 organoids, it had increased to 16.5%, the highest percentage of all conditions, and twice more than its timepoint-matched untransplanted control (Fig. 2e, supplementary data 6). Whole-mount staining of untransplanted and transplanted day 7+20 organoids with proliferative marker Ki67 (whose gene showed upregulation in the G2M-M proliferating cluster, as shown in supplementary Fig. 2a) and CD31, validated the presence of proliferating human CD31+Ki67+ ECs in both experimental settings (Fig. 2f, supplementary data 7), which appeared more abundant in transplanted organoids. Interestingly, the proportion of proliferating ECs in G2M-M phase was higher in transplanted organoids compared with untransplanted organoids (Fig. 2g). The lower percentage of proliferating ECs, in particular in G2M-M phase in untransplanted organoids, might be due to cell cycle arrest as a result of DNA damage (Fig. 1e), and could underlie the declining number of ECs in culture in vitro.

Heterogeneity and phenotypic changes in organoid ECs upon transplantation

Next, we investigated the characteristics of the quiescent or migrating EC clusters. In order to determine EC phenotype identity, we first calculated artery, vein and lymphatic module scores for the ECs in each subcluster based on known canonical marker genes. With this approach, 4 artery clusters (artery 1-4), 1 vein cluster, 1 lymphatic cluster and 5 capillary clusters (capillary 1-5 – not showing artery, vein or lymphatic phenotypes) were identified

(Fig. 3a). The identity of these subclusters was confirmed by their upregulated expression of artery, vein and lymphatic canonical marker genes (Fig. 3b). Unsupervised hierarchical clustering provided further support by grouping the vein with the lymphatic cluster, and the artery clusters together. Capillary 1,4 and 5 were more similar to the vein and lymphatic clusters while capillary 2 and 3 showed a stronger resemblance to the proliferating EC clusters (Fig. 3c). Untransplanted organoids contained mainly capillary ECs (d7+13 86.5%, d7+20 87.4%), some venous (d7+13 6.4%, d7+20 6.6%) and lymphatic (d7+13 5.7%, d7+20 4.6%) ECs and a very small amount of arterial ECs (d7+13 1.3%, d7+20 1.4%). In transplanted d7+13 organoids, the proportions were similar, with a slight decrease in venous and lymphatic ECs in favor of capillary and arterial ECs.

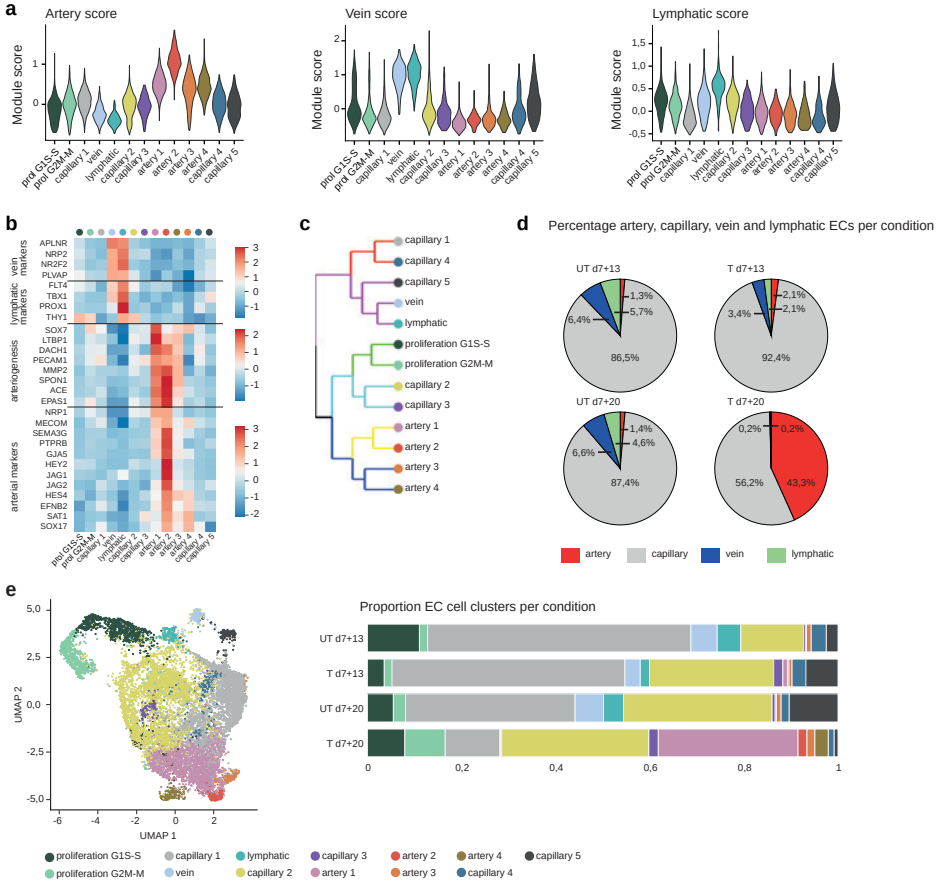

Figure 3: Kidney organoids contain venous, lymphatic, arterial and capillary ECs and transplantation induces a switch from venous to arterial phenotype. a Violin plots depicting artery (left), vein (middle) and lymphatic (right) module scores for each EC cluster. 4 artery clusters (artery 1-4), 1 vein cluster, 1 lymphatic cluster and 5 capillary clusters can be distinguished.. **b** Expression-level scaled heatmap of vein, lymphatic, arteriogenesis and arterial markers per EC cluster. Scale: z-score of the gene expression level. **c** Hierarchical clustering of EC clusters, color-

coded according to p-value from multiscale bootstrap resampling analysis on all highly variable genes. **d** Pie charts of the percentage of artery (red), capillary (grey), vein (blue) and lymphatic (green) ECs per condition. There is a large increase in the percentage of arterial ECs in transplanted day 7+20 organoids, while vein, lymphatic and capillary ECs are reduced in this condition. **e** Relative cluster quantification for each condition, showing a significant decrease in capillary 1 and 5 clusters and a significant increase in artery cluster 1,2 and 4 in transplanted day 7+20 organoids compared to the other conditions (untransplanted and transplanted d7+13 and untransplanted d7+20)

Eight days after transplantation, however, a striking shift from venous and capillary to arterial ECs had occurred, resulting in 43.3% arterial ECs, 56.2% capillary ECs and only 0.2% vein and lymphatic ECs (Fig. 3d, supplementary data 8). Further analysis of the artery subtypes revealed that the artery 1,2 and 4 clusters were nearly absent in untransplanted organoids and mostly appeared upon transplantation (Fig. 3e, supplementary data 9). The top marker genes for each of the artery clusters revealed artery 1 to represent an immature artery EC phenotype, artery 2 to express more mature artery EC markers, and artery 3 and 4 to upregulate endoMT markers including smad2/3-dependent TGFB target genes, with artery 4 showing a decreased expression of EC markers (Fig. 3b, supplementary Fig. 3a). Regarding capillary phenotypes, the proportion of capillary 1 and 5 ECs, characterized by the high expression level of OXPHOS genes and of response-to-stress and DNA damage genes, respectively, was decreased after transplantation at d7+20 (Fig. 3e, supplementary Fig. 3b, c). Capillary 3 EC cluster showing a robust glycolytic and a response-to-hypoxia phenotype was only observed in transplanted organoids, as also previously reported in podocytes upon kidney organoid transplantation (Fig. 3e, supplementary Fig. 3d)[6]. The proportion of the capillary 2 cluster, for which the phenotype was unclear, and capillary 4 cluster, with a response-to-DNA damage without activation of a response-to-stress gene signature, didn't seem much affected by the transplantation or timepoint (Fig. 3e, supplementary Fig. 3c). To summarize, ECs in kidney organoids did not represent a homogeneous population, but displayed heterogeneity consistent with arteriovenous specification, with transplantation inducing a dramatic shift to an arterial phenotype.

Tissue-specification of organoid ECs and similarities with fetal kidney ECs

In vivo, ECs display tissue-specific molecular features to support development and homeostasis. To assess the renal specification of kidney organoid ECs, we analyzed enrichment of human liver, spleen, skin, heart, pancreas, muscle, lung, vasculature, and kidney EC marker genes, identified from the Tabula Sapiens dataset[14] (supplementary Fig. 4, supplementary data 10), in organoid ECs. Kidney organoid ECs showed the highest enrichment of kidney-specific markers compared to EC markers from other

tissues, especially after transplantation (Fig. 4a). However, they also expressed marker genes associated with ECs from other tissues, including the liver, pancreas, and muscle, indicating that the tissue-specific differentiation of kidney organoid ECs is incomplete under all tested conditions (Fig. 4a).

In order to perform an in-depth comparison of organoid ECs with fetal kidney ECs, a human fetal kidney EC reference was created from publicly available scRNA-seq data resulting in a dataset of 3155 fetal kidney ECs from 8 to 17 weeks of gestation (Fig. 4b). Unsupervised subclustering resulted in 7 distinct subclusters: artery-afferent arteriole, glomeruli, efferent arteriole, capillary, vein, lymphatic and proliferation ECs (Fig. 4c,d, marker genes in supplementary data 11). Integration and co-embedding of fetal kidney and organoid ECs revealed limited overlap between the EC clusters (Fig. 4e). However, 2 organoid EC types did display similarity to fetal kidney ECs: the proliferating ECs, which were enhanced upon transplantation, and the artery ECs that newly appeared in transplanted organoids (Fig. 4e,f). Specifically, organoid proliferation G1S-S and G2M-M clusters resembled the fetal kidney proliferation cluster and organoid artery cluster 2 showed the highest similarity with the fetal kidney artery-afferent arteriole cluster, with 121 common marker genes (Fig. 4g, supplementary data 12). The enhanced renal specification of ECs from transplanted organoids appears therefore associated to the vein-to-artery phenotype shift. Since transplantation enables perfusion of organoid ECs, and shear stress is known to play a role in arterial differentiation in vivo[15], we hypothesized that this was an important factor driving arterial and renal specification of ECs upon transplantation. Indeed, analysis of the expression of laminar shear stress-associated genes by ECs from the different conditions demonstrated that these were highly expressed in transplanted day 7+20 organoids specifically (Fig. 5a). Furthermore, of all EC clusters, artery cluster 2, the cluster with the closest resemblance to fetal kidney arterial ECs, displayed the highest expression of laminar shear stress-associated genes (Fig. 5b). This gene signature suggests that artery cluster 2 consists of perfused ECs. To further investigate this, we identified JAG1, a possible mechanotransducer in ECs[16] , among the top marker genes for the artery 2 cluster that is also restricted to artery/afferent arteriolar ECs amongst fetal kidney ECs (supplementary Fig. 2b, c), and evaluated the effect of laminar flow on its expression by iPSC-derived EC using a bulk RNA-seq dataset that our group has published previously[17]. IPSC-derived ECs cultured under flow for 4 days showed significant upregulation of JAG1 expression compared to those cultured in static culture, supporting the notion that artery cluster 2 represents perfused ECs (Fig. 5c, supplementary data 13).

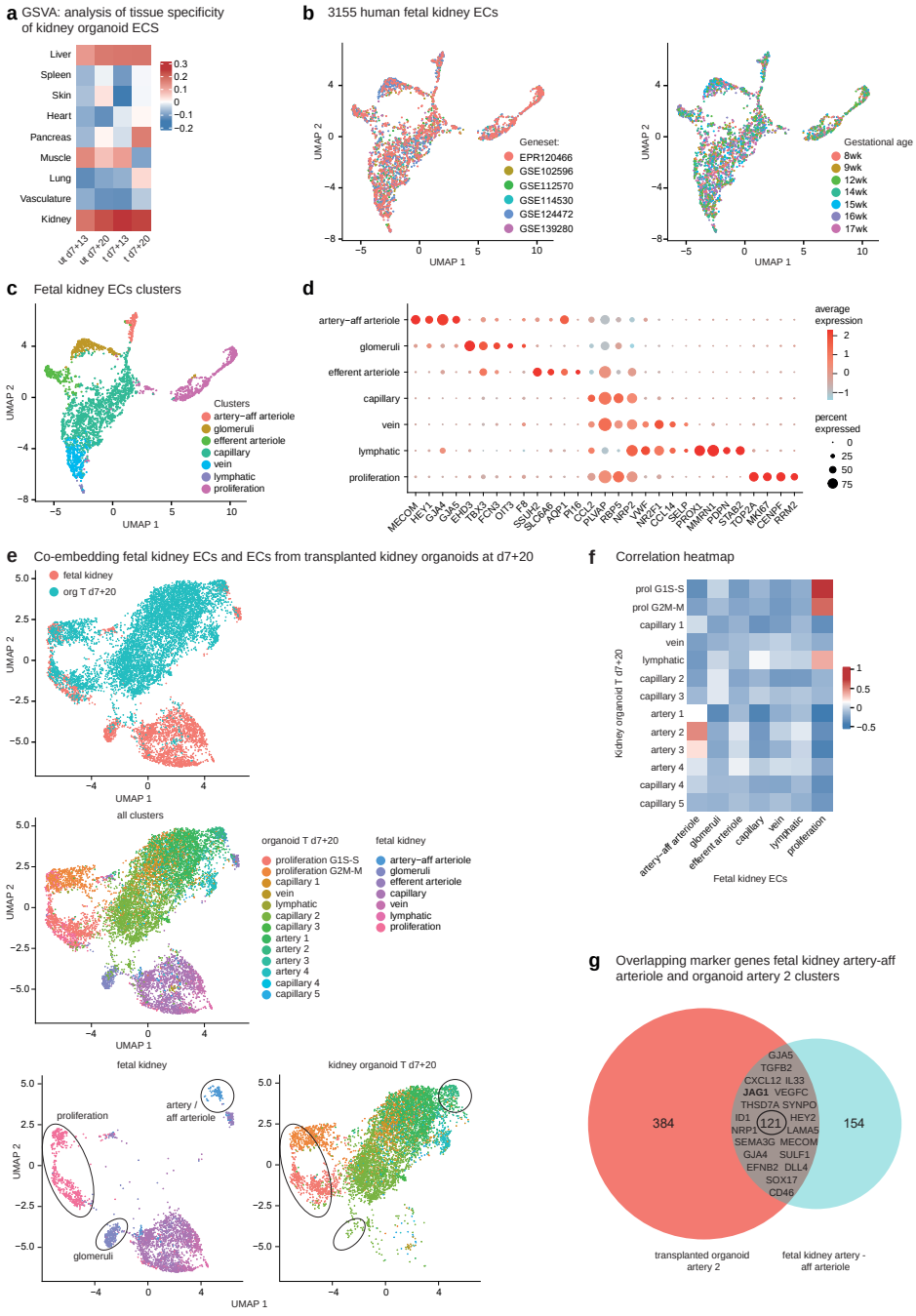

Figure 4: Kidney organoid artery and proliferating ECs resemble fetal kidney ECs. a Heatmap of the geneset variation analysis scores of tissue EC marker genes in ECs from the different kidney organoid conditions. Scale: geneset variation analysis score. **b** UMAP visualization of a total of 3155 fetal kidney ECs from publicly available scRNAseq datasets from week 8-17 of gestation,

color-coded by dataset (left) and gestational age (right). **c** UMAP visualization of the fetal kidney EC dataset, color-coded by EC subcluster. 7 clusters could be distinguished: artery-afferent arteriole, glomeruli, efferent arteriole, capillary, vein, lymphatic and proliferation. **d** Dot plot representing marker gene expression in fetal kidney EC clusters. Dot size indicates proportion of cells in cluster expressing a gene, color intensity indicates the level of expression. **e** UMAP visualization of fetal kidney ECs and ECs from transplanted kidney organoids at day 7+20, color-coded by origin (top), and cluster (bottom). **f** Heatmap visualization of the correlation between the different kidney organoid EC clusters and the fetal kidney EC clusters. The organoid proliferation clusters show high similarity to fetal kidney proliferating ECs, and the organoid artery 2 cluster correlates with the fetal kidney artery-afferent arteriole cluster. Scale: correlation coefficient. **g** Venn diagram displaying the overlap between marker genes for transplanted organoid artery 2 ECs and fetal kidney artery-afferent arteriole ECs: These clusters have 121 overlapping marker genes.

Here, we demonstrated that the transplantation of kidney organoids facilitated the differentiation of a subset of endogenous organoid ECs into a phenotype resembling kidney fetal (afferent) arteriolar cells, likely driven by blood perfusion. In contrast, the remaining quiescent organoid ECs exhibited distinct transcriptomic profiles compared to human fetal kidney ECs. Of note, despite the previously demonstrated perfusion of organoid glomeruli upon transplantation, we did not identify an organoid EC cluster with a glomerular gene signature, even in transplanted organoids. However, chicken ECs collected with the transplanted organoids did include a glomerular-like EC cluster (*GATA5* and *EHD3* positive) (supplementary Fig. 6a, b). A limitation of this analysis is that some of the chicken cells in the day 7+20 samples are derived from chicken tissue (liver) that could not be completely removed from the organoid during collection. The chicken glomerular ECs, however, display such a specific gene signature that they are almost certainly derived from the organoid glomeruli and not from the chicken liver.

Discussion

In this study, we provided an in-depth molecular analysis of kidney organoid EC subtypes and their specification in in vitro culture and upon transplantation. Given the scarcity of ECs in organoids, enrichment of ECs from hundreds of untransplanted as well as transplanted organoids was required for this analysis. To facilitate this, we performed intracoelomic transplantation in chicken embryos. Unlike mammalian models, fertilized eggs are affordable and with minimal ethical constraints at early timepoints of development. Furthermore, chicken embryos are easily accessible by opening the egg shell, lack a fully functional immune system[18,19], and the coelomic cavity is a favorable environment for the vascularization and maturation of embryonic tissues[20-22]. Unlike the commonly practiced transplantation of kidney organoids under the kidney capsule or subcutaneously in mice[5,23-25], intracoelomic transplantation enables the collection of a high number of transplanted organoids, as demonstrated here and previously published using nearly 200 chicken embryos[6]. The transplantation duration of 8 days was relatively

short compared to murine transplantation models due to our decision to sacrifice the embryos on day 12 of development, before it is believed they start experiencing pain[26]. Although extending the time in vivo would likely further improve organoid vascularization and maturation, we have previously shown that 8 days is sufficient for the establishment of a perfused vascular network within the organoids and epithelial cell maturation. To our knowledge, this is currently the only available in vivo model allowing such a high yield of ECs required for this study.

Transplantation had a major impact on organoid EC transcriptome. In line with the previously reported progressive loss of ECs in organoids cultured in vitro[6,13], we found a lower proportion of proliferating ECs in untransplanted than transplanted d7+20 organoids. This was especially clear for ECs in the G2M-M cell cycle phases. ECs in untransplanted organoids upregulated genes associated with response to DNA damage and stress as well as those involved in oxidative phosphorylation (OXPHOS). It has been well documented that ECs rely mainly on glycolysis for ATP production[27,28]. One of the advantages of utilizing glycolysis over OXPHOS is the reduced production of reactive oxygen species (ROS), decreasing oxidative stress[29,30]. Production of ROS derived from OXPHOS is promoted by the high oxygen tension from the ambient air (21%), in which kidney organoids are usually cultured. Given the oxidative effect of ROS on DNA, leading to cell cycle arrest and potentially cell death, OXPHOS in ECs from untransplanted organoids may contribute to the loss of ECs in this condition. Further studies targeting these pathways are warranted to investigate this hypothesis. The reason for the higher OXPHOS gene expression in ECs from untransplanted organoids compared to transplanted ones remains unclear, but it may indicate EC immaturity. Indeed, our group previously demonstrated that immature iPSC-derived ECs exhibit an increased number of mitochondria, albeit dysfunctional, compared to mature endothelium. This dysfunction leads to elevated ROS production and ultimately hinders proper maturation[17]. A similar phenomenon could potentially occur in ECs derived from kidney organoids. However, adapting the in vitro culture conditions to 5% O2 to promote glycolysis over OXPHOS, thereby mimicking what likely happens upon kidney organoid transplantation, did not enhance the vasculature. When placed in a hypoxia incubator in 5% O2 starting from d7+5 or d7+12 of differentiation, kidney organoids showed the same morphology and vasculature compared to organoids cultured in a regular incubator in 21% O2. There was no difference in EC volume between the different conditions and glomeruli remained avascular (supplementary Fig. 5). More extensive analysis, such as scRNAseq or metabolic profiling could possibly reveal more subtle differences that remained undetected by the readouts used. Others have reported an increase in ECs in kidney organoids cultured in ‘physiological hypoxia’ of 7% O2[31]. Perhaps the difference in oxygen tensions used partly explains the difference in findings.

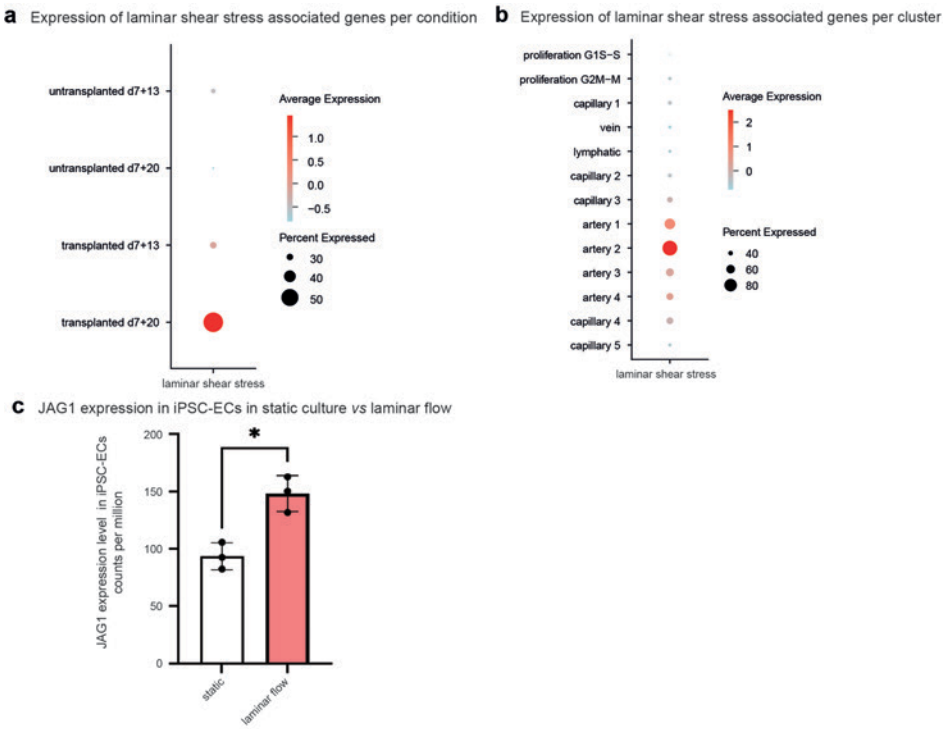

Figure 5: Upregulation of laminar shear stress associated genes in artery clusters. a Dot plot representing expression of laminar shear stress associated genes in organoid ECs per condition. ECs from transplanted organoids at day 7+20 show the highest expression. Dot size indicates proportion of cells in cluster expressing laminar shear stress associated genes, color intensity indicates the level of expression. **b** Dot plot representing expression of laminar shear stress associated genes in organoid ECs per subcluster. ECs from artery cluster 2 show the highest expression. Dot size indicates proportion of cells in cluster expressing laminar shear stress associated genes, color intensity indicates the level of expression. **c** Bar graph showing the expression of JAG1 in iPSC-derived ECs cultured under static conditions (white) or under laminar flow for 4 days. JAG1 expression is upregulated in ECs under laminar flow.

Arterio-venous specification is an essential aspect of embryonic vascular development and maturation. In kidney organoids in vitro, we identified capillary, venous, and lymphatic ECs, while artery ECs were nearly absent. After transplantation, a major shift towards artery ECs occurred. Of note, the proliferating and artery ECs formed clearly distinct clusters, with the proliferating ECs displaying a low artery score. This is consistent with the cell cycle arrest in ECs prior to arterial specification that was reported by others[15]. Although it was previously thought that in early embryology arteries mainly arise by sprouting from existing major arteries[32], recent lineage tracing studies have shown that arterialization of venous-featured ECs also plays an important role[33]. This mechanism could partly explain the observed venous to arterial shift upon transplantation. In addition, the shear stress that is induced by perfusion of ECs in transplanted organoids is likely

an important driver of arterialization. In mouse studies, shear stress has been shown to induce Notch signalling, leading to arterial specification[15]. The upregulated expression of laminar shear stress associated genes in the artery clusters in general, and the artery 2 cluster in particular, supports this theory. Consistent with this observation, another scRNA-seq study on kidney organoid cultured in suspension in spinner flasks, resulting in some levels of flow around and throughout the organoids, identified mostly arterial-like ECs[34]. Comparison of organoid ECs to fetal kidney ECs revealed that the artery 2 EC cluster was the only non-proliferating cluster resembling fetal kidney ECs. This emphasizes the importance of shear stress, implying a role not only in arterial but possibly also for renal specification in kidney organoids. Tissue specification of ECs is partly determined by their angiocrine factor profiles. Interestingly, the importance of blood flow-induced angiocrine signaling has been highlighted in different tissues, such as liver, heart or kidney, during organ development or regeneration[35-37]. Further studies linking blood flow and kidney-specific angiocrine signaling and broader, EC tissue-specification, are warranted to elucidate the underlying mechanisms.

Previously, shear stress was applied to kidney organoids in vitro in an attempt to enhance their vascularization[38,39]. Organoids were placed in a microfluidic chip and subjected to flow, resulting in an increase in ECs compared to static conditions and incidentally the appearance of perfusable vessels, reflecting to some extent what is observed upon transplantation[38]. Alternatively, co-culture with human umbilical vein endothelial cell (HUVEC)- coated microfluidic channels led to migration of HUVECs into the organoids and connection to organoid-derived ECs[39]. However, both methods failed to induce functional and glomerular vascularization. This might be partly explained by the location of shear stress, which in the microfluidic chips was applied over the top of the organoids instead of through vessels that connect to pre-existing ECs as it occurs upon transplantation. In co-culture experiments, while the flow was applied to HUVEC coated channels beneath the organoid, the characteristics of the flow and level of shear stress in the sprouting vessels vascularizing the organoid is unknown. Other factors influencing vascularization may have been suboptimal or absent, including the type of ECs used, the timing of vascularization relative to the organoid's developmental stage, or other essential cues.

Although we previously demonstrated that human organoid ECs invade glomerular structures following intracoelomic transplantation, we did not identify a human EC cluster with a glomerular signature in the transplanted organoids in the present study. The discrepancy could be due to the limited duration of transplantation and exposure to blood perfusion, with further EC specialization requiring prolonged transplantation. The previously described slightly cuboidal appearance and lack of fenestrations of organoid

glomerular ECs on transmission electron microscopy (TEM) support this theory[6]. Other possibilities are that the number of intraglomerular human ECs is too small to detect them as a separate cluster and / or that chicken derived ECs are the major contributors to the glomerular vasculature after transplantation. Indeed, chicken ECs collected together with the transplanted organoids[6] included a cluster a glomerular-like ECs (*GATA5* and *EHD3* positive ECs) (supplementary Fig. 6a, b). As no other chicken glomerular cells were detected in the chicken scRNA-seq data[6], it is unlikely that these glomerular-like ECs resulted from contamination by native chicken kidney tissue during organoid collection. The fact that a subset of chicken ECs attains a glomerular gene signature within 8 days while organoid ECs do not, suggests that endogenous organoid ECs might not be ideally suited for glomerular vascularization. This implies that an external source of ECs might be necessary for optimal vascularization in vitro. Notably, kidney vascularization, including occasional glomerular vascularization with EC-podocyte interactions, was recently achieved in vitro by mixing hiPSCs with transgenic hiPSCs that express an inducible ETS translocation variant 2 (ETV2) transcription factor during kidney organoid differentiation[34]. ETV2 expression is essential for EC specification during embryonic development and its induction in iPSCs directly differentiates them to ECs[40,41]. In this model, differentiation of a subpopulation of iPSCs to ECs without otherwise adapting the kidney organoid protocol was sufficient to enhance organoid (and glomerular) vascularization. This supports the notion that a main cause of the lack of vasculature in kidney organoids in vitro is the ECs themselves and not the (lack of) cues from the surrounding epithelium. Yet, applying flow and hypoxia in this model may further promote (glomerular) vascularization and specify (glomerular) ECs.

In the present study, kidney organoid ECs did not show expression of *ETV2* (*data not shown*) but upregulated SOX7 transcription factor and regulon in transplanted day 7+20 organoids, compared to all other conditions. SOX7 is well known for its role in vascular development, hypoxia-induced angiogenesis, and is essential for the establishment of a correct arteriovenous identity during vascular development[27-30]. In this context, ETV2 and SOX7 are concomitantly expressed in endothelial progenitor cells with ETV2 binding directly to SOX7 promoter to induce its expression[42]. SOX7 could therefore be a possible target for enhancing kidney organoid vascularization and EC specification. Further studies are required to clarify the role of endothelial SOX7 in kidney organoid vascularization. Combining hypoxia, shear stress and EC-specific overexpression of Sox7, while preventing DNA damage, could be an interesting avenue to explore in order to improve kidney organoid vascularization in vitro.

Our study has some limitations. Using only a single cell line (MAFB iPSC) for the scRNA-seq experiment prevented us from accounting for cell line–specific variations. This might confound the identified EC subclusters and is important to take into account when interpreting the results. Moreover, validation of the different EC subclusters at the protein level was not performed, due to the limited number of cells in each EC cluster per organoid, making this task particularly challenging. Human CD31 was used as a marker for EC enrichment though FACS since kidney organoid ECs display high expression levels of this marker. However, we cannot exclude the presence of CD31-negative early endothelial progenitor cells (EPCs) in the organoids, which were not captured by this approach. Follow-up studies focusing on the process of iPSC-to-EC differentiation should include a marker for EPCs.

In conclusion, transplantation of kidney organoids profoundly influenced the transcriptome of organoid ECs during the vascularization process. While organoid ECs cultured in vitro exhibited responses to DNA damage, stress, and growth arrest, those from transplanted organoids displayed enhanced proliferation and differentiation into a fetal artery/afferent arteriole-like phenotype. The transplantation-induced activation of novel transcription factors, such as SOX7, along with exposure to blood flow, likely play pivotal roles in driving these processes. Our findings therefore provide valuable insights into the potential and limitations of endogenous organoid ECs, and identify possible targets to enhance their vascularization potential in vitro.

Methods

iPSC maintenance and differentiation

hiPSC lines reporter MAFB:mTagBFP2 (hiPSC-MAFB)[43] and LUMC0072iCTRL01 were used for kidney organoid generation. LUMC0072iCTRL01 was obtained from the Leiden hiPSC hotel (approving ethics committee: Leiden University Medical Center Ethics Committee, umbrella protocol 13080, detailed information can be found at https://hpscreg.eu/). iPSC-MAFB was generated from commercially available fibroblasts (ATCC, sourced from third party suppliers that obtained informed consent). Both cell lines were maintained in Essential 8 medium (E8, Thermo Fisher Scientific) with 0.5% Penicillin-Streptomycin (Thermo Fisher Scientific) on recombinant human Vitronectin (Thermo Fisher Scientific). hiPSC-MAFB was used for the scRNAseq experiments and IF stainings. LUMC0072 for IF stainings only. Cell lines were mycoplasma free. hiPSCs were passaged twice a week using 0.5 mM UltraPure EDTA (Thermo Fisher Scientific). One day before the start of differentiation, they were dissociated to single cells using TrypLE Select (Thermo

Fisher Scientific) and plated at 15,000 – 25,000 cells / cm^2 with the addition of RevitaCell Supplement (ThermoFisher Scientific). During the entire differentiation, hiPSCs were cultured in STEMdiff APEL2 medium (Stem Cell Technologies) with 1% Protein Free Hybridoma Medium II (PFHMII, Thermo Fisher Scientific) and 1% Antibiotic-Antimycotic solution (Thermo Fisher Scientific). From day 0-4, this was supplemented with 8 μM CHIR99021 (R&D Systems), and from day 4-7, with 200 ng mL^{-1} rhFGF9 (R&D Systems) and 1 μg mL^{-1} heparin (Sigma Aldrich). On day 7, differentiating cells were treated with an 1 hour 5 μM CHIR pulse, dissociated to single cells with Trypsin-EDTA (0.25%, Thermo Fisher Scientific), centrifuged and plated on Transwell 0.4 μM pore polyester membranes as pellets of 500,000 cells. Until day 7+5, the developing organoids were cultured in APEL2-medium supplemented with 200 ng mL^{-1} rhFGF9 and 1 μg mL^{-1} heparin (only bottom compartment), and from day 7+5 onwards in APEL2 without supplements. Medium change was performed every 2 days until transplantation on day 7+12 or the end of the experiment on day 7+20.

Transplantation in chicken embryos

In accordance with Dutch law, approval by the animal welfare committee was not required for these experiments. Detailed methods were previously described [6]. Briefly, Fertilized White Leghorn eggs (*Gallus gallus domesticus*, Drost Loosdrecht B.V.) were incubated at 37 °C. On day 3 of incubation, 3mL of albumen was removed to lower the embryo inside the eggs and a window was cut into the egg shell. One day later (Hamburger Hamilton stage 23), half a kidney organoid on day 7+12 of differentiation was transplanted inside the coelomic cavity of each chicken embryo[44]. On day 5 and 12 of incubation (respectively 1 and 8 days after transplantation), the chicken embryos were euthanized by decapitation and the organoids harvested. Some of the embryos were carefully injected with 20 μL of 2,5 mg mL^{-1} rhodamine labelled *lens culinaris agglutinin* (LCA) (RL-1042, Vector Laboratories) [45] in the vitelline vein using a glass microcapillary needle before being sacrificed to enable analysis of the vasculature.

Human endothelial cell isolation

Untransplanted and transplanted organoids generated using the hiPSC-MAFB line were dissociated to single cells at d7+13 and d7+20 of differentiation. At d7+13, 94 untransplanted and 75 bisected transplanted organoids (150 chicken embryos) were dissociated, and at d7+20, 49 untransplanted and 24 bisected transplanted organoids (48 chicken embryos) were used. Organoids were incubated in a collagenase I buffer consisting of 600U ml^{-1} collagenase Type I (Worthington) and 0,75U ml^{-1} DNAse (Sigma

Aldrich) in HBSS with calcium and magnesium (Thermo Fisher Scientific) for 40 min in a water bath at 37°C with repeated pipetting. Cell suspensions were centrifuged for 7 min at 300G and resuspended in a TrypLE buffer consisting of 5U ml^{-1} DNAse I (Sigma Aldrich) and 4μg ml^{-1} heparin (Sigma Aldrich) in 80% TrypLE select 10x (Thermo Fisher Scientific) in DPBS (Thermo Fisher Scientific). They were incubated for another 5 min at 37°C before dissociation was stopped through addition of cold HBSS+/+ with 10% FCS and further diluted with HBSS+/+. Cells were centrifuged for 5 min at 400G and resuspended in wash buffer (PBS + 0,1% BSA).

Viable ECs were identified and sorted on a FACSAria II or III cell sorter using a staining for human CD31 combined with a viability dye: Organoid cells were incubated with CD31-PE (1:100, BD Biosciences 555446) and viability dye eFluor 780 (1:5000, ThermoFisher Scientific 65-0865-14) in FACS buffer (PBS + 0,1% BSA + 2mM EDTA) for 30 min at 4ºC. Viable endothelial cells (d7+13 untransplanted: 23060, transplanted: 6843. D7+20 untransplanted: 6697, transplanted: 36444) were sorted using a FACS Aria II 3L or FACS Aria III 4L (BD Biosciences) and collected in wash buffer. Cells were centrifuged for 6 min at 400G and resuspended in 10X buffer (PBS + 0,04% BSA). Cell number and viability were assessed using a Bio-Rad TC20 cell counter after staining with Trypan Blue. Due to the low number of sorted cells from transplanted d7+13 and untransplanted d7+20 organoids, these were not counted. The single cell suspensions were converted to barcoded scRNA-seq libraries with a targeted cell recovery of 6000 cells / condition using the Chromium Single Cell 3' v3 Library, Gel Bead & Multiplex Kit and Chip Kit (10x Genomics).

Immunofluorescence analysis

Untransplanted organoids from hiPSC-MAFB and LUMC0072 were fixed in 2% paraformaldehyde (PFA) for 20 min at 4°C, and transplanted organoids in 4% PFA overnight at 4°C. Both were thoroughly washed after fixation and used for whole mount staining. Organoids were permeabilized and blocked in blocking solution (PBS + 0.3% TritonX + 10% donkey serum) for 2 hours. Primary antibodies were diluted in blocking solution and incubated for 24–72 hours. After washing, secondary antibodies in blocking solution were incubated for 2–4 h at room temperature. Kidney organoids were characterized for CD31 and Ki67. Primary antibodies were detected with donkey-α-goat Alexa Fluor 568 and 647, and donkey-α-mouse Alexa Fluor 488. Antibodies and isotype controls were validated in human kidney samples. Nuclei were stained with Hoechst33258 (Thermo Fisher Scientific) and tissues embedded in ProLong Gold Antifade Mountant (Thermo Fisher Scientific) in 35 mm glass bottom dishes (MatTek corporation) or adhesive microscope

slides (StarFrost, Knittel glass). Leica White Light Laser Confocal Microscope TCS SP8 using LAS-X Image software was used for analysis of the tissues.

Kidney organoid culture in hypoxia

Kidney organoids were generated from hiPSCs in the same manner as described above until day 7+5 or day 7+12 of differentiation. From that moment until the end of the experiment on day 7+20, they were cultured in a hypoxia inbubator at 5% O2.

Quantification of CD31 positive endothelial cells

CD31 positive endothelial cells were quantified in whole mount organoids at d7+20. Imaris software was used to calculate the volume of CD31 positive cells, as a percentage of whole organoid volume. A surface of the whole mount organoids was calculated and was used to calculate the volume of the organoid with statistics function in Imaris. Next, a surface was created for the CD31 channel and the volume of this surface was obtained in the same manner. Threshold and minimum number of voxels for CD31 surface generation were set separately for each sample, to be able to correct for differences in background and if necessary, background falsely identified as endothelial cells by the software was removed manually. Graphpad Prism 9.0.1 was used for statistical analysis. Means were compared between groups using a One-way ANOVA. Normality of the distribution was tested and confirmed using the Shapiro-Wilk and Kolmogorov-Smirnov test. Individual data points and mean (SD) are presented.

Deep sequencing and data pre-processing

The snRNA-seq libraries were sequenced and the reads processed as previously described. [6] Read were demultiplexed and aligned to the human reference genome only (GRCh38) for both, samples from untransplanted and transplanted organoids, using Cell Ranger (10x Genomics, v3.1.0). Key sequencing metrics are summarized in supplementary data 1.

Raw unfiltered data matrices from the Cell Ranger output were then further processed with R (v4.1.1) and Seurat package (v4.2.0). The following quality control steps were performed for each dataset: (i) genes expressed by less than 10 cells were removed; (ii) cells that expressed fewer than 500 genes were discarded as low-quality cells (supplementary data 1, supplementary Fig. 1a); (iii) cells with a detected number of genes exceeding a “doublet” threshold as listed in supplementary data 1 were excluded (determined by inspecting the cell frequency per total number of genes expressed, for each sample).

Samples were merged resulting in 15,961 cells (supplementary data 1). Dead/dying cells with a fraction of mitochondrial genes >15% were further removed. To identify and remove remaining low-quality cells, data were normalized using the *NormalizeData()* function from Seurat Package, and the top 2000 highly variable genes were identified using *FindvariableFeatures()*. Data were scaled with the *Scaledata()* function and reduced with principal component (PC) analysis using *RunPCA()* function. The top 30 PCs were used for visualization using uniform manifold approximation and projection (UMAP) with the *RunUMAP()* function as implemented in Seurat (min.dist=0.1, n.neigbors=15). Next, a shared nearest-neighbor graph (SNN) was determined using *FindNeighbors()* function on the 30 PCs with "k.param" set at 20, and used to calculate clusters with the *FindClusters()* function with resolution 1 and other settings set as default. Remaining low-quality cell clusters were identified according to the number of genes per cell and number of UMI per cell, and removed, resulting in 12,744 high-quality cells.

ScRNAseq data analysis

In silico selection of ECs

The top 2000 highly variable genes were identified, scaled, and reduced with PC analysis. The top 30 PCs were used for visualization using UMAP with default settings. Clustering was performed as described above with "k.param" set at 30. Top marker genes were calculated with the *Findallmarkers()* function using default settings. Non-EC clusters (negative for *CDH5, PECAM1, KDR, CD34, ESM1* genes) including epithelial cells (*KRT19, CDH6, CLDN3, CLDN4, APOE*), podocytes (*NPHS1, NPSH2, MAFB, WT1, CLIC5*), mesenchymal cells (*COL1A1, COL3A1, COL6A3, POSTN, PDGFRB*) and myeloid cells (*PTPRC, LYZ, MPO, MNDA, DEFA4*), were removed from the dataset for downstream analysis.

EC dataset integration and clustering

Data were integrated according to the transplantation and timepoint conditions. For each condition, the top 2,500 variable features were identified, and used for integration running the *FindIntegrationAnchors()* function with 50 PC and anchor.features set at 2,500, and the IntegrateData() function from the Seurat package. The integrated data were scaled regressing out the percentage of mitochondrial and ribosomal genes, and reduced in 46 PCs that were further used as input for UMAP calculation with "min.dist"=0.1 and "n.neighbors"=50. Clustering was performed as described above with "k.param" set at 12 and the 46 PCs. Top marker genes for each cluster were calculated with the *Findallmarkers()* function, including genes for which Log2FC>0 only, and using other paramaters as default.

Integration of kidney organoids ECs with human fetal kidney ECs

Publicly available fetal kidney datasets were obtained from GEO and the human cell atlas repositories. All fetal kidney samples were collected with informed consent and ethical approval (supplementary data 14). Only samples containing at least ~100 ECs were retained: GSE102596 (1 sample wk16), GSE112570 (2 samples wk17), GSE114530 (1 sample wk16), GSE124472 (1 sample wk15, 2 samples wk17), GSE139280 (2 samples wk14) and ERP120466 (2 samples wk8, 1 sample wk9, 1 sample wk12, 1 sample wk14, 1 sample wk16). All count data were processed using the *NormalizeData()*, *FindVariableFeatures()*, *ScaleData()*, *RunPCA(), RunUMAP()* functions using number of PCs determined according to the output from the *ElbowPlot()* function from the Seurat package, with default settings. EC cluster(s) were obtained from *FindNeighbors()* function with "k.param" set at 30 and *FindClusters()* function using default settings, and by assessing the expression of canonical EC marker genes except for the week 16 sample from GSE114530, for which the "End" annotation was used. EC clusters from each dataset were subset and merged using *subset()* and *merge()* functions, respectively. Samples were further integrated using the canonical correlation analysis from the Seurat pipeline with 20 dimensions, 2,000 variable features, "k.filter" set at 150, and "k.weight" set at 90, from the *FindIntegrationAnchors()* and *IntegrateData()* functions. Integrated data were scaled, and dimensionally reduced to 30 dimensions. The first 8 dimensions were used to generate UMAP plot and identify nearest neighbors with "k.param" set at 30. Clusters were identified with resolution set at 1 from the *FindClusters()* function, with other default parameters. After removal of a cluster representing doublets, the integration pipeline was iterated with EC singlets only, per sample. Parameters used were 15 dimensions, 2,000 anchor features, and k.filter and k.weight set at 140 and 90, respectively. Integrated data were again scaled and dimensionally reduced to 30 dimensions. For preparing the final UMAP, the first 7 dimensions were used with "min.dist" parameter set at 0.1 in the *RunUMAP()* function. Clustering was performed again as previously described with resolution set to 0.8. Marker genes for each cluster were calculated with the *FindAllMarkers()* function setting "only.pos" to TRUE and the other settings used as default. Cluster annotation was based on canonical marker gene expression. This fetal kidney EC dataset was further integrated with the EC dataset from transplanted kidney organoids collected at d7+20. Briefly, gene annotation from the fetal kidney EC dataset was first updated from the GRCh37 to the GRCh38 reference genome using the biomaRt package (v2.58.2). The datasets were then integrated using the canonical correlation analysis from the Seurat pipeline with 20 dimensions, 2,000 anchor features and both "k.filter" and "k.weight" parameters set at 90 for the *FindIntegrationAnchors()* and *IntegrateData()* functions. Integrated data were scaled regressing out the percentage of mitochondrial and ribosomal genes and reduced to 50 PC dimensions. The 20 dimensions were used to generate the UMAP with "min.dist" set at 0.2 and "n.neihbors" at 30.

Comparison of kidney organoid EC clusters with fetal kidney EC clusters

Per cluster average expression of the integrated scaled data from both the kidney organoid ECs collected at d7+20 and fetal kidney ECs was used to assess similiraty. A correlation matrix was generated using the *cor()* function. Output was visualized as heatmap (see Visualization paragraph below).

Marker genes were identified for the “Artery 2” cluster from kidney organoid ECs collected at d7+20 and “kidney artery-afferent arteriole” cluster from fetal kidney ECs using the *FindMarkers()* function for each dataset, with running a MAST test setting the number UMIs per cell as latent variable, and “only.pos” parameter to TRUE. Only significant marker genes were retained (adjusted p-value$<$0.05). Shared marker genes were identified using the *intersect()* function.

Geneset enrichment analysis (GSEA)

Differentially expressed genes in each transplantation and timepoint combination were obtained using the *Findallmarkers()* function using the MAST test, setting the number of UMIs per cell as latent variable, and the “logfc.threshold” and “min.pct” parameters to 0. GSEA was performed on the ranked genes using *gseGO()* function from ClusterProfiler package (v.4.10.0). pValueCutoff was set to 0.05 and the biological process gene ontology was used. GO Terms were simplified using the GOSemSim package (v2.28.1) and the *simplify()* function with mesure and cutoff parameters set to “Rel” and 0.05, respectively. The top 10 upregulated genesets were filtered and visualized using the *dotplot()* function from the ClusterProfiler package.

Geneset expression analysis: module score calculation

Module scores were calculated for each cell to identify proliferating ECs in G1S/S or G2M/M cell cycle stages, and artery, vein and lymphatic EC clusters. Module scores for proliferative ECs were calculated using *CellCycleScoring()* function from the Seurat package using canonical G1S/S and G2M/M cell cycle genes, as listed in Seurat. Calculation of the other module scores was performed using the *AddModuleScore()* function and based on the expression of the canonical marker genes *NRP1, SEMA3G, MECOM, GJA4, GJA5, HEY2, JAG1, JAG2, HES4, EFNB2, SOX17, EPAS1* and *BMX* for artery ECs; *APLNR, NR2F2, NRP2, PLVAP* and *EPHB4* for vein ECs; and *FLT4, THY1, TBX1* and *PROX1* for lymphatic ECs. Quiescent or migrating EC clusters displaying low artery, vein and lymphatic module scores were labelled as capillary ECs.

For the assessment of the transcriptional response to laminar shear stress, geneset was downloaded from the molecular signature database MSigDB (https://www.gsea-msigdb.org/gsea/index.jsp) and the *AddModuleScore()* function was used.

The GOBP_RESPONSE_TO_LAMINAR_FLUID_SHEAR_STRESS geneset included the following genes *KLF2, ACE, ABCA1, MIR126, SMAD6, SMAD7, ASS1, NFE2L2, MAPK7, MAP2K5, SREBF2, TGFB3* and *KLF4*.

Geneset variation analysis (GSVA)

The EC dataset from the Tabula Sapiens study [14]was downloaded from the UCSC cell browser (https://cells.ucsc.edu/?ds=tabula-sapiens+func-compart), and used to generate a Seurat object with the *CreateSeuratObject()* function. Count data were normalized using *NormalizeData()* function. To identify tissue-specific EC marker genes, the *FindAllMarkers()* function setting the "only.pos" to TRUE, was used with selecting "organ_tissue" as grouping variable. Only significantly upregulated marker genes (adjusted p-value<0.05, log2FC>0.5) were retained for each tissue. Moreover, marker genes identified in more than one tissue were discarded. Tissue ECs defined by less than 30 marker genes were removed from the analysis. Finally, only genes also present in the kidney organoid EC dataset were retained, resulting in marker genes and tissues listed in Supplementary Data 10. GSVA was performed with these gene lists and the normalized data matrix of the kidney organoid ECs using the *gsva()* function from the GSVA package (v1.50.5).

Correlation analysis & hierarchical clustering

For correlation analysis of kidney organoid EC conditions, briefly, count data matrix was exported from the Seurat object using the *GetAssayData()* function (selected assay "RNA") and uploaded in the BIOMEX software (v1.5 - https://carmelietlab.sites.vib.be/en/biomex)[46] altogether with the corresponding metadata information. Data were normalized ("Standard" parameter) and (auto)scaled within BIOMEX. They were further grouped according to the transplantation and timepoint combinations, and highly variable genes were used to determine correlation coefficients between conditions. Hierarchical clustering was calculated using Euclidian distance and complete agglomeration method.

Visualization

Gene expression dot plots and heatmaps were created with R using the *DotPlot()* and *Heatmap()* functions from the Seurat and ComplexHeatmap packages (v2.18.0),

respectively, except for the correlation heatmap, which was prepared within BIOMEX. For gene expression heatmaps prepared with the ComplexHeatmap package, briefly, the averaged expression profiles per each cluster and for all genes were calculated using the *AverageExpression()* function from Seurat package. Next, scaled data were obtained from the RNA assay using *GetAssayFunction()* function and selected gene data were extracted from the resulting matrix. These values were used as input for the *Heatmap()* function from the ComplexHeatmap package. UMAP plots were generated using *DimPlot()* and *FeaturePlot()* functions from the Seurat package, for metadata and gene expression visualization, respectively. Violin plots were generated using *VlnPlot()* from the Seurat package. Proportions of the different EC populations were visualized as pie charts or bar plots with the ggplot2 package (v3.4.4).

Analysis of kidney organoid chicken ECs

Processed chicken scRNA-seq data from transplanted organoids at day 7+20 were downloaded from ArrayExpress repository (accession number E-MTAB-11429) and endothelial cells were subset according to the metadata information. After removal of red blood cell-EC doublets, the standard pipeline described above was used. Briefly, data were log-normalized, and the top 2,000 highly variable genes were scaled and used as input for dimensionality reduction via PCA and UMAP (first 12 principal components used, and “min.dist” parameter set at 0.1). Unsupervised clustering was performed as described above with resolution set at 0.6. Cluster-specific marker genes were identified with the *FindAllMarkers()* function from the Seurat package, with “only.pos” parameter set to TRUE. Chicken EC clusters were annotated according to canonical markers and identified top marker gene expression.

Bulk RNA-seq data analysis of iPSC-ECs exposed to laminar flow vs static culture

Raw data from NCRM1 iPSC-ECs were obtained from the BioStudies repository (E-MTAB-8392) and pre-processed as described previously [17]. The NCRM1 cell line is commercially available through RUCDR Infinite Biologics (Piscataway, New Jersey), and was generated by reprogramming of CD34+ cord blood cells using episomal vectors with approval of the institutional review board of the involved hospital. Counts per million were calculated using *cpm()* function from the EdgeR package (v4.0.14). Ensembl IDs were converted to gene symbols using the biomaRt package. *JAG1* expression dot plot was generated in GraphPad Prism (10.2.3). Statistical difference was assessed using paired Student’s t-test (significant if p-value$<$0.05) as implemented in GraphPad Prism.

Data availability

Both raw and processed sequencing data are available upon request to the European Genome-Phenome Archive (EGA): Study EGAS50000001068, Dataset EGAD50000001555.

Code availability

Custom code is available upon reasonable request.

Acknowledgements

We are grateful to Melissa Little (Murdoch Children's Research Institute, Melbourne, Australia) for providing the cell line iPSC-MAFB, and Christian Freund (hiPSC core facility, LUMC, Leiden, the Netherlands) for providing hiPSC line LUMC0072. We acknowledge the support of Saskia van der Wal-Maas (Department of Anatomy & Embryology, LUMC, Leiden, the Netherlands), Conny van Munsteren (Department of Anatomy & Embryology, LUMC, Leiden, the Netherlands), Manon Zuurmond (LUMC, Leiden, the Netherlands), George Galaris (LUMC, Leiden, the Netherlands), Lonneke Gaykema (LUMC, Leiden, the Netherlands), Loes Wiersma (LUMC, Leiden, the Netherlands), and Lin Xie (MGI, BGI-Shenzhen).

References

1 Dumas, S. J. Single-Cell RNA Sequencing Reveals Renal Endothelium Heterogeneity and Metabolic Adaptation to Water Deprivation. JASN (2019).

2 Molema, G. & Aird, W. C. Vascular heterogeneity in the kidney. Semin Nephrol ***32***, 145-155 (2012). https://doi.org:10.1016/j.semnephrol.2012.02.001

3 Jourde-Chiche, N. et al. Endothelium structure and function in kidney health and disease. Nat Rev Nephrol (2019). https://doi.org:10.1038/s41581-018-0098-z

4 Brunskill, E. W. et al. Genes that confer the identity of the renin cell. J Am Soc Nephrol ***22***, 2213-2225 (2011). https://doi.org:10.1681/ASN.2011040401

5 van den Berg, C. W. et al. Renal Subcapsular Transplantation of PSC-Derived Kidney Organoids Induces Neo-vasculogenesis and Significant Glomerular and Tubular Maturation In Vivo. Stem Cell Reports ***10***, 751-765 (2018). https://doi.org:10.1016/j.stemcr.2018.01.041

6 Koning, M. et al. Vasculogenesis in kidney organoids upon transplantation. NPJ Regen Med ***7***, 40 (2022). https://doi.org:10.1038/s41536-022-00237-4

7 Aibar, S. et al. SCENIC: single-cell regulatory network inference and clustering. Nature Methods ***14***, 1083-+ (2017). https://doi.org:10.1038/Nmeth.4463

8 Downes, M. & Koopman, P. SOX18 and the transcriptional regulation of blood vessel development. Trends Cardiovasc Med ***11***, 318-324 (2001). https://doi.org:10.1016/s1050-1738(01)00131-1

9 Wei, G. et al. Ets1 and Ets2 are required for endothelial cell survival during embryonic angiogenesis. Blood ***114***, 1123-1130 (2009). https://doi.org:10.1182/blood-2009-03-211391

10 Zhu, Q., Kim, Y. H., Wang, D., Oh, S. P. & Luo, K. SnoN facilitates ALK1-Smad1/5 signaling during embryonic angiogenesis. J Cell Biol ***202***, 937-950 (2013). https://doi.org:10.1083/jcb.201208113

11 Hermkens, D. M. et al. Sox7 controls arterial specification in conjunction with hey2 and efnb2 function. Development ***142***, 1695-1704 (2015). https://doi.org:10.1242/dev.117275

12 Lilly, A. J., Mazan, A., Scott, D. A., Lacaud, G. & Kouskoff, V. SOX7 expression is critically required in FLK1-expressing cells for vasculogenesis and angiogenesis during mouse embryonic development. Mech Dev ***146***, 31-41 (2017). https://doi.org:10.1016/j.mod.2017.05.004

13 Ryan, A. R. et al. Vascular deficiencies in renal organoids and ex vivo kidney organogenesis. Dev Biol ***477***, 98-116 (2021). https://doi.org:10.1016/j.ydbio.2021.04.009

14 Tabula Sapiens, C. et al. The Tabula Sapiens: A multiple-organ, single-cell transcriptomic atlas of humans. Science ***376***, eabl4896 (2022). https://doi.org:10.1126/science.abl4896

15 Fang, J. S. et al. Shear-induced Notch-Cx37-p27 axis arrests endothelial cell cycle to enable arterial specification. Nat Commun ***8***, 2149 (2017). https://doi.org:10.1038/s41467-017-01742-7

16 Rodriguez, F. S. et al. Jagged1 is a Notch-independent mechanotransducer in endothelial cells. bioRxiv, 2024.2011.2014.623558 (2024). https://doi.org:10.1101/2024.11.14.623558

17 Tiemeier, G. L. et al. Closing the Mitochondrial Permeability Transition Pore in hiPSC-Derived Endothelial Cells Induces Glycocalyx Formation and Functional Maturation. Stem Cell Reports ***13***, 803-816 (2019). https://doi.org:10.1016/j.stemcr.2019.10.005

18 Jankovic, B. D. et al. Immunological capacity of the chicken embryo. I. Relationship between the maturation of lymphoid tissues and the occurrence of cell-mediated immunity in the developing chicken embryo. Immunology ***29***, 497-508 (1975).

19 Alkie, T. N. et al. Development of innate immunity in chicken embryos and newly hatched chicks: a disease control perspective. Avian Pathol ***48***, 288-310 (2019). https://doi.org:10.1080/03079457.2019.1607966

20 Hamburger, V. Morphogenetic and axial self-differentiation of transplanted limb primordia of 2-day chick embryos. Journal of Experimental Zoology ***77***, 379-399 (1938).

21 Rawles, M. E. Transplantation of normal embryonic tissues. Ann N Y Acad Sci ***55***, 302-312 (1952).

22 Rawles, M. E. The Development of Melanophores from Embryonic Mouse Tissues Grown in the Coelom of Chick Embryos. Proc Natl Acad Sci U S A ***26***, 673-680 (1940).

23 Sharmin, S. et al. Human Induced Pluripotent Stem Cell-Derived Podocytes Mature into Vascularized Glomeruli upon Experimental Transplantation. J Am Soc Nephrol ***27***, 1778-1791 (2016). https://doi.org:10.1681/ASN.2015010096

24 Bantounas, I. et al. Generation of Functioning Nephrons by Implanting Human Pluripotent Stem Cell-Derived Kidney Progenitors. Stem Cell Reports ***10***, 766-779 (2018). https://doi.org:10.1016/j.stemcr.2018.01.008

25 Tran, T. et al. In Vivo Developmental Trajectories of Human Podocyte Inform In Vitro Differentiation of Pluripotent Stem Cell-Derived Podocytes. Developmental Cell ***50***, 102-+ (2019). https://doi.org:10.1016/j.devcel.2019.06.001

26 ACUC. ACUC Guideline: The Use and Euthanasia Procedures of Chicken/Avian Embryos., <https://www.cpp.edu/research/research-compliance/iacuc/docs/iacuc-guidelines-on-euthanasia-of-chicken-and-embryos.pdf> (2012).

27 De Bock, K. et al. Role of PFKFB3-driven glycolysis in vessel sprouting. Cell ***154***, 651-663 (2013). https://doi.org:10.1016/j.cell.2013.06.037

28 Xu, Y. et al. Endothelial PFKFB3 plays a critical role in angiogenesis. Arterioscler Thromb Vasc Biol ***34***, 1231-1239 (2014). https://doi.org:10.1161/ATVBAHA.113.303041

29 Rohlenova, K., Veys, K., Miranda-Santos, I., De Bock, K. & Carmeliet, P. Endothelial Cell Metabolism in Health and Disease. Trends Cell Biol ***28***, 224-236 (2018). https://doi.org:10.1016/j.tcb.2017.10.010

30 De Bock, K., Georgiadou, M. & Carmeliet, P. Role of endothelial cell metabolism in vessel sprouting. Cell Metab ***18***, 634-647 (2013). https://doi.org:10.1016/j.cmet.2013.08.001

31 Schumacher, A. et al. Enhanced Microvasculature Formation and Patterning in iPSC-Derived Kidney Organoids Cultured in Physiological Hypoxia. Front Bioeng Biotechnol ***10***, 860138 (2022). https://doi.org:10.3389/fbioe.2022.860138

32 Walls, J. R., Coultas, L., Rossant, J. & Henkelman, R. M. Three-dimensional analysis of vascular development in the mouse embryo. PLoS One ***3***, e2853 (2008). https://doi.org:10.1371/journal.pone.0002853

33 Hou, S. et al. Heterogeneity in endothelial cells and widespread venous arterialization during early vascular development in mammals. Cell Res ***32***, 333-348 (2022). https://doi.org:10.1038/s41422-022-00615-z

34 Maggiore, J. C. et al. A genetically inducible endothelial niche enables vascularization of human kidney organoids with multilineage maturation and emergence of renin expressing cells. Kidney Int (2024). https://doi.org:10.1016/j.kint.2024.05.026

35 Follert, P., Grosse-Segerath, L. & Lammert, E. Blood flow-induced angiocrine signals promote organ growth and regeneration. Bioessays, e2400207 (2024). https://doi.org:10.1002/bies.202400207

36 Bishop, D., Schwarz, Q. & Wiszniak, S. Endothelial-derived angiocrine factors as instructors of embryonic development. Frontiers in Cell and Developmental Biology ***11*** (2023). https://doi.org:ARTN 1172114 10.3389/fcell.2023.1172114

37 Lorenz, L. et al. Mechanosensing by beta1 integrin induces angiocrine signals for liver growth and survival. Nature ***562***, 128-132 (2018). https://doi.org:10.1038/s41586-018-0522-3

38 Homan, K. A. et al. Flow-enhanced vascularization and maturation of kidney organoids in vitro. Nat Methods ***16***, 255-262 (2019). https://doi.org:10.1038/s41592-019-0325-y

39 Menéndez, A. B. C. et al. Creating a kidney organoid-vasculature interaction model using a novel organ-on-chip system. Sci Rep-Uk ***12*** (2022). https://doi.org:ARTN 20699 10.1038/s41598-022-24945-5

40 Zhang, H., Yamaguchi, T., Kokubu, Y. & Kawabata, K. Transient ETV2 Expression Promotes the Generation of Mature Endothelial Cells from Human Pluripotent Stem Cells. Biol Pharm Bull ***45***, 483-490 (2022). https://doi.org:10.1248/bpb.b21-00929

41 De Val, S. & Black, B. L. Transcriptional Control of Endothelial Cell Development. Developmental Cell ***16***, 180-195 (2009). https://doi.org:10.1016/j.devcel.2009.01.014

42 Behrens, A. N. et al. Is Regulated by ETV2 During Cardiovascular Development. Stem Cells and Development ***23***, 2004-2013 (2014). https://doi.org:10.1089/scd.2013.0525

43 Vanslambrouck, J. M. et al. A Toolbox to Characterize Human Induced Pluripotent Stem Cell-Derived Kidney Cell Types and Organoids. J Am Soc Nephrol (2019). https://doi.org:10.1681/ASN.2019030303

44 Hamburger, V. & Hamilton, H. L. A series of normal stages in the development of the chick embryo. 1951. Dev Dyn ***195***, 231-272 (1992). https://doi.org:10.1002/aja.1001950404

45 Jilani, S. M. et al. Selective binding of lectins to embryonic chicken vasculature. J Histochem Cytochem ***51***, 597-604 (2003).

46 Taverna, F. et al. BIOMEX: an interactive workflow for (single cell) omics data interpretation and visualization. Nucleic Acids Res ***48***, W385-W394 (2020). https://doi.org:10.1093/nar/gkaa332

Supplementary figures

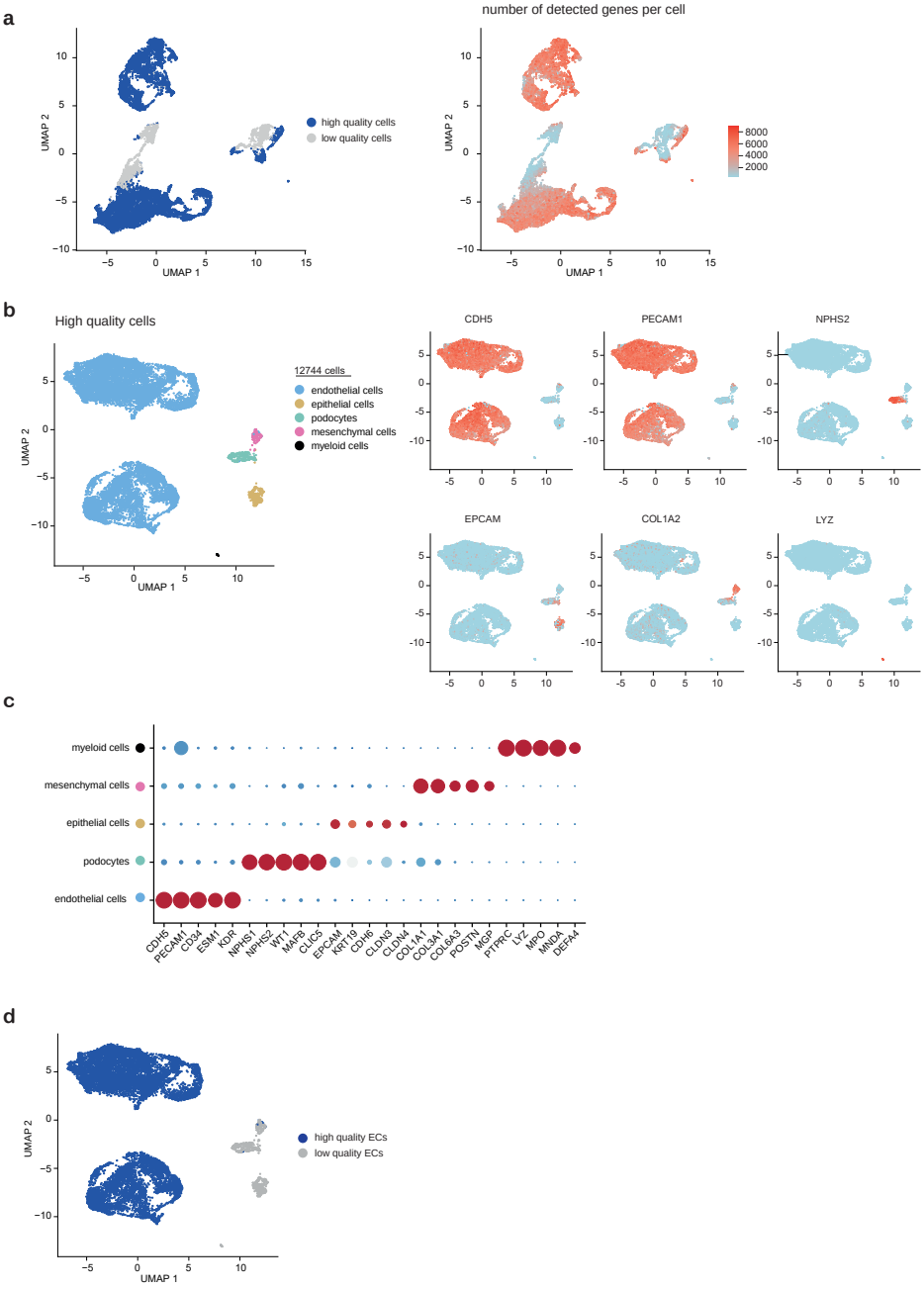

Supplementary figure 1: a UMAP visualization of (left) all enriched human cells and selection of high-quality cells (blue: high-quality cells, grey: low-quality cells and doublets), and (right) number of detected genes per cell. **b** Left: UMAP visualization of a total of 12,744 high quality cells color-coded by cell type: endothelial cells (large majority), epithelial cells, mesenchymal cells, podocytes, myeloid cells. Right: UMAP plots color-coded by the expression level of CDH5, PECAM1, NPHS2, EPCAM, COL1A2, LYZ. **c** Dot plot representing marker gene expression in the different cell clusters. Dot size indicates proportion of cells in cluster expressing a gene, color intensity indicates the level of expression. **d** UMAP visualization of all high quality human cells (grey) and selection of high quality ECs (blue) .

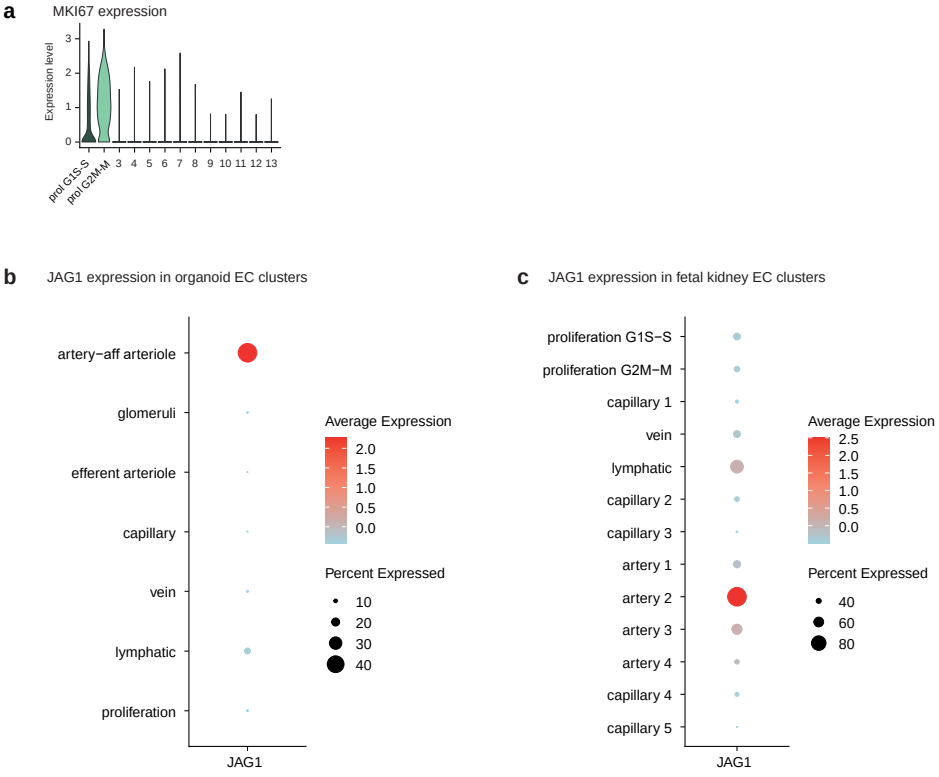

Supplementary figure 2: a Violin plot visualization of the expression level of MKI67 gene per EC cluster. The G1S-S as well as the G2M-M cluster express MKI67, with higher expression level in the G2M-M cluster. **b** Violin plot visualization of the expression level of JAG1 in organoid EC subclusters. **c** Violin plot visualization of the expression level of JAG1 in fetal kidney EC clusters.

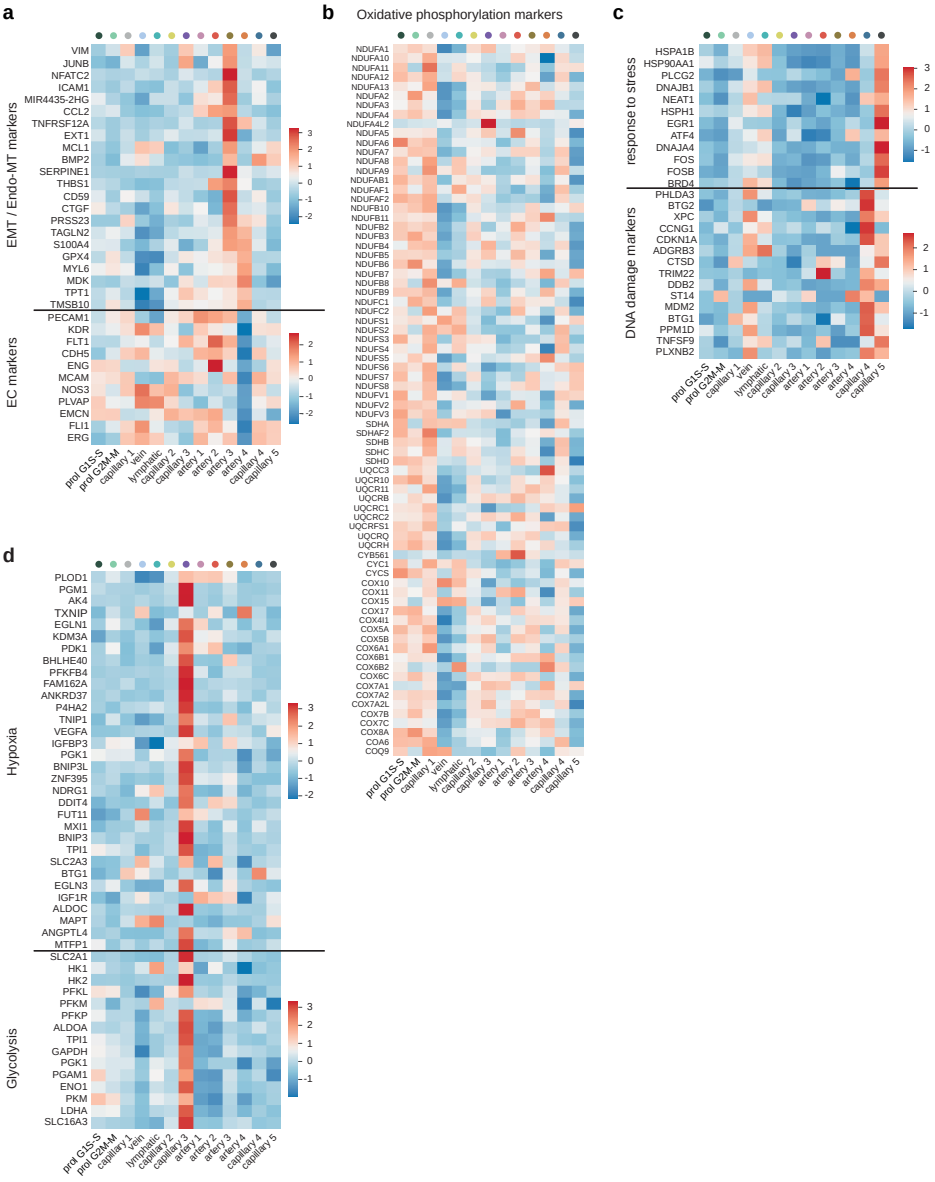

Supplementary figure 3: a Heatmap visualization of the expression of EMT / endo-MT marker genes (top) and EC marker genes (bottom) per EC cluster. Scale: z-score of the gene expression level. **b** Heatmap visualization of the expression of oxidative phosphorylation genes per EC cluster. Scale: z-score of the gene expression level. **c** Heatmap visualization of the expression of response to stress (top) and DNA damage (bottom) genes per EC cluster. Scale: z-score of the gene expression level. **d** Heatmap visualization of the expression of hypoxia (top) and glycolysis (bottom) genes per EC cluster. Scale: z-score of the gene expression level.

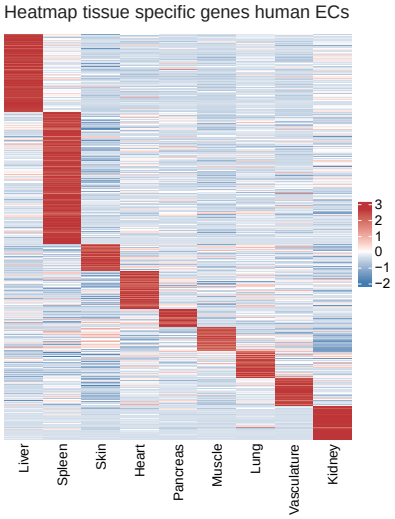

Supplementary figure.4: Heatmap visualization of tissue specific genes of human ECs from different organs. Scale: z-score of the gene expression level

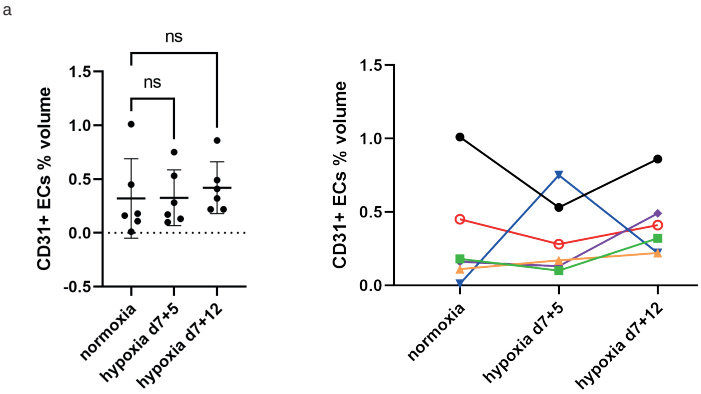

Supplementary figure 5: Quantification of CD31 positive ECs as percent volume of organoid volume in whole mount untransplanted organoids at d7+20, after culture in normoxia or in hypoxia (5%) starting from d7+5 or d7+12 of differentiation. n=6 organoids per condition. Left: There is no significant difference in EC volume between organoids cultured in normoxia and those cultured in hypoxia. Data are presented as individual data points, mean (SD). Means were compared between groups using a One-way ANOVA. Right: Alternative visualization demonstrating similar EC percent volume in normoxia and hypoxia in organoids for each differentiation.

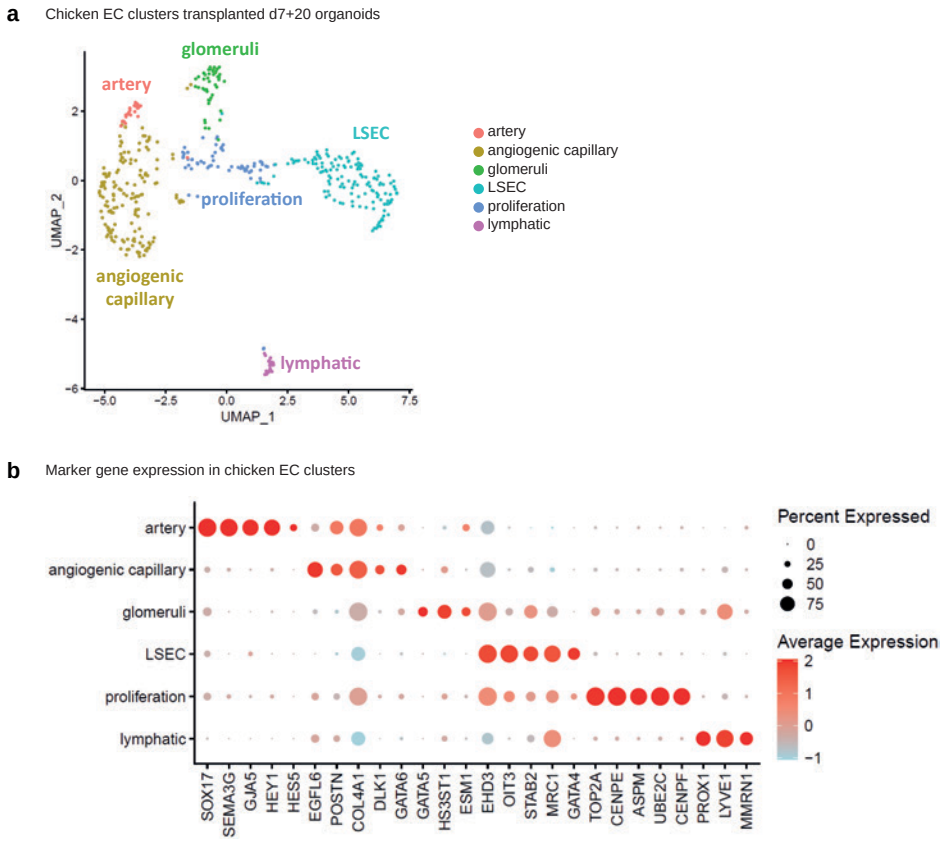

Supplementary figure 6: a UMAP visualization of all chicken ECs from transplanted kidney organoids at day 7+20, color-coded by cluster. 6 subclusters were distinguished: artery, angiogenic capillary, glomeruli, liver sinusoidal endothelial cells (LSEC), proliferation and lymphatic. **b** Dot plot representing marker gene expression in chicken EC clusters. Dot size indicates proportion of cells in a cluster expressing a gene, color intensity indicates the level of expression.

Supplementary tables and movies can be accessed through the following QR code:

CHAPTER 7

General discussion

End stage kidney disease has a major impact on the lives of patients as well as on healthcare costs. In the Netherlands, one year of dialysis for one patient costs 80.000-120.000 euros. The expenses of a kidney transplantation amount to 80.000 euros, after which the yearly costs are much lower than those for dialysis[1]. Due to the insufficient number of donor kidneys and the risks associated with the lifelong use of immunosuppression, there is an urgent need for innovative renal replacement therapies. Human induced pluripotent stem cell (hiPSC) derived kidney organoids provide an excellent base for the development of such strategies. **Chapter 2** describes the characteristics and potential of these organoids that contain nephron-like structures surrounded by stromal and scattered endothelial cells (ECs), and discusses important hurdles towards clinical application. As such, it introduces the main focus of this thesis: The lack of a functional vasculature and consequent immaturity of kidney organoids.

The kidney and its vasculature: an essential collaboration

The notion that the sole function of vasculature is the delivery of blood and nutrients to cells and tissues does not in the least do justice to the complex interaction of blood vessels and vascular ECs with their surroundings. The intricate and specialized renal vasculature is an excellent example of this symbiosis. Kidneys are burdened with the task of maintaining our fluid and electrolyte balance and removing waste products. They manage this by filtering 180L of water per day from the 1500L of blood that pass through them, allowing for passive filtration of waste products into the tubules. Through tubular reabsorption of 99% of the filtered water together with electrolytes and amino acids, around 1,8L of concentrated urine is produced and homeostasis is maintained[2]. The filtration of such large quantities of water is dependent on specialized fenestrated glomerular ECs. The post glomerular vasculature gives rise to peritubular capillaries that surround the proximal tubule, lis of Henle and distal tubules, supporting the reabsorption of water and essential solutes. Without blood vessels, the kidney is unable to execute any of these functions. In addition, the interaction between renal epithelial cells and ECs is essential for the development and maintenance of a mature kidney. During embryonic development, podocyte progenitors recruit ECs through the secretion of VEGF-A [3-5]. In turn, glomerular ECs secrete angiocrine factors including delta-like 4 (DLL4), Dickkopf-related protein 2 (DKK2), semaphorin-5A (SEMA5), VEGF-A and fibroblast growth factor 1 (FGF-1) that are implicated in the differentiation and maintenance of podocytes and mesangial cells [6,7]. Together, ECs and podocytes produce the glomerular basement membrane (GBM). Cross-talk between ECs and epithelial cells in the kidney is not limited to the glomerular

structures. Proximal tubular epithelial cells stimulate ECs to secrete increased amounts of transforming growth factor β1 (TGFβ1), its antagonist α2-macroglobulin, hepatocyte growth factor (HGF) and VEGF, supporting the maintenance and proliferation of the tubular epithelial cells [7,8].

Organoid vascularization upon transplantation: the solution to our problems?

Considering the importance of the interaction between renal progenitors and ECs, it is not surprising that unvascularized kidney organoids lack maturity. Interestingly, they do have the potential to induce sprouting angiogenesis from existing blood vessels upon transplantation in mice[9-11]. To enable detailed analysis of the process of organoid vascularization, in **Chapter 4 and 5** we develop a method for efficient vascularization of kidney organoids through intracoelomic transplantation in chicken embryos. Investigation at a transcriptomic, protein and ultrastructural level demonstrates that a perfused chimeric vascular network is formed in transplanted organoids, consistent with a combination of angiogenesis from host vessels and vasculogenesis from endogenous organoid derived ECs. The vascular network invades the glomerular structures and transplanted organoids display enhanced maturation of glomerular and tubular structures as well as the stromal compartment.

It is reassuring that kidney organoids are vascularized upon transplantation in mice or chicken embryos. It could even be argued that this relieves the need to develop strategies for in vitro vascularization: Upon transplantation of avascular organoids in patients suffering from end stage kidney disease, we might be able to depend on host-derived angiogenesis for vascularization. Indeed, the sparse hiPSC-derived products that have found their way to clinical trials in humans, such as pancreatic islets[12] and heart muscle allografts[13], did not contain a pre-formed vascular network prior to transplantation. However, these products and the vasculature they require are significantly less complex than nephrons, let alone entire kidneys. Although the optimal form and location for future transplantation of hiPSC-derived renal structures are as yet unclear, at least 100.000 functioning nephrons would be required for a clinically relevant effect that could keep a patient off dialysis. If these were delivered to a recipient without a route for blood supply, extensive angiogenesis would be required to assure functional vascularization of the entire graft. In our model of intracoelomic transplantation of bisected organoids containing an estimated 500-1000 nephron-like structures[14], glomerular vascularization commenced 3 days post transplantation, with the blood vessel network further expanding until at least day 7[15]. When transplanting much larger numbers of nephrons, this process is likely to take

even longer, leading to a high risk of ischemic injury. In kidney transplantation, increased ischemia time, defined as the time from organ removal from the donor to perfusion with warm blood in the recipient, is a well-known risk factor for delayed graft function, graft failure, and mortality[16-18]. It occurs despite the presence of a fully formed vascular network in the donor kidney which is immediately connected to the host vasculature during transplantation. While cold ischemia time (time in cold storage after removal from the donor and before transplantation in the recipient) will likely be avoided when transplanting hiPSC-derived organoids, a process akin to warm ischemia time (time from organ removal from cold storage to perfusion with warm blood in the recipient) will occur, and be more extensive than the median 35 minutes in donor kidney transplantation[16]. It is therefore highly preferable to equip iPSC-derived kidney tissue with a vascular network to ensure swift perfusion of the entire graft upon transplantation and avoid ischemic injury with loss of functioning nephrons. In addition, functional vascularization of kidney organoids in vitro would expand the possibilities for their application as models of renal physiology and pathophysiology. Microvascular injury plays a role in the most common causes of kidney disease, namely diabetes mellitus and hypertension. Auto-immune diseases such as ANCA vasculitis damage the glomerular endothelium[19], and rare diseases affecting podocytes or the GBM become most apparent in mature glomeruli. None of these conditions can be optimally modelled in an avascular kidney organoid.

Kidney organoid vascularization in vitro

In **Chapter 3**, we present a method for the in vitro co-culture of kidney organoids with 2 microvessels in a microfluidic chip that enables exposure of the ECs to bidirectional flow. The organoids induce angiogenic sprouting from the microvessels, but a connection between organoids and the newly formed vascular network is not established. Causes can be manifold, with a possible role for an inadequate gradient of angiogenic factors, suboptimal EC characteristics, lack of mural cells, and unphysiological flow. Indeed, the application of laminar flow, even when applied over the top of organoids instead of through blood vessels, has been shown to stimulate organoid EC proliferation[20]. Over the past few years, different designs of microfluidic chips have been developed, each containing a chamber for kidney organoids as well as 1 or more lanes lined with ECs that can be exposed to laminar perfusion[21,22]. These set-ups result in sprouting of ECs from the engineered microvessel toward the organoid[21] or from organoid-derived ECs toward the engineered microvessel[22], with the successful establishment of a connection between organoid and microvessel. The direction of sprouting in the model systems seems dependent on the angiogenic gradient, which is influenced by the absence or

presence of VEGF as a supplement in the medium. Unfortunately, none of these models succeed in vascularization of organoid glomeruli.

Faced with the challenge of replicating in vitro the extensive vascularization process that occurs in vivo, identifying key changes in EC gene expression profiles upon transplantation can provide important clues. Single cell RNA sequencing (scRNAseq) enables the in-depth analysis of the transcriptome of cell clusters and subclusters within tissues[23]. Despite the availability of several kidney organoid scRNAseq datasets[24-26], the characteristics of organoid ECs have long remained elusive due to their limited number within the organoids. In **Chapter 6**, we deploy the efficiency of our model of intracoelomic transplantation to acquire sufficient human organoid-derived ECs for in-depth scRNAseq analysis. Interestingly, in vitro organoid ECs display little similarity to renal ECs, while transplantation induces the appearance of a subcluster of ECs that resemble fetal kidney arterial / afferent arteriolar ECs. In addition, we identify blood flow and transcription factor Sox7 as likely drivers of arterialization and renal specification.

We did not detect a human EC cluster with a glomerular gene signature in transplanted organoids, despite their presence within podocyte clusters on confocal microscopy imaging. This, in combination with the absence of fenestrae in the glomerular ECs on electron microscopy imaging, suggests that organoid ECs might lack the capacity to fully specialize into glomerular ECs. The differentiation protocol for kidney organoids is focussed on generating nephrons from hiPSCs, with ECs appearing as a byproduct. The culture medium and growth factors are not optimized to support EC maintenance and maturation. Furthermore, even iPSC-derived ECs obtained through dedicated stepwise differentiation protocols have been shown to lack maturity[27,28]. The importance of adequate EC differentiation for interaction with the surrounding renal epithelium is supported by the recent finding that enhanced in vitro vascularization can be achieved by mixing hiPSCs with transgenic hiPSCs that express an inducible ETS translocation variant 2 (ETV2) transcription factor during kidney organoid differentiation[29]. ETV2 induction directly differentiates iPSCs to ECs[29,30]. In these organoids, an EC network is formed that encases podocyte clusters, occasionally invades them, and contains a subcluster of ECs displaying a glomerular gene signature. Of note, the EC-podocyte interaction in this model does not fully resemble the in vivo situation, as the glomeruli have an inside-out appearance with ECs encasing podocyte clusters instead of podocytes surrounding capillary loops. The random mixing of ECs with renal progenitor cells and lack of flow in the system might contribute to this organization.

Conclusion and future perspectives

In the decade that has passed since the publication of the first protocols for the generation of kidney organoids from hiPSCs[31-34], important steps have been taken to improve their suitability for regenerative medicine purposes. Progress has been made with regard to scalability[14,35,36], enhancing morphogenesis[37-39], and generation of immune-evasive iPSCs[40-42]. At the same time, the fast progression in the field of single cell transcriptomics[23] and spatial metabolomics provided new possibilities to characterize kidney organoids. This confirmed a resemblance to first trimester human fetal kidneys[24], but also brought to light variation between organoids from different batches, the presence of off-target cell populations[25,26], and metabolic immaturity of organoid proximal tubules[43]. As our knowledge of kidney organoids expands, we thus become increasingly aware of the remaining challenges.

In focussing on the vascularization of kidney organoids, this thesis addresses one of the major challenges. It provides detailed information on the process of vascularization and maturation of organoids upon transplantation in an efficient and reproducible in vivo model, demonstrates the potential and limitations of endogenous organoid ECs, and identifies modifiable factors for future research. Moving forward, robust vascularization and maturation of kidney organoids in vitro will likely require a source of well differentiated and plastic ECs exposed to laminar flow. Achieving this will advance kidney organoid applicability for modeling renal physiology and disease and be an important step towards suitability for renal replacement therapy.

References

1. Nierstichting. Nierstichting.nl Feiten en cijfers Vol. 2025 (2023).
2. Smith, H.W. From Fish to Philosopher, (The Natural History Library Anchor Books, Doubleday & Company, INC. , 1961).
3. Eremina, V., et al. Glomerular-specific alterations of VEGF-A expression lead to distinct congenital and acquired renal diseases. J Clin Invest ***111***, 707-716 (2003).
4. Kitamoto, Y., Tokunaga, H. & Tomita, K. Vascular endothelial growth factor is an essential molecule for mouse kidney development: glomerulogenesis and nephrogenesis. J Clin Invest ***99***, 2351-2357 (1997).
5. Sison, K., et al. Glomerular structure and function require paracrine, not autocrine, VEGF-VEGFR-2 signaling. J Am Soc Nephrol ***21***, 1691-1701 (2010).
6. Dumas, S.J., et al. Phenotypic diversity and metabolic specialization of renal endothelial cells. Nat Rev Nephrol ***17***, 441-464 (2021).
7. van den Berg, C.W., Dumas, S.J., Little, M.H. & Rabelink, T.J. Challenges in maturation and integration of kidney organoids for stem cell-based renal replacement therapy. Kidney Int ***107***, 262-270 (2025).
8. Tasnim, F. & Zink, D. Cross talk between primary human renal tubular cells and endothelial cells in cocultures. Am J Physiol Renal Physiol ***302***, F1055-1062 (2012).
9. van den Berg, C.W., Koudijs, A., Ritsma, L. & Rabelink, T.J. In Vivo Assessment of Size-Selective Glomerular Sieving in Transplanted Human Induced Pluripotent Stem Cell-Derived Kidney Organoids. J Am Soc Nephrol ***31***, 921-929 (2020).
10. van den Berg, C.W., et al. Renal Subcapsular Transplantation of PSC-Derived Kidney Organoids Induces Neo-vasculogenesis and Significant Glomerular and Tubular Maturation In Vivo. Stem Cell Reports ***10***, 751-765 (2018).
11. Bantounas, I., et al. Generation of Functioning Nephrons by Implanting Human Pluripotent Stem Cell-Derived Kidney Progenitors. Stem Cell Reports ***10***, 766-779 (2018).
12. Wang, S., et al. Transplantation of chemically induced pluripotent stem-cell-derived islets under abdominal anterior rectus sheath in a type 1 diabetes patient. Cell ***187***, 6152-6164 e6118 (2024).
13. Jebran, A.F., et al. Engineered heart muscle allografts for heart repair in primates and humans. Nature (2025).
14. Wiersma, L.E., Avramut, M.C., Lievers, E., Rabelink, T.J. & van den Berg, C.W. Large-scale engineering of hiPSC-derived nephron sheets and cryopreservation of their progenitors. Stem Cell Res Ther ***13***, 208 (2022).
15. Koning, M., et al. Vasculogenesis in kidney organoids upon transplantation. NPJ Regen Med ***7***, 40 (2022).
16. Tennankore, K.K., Kim, S.J., Alwayn, I.P. & Kiberd, B.A. Prolonged warm ischemia time is associated with graft failure and mortality after kidney transplantation. Kidney Int ***89***, 648-658 (2016).
17. Ponticelli, C.E. The impact of cold ischemia time on renal transplant outcome. Kidney Int ***87***, 272-275 (2015).
18. Debout, A., et al. Each additional hour of cold ischemia time significantly increases the risk of graft failure and mortality following renal transplantation. Kidney Int ***87***, 343-349 (2015).
19. Halbwachs, L. & Lesavre, P. Endothelium-neutrophil interactions in ANCA-associated diseases. J Am Soc Nephrol ***23***, 1449-1461 (2012).

20. Homan, K.A., et al. Flow-enhanced vascularization and maturation of kidney organoids in vitro. Nat Methods ***16***, 255-262 (2019).
21. Menéndez, A.B.C., et al. Creating a kidney organoid-vasculature interaction model using a novel organ-on-chip system. Sci Rep-Uk ***12***(2022).
22. Kroll, K.T., et al. A perfusable, vascularized kidney organoid-on-chip model. Biofabrication ***16***(2024).
23. Aldridge, S. & Teichmann, S.A. Single cell transcriptomics comes of age. Nat Commun ***11***, 4307 (2020).
24. Combes, A.N., Zappia, L., Er, P.X., Oshlack, A. & Little, M.H. Single-cell analysis reveals congruence between kidney organoids and human fetal kidney. Genome Med ***11***, 3 (2019).
25. Phipson, B., et al. Evaluation of variability in human kidney organoids. Nat Methods ***16***, 79-87 (2019).
26. Wu, H., et al. Comparative Analysis and Refinement of Human PSC-Derived Kidney Organoid Differentiation with Single-Cell Transcriptomics. Cell Stem Cell (2018).
27. Tiemeier, G.L., et al. Closing the Mitochondrial Permeability Transition Pore in hiPSC-Derived Endothelial Cells Induces Glycocalyx Formation and Functional Maturation. Stem Cell Reports ***13***, 803-816 (2019).
28. Tiemeier, G.L., et al. Lowering the increased intracellular pH of human-induced pluripotent stem cell-derived endothelial cells induces formation of mature Weibel-Palade bodies. Stem Cells Transl Med (2020).
29. Maggiore, J.C., et al. A genetically inducible endothelial niche enables vascularization of human kidney organoids with multilineage maturation and emergence of renin expressing cells. Kidney Int (2024).
30. Zhang, H., Yamaguchi, T., Kokubu, Y. & Kawabata, K. Transient ETV2 Expression Promotes the Generation of Mature Endothelial Cells from Human Pluripotent Stem Cells. Biol Pharm Bull ***45***, 483-490 (2022).
31. Takasato, M., et al. Kidney organoids from human iPS cells contain multiple lineages and model human nephrogenesis. Nature ***526***, 564-568 (2015).
32. Taguchi, A., et al. Redefining the in vivo origin of metanephric nephron progenitors enables generation of complex kidney structures from pluripotent stem cells. Cell Stem Cell ***14***, 53-67 (2014).
33. Morizane, R., et al. Nephron organoids derived from human pluripotent stem cells model kidney development and injury. Nat Biotechnol ***33***, 1193-1200 (2015).
34. Freedman, B.S., et al. Modelling kidney disease with CRISPR-mutant kidney organoids derived from human pluripotent epiblast spheroids. Nat Commun ***6***, 8715 (2015).
35. Kumar, S.V., et al. Kidney micro-organoids in suspension culture as a scalable source of human pluripotent stem cell-derived kidney cells. Development ***146***(2019).
36. Lawlor, K.T., et al. Cellular extrusion bioprinting improves kidney organoid reproducibility and conformation. Nat Mater ***20***, 260-271 (2021).
37. Taguchi, A. & Nishinakamura, R. Higher-Order Kidney Organogenesis from Pluripotent Stem Cells. Cell Stem Cell (2017).
38. Uchimura, K., Wu, H., Yoshimura, Y. & Humphreys, B.D. Human Pluripotent Stem Cell-Derived Kidney Organoids with Improved Collecting Duct Maturation and Injury Modeling. Cell Rep ***33***, 108514 (2020).

39. Vanslambrouck, J.M., et al. Enhanced metanephric specification to functional proximal tubule enables toxicity screening and infectious disease modelling in kidney organoids. Nat Commun ***13***, 5943 (2022).
40. Simpson, A., Hewitt, A.W. & Fairfax, K.A. Universal cell donor lines: A review of the current research. Stem Cell Reports ***18***, 2038-2046 (2023).
41. Gaykema, L.H., et al. Inhibition of complement activation by CD55 overexpression in human induced pluripotent stem cell derived kidney organoids. Front Immunol ***13***, 1058763 (2022).
42. Gaykema, L.H., et al. T-Cell Mediated Immune Rejection of Beta-2-Microglobulin Knockout Induced Pluripotent Stem Cell-Derived Kidney Organoids. Stem Cells Transl Med ***13***, 69-82 (2024).
43. Wang, G., et al. Spatial dynamic metabolomics identifies metabolic cell fate trajectories in human kidney differentiation. Cell Stem Cell ***29***, 1580-1593 e1587 (2022).

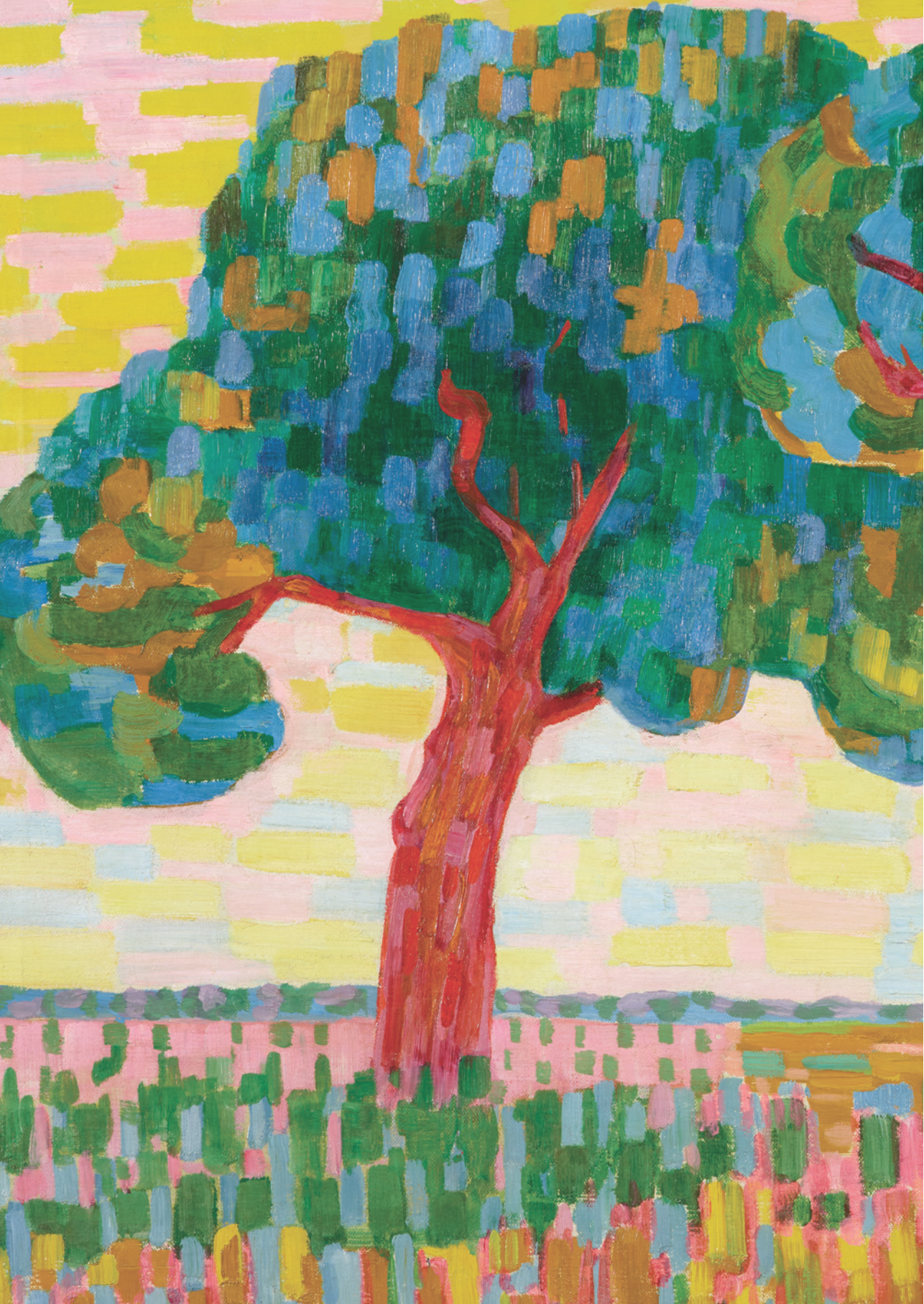

APPENDICES

Nederlandse samenvatting

Curriculum Vitae

Publicatielijst

Dankwoord

Nederlandse samenvatting

Nierfalen

Chronische nierschade komt bij ongeveer 10% van de Nederlanders voor. Een deel van de mensen met chronische nierschade ontwikkelt nierfalen, waarbij de nieren minder dan 15% werken. Bij nierfalen hopen vocht en afvalstoffen die normaal gesproken via de nieren uitgeplast worden zich op, waardoor patiënten last kunnen krijgen van onder andere kortademigheid, misselijkheid, gewichtsverlies en sufheid. Voor deze patiënten bestaan 3 behandelmogelijkheden: conservatieve behandeling, dialyse of een niertransplantatie. Conservatieve behandeling bestaat uit het met medicijnen behandelen van de symptomen van nierfalen zonder nierfunctievervangende therapie, waarbij de resterende nierfunctie zo lang mogelijk behouden wordt.

Dialyse, door middel van een kunstnier (hemodialyse) of buikspoelen (peritoneale dialyse), kan ongeveer 10-15% van de nierfunctie vervangen. Dit is een belastende behandeling, met grote invloed op het dagelijks leven en een hoog risico op hart- en vaatziekten en overlijden.

Niertransplantatie is momenteel de behandeling met de beste resultaten. Door het tekort aan donororganen is er echter een wachtlijst die in Nederland elk jaar langer wordt. Bovendien zijn sommige patiënten te kwetsbaar om een operatie en de levenslange behandeling met afweer onderdrukkende medicijnen die noodzakelijk is na transplantatie te ondergaan. Er is daarom dringend behoefte aan nieuwe behandelmethoden voor nierziekten en nierfalen.

Wat daarbij kan helpen, is de ontwikkeling van nierorganoïden, mini-niertjes die in het lab worden gemaakt.

Nierorganoïden maken uit stamcellen

Nierorganoïden kunnen gemaakt worden vanuit pluripotente stamcellen. Pluripotente stamcellen zijn aanwezig in de hele vroege embryonale ontwikkeling. Ze hebben de bijzondere eigenschap dat ze zich veelvuldig kunnen vermenigvuldigen als stamcellen, maar zich ook kunnen specialiseren tot elk celtype in het menselijk lichaam. In 2007 is ontdekt dat volwassen cellen, zoals huidcellen, geherprogrammeerd kunnen worden tot stamcellen. Deze stamcellen worden geïnduceerde pluripotente stamcellen (iPSCs) genoemd en bieden een oneindige bron van stamcellen. Sindsdien zijn methoden ontwikkeld om vanuit iPSCs vele soorten cellen te maken, zoals hartspiercellen, darmcellen en kraakbeen. En ook niercellen.

Het ingewikkelde van nieren is dat ze uit meer dan 20 gespecialiseerde celtypen bestaan die met elkaar samenwerken. Al die celtypen moeten tegelijk vanuit stamcellen gevormd worden om functionerend nierweefsel te kunnen maken.

Door iPSCs in het lab bloot te stellen aan groeifactoren waarvan we weten dat ze een belangrijke rol spelen bij de embryonale ontwikkeling van de nier, kunnen nierorganoïden gemaakt worden. Deze nierorganoïden zijn ongeveer 0,5 x 0,5 x 0,1cm groot en bevatten structuren die lijken op nierweefsel. Nierorganoïden in hun huidige vorm zijn in onderzoeksverband al gebruikt om te testen of medicatie schadelijk is voor de nieren en om bepaalde nierziekten te modelleren, wat hopelijk in de toekomst de noodzaak voor het gebruik van proefdieren zal verminderen.

De impact van nierorganoïden zou veel groter zijn als ze gebruikt konden worden om patiënten met nierfalen te behandelen. Er zijn echter belangrijke beperkingen die een dergelijke toepassing in de weg staan: Nierorganoïden bevatten cellen die niet in de nier thuishoren, ze zijn veel te klein om de nierfunctie over te nemen en hebben geen systeem voor de afvoer van urine. Een andere grote zorg is dat nierorganoïden geen functionele bloedvaten hebben en als gevolg daarvan onvolwassen zijn.

Het belang van bloedvaten in de nier

Volwassen nieren zijn zeer goed doorbloed en hebben een ingewikkeld netwerk van bloedvaten. Iedere nier bevat ongeveer 1 miljoen nefronen, de functionele eenheden van de nier. Elk nefron bestaat uit een nierfilter (glomerulus) en een systeem van nierbuisjes (tubuli). Elke dag stroomt er ongeveer 1500 liter bloed door de nieren. Daaruit wordt in de glomeruli 180 liter voorurine gemaakt. Vervolgens wordt in de tubuli bijna al het water en de zouten weer opgenomen, waardoor uiteindelijk ongeveer 1,8 liter urine overblijft. Op deze manier houden de nieren de water- en zoutbalans in het lichaam op peil en worden afvalstoffen afgevoerd.

Om zoveel bloed te kunnen filteren, zit in elke glomerulus een fijn netwerk van kleine bloedvaatjes. Deze bestaan uit speciale bloedvatwandcellen, de glomerulaire endotheelcellen. Samen met een laagje bindweefsel (de glomerulaire basaalmembraan, GBM) en gespecialiseerde cellen die daar bovenop liggen (de podocyten), vormen ze het nierfilter (Figuur 1). Zonder bloedvaten kan dit filter niet ontstaan, blijven de niercellen onvolwassen en kan de nier dus niet goed werken.

Nierorganoïden bevatten wel endotheelcellen, maar deze cellen vormen geen bloedvaten en werken niet samen met de podocyten. Daardoor wordt er geen filter gevormd en ontstaat er geen functionerend nierweefsel (Figuur 1). Dit vormt een belangrijke beperking voor het gebruik van nierorganoïden voor het modelleren van nierziekten en voor transplantatie.

Het doel van dit proefschrift is daarom het onderzoeken en bevorderen van de bloedvatvoorziening van nierorganoïden.

Bovengenoemde overwegingen worden uitgebreid besproken in de inleiding van dit proefschrift in **Hoofdstuk 1.**

In **Hoofdstuk 2** worden de verschillende manieren behandeld waarop nierorganoïden uit stamcellen kunnen worden gemaakt, inclusief hun voor- en nadelen. Deze methoden leveren wel organoïden op met structuren die lijken op nefronen, maar in geen van de gevallen ontstaat een netwerk van bloedvaten. Een methode die wél effectief blijkt om bloedvaten te laten groeien in nierorganoïden, is hun transplantatie in muizen. In zulke experimenten valt op dat bloedvaten vanuit de muis de organoïde in groeien en er vervolgens een netwerk in vormen.

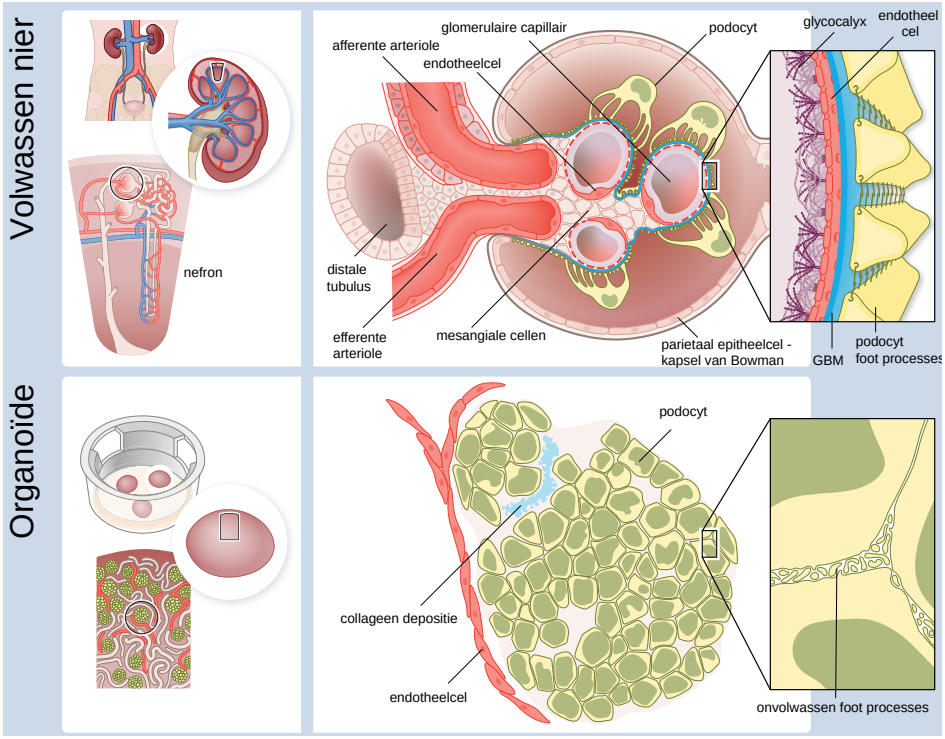

Figuur 1: Glomerulus in de volwassen nier (boven) en in een nierorganoïde (onder).
Volwassen nier: De nieren liggen aan de achterzijde van het lichaam, net onder de onderste ribben. Een nier bevat ongeveer 1 miljoen nefronen, die bestaan uit nierfilters (glomeruli) en nierbuisjes (tubuli). De glomerulus in de volwassen nier bestaat uit een netwerk van kleine bloedvaten, bekleed met endotheelcellen, die worden ondersteund door mesangiale cellen en omgeven door podocyten. Bloed komt de glomerulus binnen via het aanvoerende bloedvat, de afferente arteriole. Filtratie vindt plaats via de glomerulaire filtratiebarrière; de voorurine komt terecht in de ruimte rondom de podocyten (ruimte van Bowman) en stroomt vervolgens de nierbuisjes in. Het bloed verlaat

de glomerulus via het afvoerende bloedvat, de efferente arteriole. In de uitvergroting wordt de glomerulaire filtratiebarrière, die bestaat uit endotheelcellen, de glomerulaire basaalmembraan en de voetvormige uitsteeksels van de podocyten, in detail weergegeven.
Nierorganoïde: Nierorganoïden worden in het lab gekweekt in kweekschaaltjes met een filter erin. Ze bevatten glomerulaire structuren, tubulaire structuren en endotheelcellen. De glomerulaire structuren in nierorganoïden bestaan uit clusters van podocyten. De beperkte hoeveelheid endotheelcellen in de nierorganoïden dringt de glomerulaire structuren niet binnen. De noodzakelijke interactie tussen endotheelcellen en podocyten voor een correcte ontwikkeling van de glomerulaire filtratiebarrière vindt daardoor niet plaats. Als gevolg hiervan blijven de glomeruli en nefronen in organoïden onrijp.

In **Hoofdstuk 3** onderzoeken we of we een vergelijkbaar effect kunnen bereiken zonder transplantatie, door in het lab een andere bron van bloedvaten aan te bieden. We kweken de nierorganoïden dicht bij kleine bloedvaatjes in een speciale kweekplaat die dit soort co-kweek ondersteunt. Dit werkt gedeeltelijk. Er ontstaan nieuwe bloedvaatjes vanuit de bestaande microvaten, een proces dat angiogenese wordt genoemd. Deze bloedvaatjes groeien richting de organoïde, aangetrokken door de groeifactor VEGF, die de organoïde produceert. Helaas ontstaat er geen verbinding tussen het nieuwe bloedvatnetwerk en de organoïden. Ook aanpassing van de kweekomstandigheden verbeterde de resultaten niet. Een mogelijke verklaring is de afwezigheid van bloeddoorstroming. Hoewel de kweekplaat op een apparaat geplaatst wordt dat de plaat heen en weer beweegt om enige matige van stroming na te bootsen, komt dit niet overeen met de normale bloeddoorstroming.

We besloten daarom om een stap terug te doen en eerst goed te onderzoeken hoe nierorganoïden doorbloed worden na transplantatie. Om dit mogelijk te maken, ontwikkelen we in **Hoofdstuk 4** een nieuwe, efficiënte methode voor de transplantatie van nierorganoïden in de lichaamsholte van kippenembryo's. Kippenembryo's zijn hiervoor geschikt omdat ze tijdens hun ontwikkeling gemakkelijk toegankelijk zijn door een opening in de eierschaal te maken. Na transplantatie kunnen de embryo's zich goed verder ontwikkelen terwijl getransplanteerde weefsels uitrijpen.

En wat blijkt: nierorganoïden die volgens onze methode in kippenembryos getransplanteerd worden, raken binnen 8 dagen doorbloed. We laten zien dat de menselijke endotheelcellen die vóór transplantatie in de organoïde aanwezig zijn, na transplantatie toenemen in aantal. Samen met de endotheelcellen van het kippenembryo vormen ze een netwerk van bloedvaten dat zich door de organoïde verspreidt en waarbij ook de glomeruli doorbloed worden. In vergelijking met niet-getransplanteerde organoïden zijn de getransplanteerde organoïden verder ontwikkeld. Er ontstaat zelfs een beginnende GBM doordat de endotheelcellen in contact komen met de podocyten. Het gedetailleerde protocol voor transplantatie van nierorganoïden in kippenembryos wordt beschreven in **Hoofdstuk 5**.

De experimenten in Hoofdstuk 5 en 6 tonen aan dat transplantatie een positief effect heeft op de menselijke endotheelcellen die al in het kweekschaaltje in de organoïde aanwezig zijn. Deze cellen kunnen zich vermenigvuldigen, bloedvaten vormen en zelfs de glomeruli binnendringen wanneer ze aan de juiste omstandigheden worden blootgesteld. Om beter te begrijpen welke factoren daarbij een rol spelen, vergelijken we in **Hoofdstuk 6** de endotheelcellen uit getransplanteerde organoïden met endotheelcellen uit ongetransplanteerde organoïden. Omdat er maar weinig endotheelcellen in een organoïde zitten, verzamelen we hiervoor de endotheelcellen uit in totaal meer dan 200 organoïden. Vervolgens analyseren we deze cellen door middel van single cell RNA sequencing, een techniek waarmee we kunnen zien welke genen in individuele cellen actief zijn. Hieruit blijkt dat de endotheelcellen in ongetransplanteerde organoïden vooral lijken op bloedvatcellen in aders. Na transplantatie nemen ze daarentegen eigenschappen aan van slagaderlijke bloedvatcellen. Bovendien lijken sommige endotheelcellen in getransplanteerde organoïden op de cellen die normaal in menselijke foetale nieren voorkomen, terwijl dit bij ongetransplanteerde organoïden helemaal niet het geval is. Belangrijke factoren die hier waarschijnlijk een rol bij spelen, zijn de bloeddoorstroming na transplantatie en een gen genaamd SOX7, dat betrokken is bij de vorming van bloedvaten en slagaders. Dit zijn mogelijke aanknopingspunten om in de toekomst de bloedvoorziening van nierorganoïden te verbeteren. Helaas vinden we ook in getransplanteerde organoïden geen gespecialiseerde glomerulaire endotheelcellen. Dit kan betekenen dat de endotheelcellen in organoïden niet volwassen genoeg zijn om zich volledig te specialiseren.

Hoofdstuk 7 bevat een bespreking van de resultaten die in dit proefschrift worden gepresenteerd, evenals de toekomstige mogelijkheden van nierorganoïden voor onderzoek en regeneratieve geneeskunde.

Conclusie en toekomstperspectieven

Sinds de eerste methoden zijn ontwikkeld om nierorganoïden te maken uit iPSCs, zijn er grote stappen gezet om deze mini-nieren geschikter te maken voor transplantatie. Zo is er vooruitgang geboekt in het opschalen van de productie en in de structuur en ordening van nefronen binnen de organoïden. Daarnaast hebben nieuwe onderzoekstechnieken het mogelijk gemaakt om nierorganoïden veel gedetailleerder te bestuderen. Hierdoor werd bevestigd dat organoïden lijken op menselijke foetale nieren, maar kwamen er ook belangrijke beperkingen aan het licht. Zo is er veel variatie tussen organoïden die in verschillende batches worden gekweekt, bevatten organoïden soms celtypen die niet in een echte nier voorkomen, en zijn de cellen in de organoïden nog onvolwassen. Naarmate

we meer leren over nierorganoïden, worden we ons dus ook bewuster van de uitdagingen die nog moeten worden opgelost.

Dit proefschrift richt zich op een van de grootste uitdagingen: de vorming van bloedvaten in nierorganoïden. Het beschrijft in detail hoe bloedvaten zich ontwikkelen en organoïden verder rijpen na transplantatie, gebruikmakend van een efficiënt en goed reproduceerbaar model. Verder laat het zien wat de mogelijkheden en beperkingen zijn van de endotheelcellen in organoïden en identificeert het factoren die kunnen worden aangepast voor toekomstig onderzoek.

Om in het laboratorium nierorganoïden te maken met een functioneel bloedvatstelsel, is waarschijnlijk een bron van endotheelcellen nodig die volwassen én flexibel zijn, en die worden blootgesteld aan een gelijkmatige vloeistofstroom zoals in echte bloedvaten. Als dit lukt, zal dat de waarde van nierorganoïden voor het bestuderen van nierziekten vergroten en een belangrijke stap zijn richting hun toepassing als nierfunctievervangende therapie.

Curriculum Vitae

Marije Koning werd geboren op 28 februari 1987 in Montgomery County in de Verenigde Staten van Amerika. In 2005 behaalde ze haar middelbare school diploma aan het Stedelijk Gymnasium Leiden en startte ze met haar studie Geneeskunde aan de Universiteit Maastricht. Tijdens haar studie verbleef ze meermaals in het buitenland voor co-schappen en wetenschapsstage. Haar keuze co-schap interne geneeskunde voltooide ze in het Mulago Hospital in Kampala, Oeganda. Haar wetenschapsstage deed ze bij de afdeling Maag-, Darm- en Leverziekten (MDL) van de University of Otago in Christchurch, Nieuw-Zeeland. Ze deed hier onder begeleiding van prof. dr. Barclay en dr. Gearry onderzoek naar het gebruik van alternatieve en complementaire geneeswijzen door patiënten met inflammatoire darmziekten. Tijdens haar semi-arts stage bij de interne geneeskunde en MDL in het Orbis Medisch Centrum in Sittard werd duidelijk dat haar interesse primair bij de interne geneeskunde lag. Na het afronden van haar studie in augustus 2012 werkte ze als arts niet in opleiding tot internist in het HagaZiekenhuis in Den Haag. Vanaf 2014 begon ze in hetzelfde ziekenhuis met haar opleiding tot internist onder begeleiding van opleiders dr. van Aken en dr. van Buren. Daar ontstond haar interesse voor de nefrologie. Van 2017 tot en met 2019 en in 2022 onderbrak ze haar opleiding voor haar promotietraject op de afdeling nefrologie in het LUMC, onder begeleiding van prof. dr. Rabelink en dr. van den Berg. Gedurende deze periode presenteerde ze de resultaten van haar onderzoek op nationale en internationale stamcel congressen. In 2023 begon ze aan haar differentiatie nefrologie, die ze combineerde met de afronding van haar proefschrift. In 2025 rondde ze haar opleiding tot internist-nefroloog af. Momenteel is Marije werkzaam in het LUMC als internist-nefroloog.

Publicatielijst

M. Koning, S.J. Dumas, E. Meta, E. Lievers, A.M.A. de Graaf, M. Borri, L.J. Nai Chung Tong, X. Liang, P. Liu, F. Chen, L. Lin, Y. Luo, P. Carmeliet, C.W. van den Berg, A.J. Rabelink. Single cell transcriptomics of human kidney organoid endothelium reveals vessel growth processes and arterial maturation upon transplantation. NPJ Regenerative Medicine 2025.

J.A. de Klerk, R.C. Slieker, W.C. Parker, H. Wu, Y. Muto, R.J. Postma, L.M. ‘t Hart, J.H.D. Peerlings, F. Herrewijnen, H. Song, H.S. Spijker, S.J. Dumas, **M. Koning**, L.A.K. van der Pluijm, H.J. Baelde, T. Gerrits, J.I. Rotmans, A.J. van Zonneveld, C. van Solingen, B.D. Humphreys, R. Bijkerk. Cell type-specific expression of long noncoding RNAs in human diabetic kidneys identifies TARID as a key regulator of podocyte function. Diabetes 2025.

M. Koning, E. Lievers, T. Jaffredo, C.W. van den Berg, A.J. Rabelink. Efficient vascularization of kidney organoids through intracoelomic transplantation in chicken embryos. Journal of Visualized Experiments 2023.

G. Wang, B. Heijs, S. Kostidis, R.G.J. Rietjens, **M. Koning**, L. Yuan, G.L. Tiemeier, A. Mahfouz, S.J. Dumas, M. Giera, J. Kers, S.M. Chuva de Sousa Lopes, C.W. van den Berg, B.M. van den Berg, A.J. Rabelink. Spatial dynamic metabolomics identifies metabolic cell fate trajectories in human kidney differentiation. Cell Stem Cell 2022.

M. Koning, S.J. Dumas, M.C. Avramut, R.I. Koning, E. Meta, E. Lievers, L.E. Wiersma, M. Borri, X. Liang, L. Xie, P. Liu, F. Chen, L. Lin, Y. Luo, J. Mulder, H.S. Spijker, T. Jaffredo, B.M. van den Berg, P. Carmeliet, C.W. van den Berg, A.J. Rabelink. Vasculogenesis in kidney organoids upon transplantation. NPJ Regenerative Medicine 2022.

M. Koning, C.W. van den Berg, A.J. Rabelink. Stem cell-derived kidney organoids: engineering the vasculature. Cellular and Molecular Life Sciences 2019.

C.W. van den Berg, L. Ritsma, M.C. Avramut, L.E. Wiersma, B.M. van den Berg, D.G. Leuning, E. Lievers, **M. Koning**, J.M. Vanslambrouck, A.J. Koster, S.E. Howden, M. Takasato, M.H. Little, A.J. Rabelink. Renal subcapsular transplantation of PSC-derived kidney organoids induces neo-vasculogenesis and significant glomerular and tubular maturation in vivo. Stem Cell Reports 2018

M. Koning, L.M. van der Pol, E.F. Schippers. Peritonitis tuberculosa. Nederlands Tijdschrift voor Geneeskunde 2017.

M.Koning, R. Allabouni, R.B. Gearry, C.M.A. Frampton, M.L. Barclay. Use and predictors of oral complementary and alternative medicine by patients with inflammatory bowel disease: a population-based, case-control study. Inflammatory Bowel Diseases 2013.

Dankwoord

Dit proefschrift is tot stand gekomen met de hulp van vele anderen, die ik hier graag wil bedanken.

Prof. dr. Rabelink, beste Ton, jij gaf me de kans om mijn horizon te verbreden en de schoonheid van de fundamentele wetenschap te ontdekken. Dank voor je vertrouwen, je aanstekelijke enthousiasme voor het onderzoek en de vele gesprekken over alle facetten van de wetenschap en de kliniek, die tegelijkertijd rust boden en stof tot nadenken gaven.

Dr. van den Berg, beste Cathelijne, veel dank voor de laagdrempelige, secure en stabiele manier waarop je mij hebt begeleid. Je oprechte belangstelling voor de zaken die me zowel op als buiten het werk bezighielden waardeer ik zeer.

Het iPSC-Organoid team:
Loes, jij was er voor mij vanaf de eerste dag van mijn promotietraject en hebt me samen met Cathelijne wegwijs gemaakt in de wereld van de stamcellen en de nierorganoïden. Ik ben dankbaar dat ik erbij was toen ook jij besloot aan een promotietraject te beginnen en dat we dat nu gelijktijdig afronden.
Ellen, de vele uren in het kippenlab vlogen voorbij met jou aan mijn zijde. Dank voor je flexibiliteit, je nuchtere instelling en de fijne gesprekken. Ik ben blij dat je vandaag naast me staat als paranimf.

Wendy, Annemarie, Franca, Gesa, Lonneke, Rianne en Anneloes, het was geweldig om met jullie als team te werken. Dank voor al jullie hulp en suggesties en voor de gezelligheid binnen en buiten het lab.

Sébastien, thank you for all the single cell RNA sequencing analyses and above all for your patience with me when explaining the details of those analyses.

Cristina, jouw nauwkeurigheid bij de verwerking en analyse van elektronen microscopie samples is ongeëvenaard. Dankjewel voor de fijne en vriendschappelijke samenwerking.

Manon, jouw prachtige illustraties hebben elk hoofdstuk van mijn proefschrift verduidelijkt en verfraaid.

Collega's van C7, K5 en D3, door alle lunches, borrels en 'Heel Nefro Bakt' competities was het gemakkelijk te vergeten dat we aan het werk waren.

Lieve papa en mama, jullie warme thuis was en is voor mij de perfecte basis om open, nieuwsgierig en zelfverzekerd mijn eigen weg te vinden. Jullie hebben me geleerd dat het

leven niet uitgestippeld hoeft te zijn, maar wel vaart bij wat flexibiliteit. Bovenal hebben jullie me het vertrouwen gegeven: Het komt wel goed.

Lieve Hes en Rut, dankjulliewel voor jullie liefdevolle steun. Samenzijn met jullie is nog net zo vanzelfsprekend, ongedwongen en ontspannen als in onze kindertijd.

Lieve Kees en Jaap, jullie zijn de grootste relativerende factor in mijn leven. Op dagelijkse basis ontdekken jullie meer dan ik tijdens mijn hele promotietraject. Het is heerlijk om jullie mama te zijn en ik kan niet wachten om te zien wat jullie morgen besluiten te onderzoeken.
Lieve Ruben, jij bent mijn rustpunt. Dankjewel dat je er altijd voor me bent en alles zo makkelijk voor me maakt. Ik kijk uit naar al onze toekomstige avonturen, klein en groot.